



## **A biocompatible micro cell culture chamber (CCC) for culturing and on-line monitoring of Eukaryotic cells**

**Stangegaard, Michael**

*Publication date:*  
2005

*Document Version*  
Publisher's PDF, also known as Version of record

[Link back to DTU Orbit](#)

*Citation (APA):*  
Stangegaard, M. (2005). A biocompatible micro cell culture chamber (CCC) for culturing and on-line monitoring of Eukaryotic cells.

## **DTU Library** Technical Information Center of Denmark

---

### **General rights**

Copyright and moral rights for the publications made accessible in the public portal are retained by the authors and/or other copyright owners and it is a condition of accessing publications that users recognise and abide by the legal requirements associated with these rights.

- Users may download and print one copy of any publication from the public portal for the purpose of private study or research.
- You may not further distribute the material or use it for any profit-making activity or commercial gain
- You may freely distribute the URL identifying the publication in the public portal

If you believe that this document breaches copyright please contact us providing details, and we will remove access to the work immediately and investigate your claim.

**A biocompatible micro cell culture  
chamber ( $\mu$ CCC) for culturing and on-  
line monitoring of Eukaryotic cells**

**Ph.D. Thesis**

**Michael Stangegaard**

**Microarray Technology**

**Department of Micro and Nano Technology**

**at**

**Technical University of Denmark**

**December 2005**



## **Preface**

This thesis has been written as a partial fulfillment of the requirements for obtaining the PhD degree at the Technical University of Denmark (DTU). The PhD project has been conducted at the Department of Micro and Nano Technology (MIC) in the period from December 2002 to December 2005.

The PhD project has been carried out in the Microarray Technologies group and has been supervised by the following people:

**Associate Professor, Project leader, Dr. Claus B. V. Christensen**

Main supervisor for the first half of the project

**Associate Professor, Project leader, Dr. Anders Wolff**

Co-supervisor for the first half of the project

**Director of MIC, Dr. Pieter Telleman**

Main supervisor for the intermediate part of the project

**Associate Professor, Project leader, Dr. Martin Dufva**

Main supervisor for the last half of the project

This thesis comprises a general introduction to the subject and a summary of the results achieved during the project. The results are partially based on the submitted manuscripts, attached in the Appendix, but also include unpublished results.

The project has been financed by Danish Biotechnology Instrument Center (DABIC) project no. 2014-00-0003

### **Publication and manuscripts:**

Paper 1: S. Petronis, **M. Stangegaard**, C. B. V. Christensen and M. Dufva, "*Transparent polymeric cell culture chip with integrated temperature control and uniform media perfusion*". *Biotechniques* **40** (3), 368-375 (2006).

Paper 2: **M. Stangegaard**, S. Petronis, A. M. Jørgensen, C. B. V. Christensen and M. Dufva, "*A biocompatible micro cell culture chamber for the culturing and on-line monitoring of Eukaryote cells*". *Lab on a Chip*, **6** (8), 1045-1051 (2006).

Paper 3: **M. Stangegaard\***, Z. Wang\*, J. P. Kutter, M. Dufva and A. Wolff, "*Whole genome expression profiling using DNA microarrays for determining biocompatibility of polymeric surfaces*". *Molecular Biosystems* **2** (9), 421-428 (2006). \* Joint authorship

Paper 4: **M. Stangegaard**, I. H. Dufva and M. Dufva, "*Reverse transcription using random pentadecamer primers increases yield and quality of resulting cDNA*". *Biotechniques* **40** (5), 649-657 (2006).

### **Other Publications and manuscripts:**

Paper 5: J. Petersen\*, **M. Stangegaard\***, H. Birgens and M. Dufva, "*Detection of mutations in the beta-globin gene by colorimetric staining of DNA microarrays visualized by a flatbed scanner*". *Analytical Biochemistry* **360** (1), 169-171 (2007). \* Joint authorship

### **Peer reviewed conference proceedings:**

Poster 1: M. Dufva, **M. Stangegaard**, and C. B. V. Christensen, “*Simple bonding of PMMA microstructures to modified glass surfaces preprinted with DNA and protein microarrays*”. Miniaturized Systems for Chemistry and Life Sciences 2004 ( $\mu$ TAS 2004)

Poster 2: Z. Wang, **M. Stangegaard**, M. Dufva, J. P. Kutter, and A. Wolff, “*A simple hydrophilic treatment of SU-8 surfaces for cell culturing and cell patterning*”. Miniaturized Systems for Chemistry and Life Sciences 2005 ( $\mu$ TAS 2005)

### **Conference proceedings:**

Poster 3: **M. Stangegaard**, S. Petronis, C. B. V. Christensen, and M. Dufva, “*A micro cell culture chamber ( $\mu$ CCC) for the culturing and study of Eukaryotic cells*”. Screening Europe 2005

Poster 4: **M. Stangegaard**, I. H. Dufva, V. Wohlgehagen and M. Dufva, “*Significance of the length of random oligo primers on the yield of cDNA during reverse transcription*”. Advances in Microarray Technologies (AMT 2005)

Poster 5: S. Petronis, **M. Stangegaard**, and M. Dufva, “*Micromachined Polymeric Cell Culture Chamber with Uniform Media Perfusion and Integrated Temperature Control*”. Life Matters Conversations 2005

Poster 6: **M. Stangegaard**, S. Petronis, C. B. V. Christensen, and M. Dufva, “*A biocompatible micro cell culture chamber ( $\mu$ CCC) for culturing and on-line monitoring of mammalian cells*”. LabAutomation 2006 (ALA 2006)

### **Other conference proceedings:**

Oral 1: M. Dufva, **M. Stangegaard**, P. Mikkelsen, L. Christensen, and C. B. V. Christensen, “*A flexible and thin microarray substrate for detecting DNA microarray hybridization using a business card scanner*”. LabAutomation 2004 (ALA2004).

Michael Stangegaard

Microarray Technology

Department of Micro and Nano Technologies, DTU

## Abstract

Visualization of cellular processes over extended periods of time has been hampered by the cellular requirement for heat, humidity and a physiological pH balanced media. The advances in micro technologies have enabled the production of miniaturized cell culture devices capable of sustaining mammalian cell growth over extended periods of time.

In the present work a novel perfusion based micro cell culture chamber with imbedded thermal monitoring and regulation is presented. The chamber sustained culturing and on-line monitoring of both cancer cell lines as well as human embryonic stem cell lines over long periods of time (>2 weeks and >90 hours respectively) after which the chamber became confluent and the experiments were stopped. The culture conditions in the chamber were assessed by means of morphological observations, growths kinetics and whole genome expression profiling on transcriptome DNA microarrays. The results suggested that the culturing conditions in the  $\mu$ CCC were comparable to those in the conventional culture flask, if the intensity of the microscope and ambient light was carefully monitored.

Surface modifications of the structural photoresist SU-8 commonly used for realizing micro channels by means of lithography were assessed for their ability to sustain cell culture. The biocompatibility of the surface modifications were assessed by means of morphological observations, growths kinetics and whole genome expression profiling on transcriptome DNA microarrays. The latter method was denoted bio-comparability enabling distinction from biocompatibility. A surface modification was found to result in comparable morphology and growth kinetics to the reference cell culture flask, but showed a significantly different gene expression profile suggesting biocompatibility does not infer bio-comparability.

A novel random priming method for initiation of reverse transcription reactions and real time PCRs was developed. The impact of the simple switch of primer was found to increase the yield of cDNA by 100 % corresponding to 80 % of the RNA template was reverse transcribed into cDNA. Furthermore the random priming method increased the amount of detected genes on transcriptome DNA microarrays by 55 % in the Cy-3 channel and 72 % in the Cy-5 channel, suggesting a significant better coverage of the transcriptome.

---

## Table of contents

Preface .....	3
Abstract.....	6
Table of contents .....	7
1 Introduction.....	10
Conventional cell culturing .....	10
Cell culturing chambers.....	11
Obtaining and maintaining comparable growth conditions.....	11
Heat sensing element.....	12
Biocompatibility .....	13
Culturing surfaces.....	14
Cell patterning .....	14
Phototoxicity.....	15
Reverse transcription as a method for generating cDNA.....	15
DNA Microarrays and gene expression profiling.....	16
2 Aim of the project .....	18
3 Materials and Methods.....	19
Fabrication of $\mu$ CCC: .....	19
Imprinting of topographical features in PMMA.....	21
Temperature control .....	21
Physical modeling .....	22
Spectral analysis .....	23
Preparation of modified SU-8 surface .....	23
Patterning on SU-8 surface.....	24
Water contact angle measurements .....	24
Cell culture in CO <sub>2</sub> incubator: .....	24
Cells cultured in the $\mu$ CCC.....	25
Stem cell culturing.....	26
Conventional culturing in the CO <sub>2</sub> incubator .....	26
Culturing in the $\mu$ CCC.....	26
Surface coatings of $\mu$ CCC for stem cell culturing.....	27
RNA isolation and amplification.....	27
cDNA synthesis .....	28
DNA Microarrays.....	28



Data analysis.....	30
4 Results.....	31
Design.....	31
Materials.....	31
Device design and layout.....	32
Fabrication.....	35
Assembly of the $\mu$ CCC.....	35
Heating.....	36
Characterization of the $\mu$ CCC.....	38
Recyclable thermistor.....	39
Thin $\mu$ CCC.....	42
Multifunctional device.....	42
Operation.....	44
Cell culturing.....	44
Growth kinetics of HeLa cells in the $\mu$ CCC.....	45
Growth kinetics in the $\mu$ CCC.....	47
Temperature regulation in the $\mu$ CCC.....	48
Cell attachment.....	48
Cell proliferation.....	49
Cell-cell contact.....	50
Cell death.....	51
Bubbles.....	53
Contamination.....	56
Phototoxicity.....	58
Influence of light.....	62
Influence of surface topography.....	63
Biocompatibility.....	65
PMMA as culturing surface.....	65
Whole genome expression profiling on DNA microarrays.....	66
Whole genome expression profiling of $\mu$ CCC cultured cells.....	71
Dye-swap replicates.....	74
CACO 2 cells.....	75
Colon 205 cells.....	78
Stem cells.....	80
Biocompatible surfaces for use in microfabrication.....	87

	Morphology and growth characteristics .....	88
	Whole genome expression profile comparison cells cultured on SU-8.....	93
	Enhancement of the reverse transcription reaction for gene expression analysis .....	95
	cDNA yield of reverse transcription reactions .....	95
	Effect of R15 priming on whole genome expression profiling .....	100
5	Discussion .....	105
	Material and fabrication.....	106
	Heating strategy .....	107
	Phototoxicity.....	108
	Shear stress .....	109
	Biocompatibility .....	109
	Bio-comparability.....	111
	Growth kinetics .....	112
	Other cell culture chambers.....	113
	Random priming.....	114
6	Conclusion .....	117
7	Future outlook.....	118
8	References.....	119
9	Publications and manuscripts.....	128
	Paper 1 .....	129
	Paper 2.....	138
	Paper 3.....	147
	Paper 4.....	160
10	Conference proceedings.....	170
	Poster 1 .....	171
	Poster 2 .....	176
	Poster 3 .....	180
	Poster 4 .....	181
	Poster 5 .....	182
	Poster 6 .....	183
11	Acknowledgment .....	184
12	Appendix.....	186

## 1 Introduction

Cell culturing is a core method in biological science and clinical research, as well as in many biotechnological and biomedical engineering areas. Since the initial culturing of human cells<sup>1</sup> one objective has been to study the morphological changes in cells over time. Traditionally this has been performed by systematic inspection of a cell culture at selected time intervals. The ability to monitor cellular behavior in real time may enable new understandings of cell function or behavior. The main obstacle in imaging of cells is not to take the picture – but being able to take several continuous pictures of a few cells, without affecting culturing conditions<sup>2</sup>.

Several different solutions has been attempted to achieve on-line monitoring of cellular cultures. However, to the best of our knowledge no one has so far provided insight into how the cell culture grows in the chambers. Minute changes in culturing conditions can and most likely will induce cellular responses. These responses may be detected in terms of an altered viability, morphology, growth kinetics or whole genome expression profile, but may also be on the protein level and hence may not be identifiable with DNA microarrays.

### **Conventional cell culturing**

Typically, Eukaryotic cells are cultured in a nutrient buffer within plastic culture flasks, Petri dishes or multiwell plates. For keeping the fastidious and fragile Eukaryotic cells alive, several criteria have to be met. First, the temperature has to be controlled within a narrow range around 37 °C. Second, the pH of the media has to be maintained around the physiological 7.4. To accomplish this, most culture methods employ a buffering system similar to that found in blood, in which there is an equilibrium between dissolved CO<sub>2</sub> (bicarbonate anion) and a well-regulated usually 5 % CO<sub>2</sub> atmosphere. The two first conditions are met by placing the cell culture inside a CO<sub>2</sub> incubator maintained at 37 °C, 5 % CO<sub>2</sub> and around 80 % humidity. Third the cell culture media has to be balanced in terms of osmolality *i.e.* the concentration of osmotic active components in the media has to match physiological conditions required by the specific cell line. Fourth, the cell media has to contain nutrients, vitamins and the required amount growth regulating effectors. Conventionally this criterion is met by supplying a standard media with fetal calf or bovine

serum in volumes from around 1 % or less and up to 20 % in some instances. The amount will depend upon the specific requirement of the cell line in question. For observation under a microscope the cells are removed from the incubator and brought into room temperature and atmosphere (<0.05 % CO<sub>2</sub>), resulting in bicarbonate leaving the medium as gaseous CO<sub>2</sub> and the pH rapidly drifts up to a lethal alkaline value of over 8.5<sup>3</sup> limiting observation time to twenty minutes or less, if the temperature or pH of the cell culture is not to be adversely affected. Microscopes with CO<sub>2</sub> enriched stage environments are now commercially available and can prolong the observation time outside the CO<sub>2</sub> incubator or even replace the incubator in selected studies<sup>4,5</sup>.

### **Cell culturing chambers**

The advances in microfabrication and polymer technologies and the opportunities offered in terms of design and fabrication of miniaturized cell culture systems<sup>6</sup> has led to the development of several cell culture chambers. Some chambers focus on single cell observations over long periods of time<sup>7-13</sup>. Another group of micro chambers holding a larger amount of cells focus on large scale cell culturing<sup>14,15</sup>, wound healing processes<sup>16</sup>, heat shock<sup>17</sup>, cell-cell interactions<sup>18</sup> cell differentiation<sup>19</sup>, myocyte synchronization<sup>20</sup>, chemotaxis<sup>21</sup>, electrical characterization<sup>22-24</sup>, electroporation<sup>25</sup> and cell stress levels<sup>26</sup>. Other studies rely on arrays of interconnected cell culture chambers for on-line gene expression<sup>4,5</sup> or potential drug screening<sup>27,28</sup>. More advanced chambers seeks to elucidate the toxicological and pharmacological profiles of chemicals and pharmaceuticals relying on interconnected chambers each holding different cell lines representing the different organs and their interconnective metabolism<sup>29-31</sup>. Insight into intracellular events pose high requirement to the optical properties of the materials comprising the chamber(s)<sup>32,33</sup> hampering the use of polymeric materials due to stress and strains build up during injection molding<sup>34</sup>.

### **Obtaining and maintaining comparable growth conditions**

Maintaining the desired culturing temperature within a narrow range of *e.g.*  $\pm 0.1$  °C can be a challenge even for commercial CO<sub>2</sub> incubators. The majority of the above mentioned chambers relies on the conventional incubator to supply heat, humidity and CO<sub>2</sub> for maintaining physiological pH<sup>9,19,23,27,28</sup> or a commercial microscope equipped with a CO<sub>2</sub> enriched stage environment<sup>4,5</sup>. Alternatively the temperature of the microscope stage was regulated<sup>18</sup>, the chamber exterior was perfused with temperature balanced water<sup>17,26</sup>, or a

resistive heating coil feedback controlled based on reading from an internal temperature sensor<sup>32</sup>. In another system the chamber interior was perfused with temperature regulated media<sup>7</sup>. A more advanced system used indium tin oxide (ITO) coated glass to supply heat to the chamber bottom and/or heating of the chamber exterior walls in response to an internal temperature sensor<sup>16, 24</sup>.

### **Heat sensing element**

A vital part of the  $\mu$ CCC is the heat sensing element. The objective was to be able to monitor the actual temperature of the media inside the culturing chamber with real time accuracy. The physical dimensions of the chamber, significantly limits the amount of available measuring devices. Resistance Temperature Detectors (RTDs) operate on the principle of changes in electrical resistance of pure metals and are characterized by an almost linear positive change in resistance with temperature. They are typically made of platinum wire/film and therefore quite expensive. Another commonly used temperature devices are thermocouples. The working principle of thermocouples is that an output voltage is produced which depends on the temperature difference between the junctions of two dissimilar metal wires. Hence the measured temperature is not an absolute temperature but a temperature difference. Furthermore thermocouples would require rather complicated electronic circuits to get a correct readout of the actual temperature. Thermocouples with sub-millimeter dimensions are commercially available but are quite expensive (>400 €). The third group of temperature measurement devices commonly used is thermistors, which are temperature sensitive semiconductors exhibiting rapid and large changes in resistance for relatively small changes in temperature. Most thermistors have a negative temperature coefficient of resistance, *i.e.* as temperature increases, their resistance decreases. When connected to an electronic circuit these changes can be monitored and converted into temperature readings. The dependence of resistance on temperature is exponential. For low temperatures (< 100 °C) it is possible to approximate it to a linear dependence. By calibrating the thermistor at two different temperatures the relationship between the actual temperature and resistance is given by the simplified Steinhart - Hart equation (Formula 1).

$$\frac{1}{T} = A + B \cdot \ln(R) \quad \text{Formula 1}$$

The typical constants A and B are provided by the manufacturer, but they may vary slightly for each device, so for high precision temperature measurements, the constants may be

determined by calibration. Thermistors are commercially available with different physical dimensions, properties, accuracies, insulations composition and prices.

## **Biocompatibility**

In biology the most elementary however complete unit is the cell. It is the simplest unit that is alive. Being alive results in the cell interacts with its surrounding environment in a dynamic fashion both responding to and influencing it <sup>34</sup>. Minimizing the effect of the culturing environment requires the use of biocompatible surroundings. The term biocompatible surface refers to a surface devoid of both cytotoxic and positive effects in the sense of biofunctionality *i.e.* promotion or obstruction of biological processes compared to the reference surface <sup>35,36</sup>.

Cytotoxicity determination is an important aspect in biomaterial testing standards such as International Organization for Standardization (ISO) and American Society for Testing and Materials (ASTM). However, the absence of cytotoxicity *e.g.* measured by the 3-(4,5-dimethylthiazol-2-yl)-2,5-diphenyl-tetrazolium bromide (MTT) test <sup>37</sup> or fluorescent membrane integrity test (FMIT) <sup>38</sup> does not imply that a material is biocompatible. For each application, tests have to be conducted in settings reflecting the natural environment and the demands posed on the application to elucidate the biocompatibility of the material. The biocompatibility of a material has been related to cellular functions like adhesion <sup>38-40</sup> and spreading on the surface <sup>41</sup>, proliferation rate <sup>40</sup>, metabolic activity <sup>40</sup>, surface inhomogeneity and moderate wettability <sup>42,43</sup>. However, decreasing wettability may not represent increasing biocompatibility <sup>44,45</sup>.

Bioincompatible surfaces such as SU-8 <sup>8</sup>, modified glass and silicon <sup>24</sup>, silicon <sup>26</sup>, poly lysine coated silicon <sup>30</sup>, alkanethiol self-assembled monolayers <sup>46</sup>, polyimide <sup>47</sup>, plasma polymerized hexene <sup>48</sup>, and bovine serum albumin (BSA) coated glass <sup>49</sup> have been rendered biocompatible by coating with fibronectin <sup>30,46,47</sup>, poly-D-lysine and laminin <sup>24</sup>, poly-L-lysine <sup>8,26</sup>, adhesion peptides <sup>50,51</sup>, hydrophilic polymer materials <sup>48</sup> a special designed anchor molecule <sup>49</sup> or O<sub>2</sub> plasma treatment <sup>8</sup> to allow culturing of cells. These coatings may however be laborious, expensive, and/or unstable over time. A different strategy has been to realize micro chambers by conventional lithographical techniques *e.g.* in polydimethylsiloxane (PDMS) and bond the structures to a piece of glass functioning as culturing surface <sup>7,9,13,27,28</sup> enabling culturing and monitoring of down to single cells as well as on-line gene expression profiling of selected genes <sup>4,5</sup>.

## **Culturing surfaces**

When the culturing surface is changed several factors may influence cell attachment and proliferation. The new surface may represent changes in hydrophobicity (wettability), surface charge and the density of surface charges, surface roughness and topography, the molecular groups exposed on the surface and their reactivity as reviewed<sup>36</sup>. All of which may influence cell adhesion, cell spreading and proliferation rate. Furthermore the surface may interfere with the biosynthetic functions of the cell without affecting cell morphology or proliferation capacity<sup>52</sup>. Culturing cells on surfaces that are not biocompatible may induce changes in the gene expression profile in a cell. This was apparent when studying changes in gene expression in MG63 osteoblast-like cells grown on zirconium oxide where genes involved in immunity, cell cycle, and vesicular transport was found differently regulated<sup>53</sup>.

## **Cell patterning**

The formation of discrete locations on a surface supporting normal cell growth characteristics on a surface otherwise incapable of supporting cell growth, may be used to study cells in a well controlled manner, make precise manipulations of cell arrangement and study *e.g.* heterotypic cell interactions<sup>54</sup>. To achieve this, it is possible to select specific substrates, such as extracellular matrix proteins or specific motifs that interact with cell adhesion molecules to support cell adhesion primarily on special designed surface patterns. The resulting micropatterning techniques of living cells has made significant contributions to basic cell biology, cell-based bioelectronics and tissue engineering<sup>55,56</sup> because of the acquired spatial control of cell adhesion and growth in these fields. Several methods have previously been reported to achieve micropatterned surfaces, including photolithography<sup>57-59</sup>, electron beam (EB) polymerization using masks<sup>54</sup>, micro contact printing<sup>60-62</sup>, microfluidics<sup>63,64</sup>, and the use of elastomeric membranes with many holes<sup>65,66</sup>. Although the use of polymers simplifies fabrication of micropatterns and reduces the cost for disposable bioassay devices, these methods are intricate because of the numerous serial steps necessary for fabrication of the micropatterned surfaces<sup>61</sup>.

## **Phototoxicity**

The visible light wavelength spectrum is 400-700 nm with ultraviolet (UV) wavelengths below 400 nm. Photoeffects on media components or cells have been observed at wavelengths below 540 nm<sup>67</sup>. Common fluorescent lamps emit significant light in that range, as do sunlight and tungsten sources. Phototoxic effects of visible light was found to be related to photodecomposition of riboflavin/vitamin B2<sup>68,69</sup>, tyrosine<sup>70</sup> and tryptophan<sup>71</sup> and the generation of  $^1\text{O}_2$  and  $\cdot\text{OH}$ <sup>69-72</sup>. As riboflavin absorbs light maximally at 375 and 447 nm<sup>73</sup> this supports that photoeffects are most likely to be the result of UV or near UV light. Free radicals released due to photodecomposition of media components have been found to induce serious cell damage and fibrogenesis as reviewed in<sup>74</sup>. Whether these effects occur under typical confocal imaging conditions is unknown, but many of the photoeffects may be eliminated by antioxidants/free radical scavengers like pyruvate (2-10 mM) or vitamin C (1-5  $\mu\text{M}$ ) and E (1-5  $\mu\text{M}$ )<sup>69,75</sup>, indicating it to be advisable either to add anti-oxidants or to reduce the light intensity below the threshold. Some media designed for the low ambient  $\text{CO}_2$  levels use additional organic buffers, such as N-2-hydroxyethylpiperazine-N'-2-ethanesulfonic acid (HEPES), to maintain physiological pH. However, HEPES is highly photo sensitive, and phototoxic effects in HEPES buffered media have been reported even under standard fluorescent ceiling lights<sup>75,76</sup>.

## **Reverse transcription as a method for generating cDNA.**

Reverse transcription of RNA into cDNA is a core method for analysis of gene expression using DNA microarrays or real time PCR (RT-PCR)<sup>77-81</sup>. The reverse transcription should result in a cDNA population which reflects the original mRNA population in terms of transcript abundance and complexity. Furthermore, the reverse transcription reaction should be as efficient as possible to give maximum sensitivity in the final assay. Sensitivity is often problematic in microarray analysis of un-amplified mRNA. Sensitivity is also an issue when following fusion gene markers in cancer patients where, for instance, it is desired to detect a single cancer cell expressing the BCR/ABL fusion transcripts in a background of 100,000 normal cells in Chronic Myelogenous Leukemia (CML) patients<sup>82,83</sup>. This suggests that improvements in reverse transcription could have large impact in assay results.



Important parameters to obtain high yield cDNA of good quality is the RNA quality<sup>84-88</sup>, priming strategy<sup>89</sup> and enzyme efficiency<sup>90,91</sup>. Reverse transcription can be primed using specific primers<sup>92,93</sup> which is a possibility if relatively few different transcripts are targeted. This is not a practical option for whole transcriptome analysis using microarray since it would require synthesis and mixing of thousands of specific primers. In those cases, the reverse transcription reaction is primed with Oligo(dT)<sup>94,95</sup>, random hexamer<sup>95-99</sup> or random nonamer<sup>96,100</sup> primers. Oligo-dT priming has the virtue of producing cDNA from the 3' end of polyA mRNA allowing total RNA to be used as template, but often results in a 3' bias compared to random priming<sup>91</sup>. Random primers can and will anneal to all RNA molecules containing the complementary sequence, and as the target mRNA population only typically comprises less than 2 % of the total RNA pool, cDNA synthesis from total RNA with random priming will produce a large quantity of fragments most likely originating from ribosomal RNA that lack specificity in hybridization and can give rise to elevated background signals. As a result random priming is preferred when using poly(A) purified RNA like mRNA or amplified RNA (aRNA). However, the significance of different length of primers in the reverse transcription reaction has so far been left unaddressed.

### **DNA Microarrays and gene expression profiling**

An invaluable tool for acquiring an overview of which genes are expressed in a cell culture is the DNA microarray<sup>94,101</sup>. The DNA microarray technology utilizes a high-density array of nucleic acid probes<sup>102</sup> of various length and sequences located in discrete spots usually on a microscope slide, enabling the interrogation of a complex sample for complementary target sequences to all the arrayed probes in a single experiment.

Two different types of DNA microarrays exist, “cDNA microarrays” and “oligonucleotide microarrays” respectively. In cDNA microarrays the individual probes are derived from a physical source (*e.g.* PCR amplicons from cDNA clones or expressed sequence tagged sites (ESTs))<sup>94,103</sup>, while the probes in oligonucleotide microarrays are systematically made based on sequence information, either synthesized directly on chip<sup>104</sup> or arrayed as oligonucleotides using a spotting robot<sup>105</sup>. Utilizing two differently labeled target preparations the targets will bind to the arrayed probes in amounts reflecting their concentrations and hence abundance in each of the two analyzed samples. Conventionally the ratio between the signal intensities of the two channels are computed<sup>105</sup> and used as an indication to which genes are regulated relative to a control preparation. This allows for the comparison of two different cell cultures

or conditions on a transcription wide scale in a single experiment<sup>106</sup> or *e.g.* enables the study of cancer progression in patient material<sup>107,108</sup>.

However, much regulation is performed not on the transcriptional level but on the translational level as well as modifications to the finished proteins *i.e.* glycosylation or (de)phosphorylation are performed in response to certain stimuli. This type of regulation is not reflected in the DNA microarray data. This information could be captured using a protein array but this technology is still in its infancy and large scale protein arrays may not be commercially available for several years<sup>109</sup>.

## **2 Aim of the project**

The aim of the Ph.D. project described in this thesis was to explore the potentials of microfluidics and micro technology for realizing a platform or chip that would enable on-line monitoring of Eukaryote cells outside the CO<sub>2</sub> incubator. The intention of this was to bring light to cellular events otherwise kept in the darkness of the conventional CO<sub>2</sub> incubator. The chip was to provide culturing conditions resembling the conventional cell culture flask using non-modified conventional media enabling the comparison of results obtained in the chip with results from the literature.

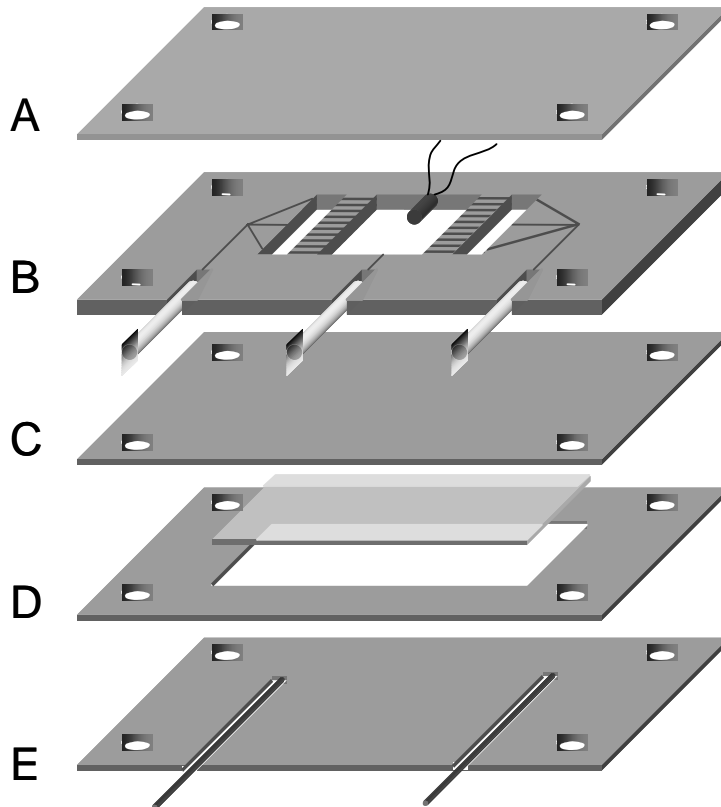
On-line monitoring of Eukaryote cells has several advantages such as real time studies of cellular events such as attachment to various surfaces, cell division, cell motility and cell death, to name a few.

During the course of the project, whole genome expression profiling was utilized as a novel tool for assessing the biocompatibility of cell culture conditions and surfaces and was denoted bio-comparability.

### 3 Materials and Methods

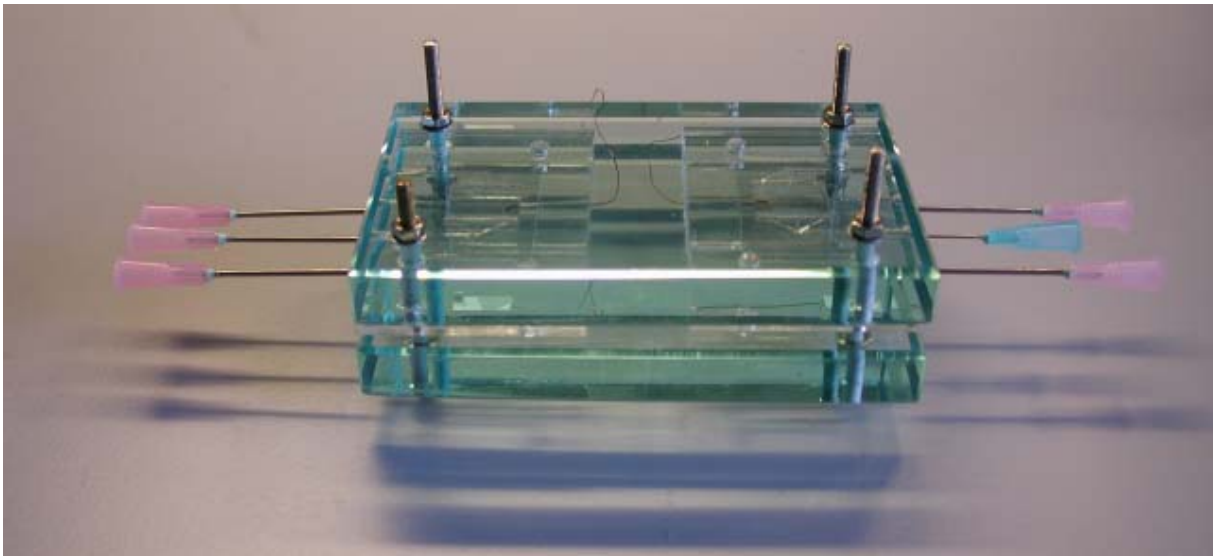
#### *Fabrication of $\mu$ CCC:*

The  $\mu$ CCC was made out of five poly-methyl-methacrylate (PMMA) sheets, each separately cut and micromachined by laser ablation (Figure 1), and assembled into a functional structure by thermal bonding as described by Klank *et al.*<sup>110</sup>.



**Figure 1: Construction of the  $\mu$ CCC.** (A) Top lid. (B) Layer defining the cell culture chamber microfluidics channels, barriers, inlet, and outlet for media perfusion as well as cell seeding. The thermistor was prior to bonding inserted between layer (A) and (B) and aligned manually. (C) Isolating layer preventing media from short circuiting the heater. (D) Layer holding the heater, which consists of a sheet of ITO coated PET film indicated with a lighter shade of gray. (E) Layer contains alignment grooves for electrodes to the heater and protects the heater from the environment. Each layer contained four alignment holes.

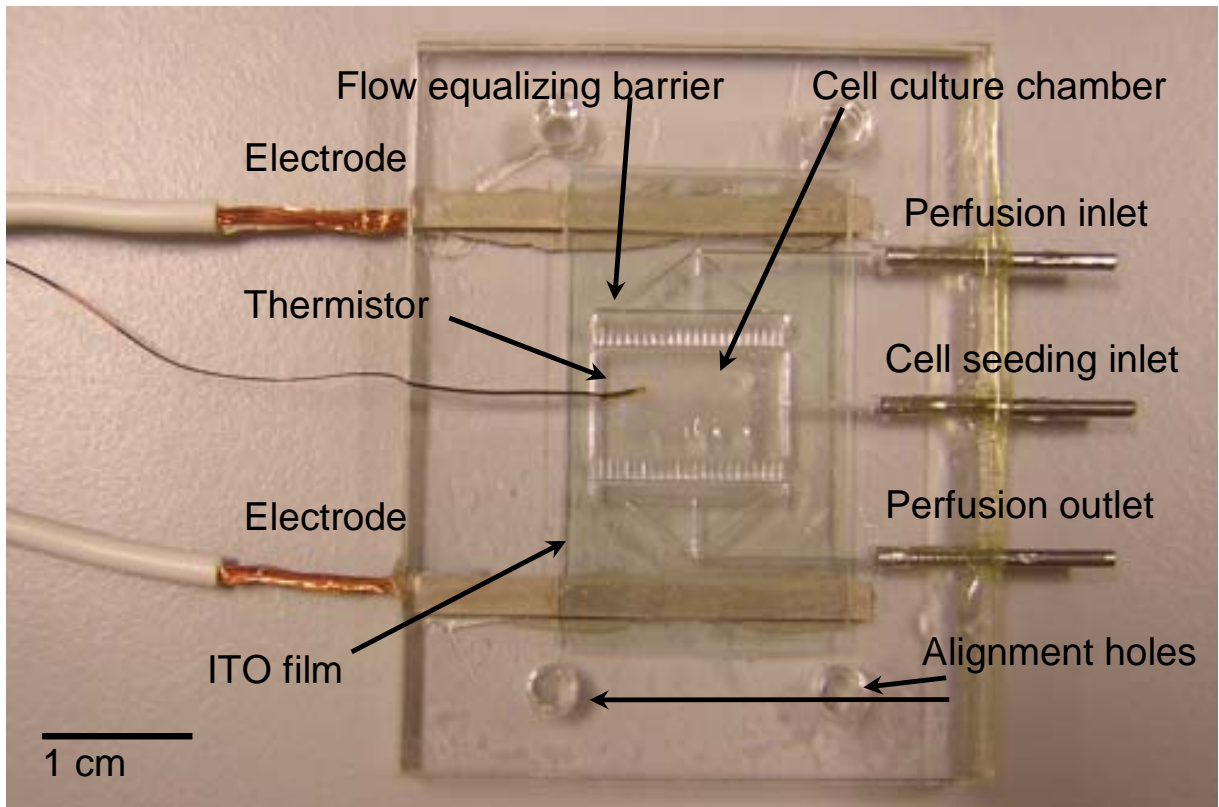
Briefly, an infrared (IR) laser ablation system (Synrad Inc., Mukilteo, USA) was run using 500-800 mm/s beam movement velocity, 28-32 W laser power and 1000 dpi exposure resolution to induce chip contours, alignment holes, chamber, heater spacers, and microfluidic channels in 1.5 mm (Figure 1 layer (A), (B) and (E)) in and 0.25 mm (Figure 1 layer (C) and (D)) thick PMMA sheets (type 99530 Röhm GmbH & Co. KG, Darmstadt, Germany). Prior to the bonding processes, the micromachined PMMA parts were annealed at 80 °C for at least 30 min in order to avoid stress cracks in the structure. After annealing, the parts were wiped with 96 % ethanol, aligned and sandwiched between two custom made glass bonding blocks (Gustav Sørensen & søn, Rødovre, Denmark) (Figure 2) and exposed to 110 °C in a Memmert oven (Memmert, Schwabach, Germany) under 100 Ncm mechanical pressure set with a 40-200 Ncm torque screwdriver (Lindstrom, Orange, CA, USA) for one hour, resulting in an irreversible bonding of the structured PMMA parts.



**Figure 2: Bonding of the  $\mu$ CCC using glass bonding blocks.** The glass bonding blocks were made of 12 mm thick glass and contained four  $\text{\O}2$  mm alignment holes. Needles were inserted in channels during bonding to maintain the integrity of the inlets and outlets channels.

After bonding, the bonding blocks with  $\mu$ CCC were allowed to cool to room temperature before the pressure was gently released. Electrical connection to the ITO coated film (15-25  $\Omega$ , Sigma-Aldrich, Steinheim, Germany) was achieved with standard copper wires and conductive epoxy based glue (Circuitworks, Chemtronics, Kennesaw, GA, USA). Curing of the glue took place at 80  $^{\circ}\text{C}$  for 15 minutes. The resistance through the ITO-film was used as a measure of the connection quality. Only chambers with a resistance lower than 17  $\Omega$  were used. Higher resistance indicated improper connection to the ITO layer which would result in inadequate heating. Inlet tubes were realized from blunt end 18 gauge stainless steel needles (Becton Dickinson, Drogheda, Ireland) that were divided in two by a metal saw and scratched on the surface for better attachment to the structure. Attachment to the structure was performed with epoxy glue (R&G GmbH, Waldenbuch, Germany). Electrical isolation of the electrodes was obtained by coating with a thin layer of epoxy glue. The layout of the  $\mu$ CCC with the functional parts labeled is provided in Figure 3.

For some chambers a UV curable glue Dymax 952-T (Dymax, Frankfurt a.M., Germany) was used to provide sealing to the  $\mu$ CCC. Curing of the glue was performed with an UV75 UV source (Thorlabs, Ontario Canada).



**Figure 3: Layout of the  $\mu$ CCC with the functional parts labeled.**

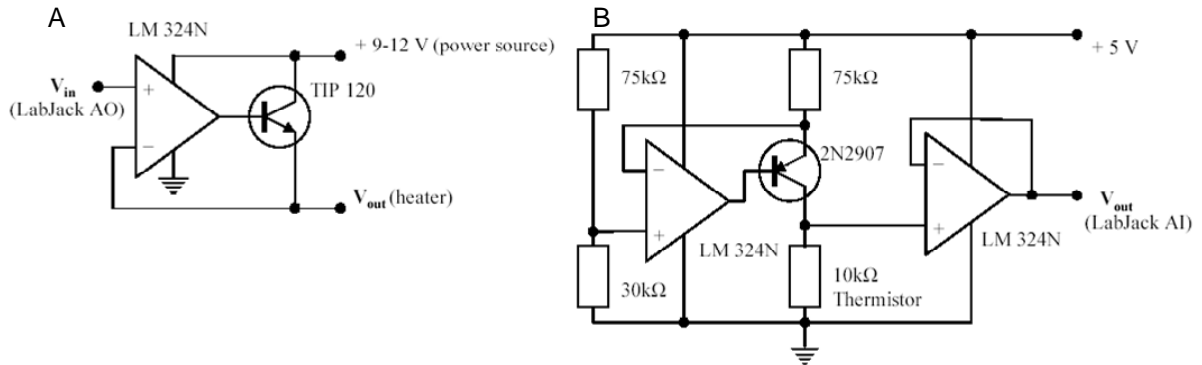
### ***Imprinting of topographical features in PMMA***

A sheet of 1.5 mm thick PMMA cut to size of a 4 inch wafer was imprinted using a wafer containing various topographical features such as lines, squares, circles etc. of various lateral dimensions ranging from tens to hundreds of  $\mu\text{m}$ . The heights of the features were 90 nm. Imprinting was performed in an EVG 520HE parallel plate nanoimprinter, setting the temperature of the lower piston to 130  $^{\circ}\text{C}$  and the upper piston to 97  $^{\circ}\text{C}$  to avoid bending of the PMMA due to the different heating/cooling rates of the pistons. A pressure of 15,000 N was applied for 2 minutes in a vacuum atmosphere.

### ***Temperature control***

The temperature inside the cell culture chamber was controlled by a proportional-integral-derivative (PID) feedback loop which was implemented using LabView v7.0 software (National Instruments, Austin, USA). The computer program controlled the voltage applied on the ITO film based heater depending on the temperature readings from the micro-BetaCHIP thermistor model 10K3MCD (BetaTHERM, Shrewsbury, MA, USA) located within the cell culture chamber (Figure 3). A USB based multifunction data input/output

board (LabJack U12; LabJack Corporation, Lakewood, USA) and two home-made electronic circuits (Figure 4) were used to connect the heater and the thermistor to the computer and the external power source (9 V, 500 mA, AC/DC converter type OTC 910801, Otron Electronics, Hong Kong). One electronic circuit controlled the electrical power provided to the heater depending on the voltage level in the analogic output (AO) port of the LabJack board. The voltage applied on the heater followed the AO voltage but with much higher current supplied from the external power source. The second electronic circuit kept constant current (50  $\mu$ A) passing through the thermistor, and therefore converted temperature dependant resistance changes of the thermistor into voltage signals that were registered by the analogic input (AI) port of the LabJack board. The voltage signal was further converted into temperature values and logged in computer memory by the same LabView code.



**Figure 4: Blueprints of home made electronic circuits.** (A) Electronic circuit for connecting the heater to an external power source to U12 LabJack USB controller. (B) Electronic circuit for connecting 10 k thermistor to the U12 LabJack USB controller for temperature logging. Design and realization of the electronic circuits was performed by Sarunas Petronis.

### *Physical modeling*

Two-dimensional finite element modeling was performed to evaluate fluidic and thermal properties of the chip. Modeling was made using Fluid Dynamics and Heat Transfer modules of FEMLAB v3.1b software (COMSOL A/S, Kgs. Lyngby, Denmark). The physical parameters of the materials used in simulations are listed in Table 1. First, the incompressible Navier-Stokes equations were solved to simulate steady state velocity field of the culture media perfusion. No-slip boundary conditions were applied on the walls of the channels and the chamber, a parabolic velocity profile with average speed corresponding to 0.1 mL/h perfusion rate was used at the inlet, and zero pressure conditions were set at the outlet.

**Table 1: Material properties used in 2D finite element modeling of fluid and heat transfer within the  $\mu$ CCC**

PMMA density	1180 kg/m <sup>3</sup>
PMMA heat capacity	1500 J/(kg·K)
PMMA thermal conductivity	0.18 W/(m·K)
Buffer density	1007 kg/m <sup>3</sup>
Buffer dynamic viscosity (37 °C)	0.0007 N·s/m <sup>2</sup>
Buffer heat capacity (37 °C)	4000 J/(kg·K)
Buffer thermal conductivity (37 °C)	0.62 W/(m·K)
Heat dissipation to ambient	20 W/(m <sup>2</sup> ·K)

### *Spectral analysis*

The spectrum of the light emitted by the microscope halogen lamp was measured using an AvaSpec2048 spectrometer (Avantes, Netherlands). The spectrometer was connected to a stepindex optical fiber with a core diameter of 50  $\mu$ m and a numerical aperture of 0.22. This fiber was mounted on the microscope fixture and aligned with the collimated illumination light. The spectrum was measured both in the dark and for several settings of the microscope light intensity using integration times between 2 and 20 ms. The measurements were scaled to an integration time of 20 ms and the dark spectrum was subtracted. Each measurement was obtained ten times.

### *Preparation of modified SU-8 surface*

A 5  $\mu$ m thin layer of SU-8 XP2005 negative photoresist (Microchem, Switzerland) was spin-coated on a 4" 500  $\mu$ m thick Pyrex wafer (Schott corporation, Germany). The SU-8 layer was fully cross-linked by UV flood exposure and a post bake processes. The SU-8 surface was modified by incubation with 1 M nitric acid (Fluka, Germany), catalyzed by 0.1 M Ceric ammonium nitrate (CAN, (NH<sub>4</sub>)<sub>2</sub>Ce(NO<sub>3</sub>)<sub>6</sub>) (Sigma) at 50 °C for 1 hour and subsequently washed with MilliQ water. The material samples were dried and, optionally, treated with 0.1 M ethanolamine (Fluka) in 0.1 M sodium phosphate (Sigma) buffer (pH 9.0) for 20 minutes at 50 °C. Finally, the material samples were washed MilliQ water and dried.



### ***Patterning on SU-8 surface***

A two-step photolithography process was established to create the hydrophilic SU-8 patterns on the SU-8 surface for the cell patterning experiments. A 1.5  $\mu\text{m}$  thick AZ5214e photoresist (Honeywell, USA) film was created on fully developed 5  $\mu\text{m}$  thick SU-8 layers by spin coating. A shadow mask was applied to define the patterns created by standard light lithography. Then the whole wafer was dipped into the  $\text{HNO}_3$ -CAN solution for the first step surface treatment. After the  $\text{HNO}_3$ -CAN surface treatment, the AZ5214e photoresist shadow mask was lifted off in acetone (Fluka) utilizing 4 minutes ultrasonic agitation. Finally, the whole wafer was dipped into the ethanolamine solution to finish the second step surface treatment. Thus on the SU-8 surface, patterned areas were rendered to own hydrophilic characters for cell patterning and the rest areas kept original hydrophobic characters.

### ***Water contact angle measurements***

Contact angles between the different surfaces and MilliQ water was measured using a DSA 10 MK2 (Krüss GMBH, Germany).

### ***Cell culture in $\text{CO}_2$ incubator:***

Human epithelial carcinoma cells (HeLa), human colon adenocarcinoma cells (CACO 2) and human colon adenocarcinoma cells with a round and refractile morphology (COLO 205) were cultured in 75  $\text{cm}^2$  culture flasks (Easyflask, Nalge Nunc International Rochester, NY, USA) in 25 mL media (RPMI 1640 media (Sigma) supplemented with 10 % Fetal Bovine Serum (FBS) (Sigma), penicillin (100 U/mL) and streptomycin (100  $\mu\text{g}/\text{mL}$ ) (Sigma)). Cells were cultured at 37  $^\circ\text{C}$  in an atmosphere containing 5 %  $\text{CO}_2$  (AGA, Copenhagen, Denmark) in a  $\text{CO}_2$  incubator (Assab, Don Whitley Scientific Ltd., Shipley, West Yorkshire, United Kingdom). Seeding of the cells was performed with a density of about 6660 cells per  $\text{cm}^2$  and subcultured every three to four days when around 90 % confluence was reached. Cell passaging was performed by trypsinization (Sigma). Cell count was performed in a Bürker chamber (Paul Marienfeld GmbH & Co. KG, Lauda-Koenigshofen, Germany). Cell counting in the culture flasks for growth kinetics determination was performed using microscopic images of the cell culture obtained by temporarily removing the cell culture flasks from the  $\text{CO}_2$  incubator and placing them on the stage of the microscope (Zeiss Axiovert 200M, Carl

Zeiss, Oberkochen, Germany). Three to four images were grabbed using the accompanying software of each culture flask on each day over a four day period (twenty seven images in total).

### ***Cells cultured in the $\mu$ CCC***

Prior to culturing the  $\mu$ CCC was sterilized by sandwiching the chamber between the two glass bonding blocks at 100 °C for one hour. No other pressure than the weight of the glass bonding block (185 g) was applied. After cooling to room temperature the sterilized chamber was removed from the glass bonding blocks and the thermistor in the  $\mu$ CCC was calibrated at room temperature and 37 °C. Media (RPMI 1640 media (Sigma) supplemented with 10 % Fetal Bovine Serum (FBS) (Sigma), penicillin (100 U/mL) and streptomycin (100  $\mu$ g/mL) (Sigma)) was brought to room temperature prior to loading in a 20 mL sterile syringe (Becton Dickinson, Drogheda, Ireland). The perfusion inlet of the chip was connected to a 20 mL sterile syringe (Becton Dickinson) by freshly autoclaved polytetrafluoroethylene (PTFE) tubing ( $\varnothing$  0.8 mm, Bohlender GmbH, Grünsfeld, Germany), which were attached by 2 cm long flexible polydimethylsiloxane (PDMS) connectors. Continuous media perfusion was realized with a stepper pump (Harvard Apparatus 22, Holliston, MA, USA) and a perfusion rate of 0.1 mL/h (1.67  $\mu$ L/min).

Cells were seeded into the  $\mu$ CCC through blunt end 18 gauge needles (1.2 mm) (Becton Dickinson) unless otherwise mentioned. Cells were seeded in a density of 10 to 100 cells visible in the view field of the camera (Nikon Cybershot E990) viewed through the 10 x magnification objective of the microscope (Nikon model Alphashot 2 YS2, Nikon Corporation, Tokyo, Japan) by manually adjusting seeding volume. Cells were cultured in the  $\mu$ CCC either on a microscope stage of a standard phase contrast microscope or on the laboratory desk. Light to the microscope was provided by a 6 V 30 W G4 halogen projection bulb (Phillips, Germany). Cell culture images were digitally recorded using a Nikon Coolpix 990 camera attached to the microscope via a Nikon Coolpix MDC lens and equipped with a Nikon MC-EU1 remote control unit operating in time-lapse mode, typically with five-minute period. Images were converted to grayscale tiff images using the program IrfanView (version 3.97). Time stamps were created using the program Scion Image (version Beta 4.0.2) and a home written macro. Time lapse videos were generated using the program AxioVision (version 3.1.2.1). Cell counting for growth kinetics estimation was performed manually at selected time intervals with the program ImageJ (version 1.33u).

Cells cultured in the  $\mu$ CCC were extracted by replacing the syringe holding media with a syringe containing Phosphate Buffered Saline (PBS) (Sigma) and replace the media in the culture chamber by manual gentle perfusion with 2 mL of the PBS buffer. The cells were released by trypsinization by replacing the PBS with trypsin in a similar fashion. When the trypsin solution had completely replaced the PBS, the  $\mu$ CCC was incubated for 5 minutes after which the cells were released by a gentle knock on the  $\mu$ CCC. Isolation of the cells was performed by blocking the perfusion outlet with a solid stainless steel plug and manually controlled gentle perfusion of cell culture media into the  $\mu$ CCC, forcing media and cells to exit through the cell seeding inlet into 1.5 mL Eppendorf tubes (Eppendorf, Hamburg, Germany). Cells were concentrated by centrifugation ( $300 \times g$  for 5 min) in a centrifuge (5804R, Eppendorf).

## ***Stem cell culturing***

### **Conventional culturing in the CO<sub>2</sub> incubator**

Stem cells were cultured in DMEM/F12 (1:1, Gibco BRL, Invitrogen Life Technologies) added penicillin/streptomycin (Sigma), HEPES (Sigma), N<sub>2</sub> supplement, Albumax (Invitrogen) and Glutamax (Invitrogen). For proliferation, cells were cultured in the presence of recombinant human (rh) epidermal growth factor (EGF) (20 ng/mL; R&D Systems, Minneapolis, MN, USA) and rh fibroblast growth factor 2 (FGF2) (20 ng/mL; R&D Systems). No serum was added to the medium. The cells were kept at 37 °C in an atmosphere of 5 % CO<sub>2</sub> in T-25 culturing flasks coated with 5  $\mu$ g/mL poly-L-lysine (PLL), on which the cells were growing as a single attached layer. The cells were passaged by trypsinization (Sigma) every two to four days to a density of about 600,000 cells per T-25 flask.

### **Culturing in the $\mu$ CCC**

The sterilized  $\mu$ CCC was seeded by injecting a suspension of cells of 100,000 – 200,000 cells/mL. Seeding density was performed by manually adjusting the injection volume of the cell suspension according to visual inspection of the cell density in the chamber. To increase the cell density in the chamber, cells were allowed to settle on the bottom of the  $\mu$ CCC before injecting additional cell suspension. The medium was similar to the culturing medium described above.

**Surface coatings of  $\mu$ CCC for stem cell culturing**

Polyethyleneimine (PEI) coating:

A sterilized  $\mu$ CCC was filled with PEI (10  $\mu$ g/ $\mu$ L) and incubated for 30 minutes at room temperature and gently flushed with PBS buffer. Prior to seeding cells the  $\mu$ CCC was filled with culturing media and allowed to achieve a steady culturing temperature of 37 °C. Seeding was performed by manually injection of the cell suspension until the desired culturing density was achieved. The seeding density was evaluated by visual inspection of the  $\mu$ CCC.

Poly-L-Lysine (PLL) coating:

The sterilized  $\mu$ CCC was filled with PLL (20  $\mu$ g/mL) and incubated for 2 hours at 37 °C prior to 30 minutes of UV-light exposure. The  $\mu$ CCC was subsequently gently flushed with 10 mL of PBS buffer. Seeding of cells was performed similar to PEI coated chambers.

***RNA isolation and amplification***

Total RNA was isolated by RNeasy total RNA isolation kit (Qiagen, Valencia, CA, USA) according to the manufacturer's instructions. Quantification of total RNA was performed in an Ultraspec 3000 spectrophotometer (Pharmacia Biotech, Cambridge, England) using 1  $\mu$ L RNA and 59  $\mu$ L elution buffer (Qiagen) using a 60  $\mu$ L micro-cuvette (Hellma, Müllheim, Germany). Validation of RNA quality was performed on an Agilent 2100 Bioanalyzer using the RNA 6000 nano kit (Agilent Technologies, Palo Alto, CA, USA). Only total RNA with a RNA Integrity Number (RIN) greater than 9.7, assessed by the bioanalyzer was used for amplification reactions. Amplification was performed with the Riboamp T7-based RNA amplification kit (Arcturus Engineering, Mountain View, CA, USA) according to the manufacturer's instructions using 2  $\mu$ g total RNA as starting material and yielding 35-40  $\mu$ g aRNA after one round of amplification which was considered sufficient. The quality of the resulting aRNA was assessed on the Agilent 2100 bioanalyzer using the RNA 6000 nano kit (Agilent). mRNA was isolated from 100  $\mu$ g total RNA using oligo-d(T)25 Dynabeads (Dyna, Oslo, Norway) and following the manufacturer's directions yielded 2-3  $\mu$ g poly(A)<sup>+</sup>-enriched RNA (mRNA) in 20  $\mu$ l 10 mM Tris-HCl, pH 7.5.

### ***cDNA synthesis***

cDNA was synthesized as described elsewhere <sup>96</sup>, with modifications. In brief: each reaction was unless otherwise mentioned primed with 3.35 nmoles of random primers (Sigma-Genosys, Haverhill, UK or Invitrogen, Paisley, UK) corresponding to 6 µg random hexamers in 18.5 µL reactions containing 2-3 µg aRNA by heating at 70 °C for 10 minutes, snap cooling on ice for at least one minute. Reverse transcription reaction mixture lacking enzyme was added to final concentration of 500 µM of each of dATP, dCTP, and dGTP, 300 µM dTTP (Larova Biochemie GMBH, Teltow, Germany), 200 µM 5-aminoallyl-dUTP (Sigma), 40 U RNasin (Promega, Mannheim, Germany), 1x first-strand buffer (Life Technologies), 10 mM dithiothreitol (DTT) (Life Technologies) in final volume of 30 µL. The mixture was incubated for 3-5 minutes at room temperature to let the primers anneal. 400 U (2 µL) of Superscript II (Life Technologies) was added and the mixture was incubated for at 42 °C for 5 hours. Reactions were quenched by addition of 10 µL of 0.5 M EDTA (Sigma) and RNA hydrolyzed by the addition of 10 µL of 1 M NaOH followed by heating at 65 °C for 15 min. Reactions were neutralization by addition of 10 µL 1 M HCl, and cDNA was purified on QIAquick columns (Qiagen, Valencia, CA, USA) according to the manufacturer's instructions but substituting phosphate wash buffer (5 mM potassium phosphate pH 8.0, 80% ethanol) for buffer PE, and phosphate elution buffer (4 mM potassium phosphate pH 8.5) for buffer EB.

cDNA was lyophilized to dryness and resuspended in 4.5 µL of 0.1 M sodium carbonate buffer, pH 9.0. NHS ester (4.5 µL) of Cy-3 or Cy-5 dye (Amersham Biosciences, Piscataway, NJ, USA) in DMSO (dye from one tube was dissolved in 73 µl of DMSO) were added and reactions were incubated at room temperature in the dark for 1 h. Coupling reactions were quenched by the addition of 35 µL of 0.1 M sodium acetate pH 5.2, and unincorporated dye was removed using QIAquick columns according to the manufacturer's instructions. Labeling efficiency was determined by analyzing the whole undiluted sample in a spectrophotometer using a 50 µL micro-cuvette (Hellma).

### ***DNA Microarrays***

Slides pre-spotted with 44,290 60 nt. long oligos directed against the human transcriptome were obtained (Agilent). Labeled cDNA were co-hybridized to the DNA microarrays according to supplier's instructions. In brief; 200 pmol of each of the differently Cy labeled cDNA were combined in 200 µL milliQ water were denatured at 98 °C for 3 minutes

followed by incubation at room temperature for 2-3 minutes and addition of 50  $\mu$ L 10 x control (Agilent) and 250  $\mu$ L 2 x hybridization buffer (Agilent). 490  $\mu$ L was applied to a gasket slide (Agilent) in a hybridization chamber (Agilent). The slide containing the microarray was placed on top and the hybridization chamber was closed and mounted on a rotation device and placed in a Hybaid Shake 'n' Stack hybridization oven (Thermo Electron Corporation, San Diego, CA, USA) for 17 hours at 60 °C with the lowest rotation setting (~ 4 rpm).

Following hybridization the gasket slide was removed while the slides were submerged in washing solution 1 (6 x Saline Sodium Citrate buffer (SSC) (AppliChem, Darmstadt, Germany), 0.005 % Triton-X-102 (Agilent)) and the slides were washed for 10 minutes at room temperature (RT) in washing solution 1 followed by 5 minutes in wash solution 2 (0.1 x SSC (AppliChem), 0.005 % Triton-X-102 (Agilent)) at 4 °C in an in-house fabricated microarray washing station. The slides were dried by centrifugation.

In house fabricated arrays were fabricated on silylated slides (CSS-100, Telechem, Sunnyvale, CA, USA). Slides were printed with a Qarray micro spotting robot (Genetix, Hampshire, UK) holding standard stainless steel micro spotting pin (CMP3-B, Telechem). For all in-house printing a 300 mM phosphate buffer, pH 9.6 was utilized as a 2 times spotting buffer unless otherwise mentioned.

Following spotting silylated slides were blocked using 10 washing in 0.2 % sodium dodecyl sulphate (SDS) (Sigma), 10 minutes in milliQ water, 5 minutes in NaBH<sub>4</sub> freshly prepared by dissolving 1 tablet (1 g) NaBH<sub>4</sub> (Sigma) in 300 mL phosphate buffers saline (PBS), pH 7.4 (Sigma) when dissolved, 100 mL absolute ethanol (Honeywell, Seelze, Germany) was added. Finally the slides were washed in 0.2 % SDS for 3 minutes and cleaned with milliQ water and dried by centrifugation.

A solution of 5 x SSC (Promega, Madison, WI, USA) and 0.5 % SDS was used as hybridization buffer for hybridizations on silylated slides. Following hybridization, the slides were washed in 0.5 % SDS and 0.1 x SSC for 10 minutes and in 0.1 x SSC for 5 minutes and dried by centrifugation

The DNA microarrays were scanned in an ArrayWoRx microarray scanner (Applied Precision, Issaquah, WA, USA) and the accompanying software was used for quantification.

### ***Data analysis***

The data was normalized using the non-linear method Qspline<sup>111</sup> included in the affy package (version 1.6.7)<sup>112</sup> in Bioconductor (version 1.6)<sup>113</sup> run under the statistical freeware program R (version 2.1.1)<sup>114</sup> and further processed in Excel unless otherwise mentioned.

## 4 Results

The aim of the project was the realization of a micro cell culture chamber ( $\mu$ CCC) capable of supporting culturing of mammalian cells over extended periods of time under culturing conditions similar to the reference cell culture flask. The  $\mu$ CCC was to support continuous on-line observation of the cells during culturing and should not rely on external heating sources. Furthermore the  $\mu$ CCC was to be large enough to accommodate enough cells for *e.g.* genetic analysis of the cultured cells.

### *Design*

#### **Materials**

To enable continuous on-line monitoring of cells during culturing the material comprising the device was to be transparent. Conventional glass has previously been used as culturing surface for cell culturing devices. However, fabrication of glass devices is laborious and glass is a fragile material. Many polymeric materials are less fragile and transparent and may more easily be shaped in to 3-dimensional structures. As the number of different polymeric materials available is approaching the infinite, testing of a representative selection of the polymeric materials was not possible. Two strategies for the construction of three dimensional structures seemed likely to result in a functional device. Using epoxy based negative resist SU-8 three dimensional structures can be created with the high resolution attainable with photolithographic techniques. This structure can then serve as a negative mold for PDMS<sup>15</sup>. This makes it relatively simple to make several replicas of the same structure. PDMS is notorious to strongly adsorb molecules to the surface as well as being extremely hydrophobic making PDMS structures hard to fill with aqueous solutions<sup>115</sup> as well as it is highly gas permeable<sup>116-118</sup>. Furthermore, photolithography is highly labor intensive and expensive. Laser ablation of PMMA<sup>110</sup> sacrifices the high resolution attainable with photolithography and substitutes it with ease of manufacture and less labor intensive and was hence chosen as the polymer for realization of the  $\mu$ CCC. The size of the actual culturing surface was set to 1 cm<sup>2</sup>. This would support the culturing of more than 100,000 cells which was considered sufficient for most genetic analysis purposes. Furthermore the dimensions of the accompanying microfluidics channels would be attainable using laser ablation of PMMA.

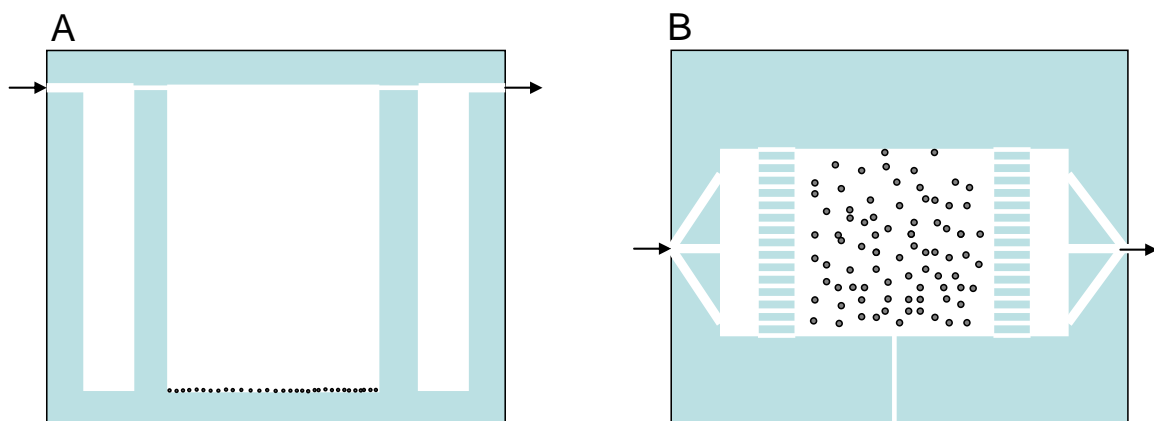


## Device design and layout

To simplify the design the need for CO<sub>2</sub> as a pH stabilizing agent was sought eliminated. Utilization of continuous perfusion would provide a constant removal of waste products as well as providing fresh pH balanced media, provided the media reservoir is impermeable to O<sub>2</sub> and CO<sub>2</sub>. However, introducing continuous perfusion posed considerations regarding flow rate and temperature regulation.

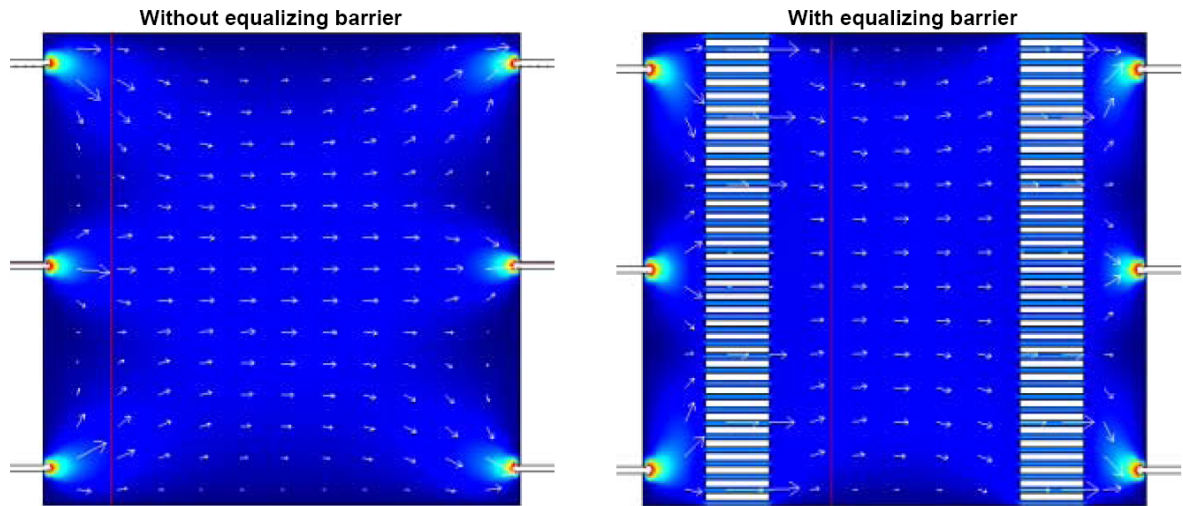
In order to minimize shear stress on the cells the PMMA layer of the chip comprising the cell culture chamber was made of 1.5 mm thick PMMA. This resulted in the distance from the media inlet to the cells was more than 1 mm after thermal bonding, corresponding to more than 100 times the height of a cell (Figure 5 A).

Equalization of the flow was performed with flow equalizing barriers. The inlet flow was divided in three and led to pre-heating part of the chamber from where the media was distributed between at least 22 Gaussian shaped channels each roughly 250 μm wide and 300 μm deep into the actual culturing chamber (Figure 5 B and Figure 11). The preheating part of the chamber also functioned as a bubble trap collecting bubbles formed from storing media in the syringe. Cell washout was reduced by the flow equalization barriers, but could not be eliminated due to the resolution limitations of the laser ablation system.



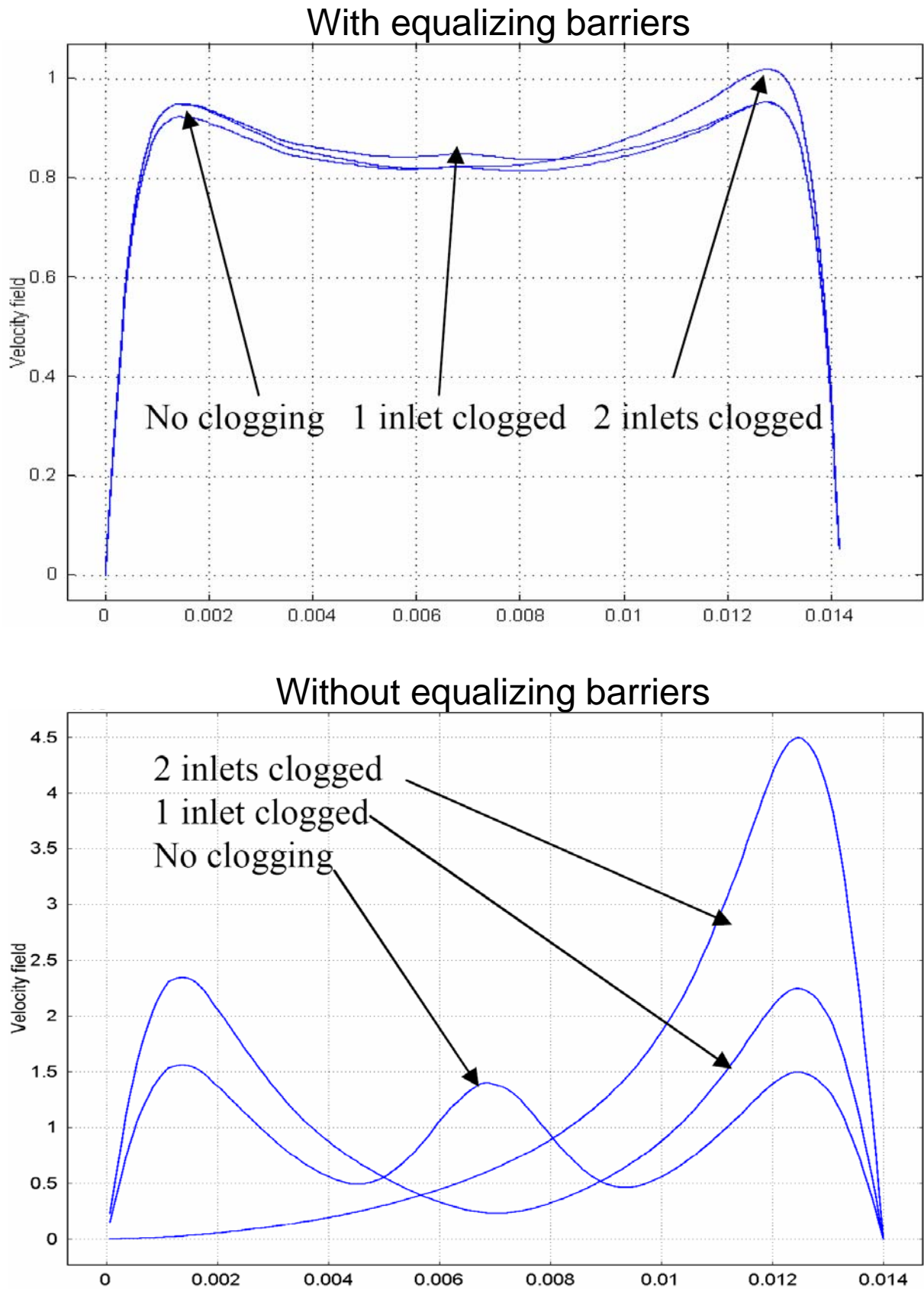
**Figure 5: Layout of the μCCC.** Cells are for simplicity depicted as spheres. (A) View from the side. The distance from the culturing surface to the inlet is between 1.2 and 1.3 mm. Assuming the cells has a height of 10 μm results in media is perfused into the chamber more than 100 cell heights above the cells. The scale between cell diameter and height of the chamber is roughly 1 to 100. Other chamber dimensions are not drawn to scale. (B) View from above. The size of the cells and the equalization barriers relative to chamber dimensions is not drawn to scale.

In order to simulate the liquid flow profile of media in the  $\mu$ CCC this was simulated using the program FEMLAB. Simulations were performed of a  $\mu$ CCC with and without the flow equalizing barriers (Figure 6).



**Figure 6: Simulations of the liquid flow in the  $\mu$ CCC.** The length of the white arrows represents the velocity of the liquid at the particular location in the chamber. The left-hand image shows the flow distribution of the perfusion media entering the chamber via the three inlet apertures. The right-hand image shows the flow distribution of the media entering the chamber via the multiple apertures of the equalization barriers. Flow velocity profiles were generated two millimeters away from the culture chamber wall indicated by vertical dark red lines (Figure 7).

The 2-dimensional simulations (Figure 6) demonstrated the significance of the flow equalizing barriers. Without the equalizing barriers a less uniform flow was obtained and larger variations in the local media velocities were observed. Plots of flow velocity profiles were generated to simulate the significance of the flow equalizing barriers upon clogging of one or two of the inlet channels *i.e.* by an air bubble (Figure 7).



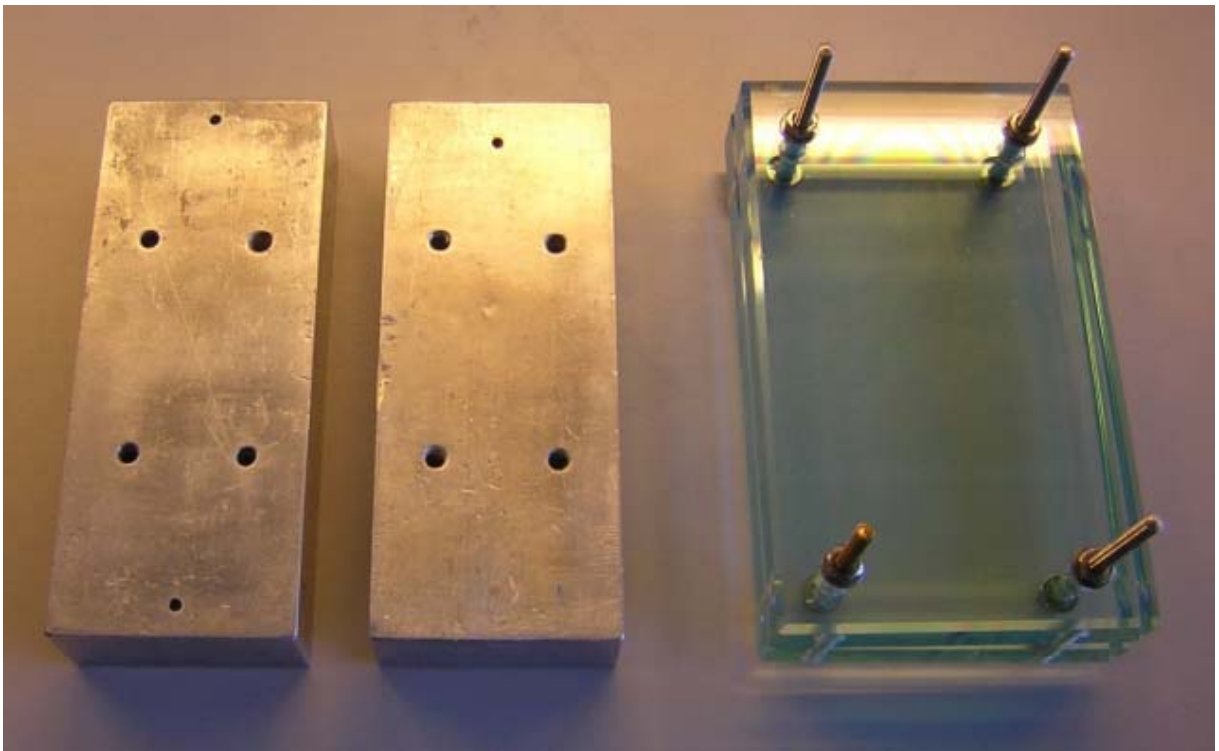
**Figure 7: Liquid velocity profiles.** Plots of velocity profiles generated two millimeters away from the cell chamber wall (marked by the vertical dark red lines on Figure 6)

The flow velocity plots (Figure 7) clearly demonstrated the significance of the flow equalizing barriers to compensate if one or two of the inlet channels were clogged *i.e.* by an air bubble.

## ***Fabrication***

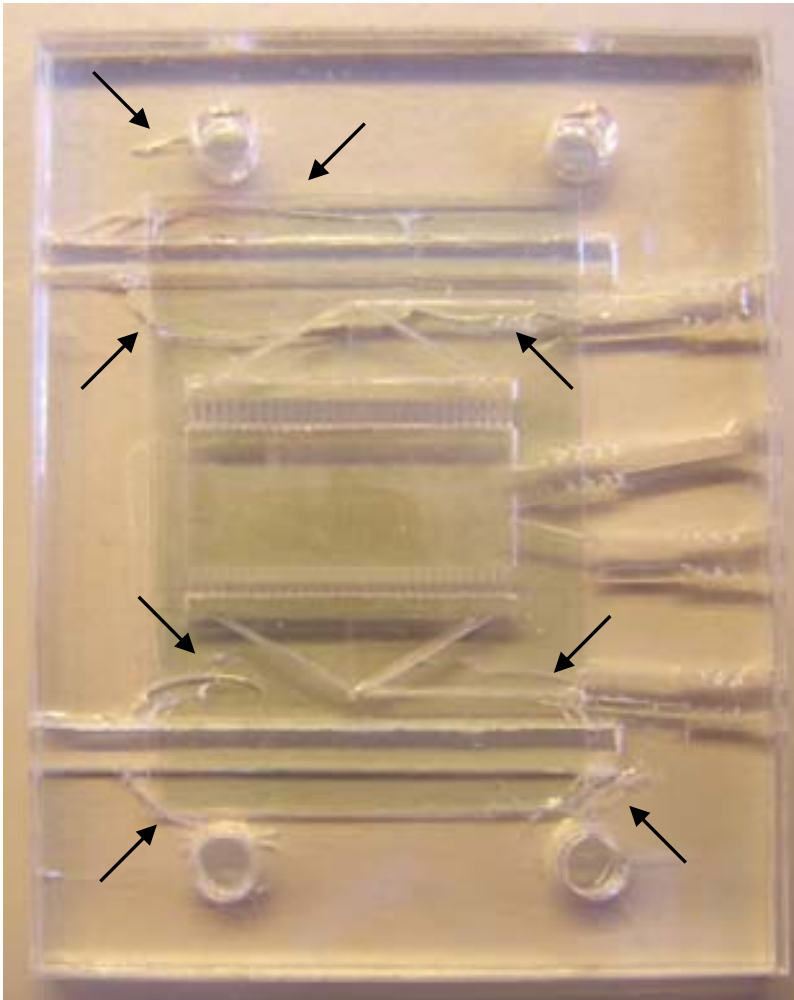
### **Assembly of the $\mu$ CCC**

A tight seal between the different layers was required in order to prevent air to enter the  $\mu$ CCC during culturing resulting in bubbles formation as well as to prevent cell culture media from leaking out. PMMA can either be bonded chemically <sup>119</sup> using either acetone or dichloromethane or using pressure at a temperature close to the glass transition temperature ( $T_g$ ) <sup>110</sup>. Chemical bonding proved difficult as aligning of the individual parts was difficult as well as the channels rapidly melted when exposed to especially dichloromethane resulting in blocking of channels. Aligning of the individual parts was easier using thermal bonding. However, when metal bonding blocks were used for application of uniform pressure, the surface roughness of the metal was transferred to the polymer substrate resulting in decreased optical properties. This was eliminated when the metal bonding blocks were replaced by a set of custom made glass bonding block (Figure 8).



**Figure 8: Metal and glass bonding blocks.** The metal bonding blocks were made custom made of aluminum and pressure was applied using a clamp.

During bonding it was observed that cracks in the PMMA could occur (Figure 9). These cracks were most likely the result of stress built up in the polymer during laser ablation. The amount of stress was significantly reduced when the individual PMMA layers were annealed prior to assembly into the finished device.



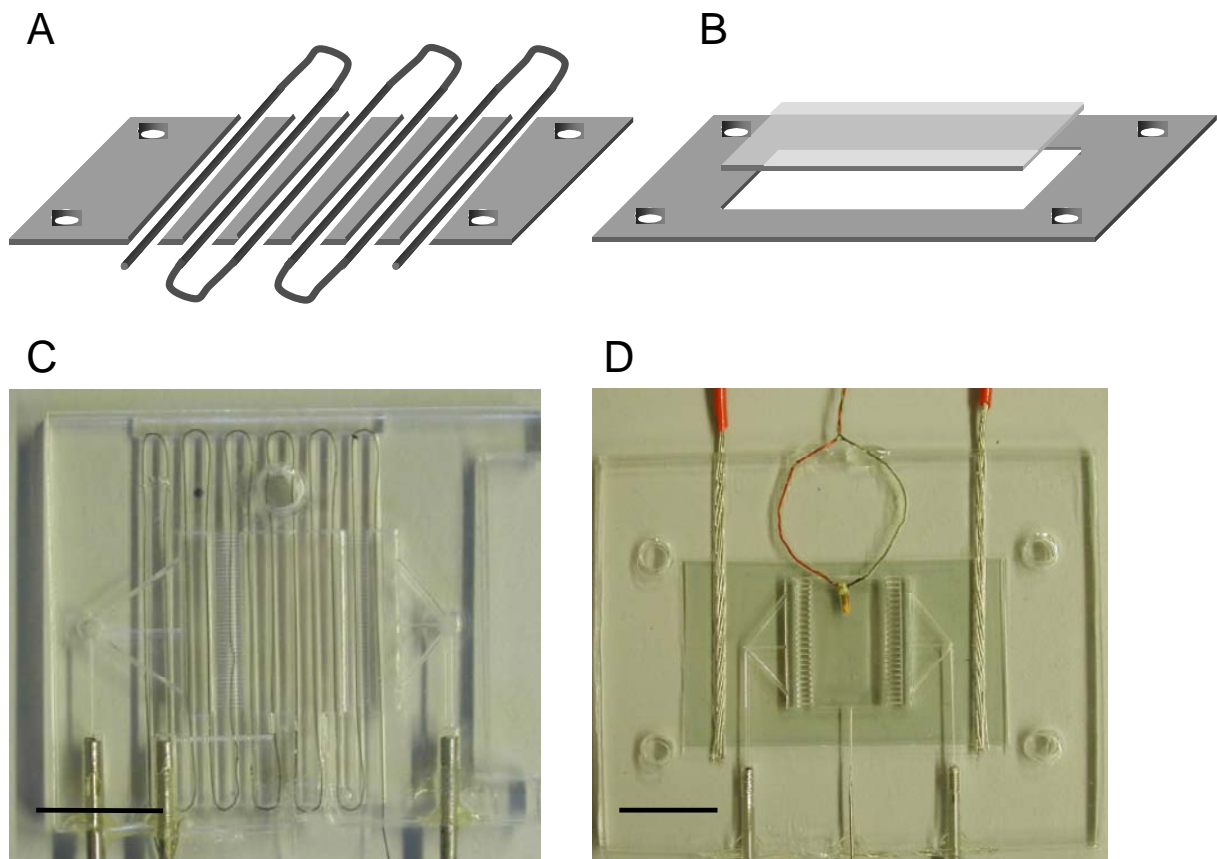
**Figure 9: Cracks resulting from stress in the PMMA.** The black arrows indicate the location of some of the cracks resulting from stress. The individual parts were aligned without prior annealing (30 minutes at 80 °C) and bonded using 100 Ncm of force between the glass bonding blocks.

## Heating

Initially heating was obtained by using a thin metal wire placed in a zigzag fashion over the culture chip during chip assembly and bonded to the culture chip by thermal bonding. The wire was connected to an adjustable resistor. An example of the initial culture chip with wire heating is given in Figure 10 A and C. The temperature was measured using a thermistor embedded inside the culture chamber and the resistance was manually adjusted until the desired culturing temperature was achieved. The wire heating was used for successful

culturing of HeLa cells for more than 50 hours (data not shown). During culturing experiments, constant minor adjustment needed be performed in order to compensate for variations in ambient temperature due to the day and night cycles. Another disadvantage of this type of heating was the lack of transparency of the chip throughout the culturing area. This resulted in the need for aligning the culture chip below the field of view under the microscope in such a way so shadowing of the heating wires was minimized. Most importantly was that heating was not distributed evenly throughout the culturing area. Furthermore aligning the wire evenly in the chip was cumbersome and laborious.

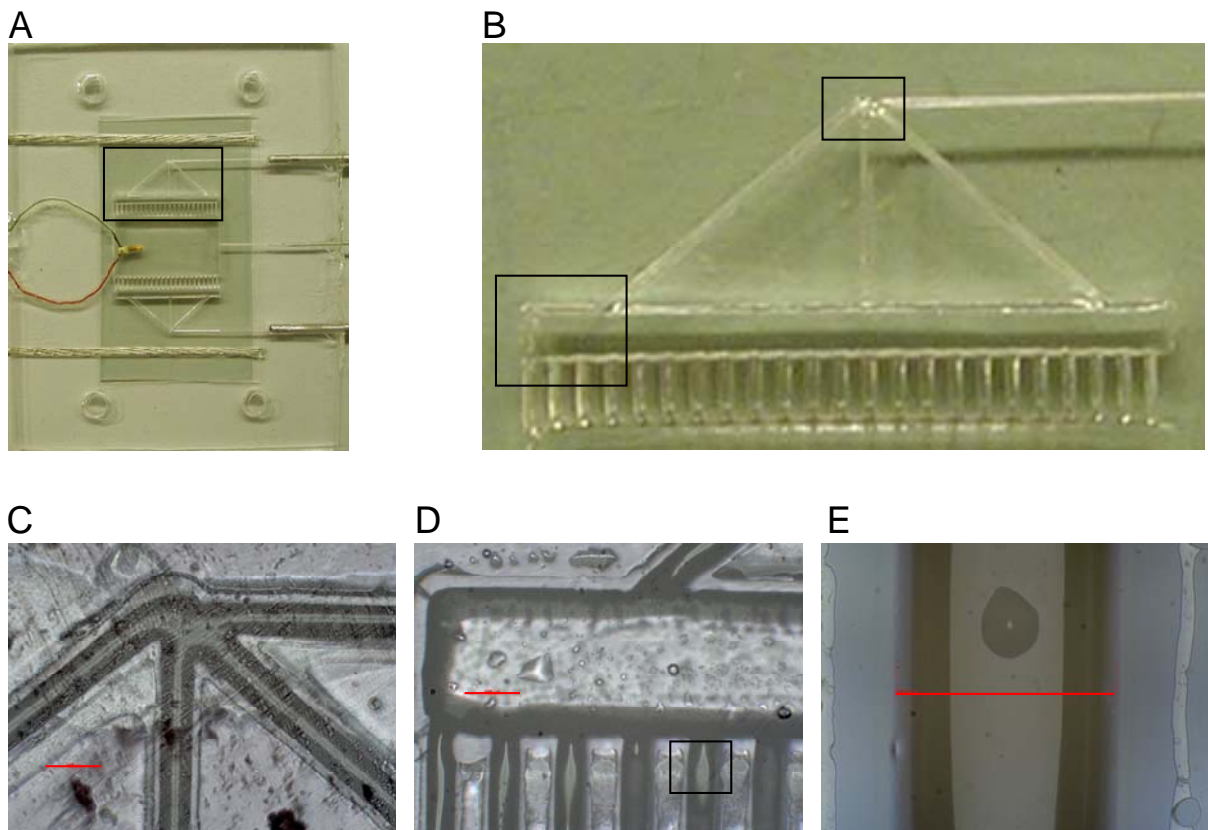
Replacing the wire based heating with a 0.2 mm thick optically transparent polyethylene terephthalate (PET) coated with a thin layer of conductive indium tin oxide (ITO) resulted in a more uniform heating of the culture area with better optical properties and easier manufacturing (Figure 10 B and D).



**Figure 10: Wire heating and thin film resistive element heating.** (A) Schematic view of the layout of the resistive wire heating. The wire was manually “sewed” into the structure. (B) Schematic view of ITO heater. The resistive ITO coated film was cut to size and placed in a 0.25 mm thick PMMA sheet laser ablated to contain free space for the ITO film and alignment holes. (C) An initial culture chamber with wire heating. (D) A culture chamber with ITO heating. Scale bar in the lower left corner of (C) and (D) represents 10 mm.

## Characterization of the $\mu$ CCC

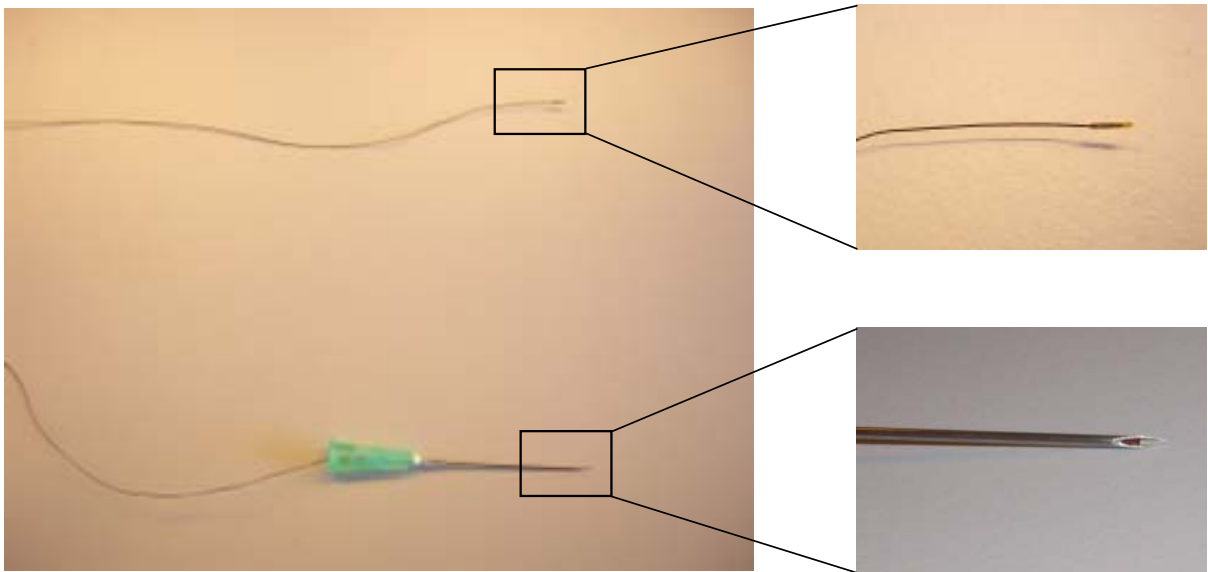
The  $\mu$ CCC was characterized with respect to the dimensions of the channels. The final dimensions were highly dependent upon the laser settings with respect to the resolution used, the speed at which the laser beam was moved, the power of the beam and how many times the beam passed the individual features of the device. Using the settings mentioned in the materials and methods section, the microchannels had a Gaussian cross-section<sup>110</sup> and were measured to be 250  $\mu$ m wide and 350  $\mu$ m deep (Figure 11 C). The flow equalizing barriers were comprised of 22 microchannels, each 250  $\mu$ m wide and 350  $\mu$ m deep separated with 0.6 mm pitch (Figure 11 B, D-E).



**Figure 11: Physical dimensions of the features of the  $\mu$ CCC.** (A) Full size view of the  $\mu$ CCC. The actual culturing area is 7.6x13.0 mm. The black rectangle is magnified in (B) where the inlet channel dividing the media flow in three is indicated with the small rectangle located at the top center and further magnified in (C). The red scale bar represent 500  $\mu$ m. In (B) the flow equalizing barriers as well as the bubble trap are more clearly seen and one section of the flow equalizing barriers, indicated by the larger rectangle in the lower left corner is further magnified in (D). In (D) the red scale bar represent 500  $\mu$ m. A part of a single channel of the 22 channels comprising the flow equalizing barrier was further magnified in (E). The channel was measured to be 250  $\mu$ m wide, indicated by the red line.

## Recyclable thermistor

Looking at the cost price of the  $\mu$ CCC, the most expensive part was the thermistor. The thermistor was also the most vulnerable part in the  $\mu$ CCC as the salinity in the media was found to decompose the thin insulating polymer layer around the thermistor and introducing a short circuit resulting in loss of temperature control and the failure of a culturing experiment. As thermistors are available with very small dimensions, one thermistor small enough was fitted inside a 21 gauge needle (Figure 12).



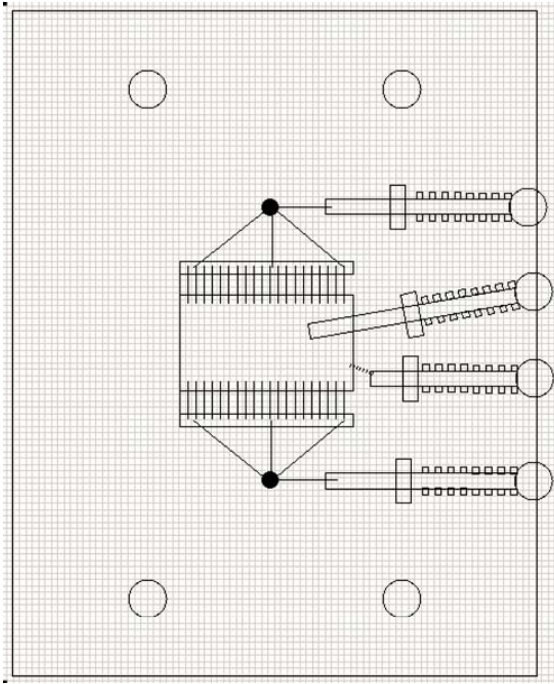
**Figure 12: Fitting the thermistor in a needle.** Using a small thermistor with a diameter of 0.46 mm (upper thermistor on big image and the upper small image) it was possible to fit the thermistor inside a 21 gauge needle diameter 0.8 mm (lower right). The thermistor was sealed inside the needle with epoxy glue.

As the diameter of the thermistor (0.46 mm) was significant less than the diameter of the needle (0.8 mm) the thermistor did not make an efficient seal in the needle. To prevent air from intruding the  $\mu$ CCC resulting in the flooding of bubbles and contamination of the cell culture, an air tight seal was required. This seal was accomplished with epoxy glue.

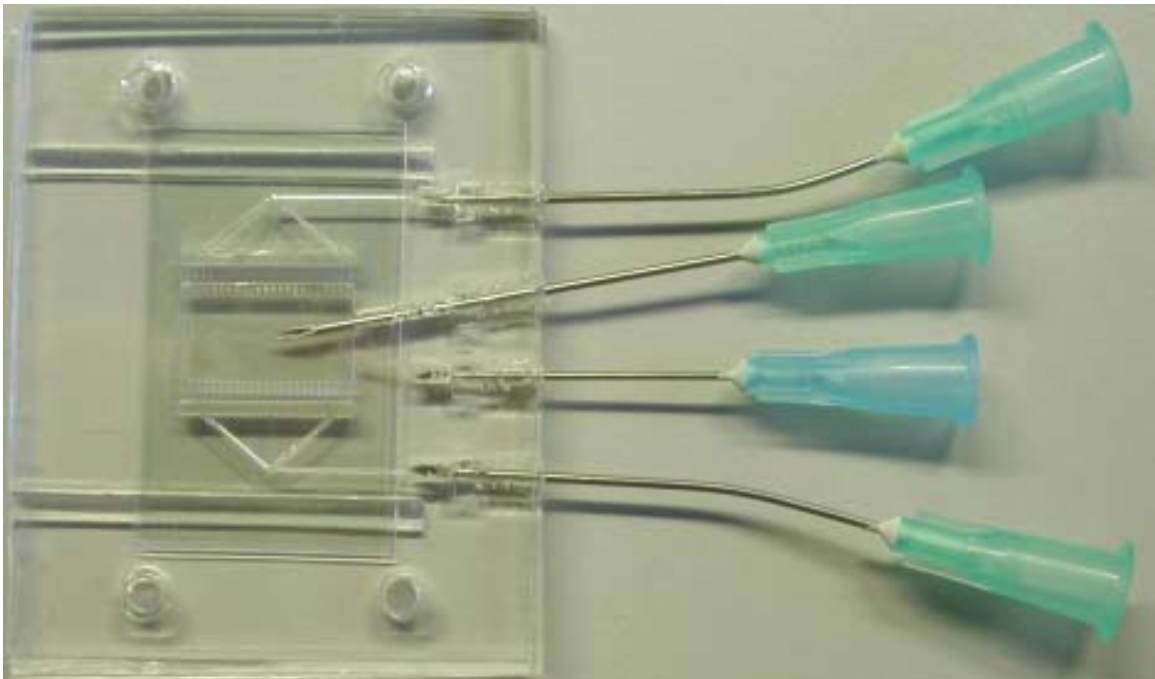
The  $\mu$ CCC was modified enabling the needle containing the thermistor to be inserted in to the  $\mu$ CCC and removed without damaging the thermistor after the culturing experiment (Figure 13). Crucial to this modification was the possibility of obtaining an airtight seal around the needle holding the thermistor. This seal was achieved by use of UV-curable glue. By timing the exposure time to UV-light an elastic rubber like consistency was achieved and the needle could be inserted through this layer without creating tiny cracks which would enable air to enter the  $\mu$ CCC causing it to fill with bubbles.



A



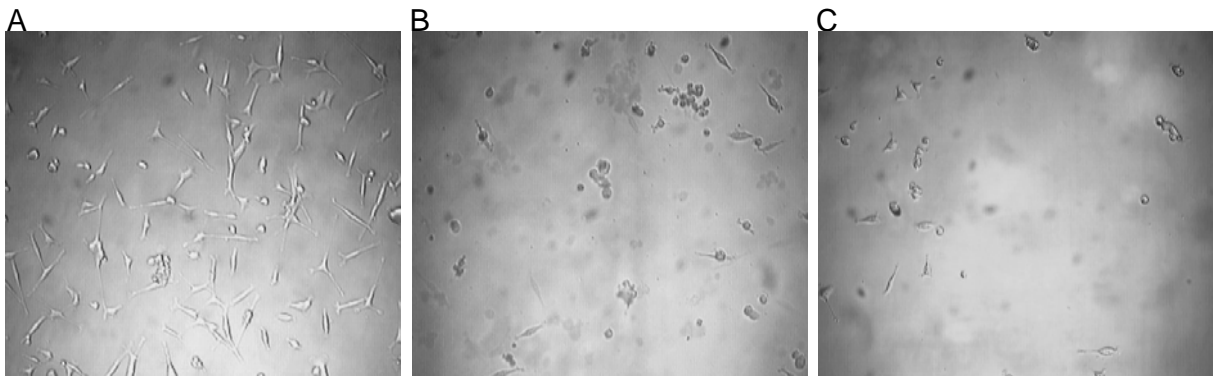
B



**Figure 13: Modifications of the  $\mu$ CCC enabled recycling of the thermistor.** (A) Screen dump from the laser ablation program displaying the layout of the modified  $\mu$ CCC. The channels were redesigned enabling sealing with UV curable glue. After filling the channels with UV-curable glue, each channel was exposed to UV-light for 10 seconds which was sufficient for curing. After sealing the  $\mu$ CCC was left over night for the evaporation of potentially toxic gasses. Media inlet and outlets were realized from 21 gauge needles while cell seeding was performed with a 23 gauge needle. (B) The actual chip containing needles for inlet, outlet, cell seeding and thermistor. The needles for media inlet and outlet were bended to avoid physical contact between the needles during handling which might introduce air bubbles.

Initial filling results indicated that by careful timing the curing time of the UV-curable glue it would remain flexible enough to inject cells and retrieve the needle from the cell loading syringe without having air leaking into the chamber.

Culturing in the modified  $\mu$ CCC resulted in cell death within 48 hours. This indicated that the UV-curable glue was toxic to the cells. Seeking to confirm this, a crude viability test of the UV curable glue was performed (Figure 14 A-B). Seeking to elucidate if the epoxy glue used for sealing of the needles used for attachment of the connection tubings and sealing of thermistor in the needle would result in cell death when used in direct contact with the cells, the same approach was used replacing the UV-curable glue with epoxy (Figure 14 A and C).



**Figure 14: Viability testing of the UV-curable glue and epoxy.** The UV-curable glue was added in drops spaced roughly three to four cm apart on the culturing surface of a culture grade Petri dish and cured with a UV light gun. The culture dish was wiped with a towel wetted with 70 % ethanol and placed in the LAF bench for one hour for the evaporation of potentially toxic gasses. After addition of cell culture media  $2.5 \cdot 10^5$  cells were added to the culture dish and to a control culture dish without UV-curable glue. The culture dishes were incubated in the  $\text{CO}_2$  incubator for 24 hours at  $37^\circ\text{C}$  and 5 %  $\text{CO}_2$  and inspected. (A) Control culture dish. (B) Culture dish with UV-curable glue. (C) Culture dish with epoxy glue. The dark shadows in (B-C) are dead cells floating in the media above the focal plane.

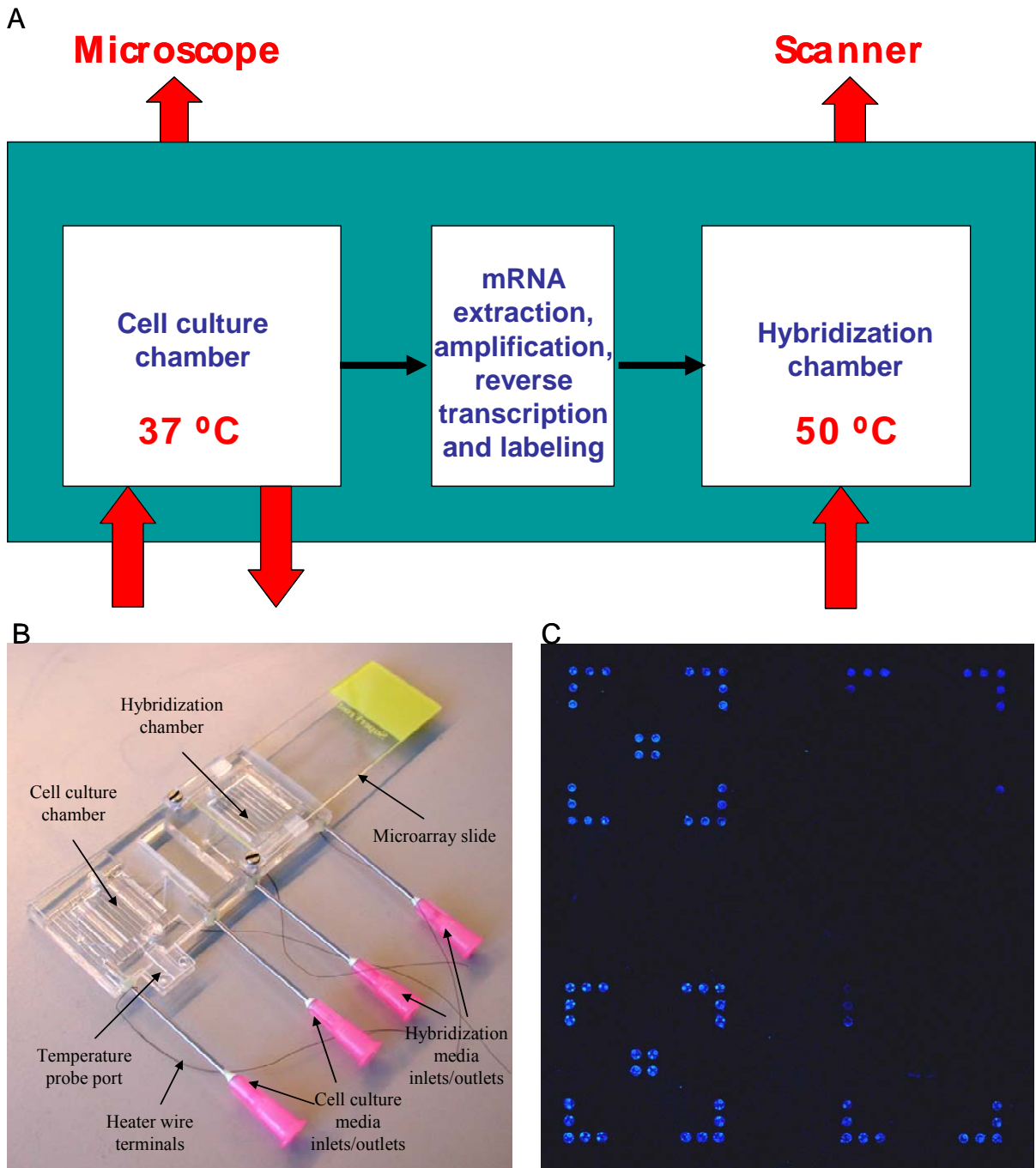
The results indicated that the both the UV-curable glue and the epoxy glue used to seal the thermistor in the needle and the inlets to the  $\mu$ CCC were inducing cell death. However, if the UV-curable glue could be replaced with a biocompatible UV-curable glue of similar physical properties, recycling of the thermistor seems very likely as this glue could also be used to seal the thermistor in the needle. The results also indicated that caution must be applied when sealing of the tubing is performed with epoxy as exposure to media might result in adverse effects on the cells.

### **Thin $\mu$ CCC**

Another idea to improve the temperature performance of the  $\mu$ CCC was to reduce the number of 1.5 mm thick PMMA layers comprising the  $\mu$ CCC and replace them with 0.25 mm PMMA. This would reduce the heat capacity of the chamber enabling a faster response time of the ITO heater to changes in ambient temperature. The  $\mu$ CCC was successfully fabricated replacing the 1.5 mm thick top and bottom layer (Figure 1 A and E) with 0.25 mm thick PMMA. The layer defining the actual culture chamber and the micro channels was not replaced with 0.25 mm thick PMMA to avoid shear stress as the distance from the media inlet to the culturing surface would be reduced significantly. The resulting  $\mu$ CCC proved too flexible causing the electrical connection to the ITO layer to fail resulting in inadequate and unstable heating. Hence, no further experiments were performed to decrease the thickness of the  $\mu$ CCC.

### **Multifunctional device**

A future goal envision a complete chip holding a cell culturing part, sample preparation part and an array part (Figure 15 A-B). The idea was for the chip to sustain culturing of mammalian cells, extract total RNA from the cultured cells, isolate and amplify the mRNA fraction, reverse transcribe the amplified RNA into cDNA, incorporate fluorescent label into the cDNA and finally hybridize the cDNA to a DNA microarray. Practical experience with the protocols indicated that the current standards of microfluidics were insufficient for realizing sample pretreatment on chip for gene expression studies. The effect of bubbles during hybridization was clearly visible (Figure 15 C) where an air-bubble partially covered two of four sub-arrays on a test array, hampering hybridization at this location. Realization of the multifunctional device seems not possible until microfluidics techniques are developed that can perform the rather complicated and laborious sample pretreatment for genetic analysis.

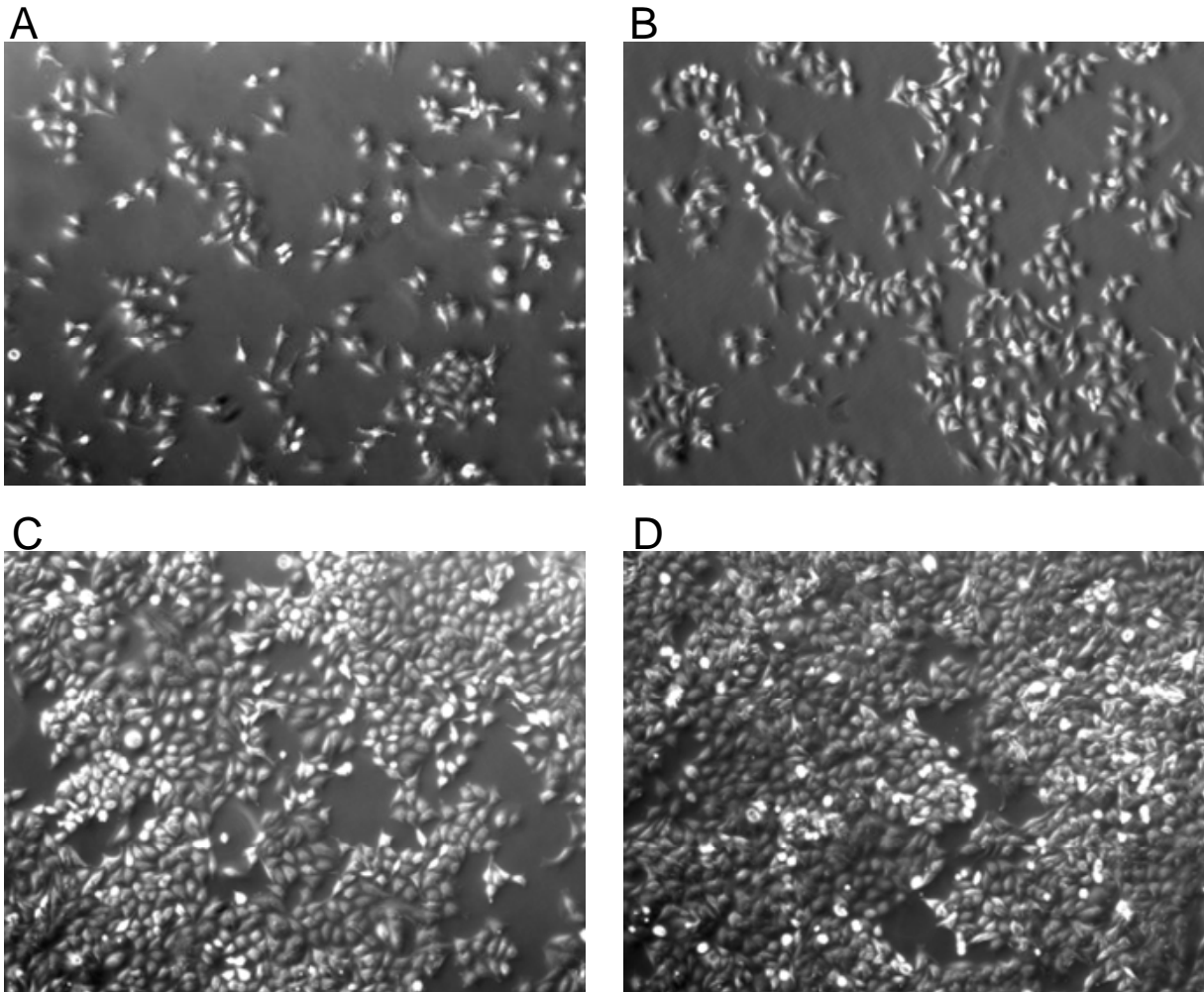


**Figure 15:** Initial layout of the complete chip. **(A)** An illustration of the complete chip layout. The size of the chip was set to match a standard laboratory glass slide at three by one inch. **(B)** Image of an actual chip. The wires were used as resistive heating elements enabling separate heating of either the cell culture part or the hybridization part. The hybridization part is connected to a conventional microscope slide. **(C)** One result of hybridization on chip with complementary 60 nt. long oligos. Hybridization was performed with 60 nt long 10 nM cy-3 labeled target oligo (5' Cy-3-GCGCGGAGGAGTTGTGTTTGTGGACGAAGTACCGAAAGGTCTTACCG-GAAAACCTCGACGC 3') directed against a complementary 60 nt. long probe (5' NH<sub>2</sub>- GCGTCGAGTTTTCCG-GTAAGAC-CTTTCGGTACTTCGTCCACAAACACAACCTCCTCCGCGC-3') spotted at 10  $\mu$ M concentration on a silylated slide. The slide contained four identical sub-arrays each containing 24 spots distributed with 5 in each corner and four spots in the center of each sub-array. Hybridization was allowed to take place for one hour at 50 °C. Following hybridization the array containing slide was removed, washed and scanned. The missing spots in the two sub-arrays to the right were the result of a stationary air-bubble which partially covered these two sub-arrays.

## *Operation*

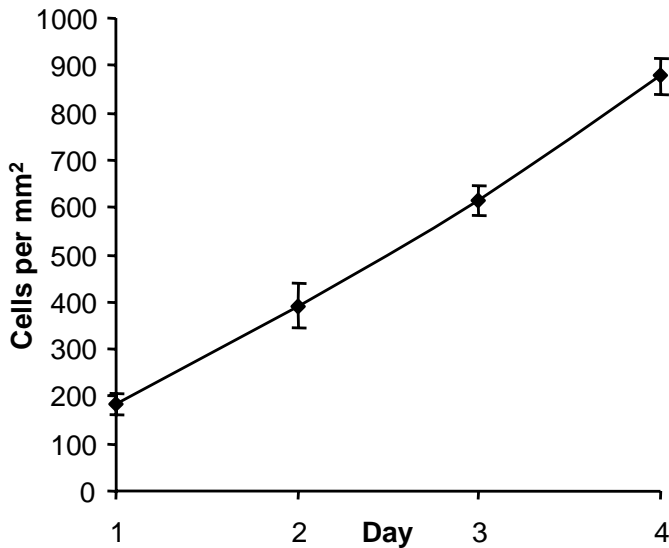
### **Cell culturing**

HeLa cells were studied in order to compare the growth kinetics in the  $\mu$ CCC with the growth kinetics in the culture flask. As alignment of the culture flask in order to take pictures of the exact same area proved too uncertain, several pictures of the same culture flask at various locations were obtained over several days (Figure 16).



**Figure 16: HeLa cells in culture flask over time.** HeLa cells were seeded in  $75 \text{ cm}^2$  culture flasks using  $5 \cdot 10^5$  cells per flask. The flasks were inspected daily and three to four representative pictures were obtained each day of each flask. **(A)** One day post seeding. **(B)** Two days post seeding. **(C)** three days post seeding. **(D)** Four days post seeding.

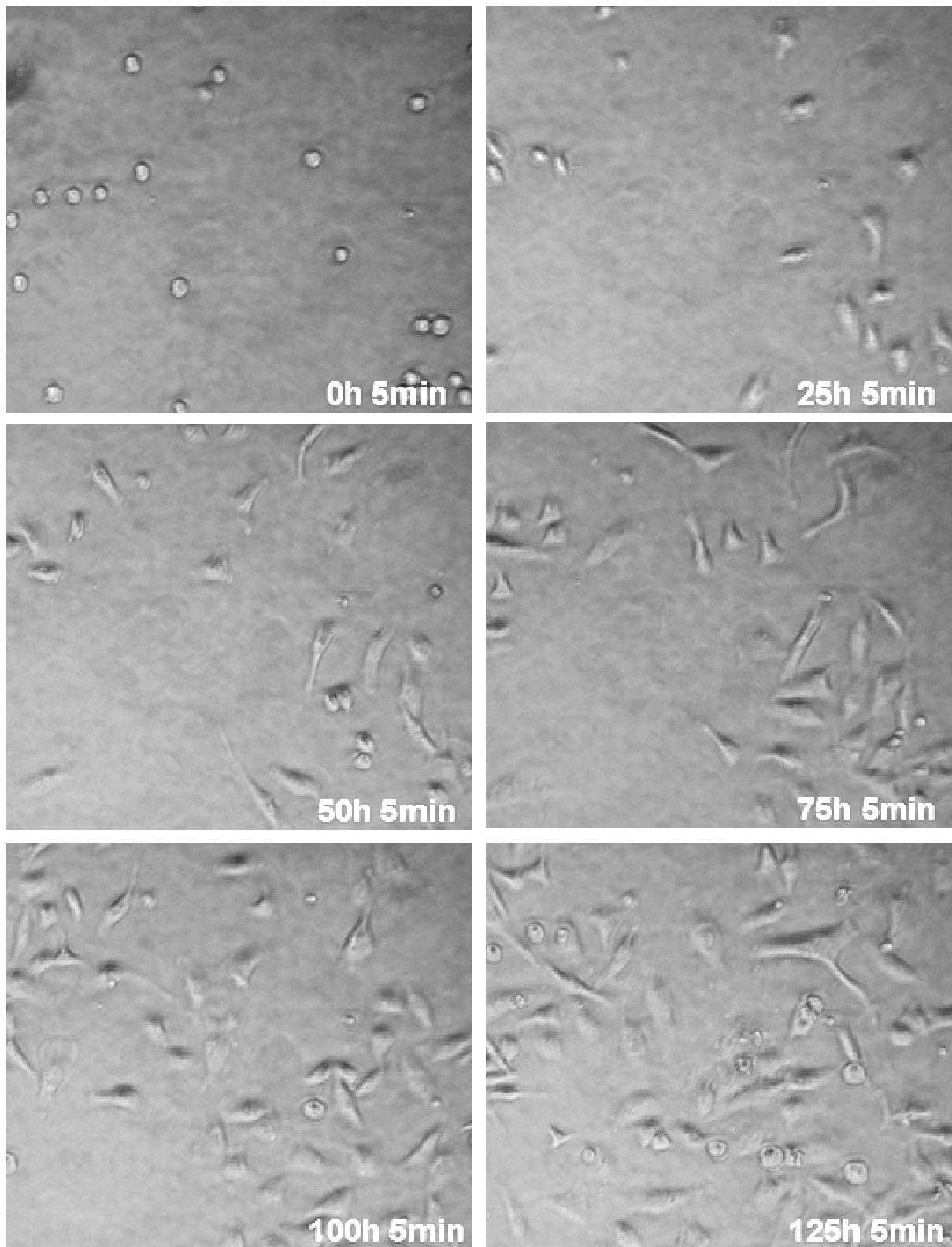
Using the pictures obtained during culturing the cell count on each picture was manually computed. The different cell counts were averaged and plotted (Figure 17). Using the average cell counts, the results indicated that the HeLa cells in culture flask inside the  $\text{CO}_2$  incubator had a doubling time of 32 hours.



**Figure 17: Growth rate of HeLa cells in the culture flask.** Two flasks seeded simultaneous with equal amount of HeLa cells (Figure 16) were inspected daily and three to four representative pictures were obtained from each flask each day (27 pictures in total). The number of cells on each picture was manually computed and the cell density was computed using the relation that one pixel on the image correspond to 1  $\mu\text{m}$  and the size of the picture is 1340 by 1025 pixels. The error bars represent the standard error of the mean (SEM).

### Growth kinetics of HeLa cells in the $\mu\text{CCC}$

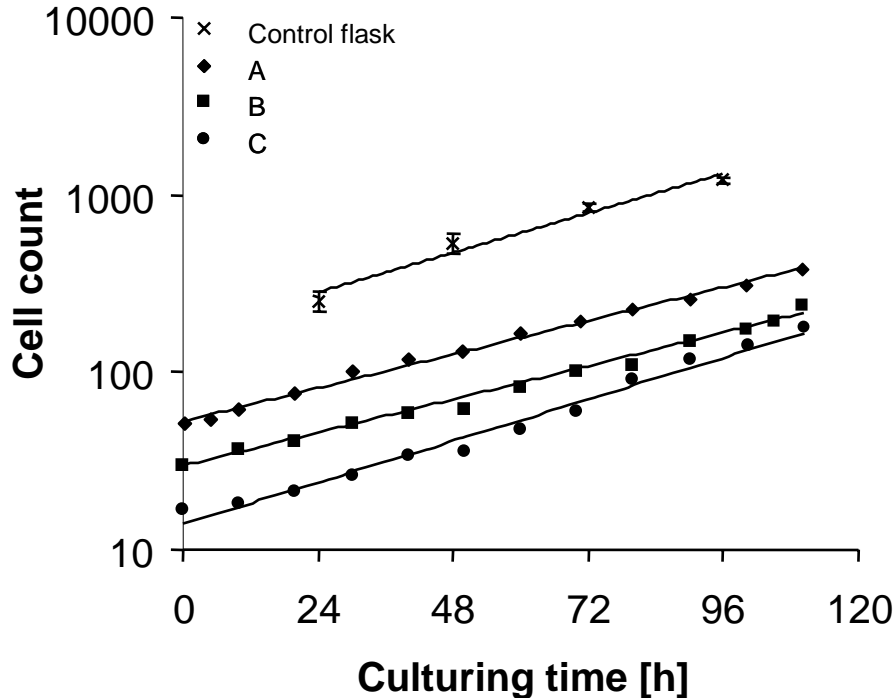
Following sterilization and calibration of a  $\mu\text{CCC}$ , freshly passaged HeLa cells were seeded adjusting the seeding volume to 20 cells visible in the camera using 10 x magnification on the microscope. After 140 hours of culturing the  $\mu\text{CCC}$  was confluent (Figure 18) and the cells were collected for later genetic analysis.



**Figure 18: Growth rate of HeLa cells in the  $\mu$ CCC.** Following seeding of cells, pictures were obtained with 15 minutes increment over 140 hours of culturing. The time stamp in the lower right corner indicates the elapsed culture time. A movie of the entire culturing is available on the accompanying data disc (Movie 1).

## Growth kinetics in the $\mu$ CCC

One method commonly used to assess differences in culture conditions is the proliferation rate of comparable cells.



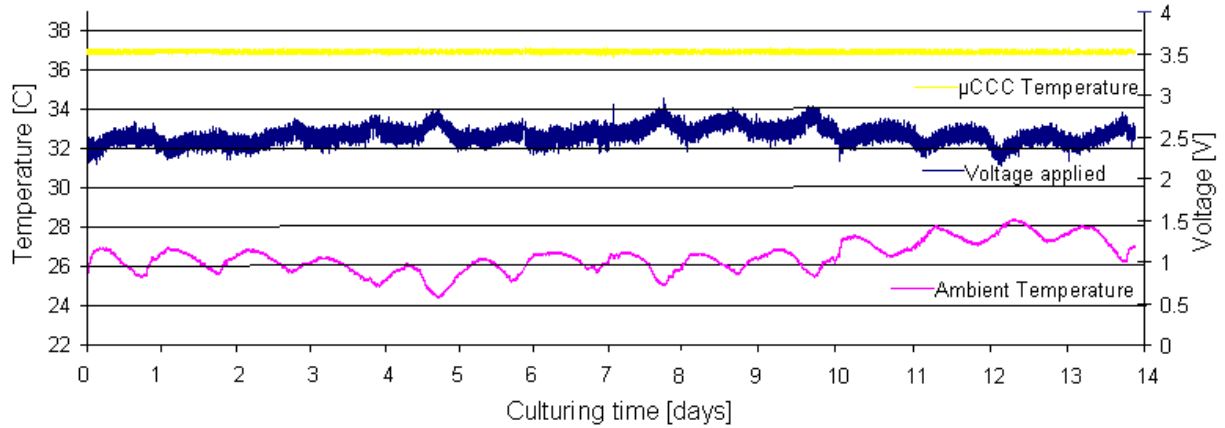
**Figure 19: Comparison of the proliferation rate of HeLa cells in the  $\mu$ CCC.** Cell counts were manually counted at selected time points for three culture experiments in the  $\mu$ CCC (A-C). Exponential regression lines were fitted through these time points. The computed  $R^2$  were 0.9946, 0.9895 and 0.9828 for culture A, B and C respectively.

The proliferation rates of HeLa cells in  $\mu$ CCCs (Figure 19) were compared to the proliferation rates of HeLa cells in culture flasks presented in more detail in Figure 17. The results indicated that the proliferation rates were comparable. The doubling times for the control flask,  $\mu$ CCC culture A, B and C were 32.0 h, 37.9 h, 36.7 h and 32.6 h, respectively. This indicates a slightly increased generation time possibly arising from continuous perfusion removing autocrine and paracrine growth promoting factors.



## Temperature regulation in the $\mu$ CCC

During culture experiments the  $\mu$ CCC was subjected to changes in ambient temperature due to the day-night cycle. The  $\mu$ CCC was tested for the ability to maintain the desired culturing temperature over time when the day and night cycle varied significantly (Figure 20).

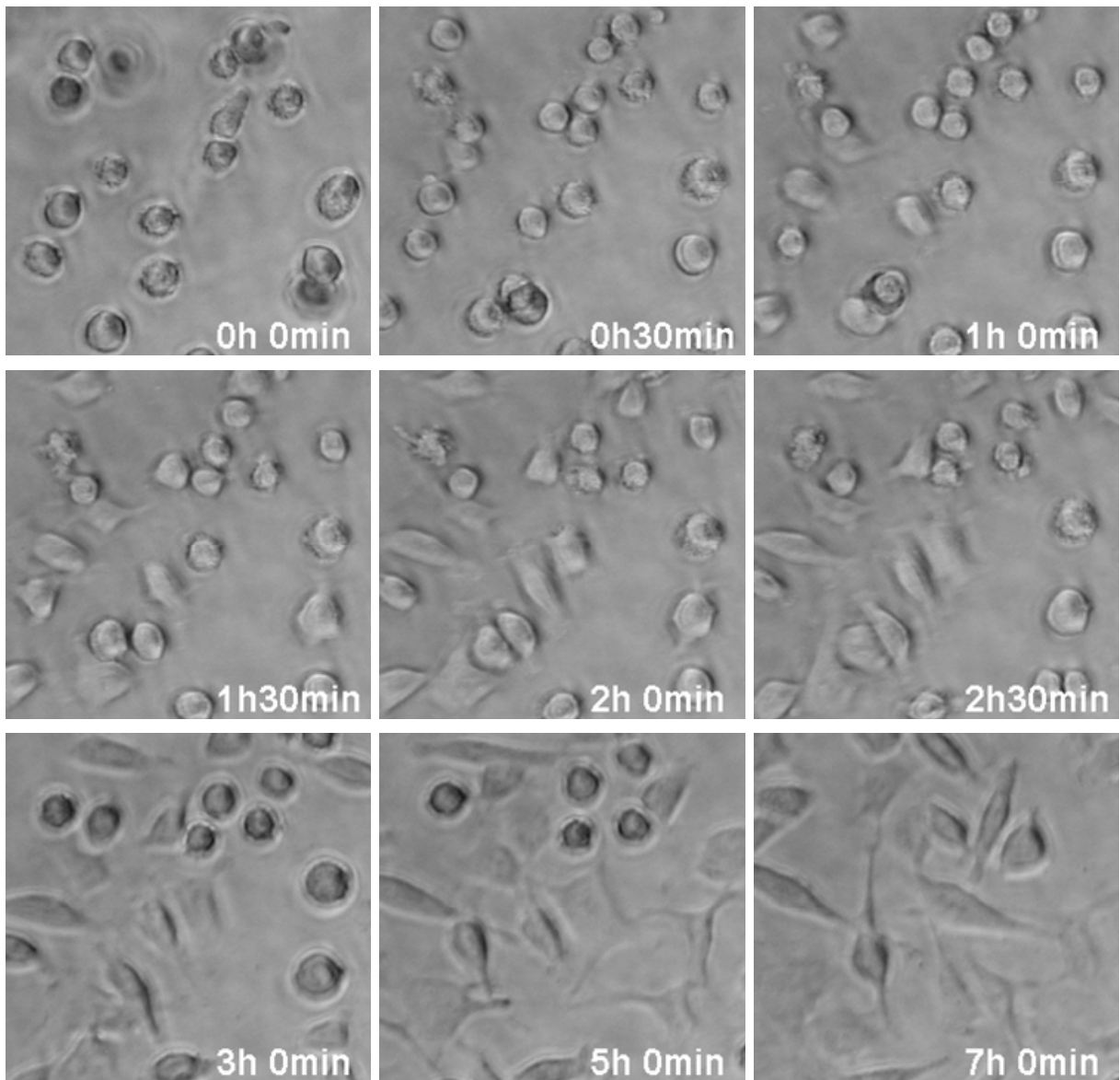


**Figure 20: Thermal performance of the  $\mu$ CCC during fourteen days of culturing.** Ambient temperature was recorded using a second  $\mu$ CCC with only the calibrated thermistor connected to the electronics. Temperature and applied voltage were recorded every 23 seconds over the entire culturing period.

The results indicated that despite significant fluctuations in ambient temperature (24.4 - 28.4 °C) due to the day and night cycle, the temperature within the  $\mu$ CCC maintained unperturbed ( $37.0 \pm 0.21$  °C) due to the computer controlled PID feedback loop, which continuously adapted the voltage amplitude applied to the heater (2.2 - 3.0 V) reflecting the actual temperature inside the  $\mu$ CCC.

## Cell attachment

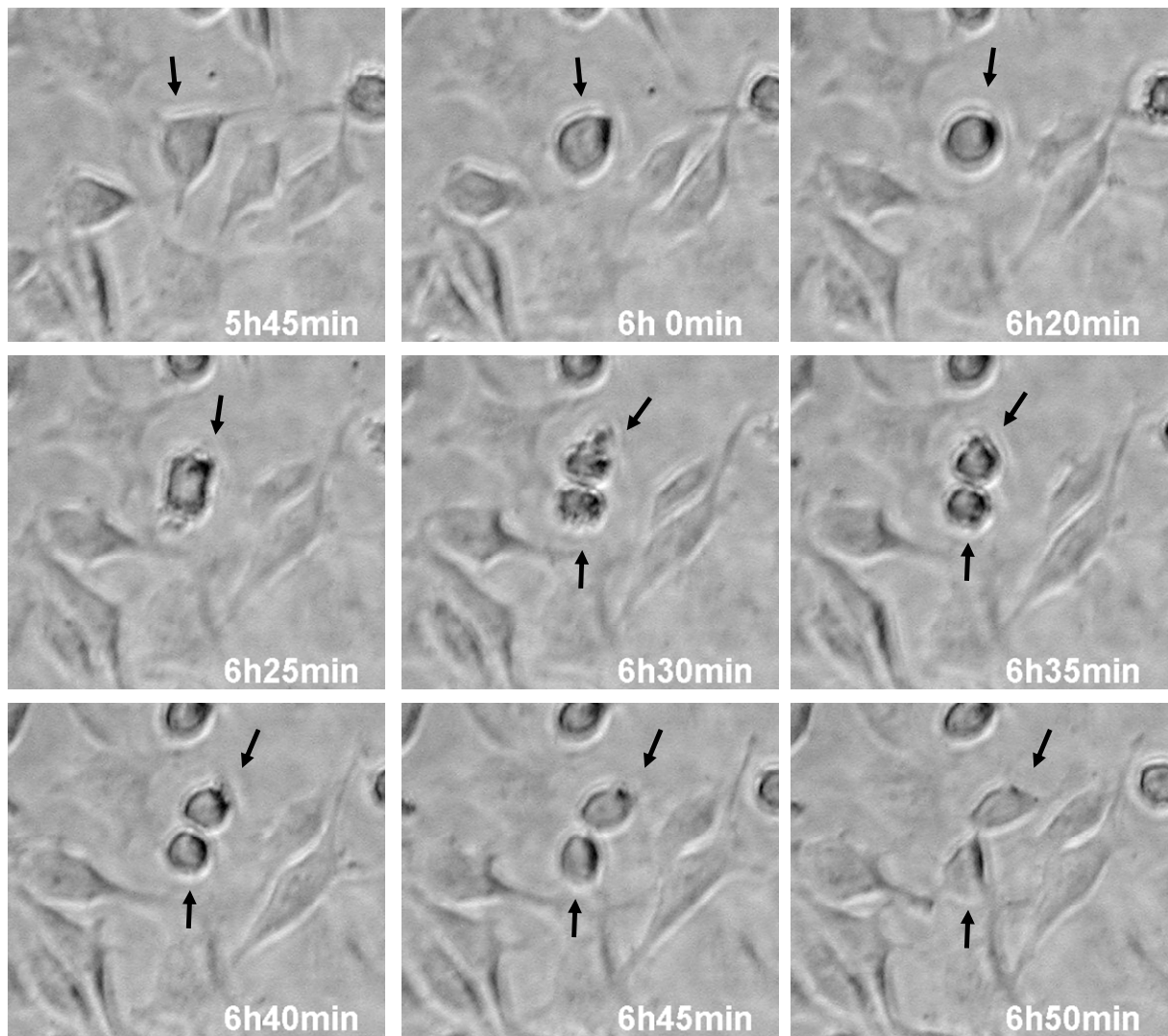
On-line monitoring of cell cultures enabled the study of many aspects in a cells life. Interesting was the possibility to study the attachment process over time (Figure 21). The first signs of the attachment process were frequently observed within minutes after seeding of the cells. Some cells would take several hours before they attached to the surface. This is observable on Figure 21 where some cells remain detached following more than 2 hours and 30 minutes of culturing. Following 7 hours of culturing all cells in the images on Figure 21 showed signs of attachment to the surface. The reason for this may be found in the cells was not synchronized prior to seeding in the  $\mu$ CCC. Hence the cells would most likely be at different stages of the cell cycle and thus responded differently to treatment with trypsin, handling and seeding.



**Figure 21: On-line studies of HeLa cell attachment.** Selected cropped frames of the same culturing area showing the initial attachment process of HeLa cells. The time stamp indicates the time elapsed since the cells were seeded. A movie of the entire attachment is available on the accompanying data disc (Movie 2).

### Cell proliferation

Another phase in cell culturing is the cell proliferation process. It was noted that prior to division a HeLa cell would grow physically larger, detach from the surface and until division appear round like a freshly passaged cell prior to attachment, only larger (Figure 22).

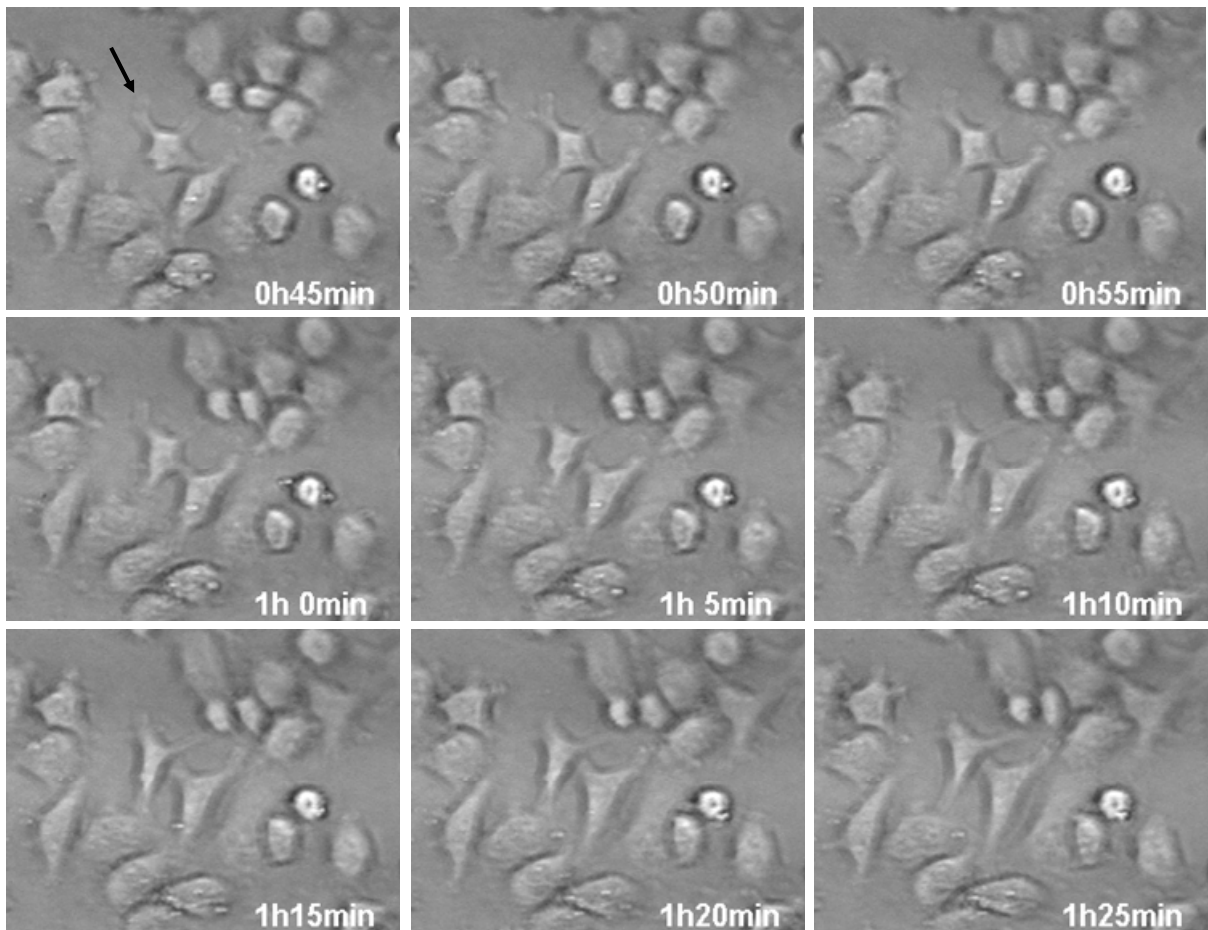


**Figure 22: On-line monitoring of a dividing HeLa cell.** Selected cropped frames were selected showing a dividing cell in the center of the images indicated by an arrow. Following division the two new cells are indicated with arrows. The time stamp indicates the time since the cells were seeded.

The results indicated that the detachment from the surface took around 20 minutes. The actual division of the mother cell into two daughter cells was rapid and took place in less than five minutes and is visible on the frames 6h25min and 6h30min on Figure 22. Following the division, the two daughter cells attached to the surface within 20 minutes. Interestingly for this division, the time required for detachment of the original cell was strikingly similar to the attachment time for the two daughter cells.

### Cell-cell contact

Another interesting observation was cell-cell contact. When two cells came in physical contact with each other they appeared to recognize the presence of either another cell or another object (Figure 23).

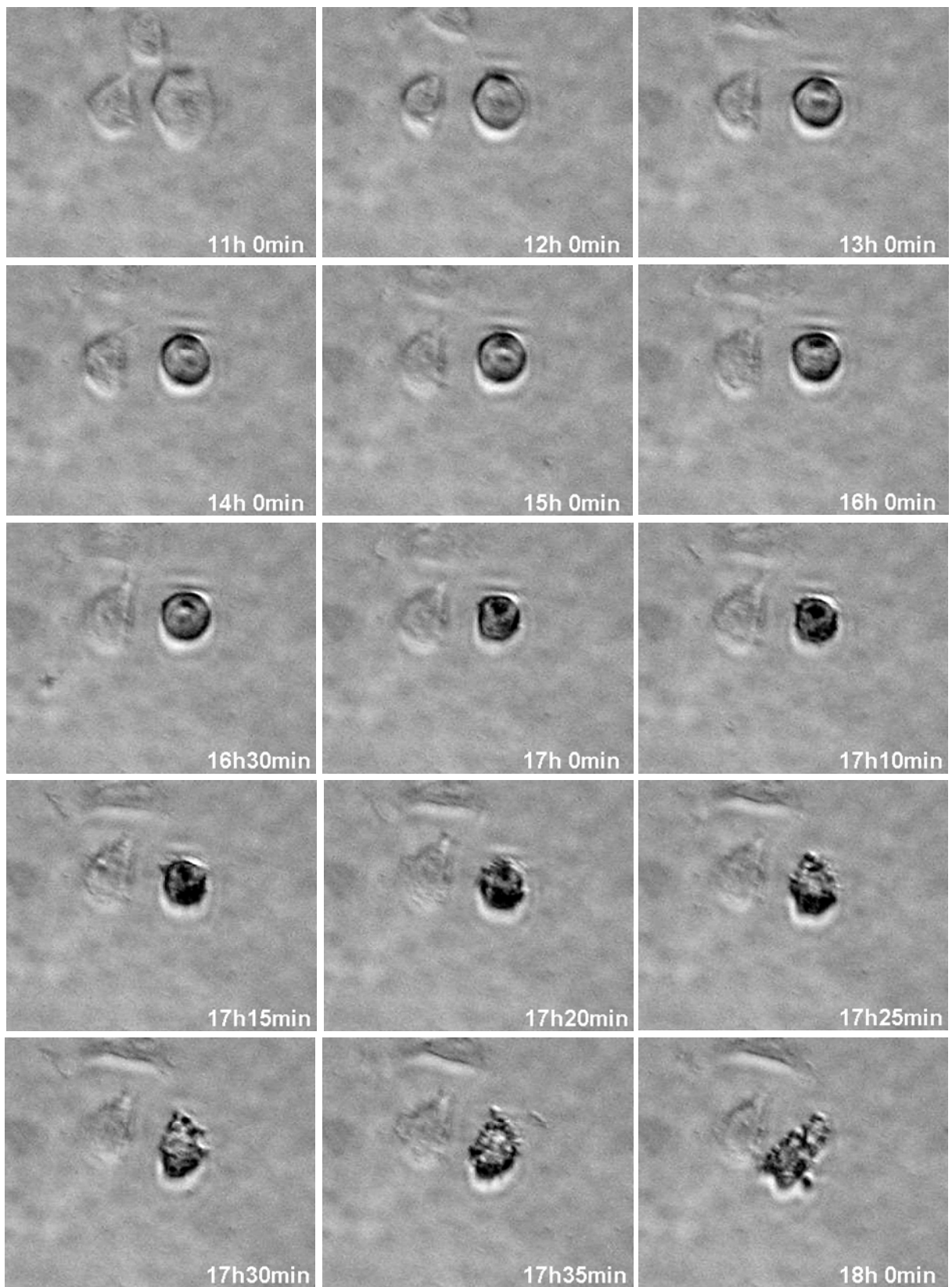


**Figure 23: Cell-cell contact during culturing.** Selected images were cropped from a culture sequence of images. The arrow indicates the cell which first came into contact with the adjacent cell. The label in the lower right corner indicated the elapsed time since the cells were seeded.

In the central region on the images comprising Figure 23 the physical contact between the protrusions of two cells can be observed over time. Initially the top cell (marked by an arrow on Figure 23 0h 45min) recognizes a cell situated below it. Upon the physical contact the lower cell extends a protrusion directed at the cell touching it within 10 minutes (Figure 23 0h 45min - 0h 55min). The first cell then withdrew its protrusion and directed the other protrusion in other directions.

### Cell death

During culturing occasional cell deaths were observed. Initialization of cell death usually commenced with an unusual slow detachment of the dying cell from the surface forming a big round cell similar to a dividing cell (Figure 24).



**Figure 24: Initialization of cell death.** Selected images were cropped from a culture sequence. The time-tag indicates the time since the cells were seeded. A movie of the cell death is available on the accompanying data disc (Movie 3).

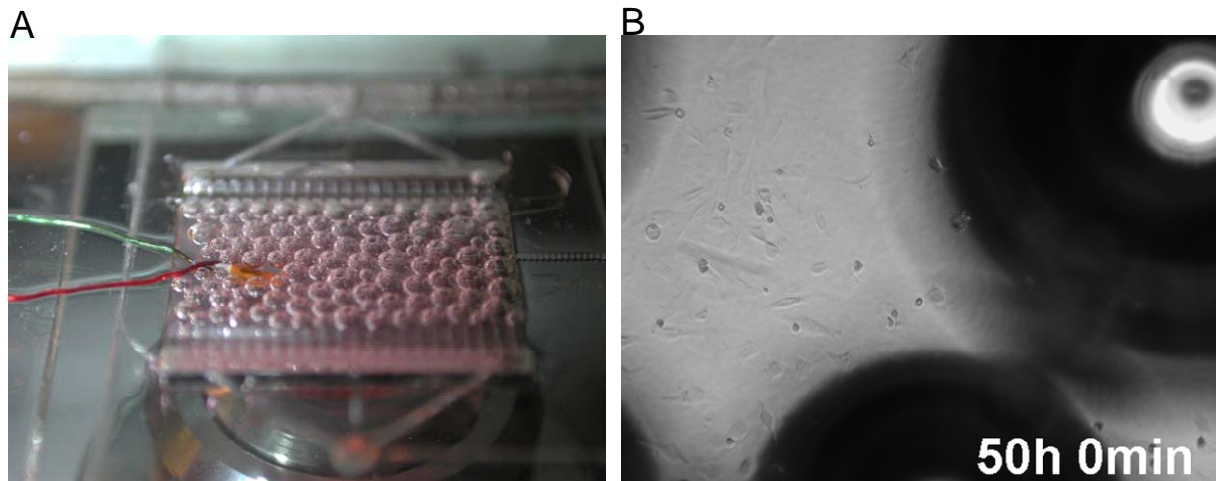
Opposed to a dividing cell, the dying cells were observed to remain detached and round for several hours until the membrane ruptured. Initially this can be observed by the several small

protrusions extending from the cell membrane. These can be observed on at the time 17h 10 min and forth on Figure 24. The time from the initial observation of these protrusions until the cell lysed was less than one hour. The adjacent cells seemed unaffected of the dying cell (data not shown) indicating that no apoptotic effectors were released in concentrations great enough to initiate cell death in these adjacent cells.

## **Bubbles**

As with any microsystem bubbles arising from improper sealing of the  $\mu$ CCC to the surroundings would most likely result in either obstruction of the camera view to the cells (Figure 25 A-B) or influencing on the local microenvironment experienced by the cells possibly leading to non-reproducible effects.

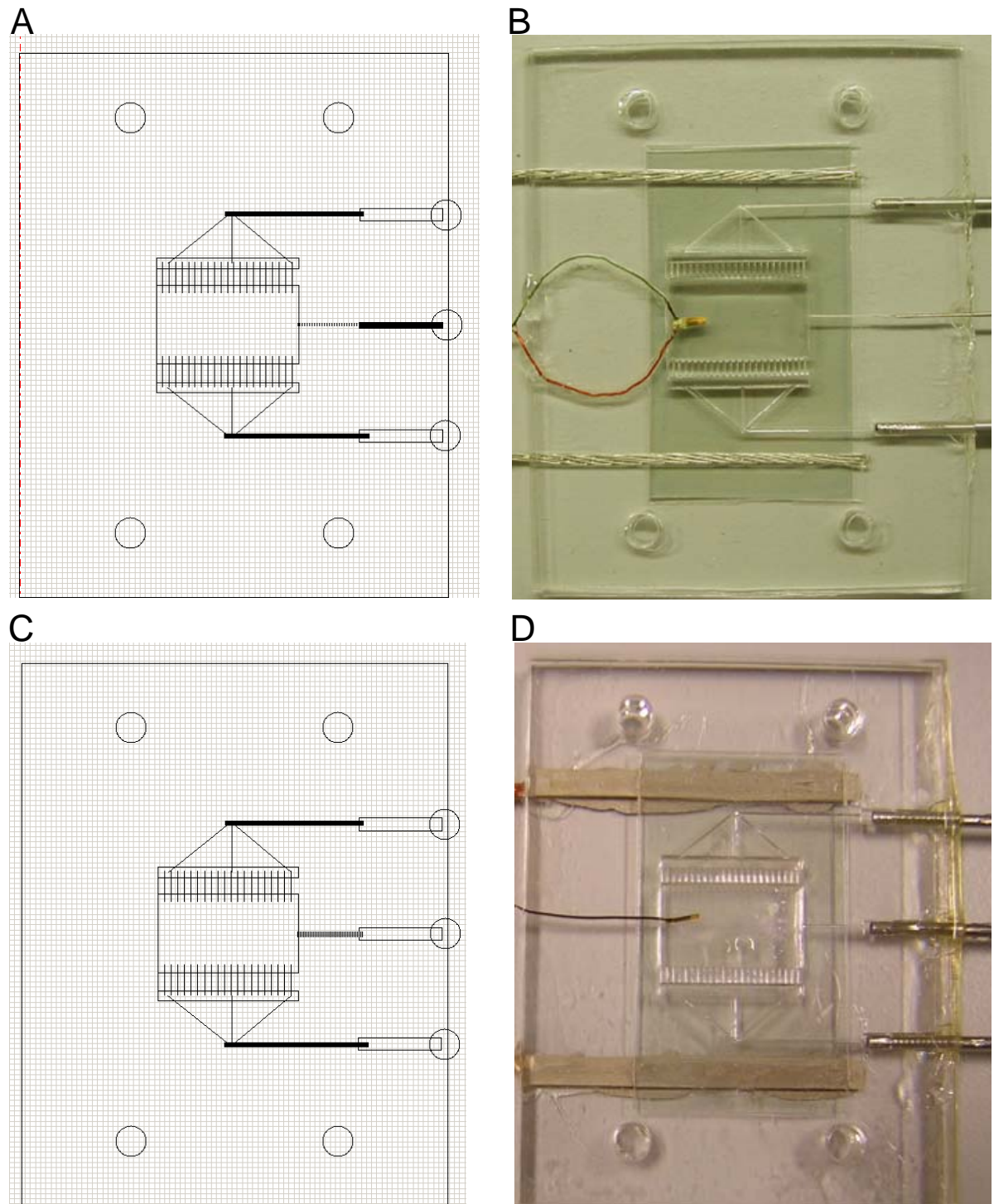
In microfluidics the traditional approach for reducing bubble formation is degassing any liquid introduced to the microsystem. Degassing the media prior to culturing would remove dissolved oxygen resulting in the asphyxiation of cells and was hence not attempted. Special cell loading procedures were developed in which a tiny portion of the cells were loaded prior to filling of the culture area with media. This enabled the filling of the channels around the cell loading port. Subsequently media was perfused initially at a rate of one to five mL per hour until the entire chamber was filled. Reducing the flow rate to 0.1 mL per hour enabled the archival of steady state conditions with regards to temperature distribution within the chamber. It was noted that when cells were injected following the achievement of steady state resulted in minimal exposure to reduced or elevated temperatures and also reduced bubble formation.



**Figure 25: The effect of air bubbles on the  $\mu$ CCC.** (A) Close-up of the  $\mu$ CCC filled with bubbles. As a result of improper sealing air from the surroundings can enter the culturing chamber resulting in the formation of bubbles. (B) Example of the resulting image obtained from a  $\mu$ CCC partially filled with bubbles during culture of cells. The growing attached HeLa cells are visible on the surface, but the air bubbles obstruct the view of the cells from the camera.

Seeking to elucidate if different sizes of cell inlet needles influenced the rate of bubble formation, two versions of the  $\mu$ CCC were designed enabling the seeding of cells through either an 18 gauge (1.2 mm diameter) needle or a thinner 25 gauge needle (0.4 mm diameter) (Figure 26).

Utilizing the thinner 25 gauge needle (Figure 26 A-B) resulted in more frequent bubble formation (Figure 25) as it was difficult to obtain an air tight seal around the needle with epoxy glue. Furthermore after seeding of cells through a 1 mL syringe the syringe had to remain attached to the seeding needle as the creation of an airtight seal of the needle after the removal of the syringe proved virtually impossible. A tighter seal was obtained when the thicker 18 gauge needle was used (Figure 26 C-D). The larger size of the needle enabled abrasion of the needle, resulting in a more air tight seal with the epoxy sealing glue.

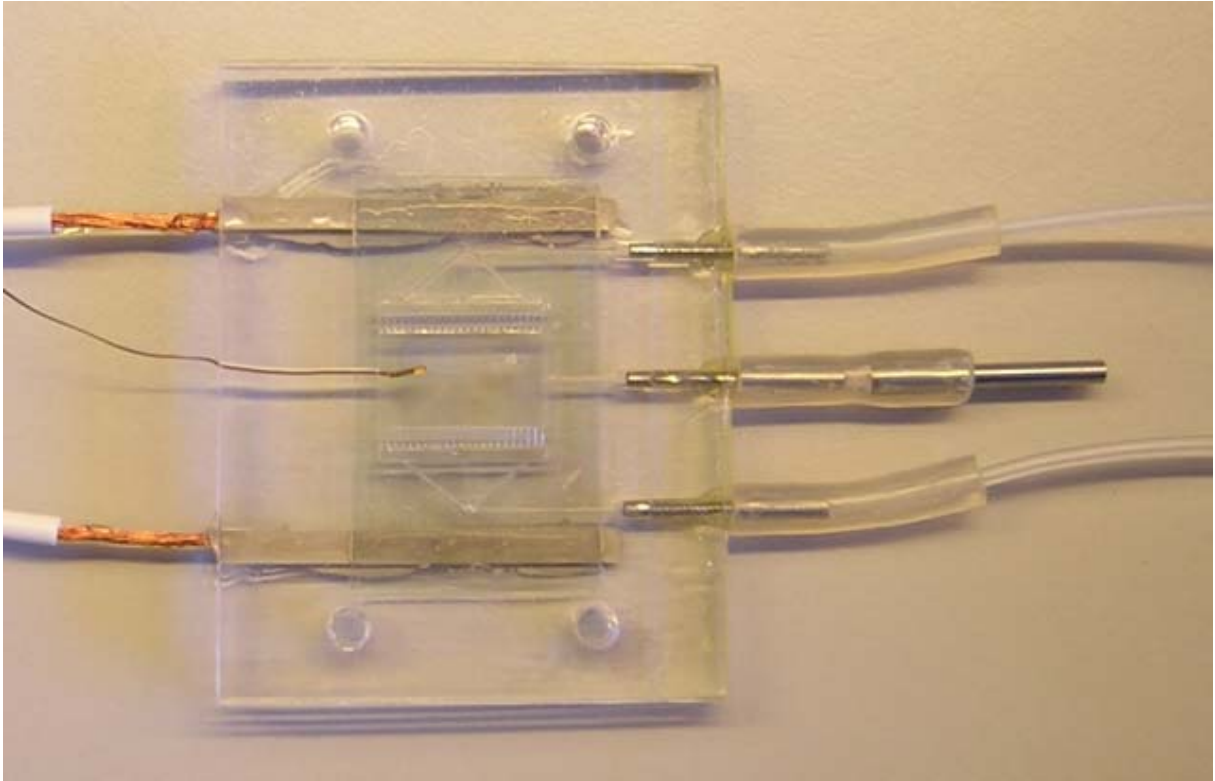


**Figure 26: Different sizes of loading inlets for the  $\mu$ CCC.** (A) Screen dump from the laser ablation program displaying the layout of the  $\mu$ CCC with a 25 gauge cell seeding needle. The grid size is 0.5 mm. (B) An actual chip utilizing the thin cell seeding needle. (C) Screen dump from the laser ablation program displaying the layout of the  $\mu$ CCC with the larger 18 gauge cell seeding needle. The grid size is 0.5 mm. (D) An actual chip with the larger 18 gauge cell seeding needle.

An air tight connection between the inlet channels as well as the thicker 18 gauge needle was realized with a PDMS connection tube. After seeding of the cells through a 1 mL syringe



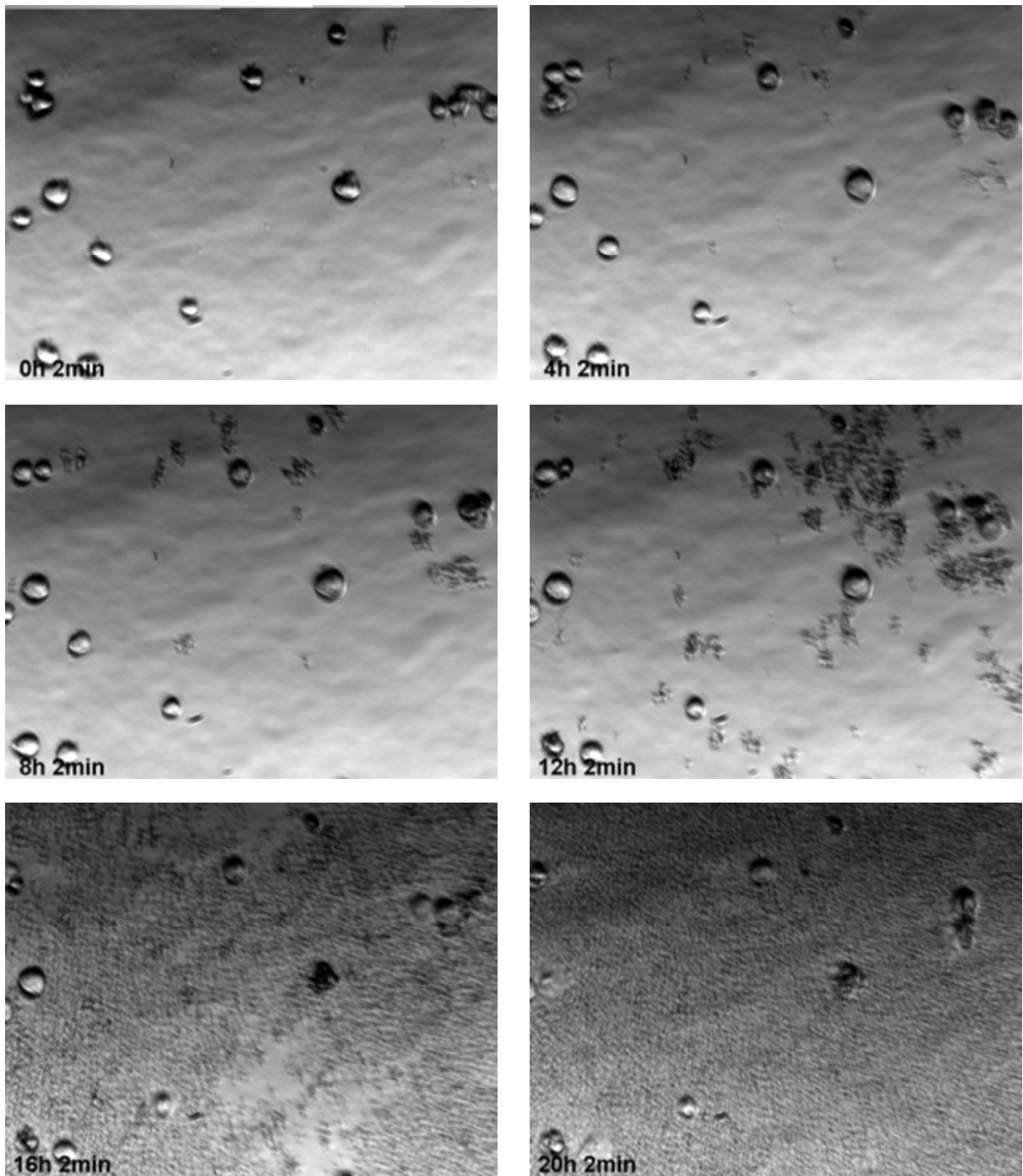
attached with another 18 gauge needle, the syringe with needle could be removed and replaced with a solid stainless steel plug (Figure 27).



**Figure 27:  $\mu$ CCC with connection tubings.** Attachment of the tubings was facilitated by use of flexible PDMS connectors. Seeding of cells was performed by replacing the stainless steel plug with an 18 gauge needle attached to a 1 mL syringe containing the cells.

## Contamination

As the glass transition temperature ( $T_g$ ) for PMMA is 110 °C it was not possible to autoclave the  $\mu$ CCC prior to culture experiments. Instead the  $\mu$ CCC was dry-sterilized at 100 °C for one hour between the two glass bonding blocks (Figure 2) each weighing 185 grams. No additional pressure was applied other than the weight of the glass bonding blocks. The pressure prevented the separation of the individual layers. Maintaining the temperature below  $T_g$  prevented melting of the chip and blocking of the microfluidics channels. Failure to use proper sterile techniques during seeding or handling the  $\mu$ CCC after sterilization occasionally resulted in contamination of the culture (Figure 28). The much shorter generation time of the contamination resulted in rapid flooding of the  $\mu$ CCC with microorganisms.

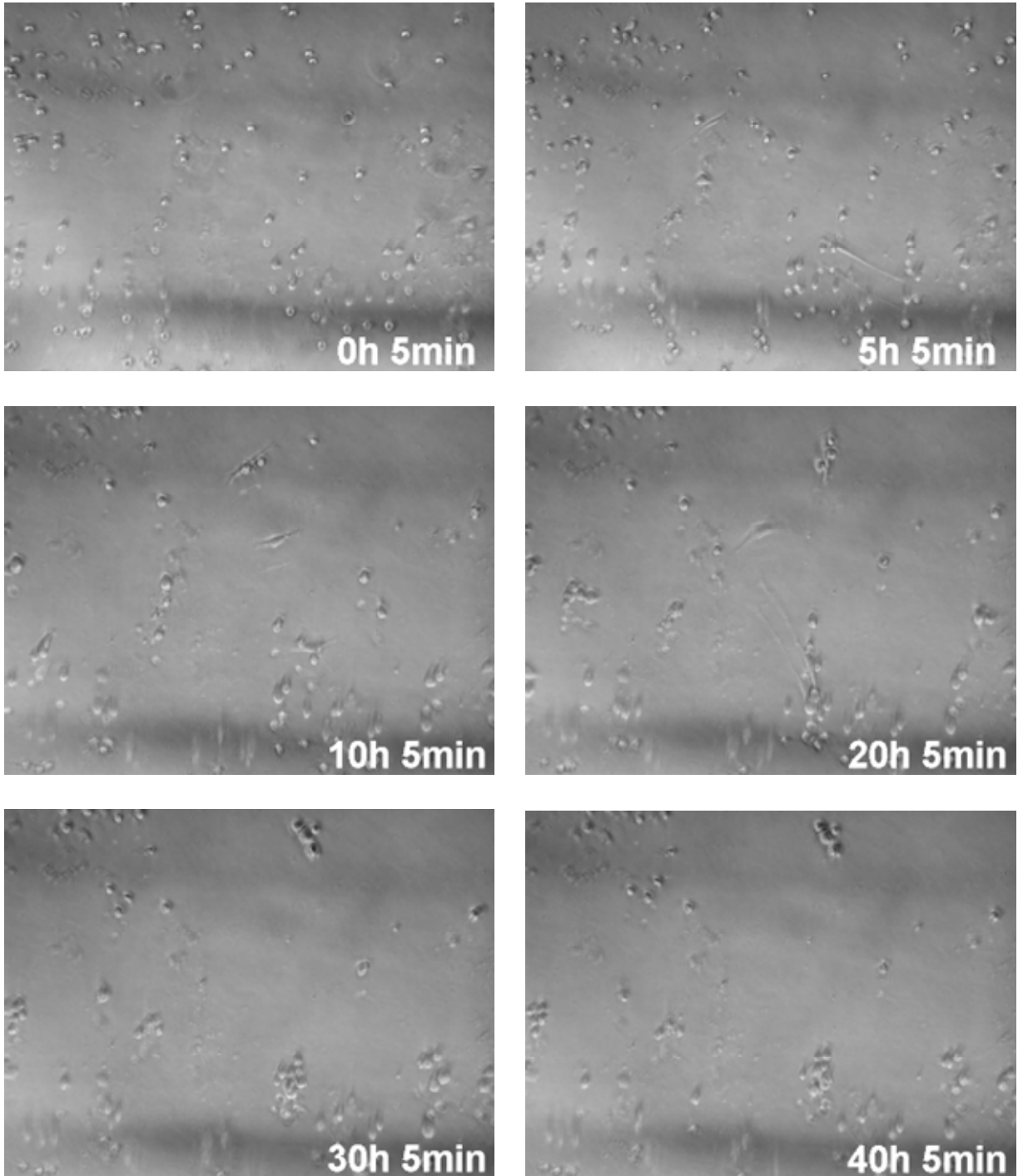


**Figure 28: Contamination of the  $\mu$ CCC.** The time stamp in the lower left corner indicates the time elapsed after seeding. No anti biotic agents were added to the media formulation.

After just 4 hours of culturing the first signs of the contaminating microorganism are evident (Figure 28). Following just 20 hours of culturing the view field of the camera was completely blocked by the contaminating microorganism. After addition of antibiotics to the culturing media only a single contamination occurred in more than 30 culture experiments.

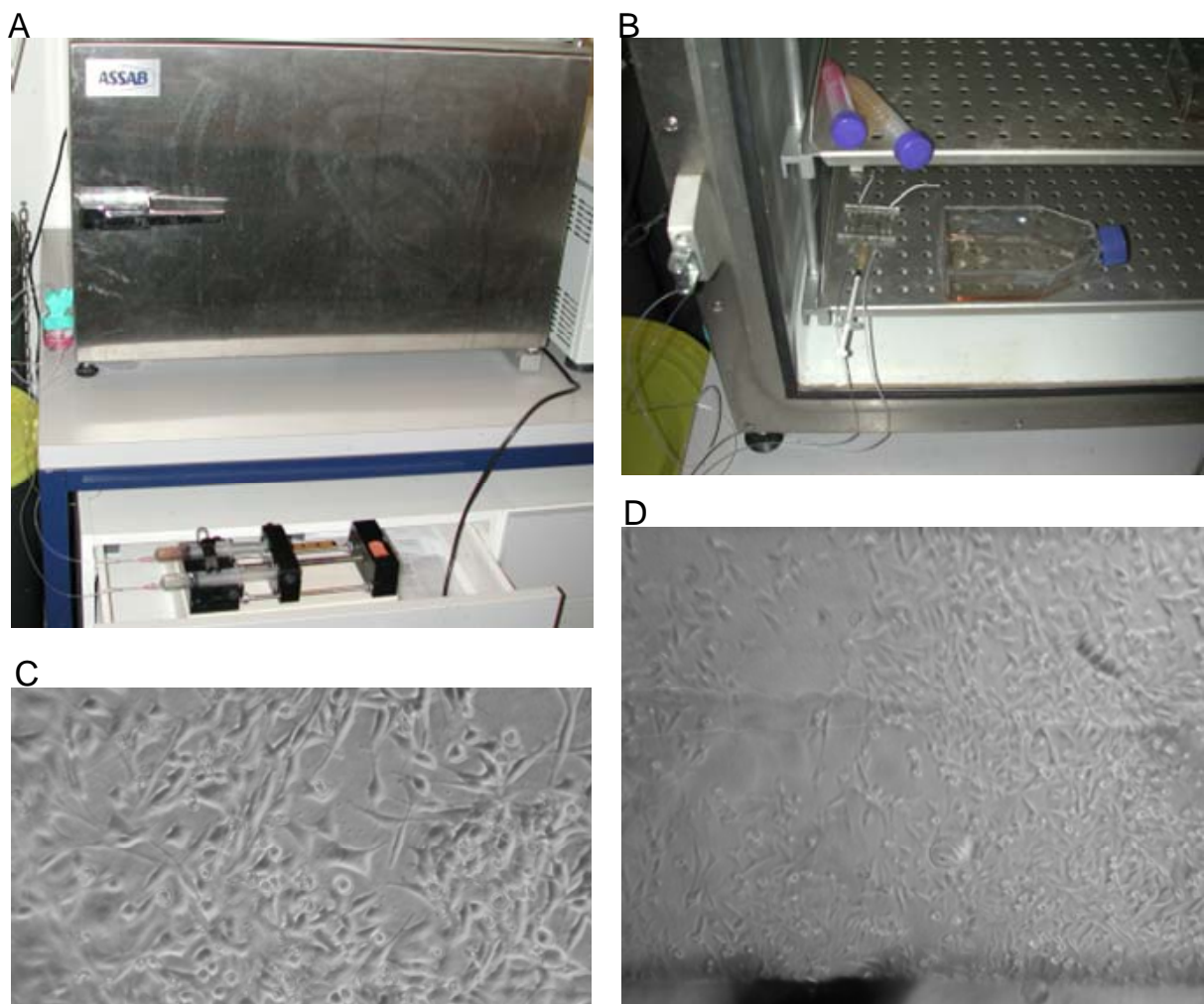
## Phototoxicity

During initial culture experiments, it was noted that cells appeared to attach to the surface of the  $\mu$ CCC and following one or two days of culturing they would detach from the surface and die (Figure 29).



**Figure 29: Cell death in the  $\mu$ CCC.** Cell attachment was occurring up to around 20 hours of culturing after which cells detached, became immobile and subsequently died. The labels in the lower right corner indicates the time post seeding in the culturing experiment.

As the cells in the control flask remained viable and proliferated and the media used in the  $\mu$ CCC culturing and the control was identical, the incentive to the cell death was sought in the cell culturing conditions. Speculating that shear stress, inadequate pH buffering, localized heating or the fact that the  $\mu$ CCC was exposed to light might be the course of the cell death, a  $\mu$ CCC was seeded with freshly passaged cells, connected to the perfusion pump operating at 0.1 mL/h and placed inside the CO<sub>2</sub> incubator to supply heat (Figure 30 A-B). As control cells from the same passage was simultaneously seeded in a culture flask and incubated next to the  $\mu$ CCC in the CO<sub>2</sub> incubator (Figure 30 A-B).

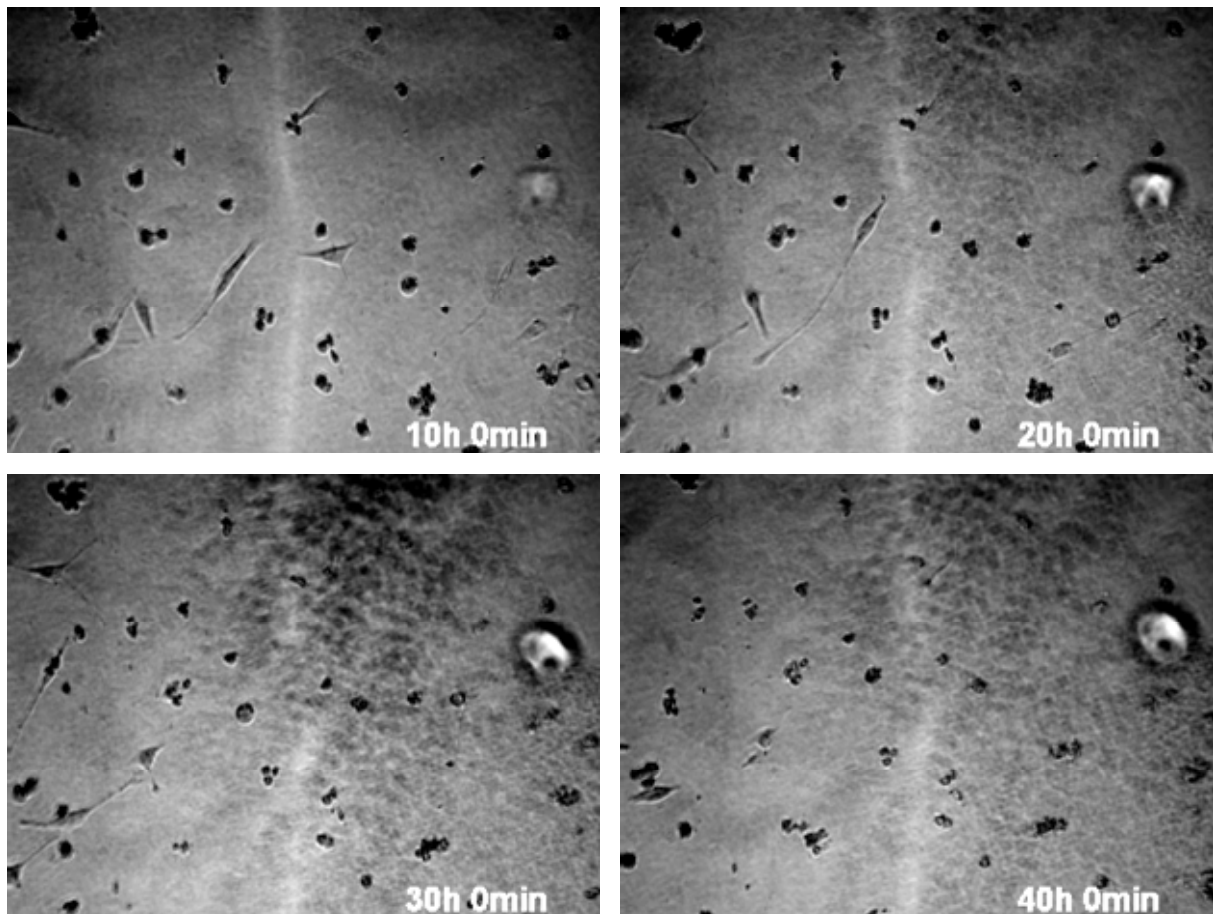


**Figure 30: Culturing of cells in the  $\mu$ CCC inside the CO<sub>2</sub> incubator.** (A-B) The setup and the location of the  $\mu$ CCC relative to the reference culture flask. (C) View of cells in the  $\mu$ CCC following two days of incubation through the 10 x magnification objective. (D) View of cells through the 4 x objective in the  $\mu$ CCC following two days of incubation. The line in the bottom is the  $\mu$ CCC chamber wall and the dark region is the cell seeding inlet.

Following two days of culturing, the cells in the  $\mu$ CCC were viable and proliferated indistinguishable from the cells in the reference cell culture flask, indicating that continuous media perfusion may not be responsible for the observed cell death (Figure 30 C-D).

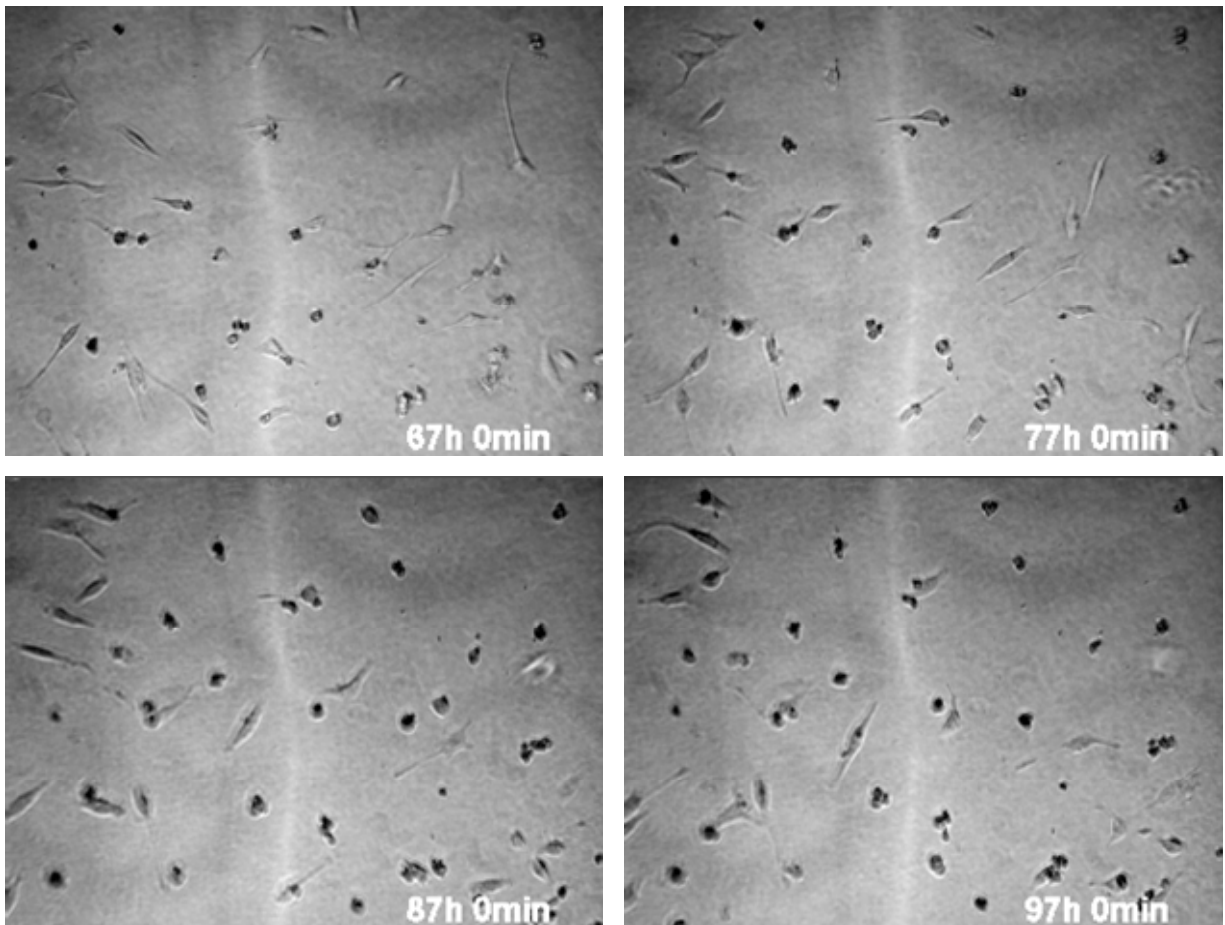
If the  $\mu$ CCC was permeable to either  $O_2$  or  $CO_2$ ,  $CO_2$  dissolved in the media might diffuse through the PMMA comprising the  $\mu$ CCC, causing the pH of the culture media to drift up to lethal alkaline values of over 8.5 when the  $\mu$ CCC was left at atmospheric conditions ( $<0.05\%$   $CO_2$ ) resulting in cell death. As the conventional cell culture media depended on  $CO_2$  for pH buffering, a  $CO_2$  independent medium containing HEPES was tested (Figure 31).

The results indicated that when culturing cells in a HEPES buffered media in the  $\mu$ CCC outside the  $CO_2$  incubator, only few cells attached and cell death occurred within two days of culturing. Inspecting other areas of the  $\mu$ CCC previously not directly exposed to light of the microscope lamp indicated that viable cells were attached and proliferating in the same  $\mu$ CCC. This indicated that the shift of culture media may not be lethal to the cells. Repositioning the  $\mu$ CCC enabled the observation of these cells over time (Figure 32).



**Figure 31: Use of HEPES buffered medium in the  $\mu$ CCC.** The conventional  $CO_2$  dependent media was replaced with HEPES buffered media.

The results indicated that when cells were exposed to the light of the microscope light they would detach from the surface and die within two days. This indicated that the light from the microscope lamp may be responsible for the observed cell death. As HEPES buffered medium previously has been found to be especially susceptible for photo damage<sup>68,75,76,120</sup> further experiments were conducted with conventional CO<sub>2</sub> dependent media (RPMI-1640).

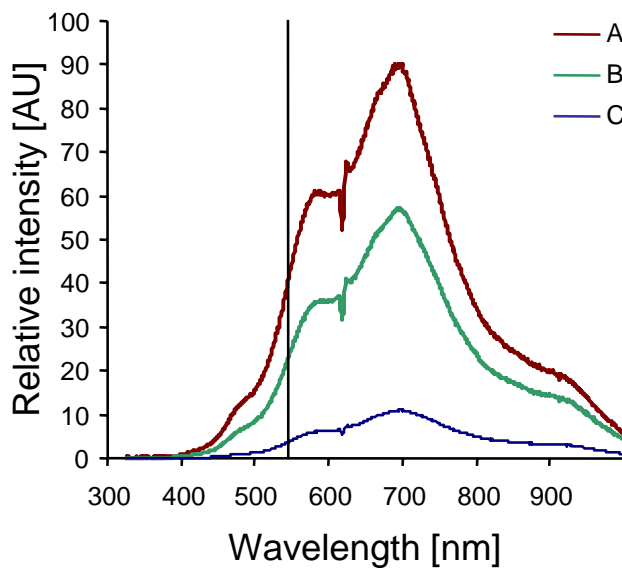


**Figure 32: Use of HEPES buffered in the  $\mu$ CCC.** Following 67 hours of culturing the  $\mu$ CCC was repositioned enabling monitoring of attached and proliferating cells from an area of the  $\mu$ CCC not directly exposed to the light of the microscope. No other parameters of the  $\mu$ CCC were changed.

## Influence of light

As the temperature was continuously monitored with a thermistor inside the culturing chamber and regulated by the by the ITO heater, and cell death also occurred in close vicinity to the thermistor, light induced localized heating was suspected not to be the cause of cell death. Seeking to elucidate if the microscope lamp used to provide light to the camera during culturing induced phototoxic effects, the light spectra was collected at different light intensity settings (Figure 33). Due to the intensity of the light it was not possible to obtain the light spectra at higher light intensities than half power.

The intensity of the microscope lamp was continuously adjustable resulting in the light spectra was obtained at power settings denoted “minimal setting”, “one third intensity” and “half intensity”. The amount of light at each wavelength was counted and plotted against the wavelength. The results indicated that when the light intensity was set either to half or one third power, significant amounts of light with wavelength below 540 nm was recorded (Figure 33). However, when the light intensity was reduced to the minimal setting the amount of light with wavelengths below 540 nm was significantly reduced. As light below 540 nm is known to introduce phototoxic effect on media components like riboflavin, tryptophan and tyrosine<sup>69-72</sup>. Future experiments were carried out using a darkened room and minimal settings of the microscope lamp and keeping media secluded from light as much as possible.

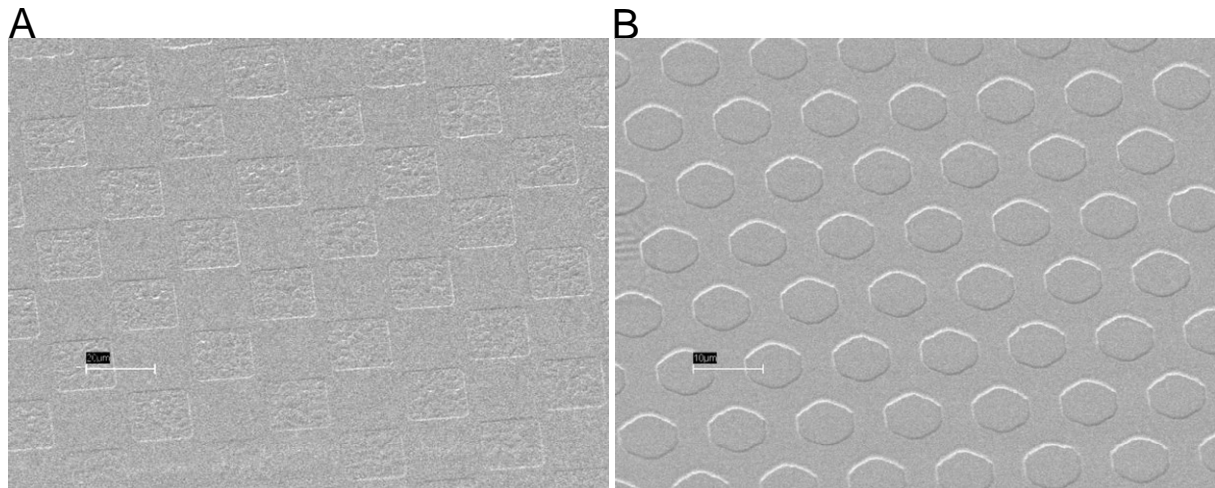


**Figure 33: Light spectra obtained at different intensity settings.** Each measurement was obtained ten times and the plotted values are average values of these measurements. All values were corrected for background by subtracting measurements obtained in complete darkness. **(A)** Spectra recorded with the half the possible light intensity. **(B)** Spectra with the one third of the possible light intensity. **(C)** Spectra obtained with minimal light intensity. The black vertical

## Influence of surface topography

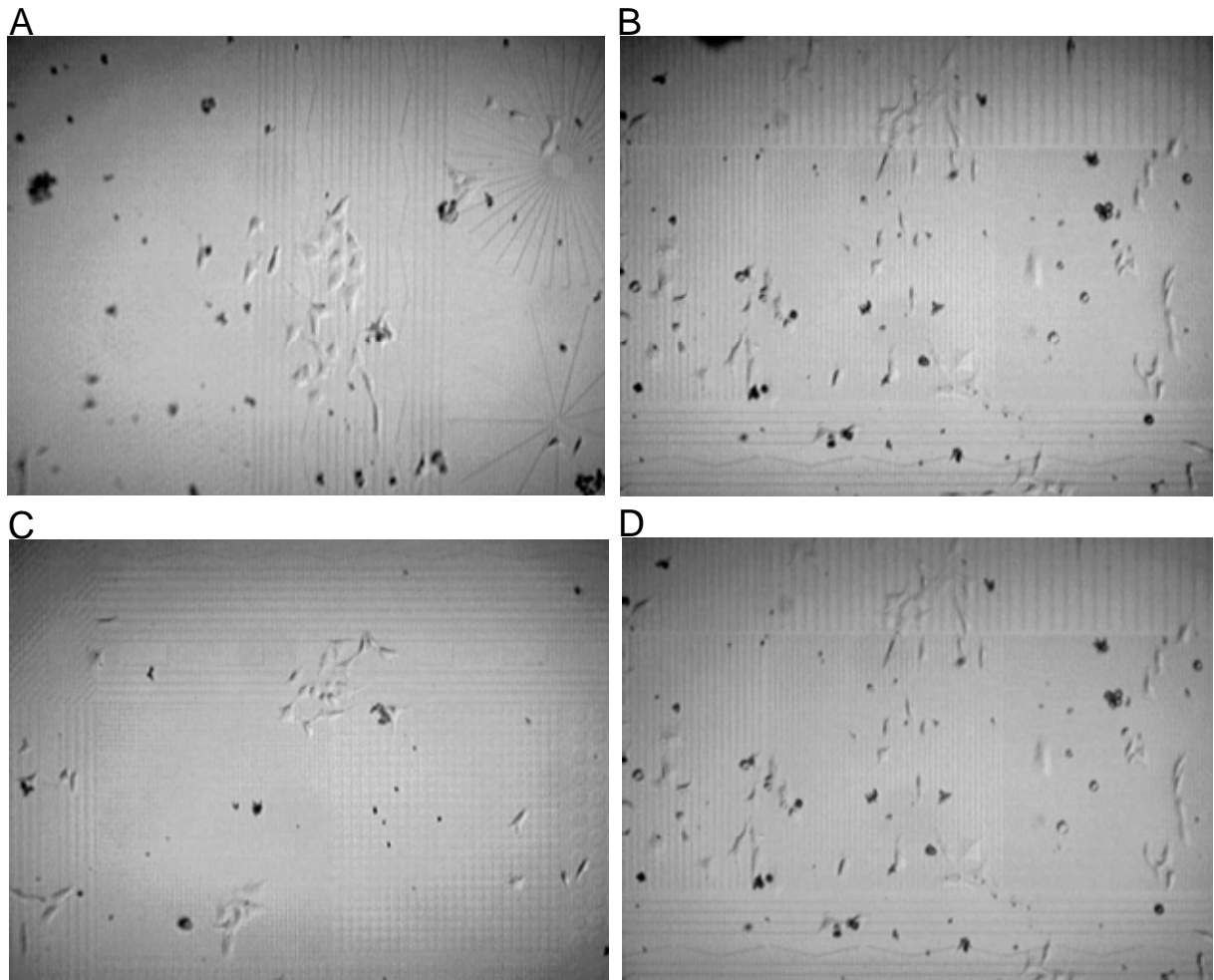
The low  $T_g$  (110 °C) of the PMMA enables imprinting of structures using the hot-embossing technique. By heating the sheet of PMMA to be imprinted to temperatures above the  $T_g$  and pressing a stamp with the desired design features into the PMMA a replica of the of the features are created in the PMMA. Using an available stamp containing various topographical features of different lateral dimensions with a height of 90 nm, this was transferred into PMMA. Verification of the features in the PMMA was performed with a scanning electron microscope (SEM) (Figure 34).

Using the imprinted piece of PMMA it was tested if HeLa cells would be affected of substituting the flat PMMA with a piece of PMMA containing imprints. Prior to seeding of cells the PMMA was sterilized by wiping with 70 % ethanol following drying for one hour in the LAF bench. The imprinted PMMA was placed in a cell culture Petri dish and covered with media and incubated for 30 minutes in the CO<sub>2</sub> incubator at 37 °C to equilibrate the media. Freshly passaged HeLa cells were seeded on the PMMA and incubated for 2 days in the CO<sub>2</sub> incubator (Figure 35).



**Figure 34: SEM pictures of PMMA imprinted with topographical features.** The imprint was made using 97 °C temperature on the upper piston and 130 °C on the lower piston and 15,000 N of pressure for 2 minutes in vacuum. The height of the features on the stamp was 90 nm. (A) A square pattern. Scale bar represents 20 µm. (B) Pattern consisting of circles. The scale bar represents 10 µm.





**Figure 35: Effect of topographical features on HeLa cell attachment. (A-D)** Topographical features of various dimensions hot-embossed into a 1.5 mm thick piece of PMMA. The circular pattern in Figure 34 B can be seen in Figure 35 C.

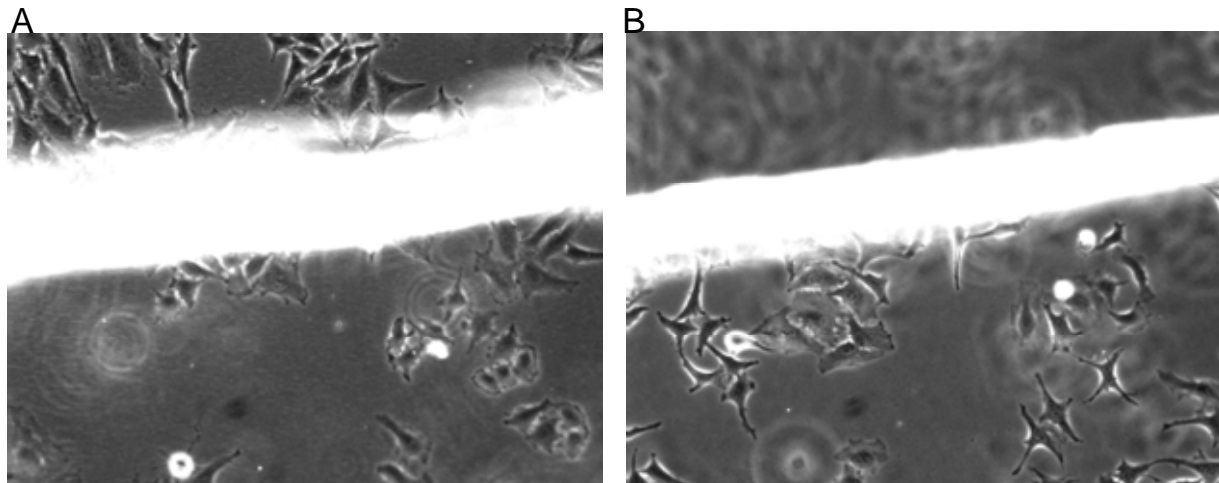
The result indicated that with the physical dimensions used no effect of the features was observed (Figure 35). This suggests the need for larger dimensions than those used in the experiment. This is most apparent as the no alignment of cellular protrusions was observed on the regions containing lines of various dimensions. In Figure 35 C circular patterns with various diameters seem not to affect the HeLa cells as the cells spread over the imprinted circles.

## ***Biocompatibility***

As one of the primary goals with the  $\mu$ CCC was the realization of a device capable of sustaining culturing of mammalian cells under culturing conditions similar to the reference culture flask test had to be conducted to verify this. Typical parameters used to evaluate the biocompatibility of a surface or components are cellular viability, morphological observations, growth kinetics or the activity of selected enzymes. As various cells may respond differently to the same stimuli another parameter may be to evaluate the  $\mu$ CCC with different cell lines.

### **PMMA as culturing surface**

Initial studies sought to elucidate if switching from the tissue culture polystyrene (TC-PS) surface of the conventional culture flask to a sheet of PMMA resulted adverse effects. As the intended culturing surface of the  $\mu$ CCC was PMMA, this was tested by inserting a 0.25 mm thick sheet cut to practical dimensions (5 cm long and 1 cm wide) in to a cell culture flask following the addition of media and cells. There were no major differences in cell morphology following 2 days of culturing (Figure 36).

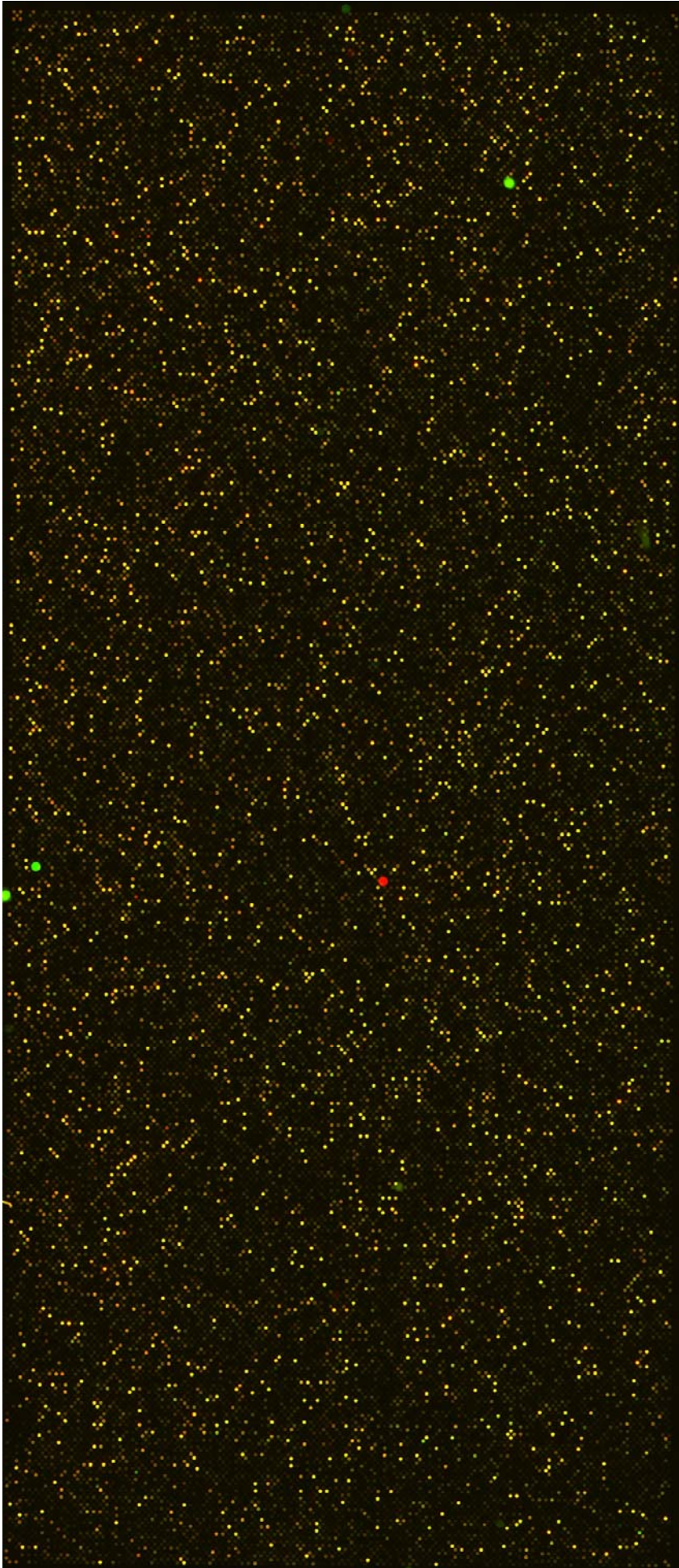


**Figure 36: Cell culturing on PMMA and culture flasks.** PMMA was evaluated as cell culturing surface by placing a section of a 0.25 mm thick PMMA sheet inside a cell culture flask following the addition of media and cells. The PMMA was sterilized by cleaning with 70 % ethanol and was left in the LAF bench for one hour to let the ethanol evaporate. Following 48 hours of culturing in the CO<sub>2</sub> incubator the cells were inspected. (A) The focal plane was adjusted to the culture flask surface. The white line is the edge of the sheet of PMMA. (B) The focal plane was adjusted to the PMMA surface. The cells appearing out of focus are growing on the culture flask surface.

## **Whole genome expression profiling on DNA microarrays**

Gene expression profiling using DNA microarrays has been widely used in the past 10 years to unravel molecular events of cell cycle regulation<sup>121,122</sup>, response to growth factors<sup>123</sup> and cellular responses to irradiation<sup>124</sup>. DNA microarrays are used as cancer classifiers<sup>107,125,126</sup> since it is strongly likely that the gene expression profile differs in cancer cells compared to the normal counterpart. The DNA microarrays used usually consist of DNA (probes) complementary to about 40,000 genes or possible genes (targets). In one batch process the expression level of these 40,000 genes in a cell can be monitored and compared to a reference cell. Whole genome expression profiling of cells cultured under conditions that are not comparable will most likely induce changes in the mRNA expression profile in a cell. Previous studies have indicated that cells appearing morphological similar might have a different gene expression profile<sup>111</sup>.

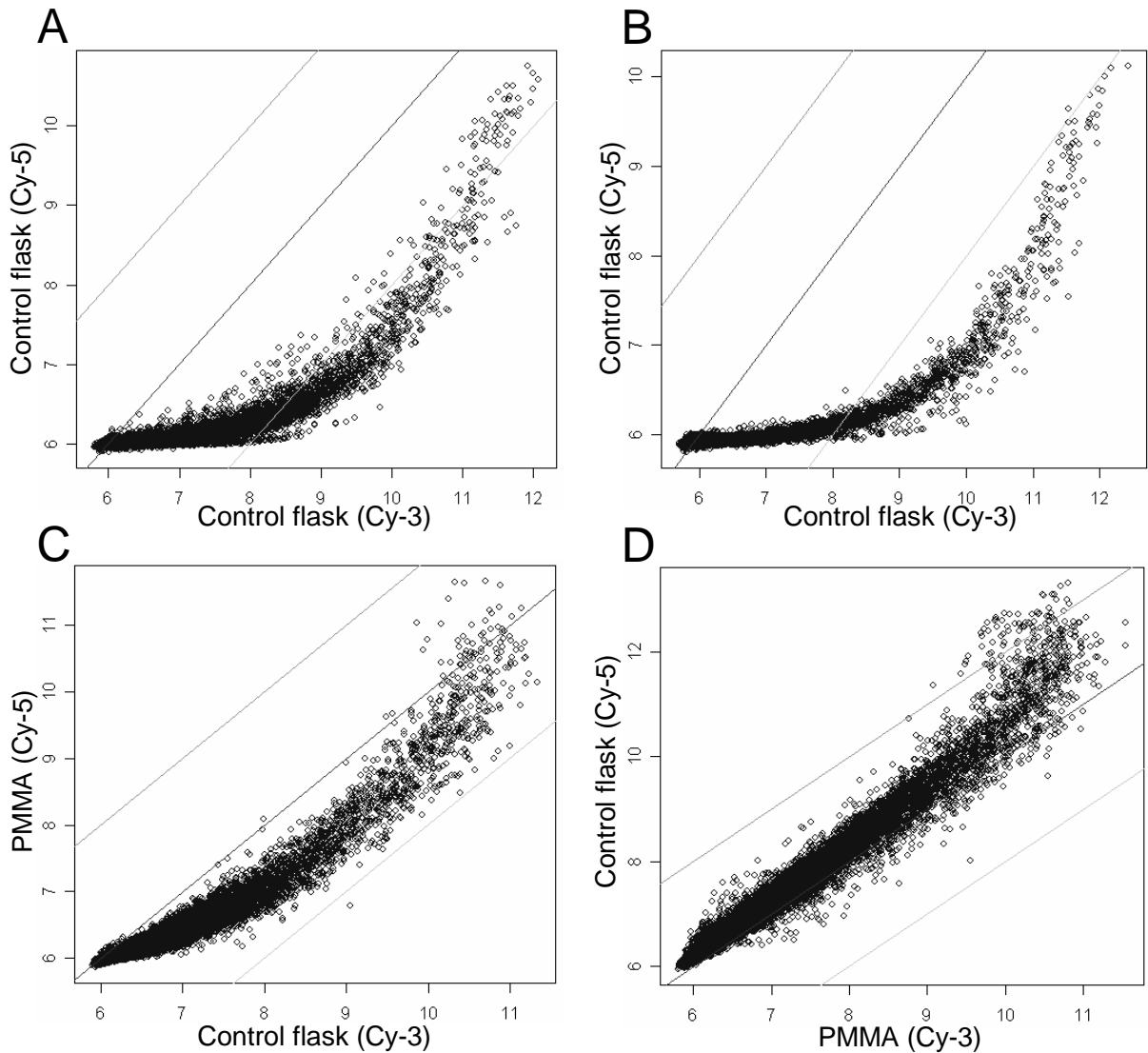
As the PMMA surface might induce an altered gene expression profile of the cells relative to the conventional TC-PS surface of the cell culture flask, this was tested by culturing HeLa cells inside a culture flask in the CO<sub>2</sub> incubator on a sheet of 0.25 mm thick PMMA. Following four days of culturing the sheet of PMMA was removed and non-attached cells were removed by washing of the PMMA with PBS buffer. The attached HeLa cells were collected by trypsinization and total RNA was extracted. As control, cells seeded simultaneously in a culture flask without PMMA were used. RNA isolated from cells cultured on PMMA as well as RNA isolated from cells cultured in unperturbed culture flasks was amplified to avoid introducing a bias<sup>127</sup>. Following reverse transcription and incorporation of Cy-3 or Cy-5 dyes, cDNA containing 200 pmol dye originating from each culture condition were pooled and co-hybridized to a whole human genome DNA microarrays containing 44,290 60 nt. long probes directed against the transcriptome (Figure 37).



**Figure 37: Scan of whole human genome DNA microarray.** Cy-3 (green) labeled cDNA originated from HeLa cells cultured on PMMA, while Cy-5 (red) labeled cDNA originated from cells cultured in the culture flask.

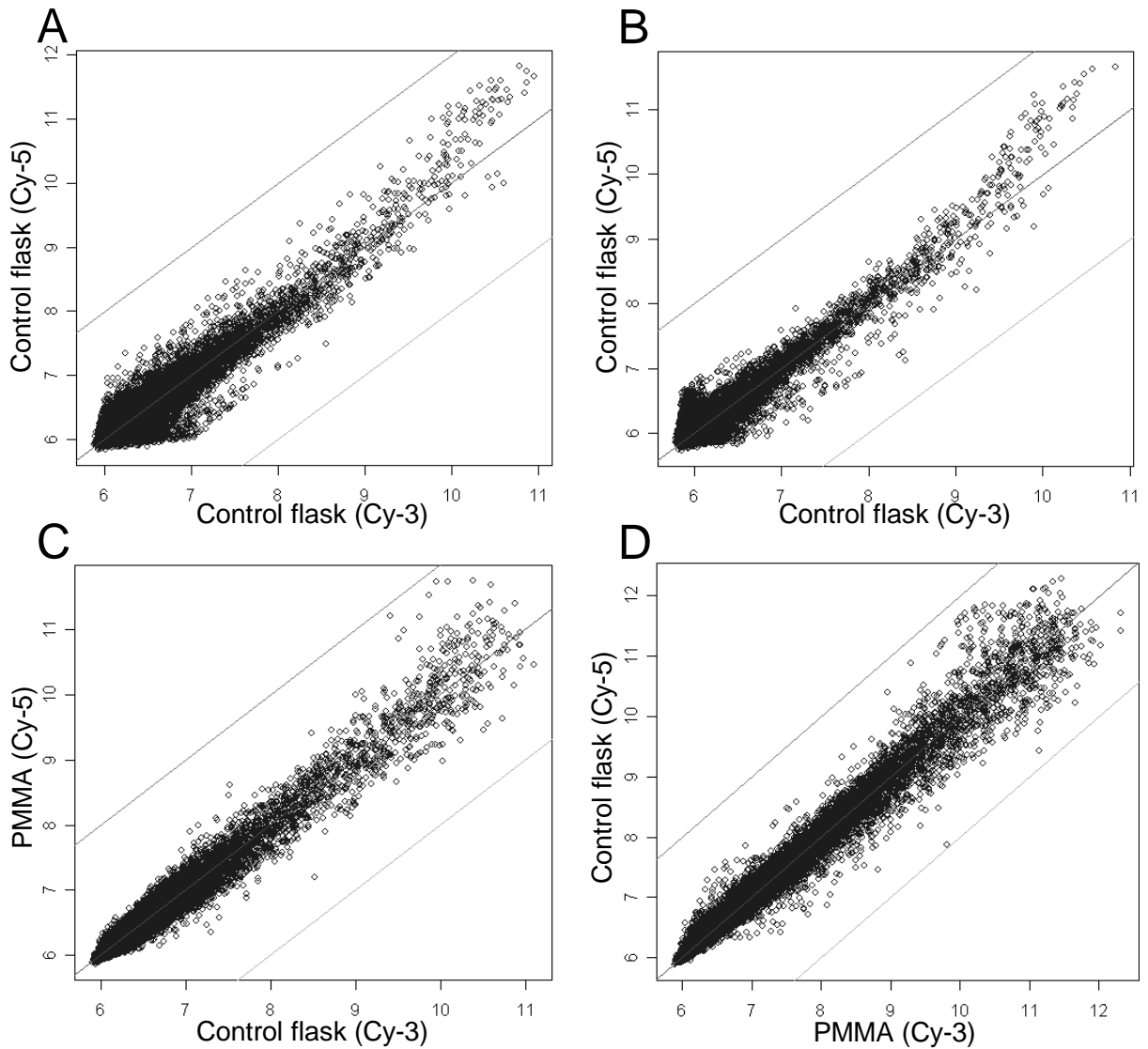
The entire experiment was repeated with the order of the dyes reversed. Furthermore two arrays were hybridized with cDNA originating from the same pool of aRNA isolated from cells cultured in the culture flask. These two self-self hybridizations served as a measure of the amount of noise to be expected in hybridizations involving cDNA originating from different sources of RNA.

Following quantification of the data, the  $\log_2$  values of the data was plotted in a scatter plot with the  $\log_2$  values of the Cy-3 labeled cDNA on the x-axis and the  $\log_2$  values of the Cy-5 labeled cDNA on the y-axis (Figure 38). Transcripts having the same intensity of Cy-3 and Cy-5 would lie on a straight median line passing through the points (0,0) and (1,1). Hybridizations in which a transcript is more abundant in the cDNA pool incorporated with Cy-5 would have a larger intensity in the Cy-5 channels relative to the Cy-3 channels and will hence lie above the median line. Hybridizations in which a transcript is less abundant in the cDNA pool incorporated with Cy-5 would have a smaller intensity in the Cy-5 channels relative to the Cy-3 channels and will hence lie below the median line.



**Figure 38: Non normalized scatter plots from whole human genome expression profiling of HeLa cells cultured on PMMA.** All cDNA reactions were primed with random nonamer primers. Prior to hybridizations, cDNA pools were normalized to 200 pmol of incorporated Cy-dye. **(A-B)** Self-self hybridizations of HeLa cells cultured in the culture flask for 4 days. The same pool of aRNA was used as template for all cDNA reactions for the self-self experiments. The upper and lower line represent a fold change of 3 up and down, respectively. The central line is the median. **(C)** Co-hybridizaion of cells cultured on PMMA and cells cultured in the reference culture flask. **(D)** The experiment in **(C)** was repeated with the order of the dyes reversed.

The plots in Figure 38 indicated that data appeared non-linearly skewed. This most likely originates from the two Cy-dyes having different physical properties. To compensate for this the data was normalized using Qspline<sup>128</sup> which is a non-linear normalization method in which cubic splines are fitted to the data and systematic errors are removed (Figure 39).



**Figure 39: Normalized scatter plots from whole human genome expression profiling of HeLa cells cultured on PMMA.** The raw data (Figure 38) was normalized using Qspline. **(A-B)** Self-self hybridizations of HeLa cells cultured in the culture flask for 4 days. The upper and lower line represent a fold change of 3 up and down, respectively. The central line is the median. **(C)** Co-hybridization of cells cultured on PMMA and cells cultured in the reference culture flask. **(B)** The experiment in **(D)** was repeated with the order of the dyes reversed.

The self-self hybridization results indicated that whole genome expression profiling of cDNA reverse transcribed from the same pool of RNA yielded very similar looking scatter plots (Figure 39 A-B) indicating the robustness of the method. Inspection of the data showed that no transcripts were found more than three fold regulated. However, 37 transcripts were more than 2 fold regulated, indicating the need for a more conservative 3-fold cut-off to reduce the number of false positive results.

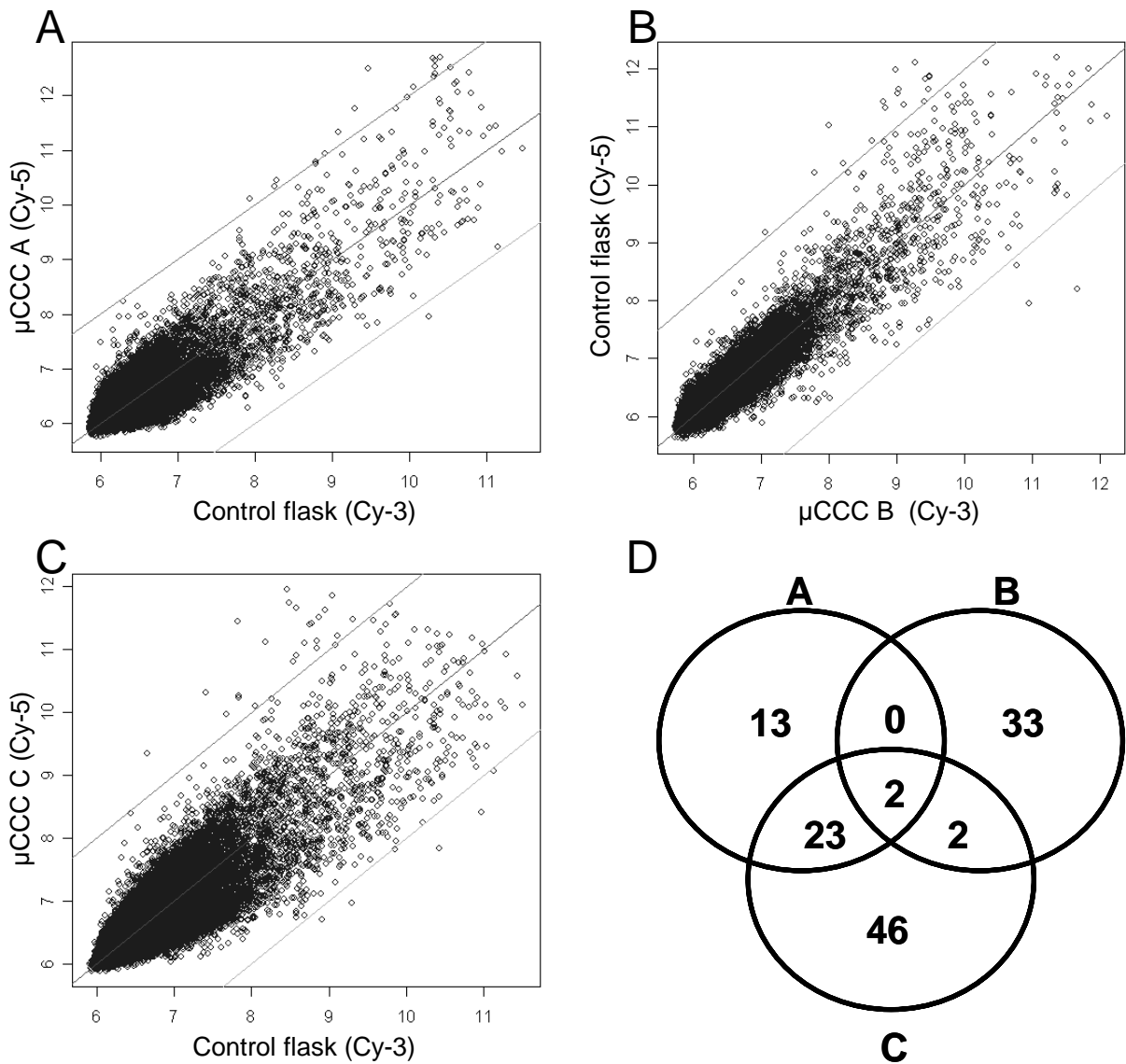
Cells cultured on PMMA were found to have a whole genome expression profile indistinguishable from that of cells cultured in the reference cell culture flask (Figure 39 C-D). No transcripts were found more than three fold regulated. Using a 2 fold regulation as cut-off resulted in 85 transcripts being significantly regulated. However, statistical analysis revealed that no transcript was more than 2 fold regulated with a P-value less than 0.05 (data not shown). This indicated that PMMA did not induce reproducible identifiable effects on the evaluated HeLa cell line.

### **Whole genome expression profiling of $\mu$ CCC cultured cells**

Seeking to elucidate if culturing of HeLa cells in the  $\mu$ CCC gave rise to a different whole genome expression profile relative to comparable cells cultured in culture flasks in the CO<sub>2</sub> incubator, cells from three independent cultures each lasting more than 100 hours (Figure 19) were isolated from both the  $\mu$ CCC and the corresponding culture flasks. Following isolation of total RNA, RNA amplification and reverse transcription utilizing random pentadecamer priming<sup>129</sup> the labeled cDNA was hybridized to whole human genome DNA microarrays (Figure 40).

Visualization of the number of significantly regulated genes was performed by using a Venn diagram (Figure 40 D) where each hybridization experiment was depicted as a circle containing the number of significantly regulated transcripts relative to the culture flask. Transcripts regulated more than three-fold on more than one array were depicted in the overlapping region(s) of the representative circles. Two transcripts were found regulated on all three arrays and were listed in Table 2.





**Figure 40: Whole human genome expression profiling of cells cultured in the  $\mu$ CCC.** (A-C) Qspline normalized scatter plots obtained from three independent culture experiments in the  $\mu$ CCC and the culture flask. (D) A Venn diagram was utilized depicting each array as a circle enclosing the number of more than three fold regulated genes (up and down) relative to the culture flask. The number of genes similarly regulated on more than one array was placed in the overlapping region of the corresponding circle(s).

The Venn diagram (Figure 40 D) indicated that 23 transcripts were three-fold or more regulated in both culture A and C while only 2 transcripts were more than three-fold regulated in both culture B and C. No transcripts other than the two regulated in all three cultures were more than three fold regulated in culture A and B. Inspection of the order of dye incorporation (Figure 40 A-C) revealed that cDNA derived from  $\mu$ CCC cultured cells A and C was labeled with Cy-5 while culture B was labeled with Cy-3. This may indicate that some of the transcripts found more than three fold regulated in both culture A and C results from dye dependant effects as they were removed when the order of the dyes were reversed.

**Table 2: The two transcripts regulated more than three fold on all three arrays.** The average fold change is calculated as the average fold change for cells cultured in the  $\mu$ CCC divided by the average fold change for cells cultured in the control flask. Blast searches on the probe sequences revealed that probe number Probe number A\_32\_P162760 had a perfect match to the Ataxin 10 gene while probe number A\_23\_P141785 yielded no additional information.

Probe name	Gene Name	Average fold change	Genbank entry	Description	Probe Sequence
A_32_P162760	BI003432 (ATXN10: Ataxin 10)	0.25	BI003432 AI873036 AI364565 D80033 NM_013236	PM0-HN0073- 080201-005- d02_1 HN0073 Homo sapiens cDNA, mRNA sequence	TATTCTTTAAATGCAC GTTCTATCCAGGGGG ACAAAGGCAAACCAC ACAGTTACATTAAT
A_23_P141785	A_23_P141785	5.0	AC025018	Homo sapiens chromosome 18, clone RP11- 320C19, complete sequence.	TGCTTTTGGTGTTTTA GACGTGAAGCCTTTC CCATACCTATGCACTG AATGGTAATGCC

No additional information regarding the two transcripts was found by Blast searches indicating that the function of transcripts may still be unknown.

For the determination if the scattering was a result of experimental variation or a reproducible effect of the  $\mu$ CCC the data was statistically compared using the t-test. For this analysis the fold change calculated as the normalized intensity obtained from the  $\mu$ CCC cultured cells divided by the normalized intensity of the culture flask cultured cells of each transcript from each array was averaged. This average was compared to the null hypothesis that the fold change was 1 *i.e.* no regulation of the transcript. Transcripts found regulated more than three fold with  $P < 0.05$  were considered significant and listed in Table 3. Blast searches performed on the probe sequences failed to reveal the biological functions of the regulated transcripts.

**Table 3: Statistical analysis of the whole genome expression data from  $\mu$ CCC culturing of HeLa cells.** The data was averaged and tested against the null-hypothesis (a fold change of 1) corresponding to no regulation using the t-test.

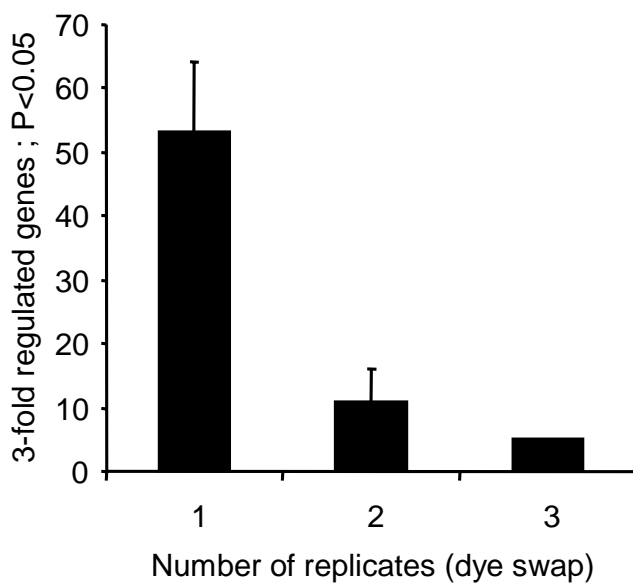
Probe name	Gene Name	Average fold change	P-Value	Genbank entry	Description	Probe Sequence
A_32_P162760	BI003432 (ATXN10: Ataxin 10)	0.25	2.28E-05	BI003432 AI873036 AI364565 D80033	PM0-HN0073 Homo sapiens cDNA, mRNA sequence	TATTCTTTAAATGCA CGTTCTATCCAGGG GGACAAAGGCAAAC CACACAGTTACATT AAT
A_23_P119407	A_23_P11 9407	3.01	0.0121	AC007785	Homo sapiens chromosome 19, BAC 282485 (CIT- B-344H19), complete sequence.	CATTTATCTTGCTTG GTGTTCTCTGAGCTT CCTGGATCTGTGGTT TGGTGTCTGACATG A
A_32_P175313	BF960555 (TNRC6B)	3.28	0.0154	BF960555	PM1-NN1207 Homo sapiens cDNA, mRNA sequence (Trinucleotide repeat containing 6B).	TACTCAAGGGGTG TGTATGTGTGTGCT GAACCAAGAAAGGT TGAGAGCTCCAGGT ATT
A_23_P141785	A_23_P14 1785	5.02	0.0422	AC025018	Homo sapiens chromosome 18, clone RP11-320C19, complete sequence.	TGCTTTTGGTGTTTT AGACGTGAAGCCTT TGCCCATACCTATGC ACTGAATGGTAATG CC

The result indicated that 4 transcripts statistically were more than three fold regulated with a P-value less than 0.05. Of these 4 transcripts 2 were also identified using solely comparison of more than 3 fold regulated genes in the Venn diagram (Figure 40 D). No additional information was obtained from Blast searches on the probe sequences from the two additional transcripts identified with the t-test. This may indicate that no function has been assigned to the transcripts yet.

### Dye-swap replicates

As the properties of in terms of photo stability, quantum efficiency, of the dyes Cy-3 and Cy-5 are quite different, a bias between the two channels will occur. During gene expression studies this may lead to false positive results. One way to identify these false positive results is to repeat the experiment with the order of the dyes reversed – dye-swap. As transcriptome

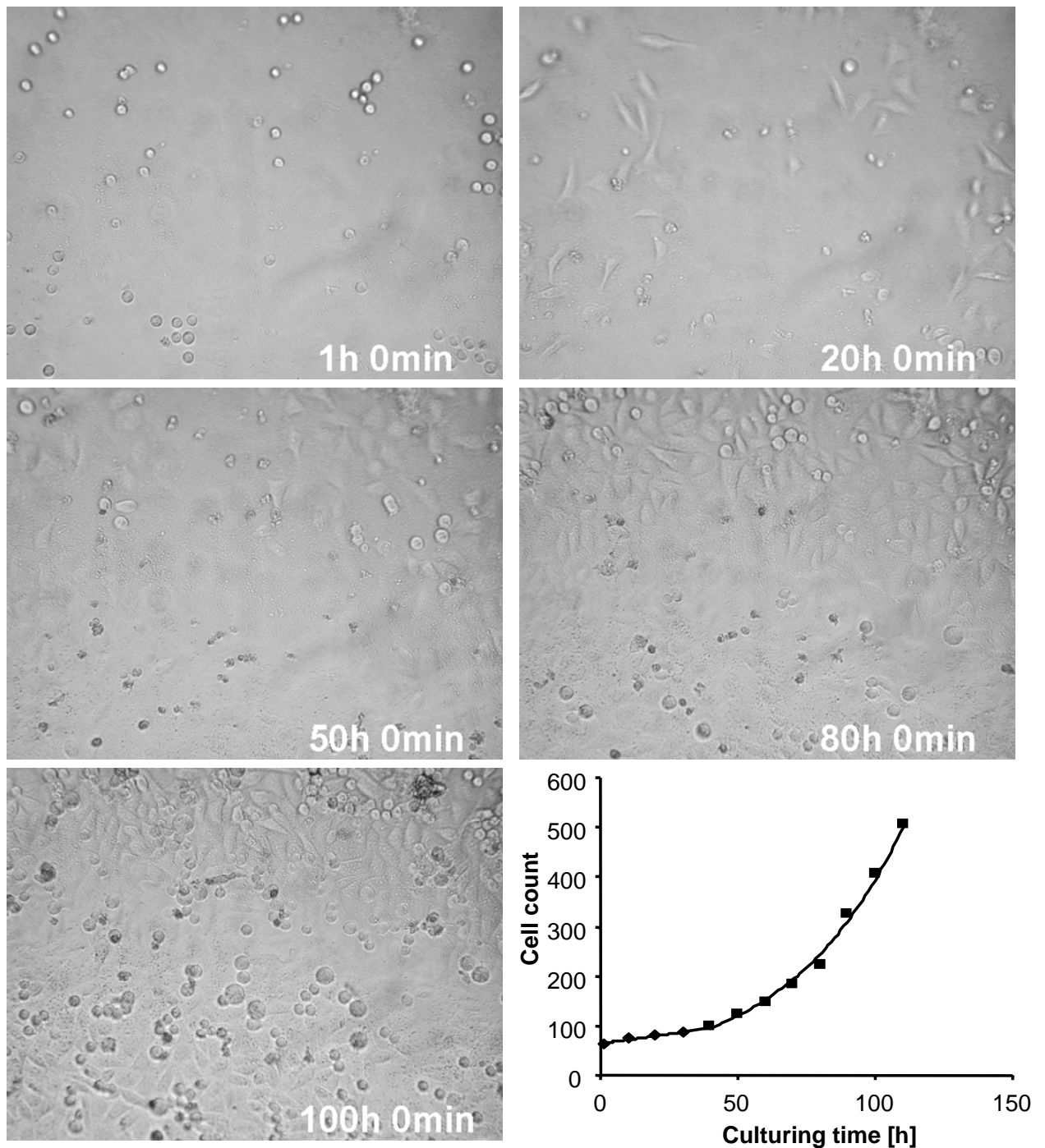
microarrays are quite costly it is desirable to use as few replications of the experiment as possible. Hybridization to transcriptome arrays using cDNA generated from RNA isolated from cells cultured in the  $\mu$ CCC and the culture flask was performed three times (Figure 40). Inspection of the raw data with respect to the number of genes regulated more than three-fold on the different arrays indicated that repeating the experiment once with the orders of the dyes reversed reduced the number of significant genes from  $53 \pm 10$  to  $11 \pm 5$  (Figure 41). A third replication further reduced the number of significant genes to 5. Combined this indicates the need for performing at least one dye-swap replication of microarray experiments when the results are not validated by *e.g.* Western blotting or real-time PCR.



**Figure 41: Effect of dye-swap replicates on the number of significant genes.** Three separate hybridizations to whole human genome arrays were performed, each co-hybridizing 200 pmol of Cy-3 and Cy-5 incorporated cDNA. The number of genes more than three fold regulated on each array was counted. Using the t-test and the null hypothesis that the fold change was equal to one the P-values were computed. The error bars represent the standard deviation.

## CACO 2 cells

Attempting to clarify if the  $\mu$ CCC could sustain culturing of other cell types than the more common HeLa cell line, a human Caucasian colon adenocarcinoma cell line displaying epithelial morphology isolated from a primary colonic tumor in a 72-year-old male using the explant culture technique<sup>130</sup>, denoted CACO 2 was seeded in the  $\mu$ CCC using similar techniques as for the HeLa cell line.

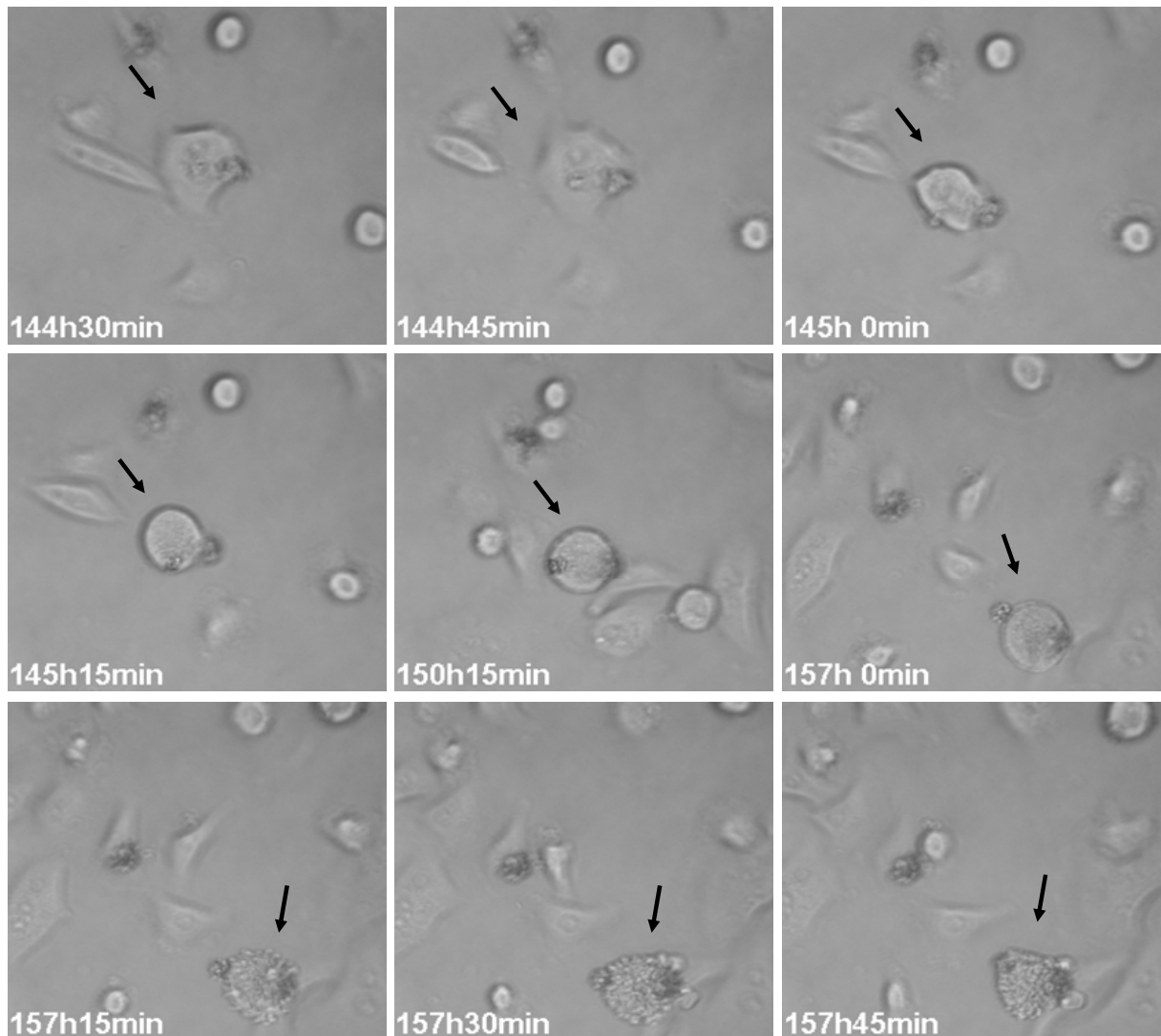


**Figure 42: Culturing of CACO 2 cells in the  $\mu$ CCC.** Images were obtained using a 15 minute increment over a 110 hour culturing period. Following roughly 40 hours of lag time ( $\blacklozenge$ ) exponential growth ( $\blacksquare$ ) commenced. Cell counts were performed at selected time intervals and an exponential regression line ( $R^2=0.9926$ ) was fitted to through the data points. A movie of the entire culturing experiment is available on the accompanying data disc (Movie 4).

The results indicated that the doubling time of the CACO 2 cell line in the  $\mu$ CCC was 34 hours. The doubling time of CACO 2 cells have previously been reported to be between 24

and 34 hours and increasing with the passage number of the cells <sup>131</sup>, indicating that culturing of CACO 2 cells in the  $\mu$ CCC does not significantly influence the doubling time.

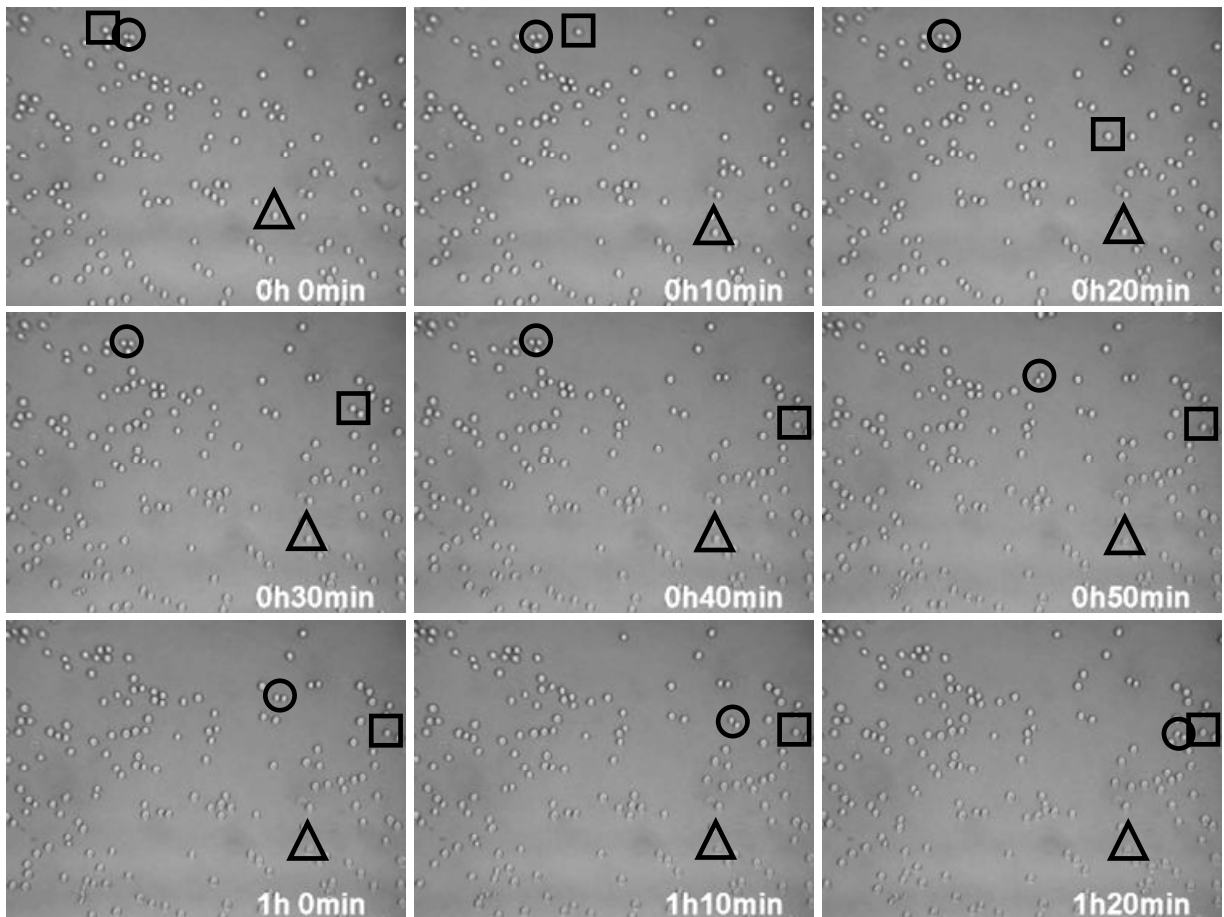
Cell death appeared similar in the CACO 2 cell line as in the HeLa cell line. The dying cell would detach from the surface, swallow in size and look like a freshly passed cell only larger for several hours prior to cell lysis (Figure 43). The time this CACO 2 cell was observed to remain detached from the surface was significant longer than the HeLa cell (Figure 24) which remained detached from the surface around 5 hours prior to cell lysis.



**Figure 43: Death of a CACO 2 cell.** The black arrow indicates the dying cell. Prior to death, a CACO 2 cell would detach from the surface.

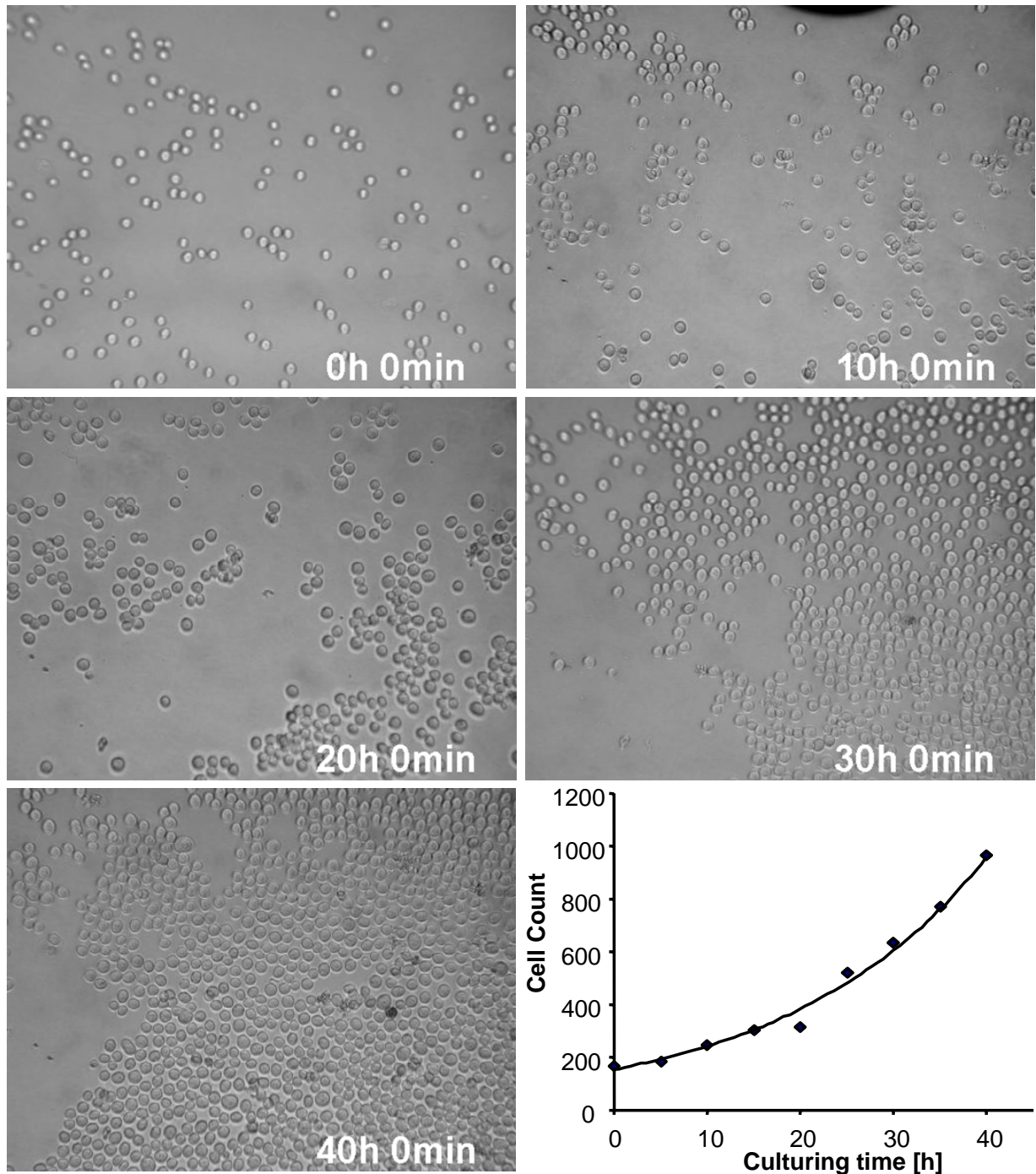
## Colon 205 cells

Another colon cancer cell line isolated from ascitic fluid of a 70 year old Caucasian male with carcinoma of the colon having a round and refractile morphology, denoted COLO 205<sup>131</sup> was used to test the versatility of the  $\mu$ CCC to provide culture conditions which could facilitate proliferation of other mammalian cells lines (Figure 44).



**Figure 44: Culturing of the COLO 205 cell line in the  $\mu$ CCC.** Images were grabbed with 5 minutes increment throughout the entire culture experiment which lasted more than 115 hours. The figure displays images with 10 minutes increment of the first 120 minutes of the culturing. Three cells are indicated with a triangle, a square or a circle enabling the visualization of cellular movement over time. The time stamp in the lower right corner indicated the elapsed time post seeding.

Inspection of the images obtained from culturing of the COLO 205 cell line frame by frame indicated an unusually high degree of mobility (Figure 44). Opposed to the HeLa and the CACO 2 cell line, the COLO 205 cells appeared to move around the surface forming aggregates of cells. Long term culturing of COLO 205 cell line indicated that the  $\mu$ CCC was capable of providing conditions suitable for culturing of this cell line (Figure 45). The results also indicate the high degree of mobility can be studied in greater detail using the  $\mu$ CCC.



**Figure 45: Culturing of COLO 205 cells in the  $\mu$ CCC.** The graph illustrates the cell count at selected time points. An exponential regression line ( $R^2=0.9837$ ) was fitted to through the data points. A movie of the first 50 hours of culturing is available on the accompanying data disc (Movie 5).

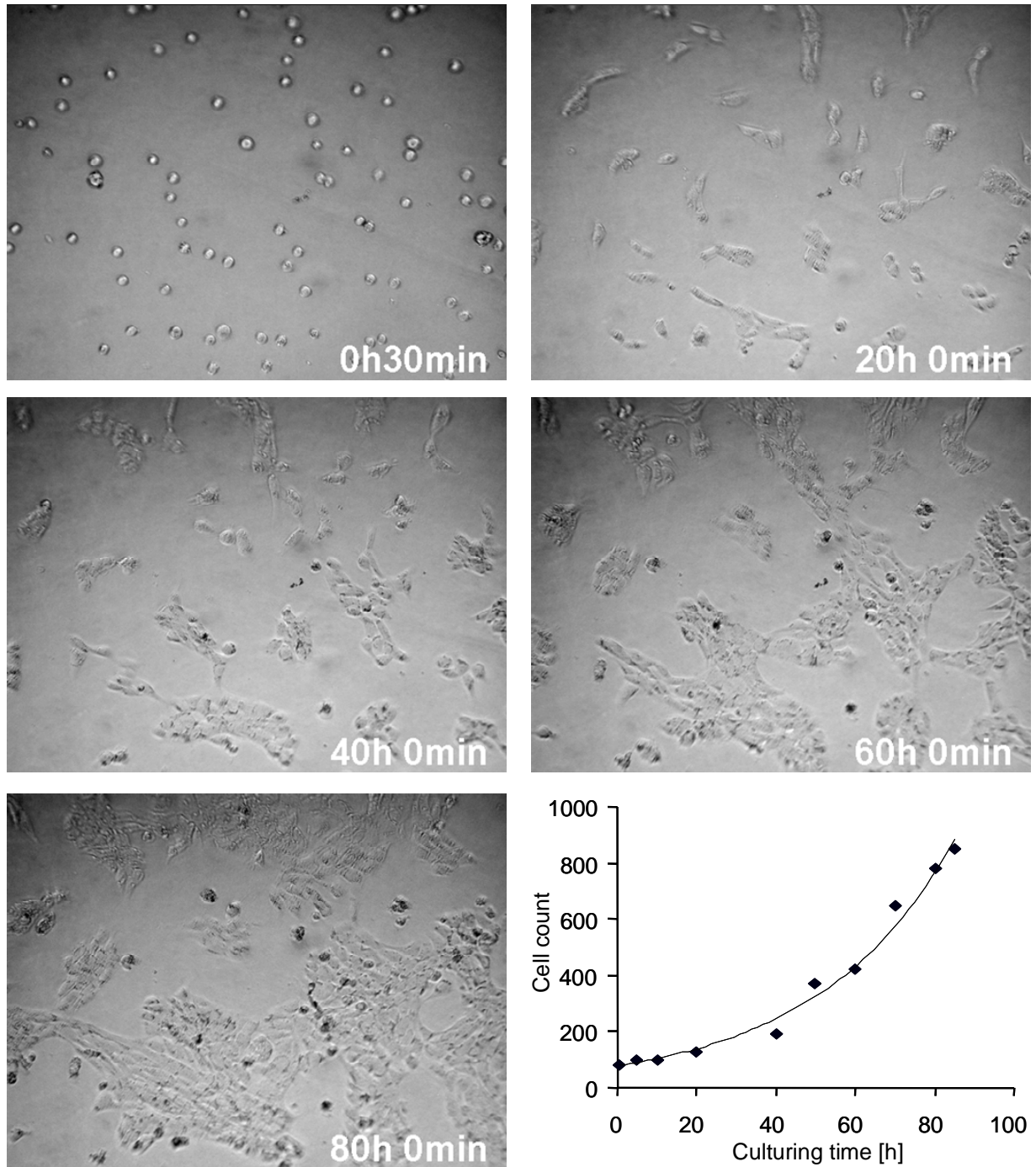


The high degree of mobility of this cell line possibly hampered estimation of cell growth rates utilizing counting of cells at selected time intervals. The doubling time was estimated to be 15 hours which seem unrealistic fast, supporting that the mobility of the cell line hampers the estimation of growth rate utilizing this method. Following confluence which was achieved after 50 hours, the cells were still proliferating on top of the initial layer of cells until the experiment was stopped after 115 hours of culturing. Cell death appeared to follow the same traits like the HeLa and the CACO 2 cell line. Prior to death, the cell would swell in size and remain large for several hours prior to a rapid lysis.

### **Stem cells**

Stem cells are undifferentiated cells that give rise to of the body's cells and organs. Stem cells are by many are considered to be hold the key for successful treatment of many diseases or disorders. On-line monitoring might help elucidate the morphological changes accompanying both the proliferation and the differentiation of these cells in response to changes in either media composition or culturing conditions. Furthermore, changes in proliferation rate or viability might also be compared to concentration of various media components. As the  $\mu$ CCC seemed an ideal platform for testing and further development of stem cell assays, initial culturing experiments were performed in order to prove the flexibility and the power of this platform. Two different stem cell lines were tested in the  $\mu$ CCC, human Neuronal Stem Cells (HNSC.100 or hNS1)<sup>132</sup> and hNS1 transfected with Bcl-X<sub>L</sub><sup>133</sup> respectively. The latter was for simplicity denoted Bcl-X<sub>L</sub>. The hNS1 clone was an EGF/bFGF-dependent cell line of human progenitor cells derived from the telencephalic and diencephalic regions of a 10-10.5 week of gestation old human Caucasian embryo. The clone was genetically perpetuated using v-myc. Removal of the growth factors EGF and FGF-2 would result in differentiation of the cells. No attempt was made to differentiate the cells. Both cell lines have a doubling time in the range of 40 hours depending on cell density and growth auto regulation by secretion of growth-influencing factors and/or cell-cell contact. The Bcl-X<sub>L</sub> transfected cells were passage 40 and the un-transfected hNS1 clone was passage 61.

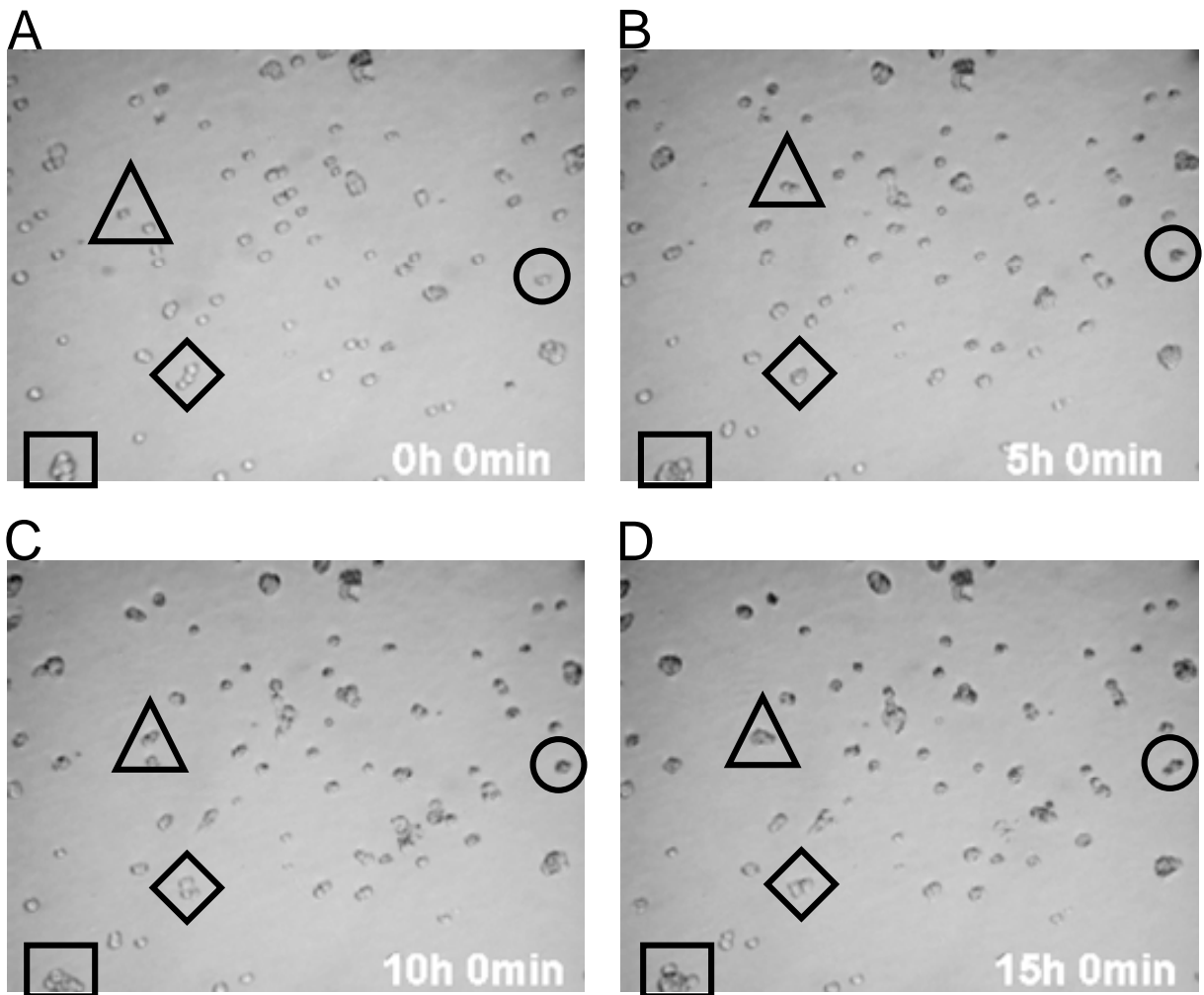
Experience from culturing of hNS1 cells in culture flasks, indicated that coating of the culture flask surface with poly-L-lysine (PLL) resulted in significant better culturing conditions. A  $\mu$ CCC was coated with PLL prior seeding of the  $\mu$ CCC with freshly passaged hNS1 cells (Figure 46).



**Figure 46: Culturing of hNS1 in PLL treated  $\mu$ CCC.** The  $\mu$ CCC was prior to seeding with hNS1 cells incubated with 20 mg/mL PLL in PBS for three hours in the  $\text{CO}_2$  incubator. Following UV-treatment for 30 minutes in the LAF bench the  $\mu$ CCC was flushed with 10 mL PBS for removal of unbound PLL remnants. The  $\mu$ CCC was connected to the electronics and the PBS was replaced with culturing media. After archival of steady state temperature, hNS1 cells were gently seeded to an acceptable density determined by visual inspection of the chamber. Cell counts were performed at selected time intervals and an exponential regression line ( $R^2=0.9866$ ) was fitted to through the data points. A movie of the entire culturing experiment is available on the accompanying data disc (Movie 6).

The results indicated that PLL treated PMMA supported culturing of hNS1 cells over long periods of time. The culturing was stopped after 90 hours of culturing when the  $\mu$ CCC was almost confluent. The doubling time was slightly above 25 hours indicating a faster growth than the previously reported 40 hours<sup>110</sup>. The faster generation time possibly arises from the continuous perfusion of fresh growth factor containing media conceivably increasing the availability of growth factors to the cells. As removal of growth factors from the media would result in differentiation of the cells this was not attempted. If continuous perfusion reduces the concentration requirements for growth factors, this hypothesis could easily be verified experimentally.

As culturing of HeLa, CACO 2 and COLO 205 has successfully been performed on unmodified PMMA, it was sought to investigate if the unmodified PMMA surface of the  $\mu$ CCC could sustain cell culturing of hNS1 stem cells (Figure 47).



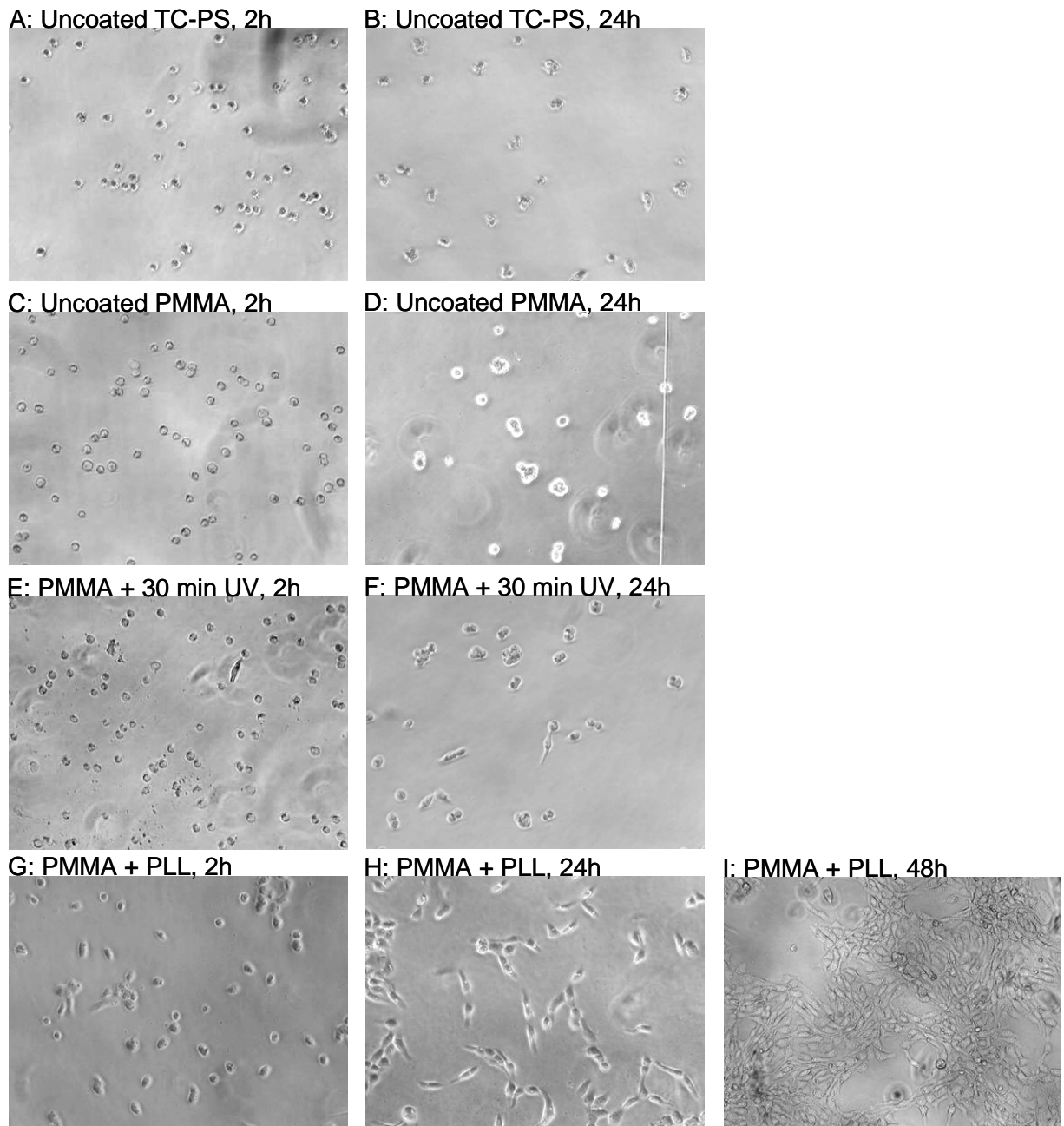
**Figure 47: Culturing of hNS1 stem cells in the unmodified  $\mu$ CCC.** Pictures were obtained with five minutes increment over almost 17 hours of culturing. (A) Immediately after seeding of cells. (B) Five hours post seeding. (C) Ten hours post seeding. (D) Fifteen hours post seeding. Moving cells are indicated with various shaped figures. A movie of the entire culturing experiment is available on the accompanying data disc (Movie 7).

---

The culturing was followed for almost 17 hours after which it was concluded that no real attachment had occurred and the cell morphology did not resemble the PLL coated  $\mu$ CCC (Figure 46 and Figure 47). The culturing was hence abandoned. The results indicated that the unmodified  $\mu$ CCC did not support culturing of the hNS1 cells. There were occasional few signs of cell attachments indicated by elongations of the cell rather than spreading. However, upon inspection of the grabbed images frame by frame, clear indications of cellular movement was observed. Some indications of this were highlighted with various geometrical shapes on Figure 47. This indicated the cells were alive but not attached and proliferating. Cell movement can be observed *e.g.* by comparing the image obtained ten hours post seeding (Figure 47 C) with the image obtained fifteen hours post seeding (Figure 47 D).

During the PLL treatment the surface was exposed to UV-light for 30 minutes. Attempting to elucidate if this step alone was responsible for the enhanced biocompatibility observed after PLL coating, a piece of PMMA was divided in three. The one part was used directly without modification after being sterilized. The two other pieces was subjected to the PLL treatment, substituting the PLL solution with PBS on one of the two pieces, which served as a control for the significance of the PLL. The unmodified surface of the TC-PS culture plate served as an additional control. Following seeding of hNS1 cells the culture plates were incubated for 2 hours in the CO<sub>2</sub> incubator after which they were inspected (Figure 48).

Following 24 hours of incubation in the CO<sub>2</sub> incubator the culture plates were inspected again (Figure 48). The results indicated that only the PLL treated PMMA supported growth of the hNS1 cells. No signs of attachment were observed on the unmodified PMMA and the unmodified culture plate (Figure 48 A-D) supporting the  $\mu$ CCC culture experiment (Figure 46 and Figure 47). The UV-treated PMMA showed some signs of attachment (Figure 48 E-F) but the extent of attachment were significantly less than the PLL coated PMMA (Figure 48 G-H) indicating the significance of the PLL in the coating. As neither the unmodified PMMA, the UV exposed PMMA nor the conventional TC-PS surfaces yielded acceptable culturing conditions they were abandoned after one day of incubation. However, PLL coating of the PMMA followed by UV-treatment did have a significant positive effect (Figure 48 G-I). The morphology of the hNS1 cells on PLL coated PMMA resembled the morphology of hNS1 cells on PLL coated TC-PS indicating the two surfaces might be comparable.

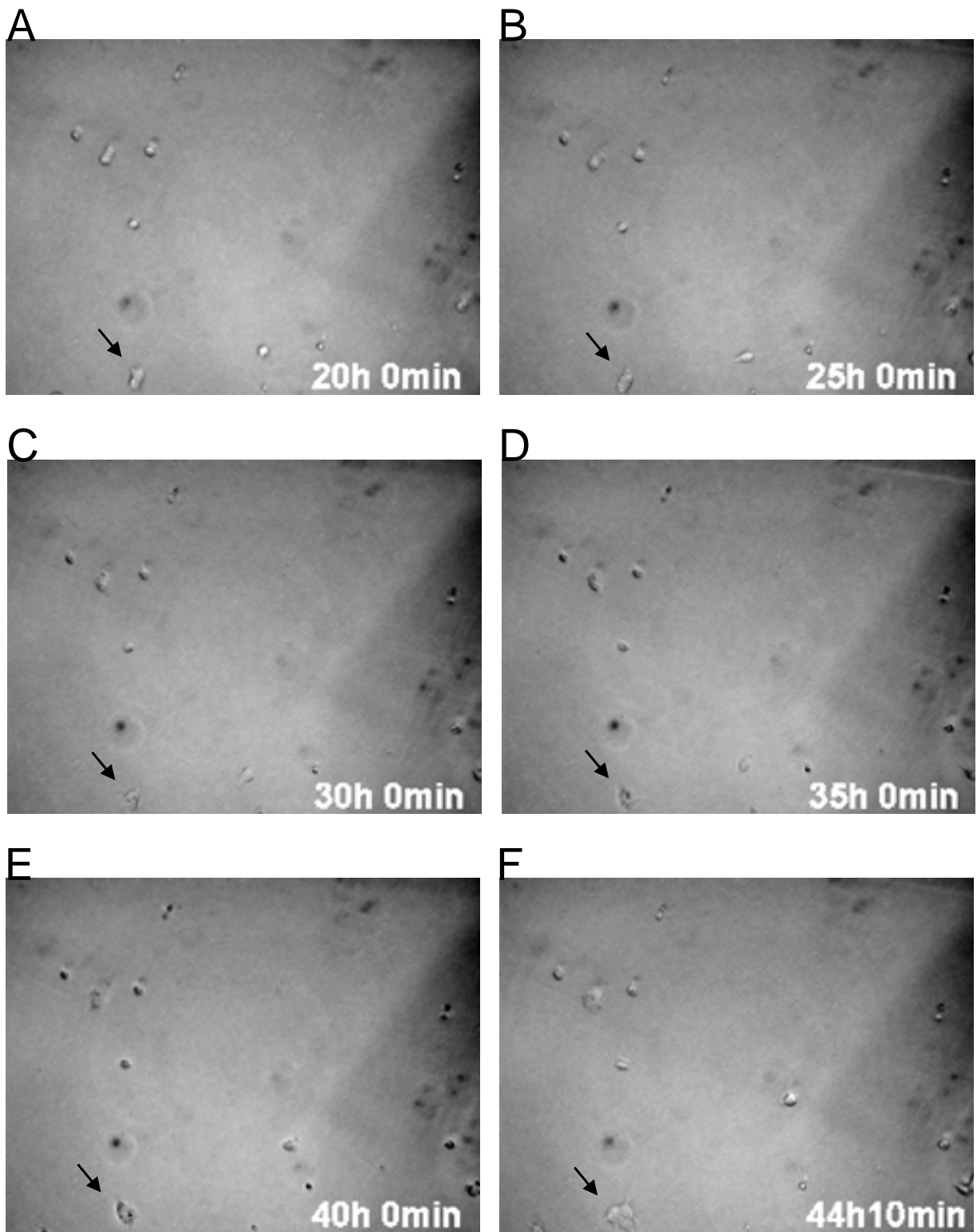


**Figure 48: Culturing of hNS1 cells on modifications of the PMMA surface.** The experiments were performed simultaneously in four well culture plates. All wells contained the same media both on amount and composition and were seeded with equal amount of cells. All images were obtained using 10 x magnifications, except (I) in which 5 x magnification was used. **(A)** Uncoated TC-PS culture well 2 hours post seeding. **(B)** Uncoated TC-PS culture well 24 hours post seeding. **(C)** Unmodified PMMA 2 hours post seeding. **(D)** Unmodified PMMA 24 hours post seeding. **(E)** PMMA exposed to 30 minutes of UV light 2 hours post seeding. **(F)** PMMA exposed to 30 minutes of UV light 24 hours post seeding. **(G)** PMMA exposed to PLL treatment (20  $\mu$ g per mL for 2 hours followed by 30 minutes of UV treatment, washed in milliQ water and dried) 2 hours post seeding. **(H)** PMMA exposed to PLL treatment, 24 hours post seeding. **(I)** The PLL coated PMMA surface was further inspected two days post seeding.

Culturing of the Bcl-X<sub>L</sub> transfected hNS1 cells was attempted in the  $\mu$ CCC utilizing a faster and less cumbersome coating, polyethyleneimine (PEI) coating. Freshly passaged Bcl-X<sub>L</sub> cells were seeded in a freshly coated  $\mu$ CCC. Following 19 hours of culturing no cell movement or attachment was observed. Upon repositioning of the  $\mu$ CCC several attached cells were observed. The culturing was continued with the  $\mu$ CCC repositioned (Figure 49).

The results indicated the  $\mu$ CCC was capable of supporting culturing of Bcl-X<sub>L</sub> stem cells for more than forty hours (Figure 49). Several cell divisions were observed. On Figure 49 a group of cells are highlighted with an arrow. Initially after 20 hours of culturing two distinct cells are visible. During the culturing these cells would proliferate and following 44 hours of culturing three attached cells are visible.

Combined this indicates that the  $\mu$ CCC is capable of sustaining long term culturing of HeLa, CACO 2, COLO 205 and hNS1 cells. The results also indicate that changes in the molecular structure or composition of the surface might be of importance for cell proliferation.

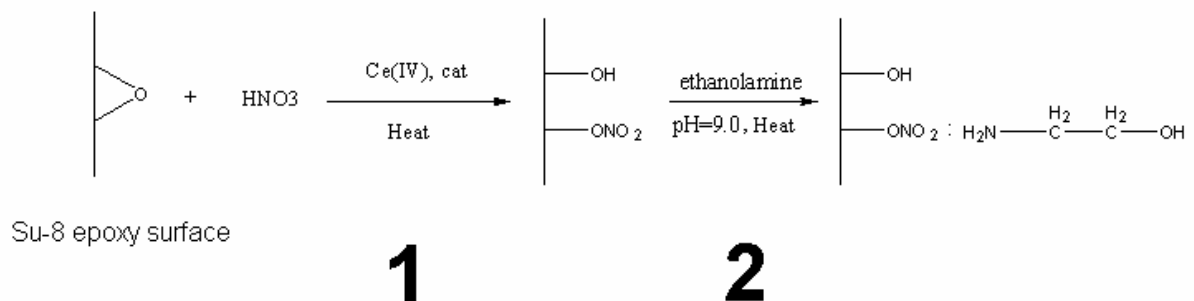


**Figure 49: Culturing of Bcl-X<sub>L</sub> stem cells in the  $\mu$ CCC.** Pictures were obtained with five minutes increment over almost 45 hours of culturing. The arrows indicates proliferating cells. **(A)** 20 hours after seeding of cells. **(B)** 25 hours post seeding. **(C)** 30 hours post seeding. **(D)** 35 hours post seeding. **(E)** 40 hours post seeding. **(F)** 44 hours and 10 minutes hours post seeding. A movie of the entire culturing experiment is available on the accompanying data disc (Movie 8).

## ***Biocompatible surfaces for use in microfabrication***

As the resolution attainable with laser ablation is larger than  $100\ \mu\text{m}$ <sup>134</sup>, photolithography is required for realization of smaller feature sizes. SU-8 is an epoxy-based negative constructional photoresist widely used for fabricating microstructures in various micro total analysis system ( $\mu\text{TAS}$ ) devices<sup>135-140</sup> because of its excellent chemical stability, optical properties and fast fabrication process<sup>141</sup>. However, the SU-8 epoxy surface is not biocompatible<sup>142</sup>. Not only cell adhesion and culturing is hampered in the SU-8 based microsystems, but also the PCR reaction is inhibited in the SU-8 structured reaction chamber<sup>142</sup>. Chemical treatments have the potential to modify the SU-8 surface properties for extended time periods, and can easily be combined with other micro fabrication processes. The epoxy rings on the SU-8 surface are generally not reactive with standard corrodents (*e.g.*, tetrahydrofuran (THF), HCl or  $\text{HNO}_3$ ), resulting in the pronounced chemical stability of SU-8<sup>143</sup>.

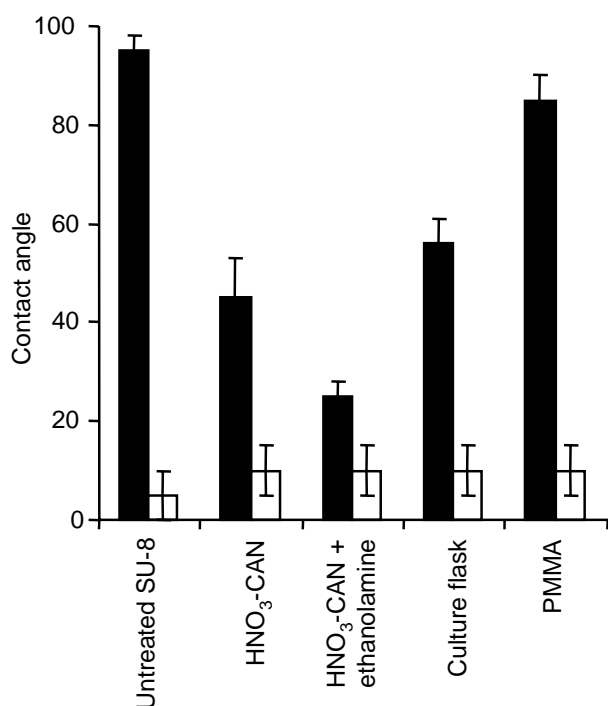
SU-8 was investigated for its use as a cell culture surface and compared to tissue culture quality polystyrene (TC-PS) cell culturing flasks. SU-8 as well as PMMA are highly hydrophobic suggesting that they may be less suitable for cell growth<sup>42,43</sup>. Therefore, a method was sought developed to modulate the hydrophobicity of SU-8. A simple two-step chemical surface treatment resulted in a hydrophilic SU-8 surface. The assumed chemical reaction mechanism of the protocol is shown in Figure 50. The  $\text{HNO}_3$ -CAN treatment opens the SU-8 epoxy groups and converts them into nitro groups<sup>144</sup>. This surface can subsequently be modified with ethanolamine<sup>111</sup>.



**Figure 50: Proposed reaction scheme of the two-step SU-8 surface modification:** 1: The epoxy ring on the SU-8 surface is believed to be opened by treatment with  $\text{HNO}_3$ -CAN; 2: The nitro radical on the modified SU-8 surface reacts with the amino group of ethanolamine.



The water contact angle was measured on the differently modified SU-8 surfaces, PMMA and TC-PS cell culturing flasks. Treatment of SU-8 with HNO<sub>3</sub>-CAN decreased the contact angle from 95 ° to 45 ° (Figure 51). The HNO<sub>3</sub>-CAN treated SU-8 surface was chemically stable. It tolerated an ultrasonic agitation lift off process of photoresist in acetone. The contact angle of SU-8 could be decreased to 25 ° by treating SU-8 first with HNO<sub>3</sub>-CAN and subsequently with ethanolamine. Ethanolamine had no effect on the contact angle without the initial HNO<sub>3</sub>-CAN treatment. The contact angle of the treated SU-8 surface returned to 50° after storage at room temperature for two months. In comparison, the contact angle of a PMMA sheet was 85 ° and the TC-PS cell culturing flask was 56 ° (Figure 51). These two surfaces served as control surfaces for the study of the differently treated SU-8 surfaces. As contact angles measured on a dry surface hardly reflects the environment encountered by the cells during culturing, the different surfaces were immersed in cell culture media and incubated for 24 hours under cell culturing conditions. After drying under a gentle stream of N<sub>2</sub>, all surfaces had a contact angle with water less that were less than 15 °, indicating protein adsorption took place on all surfaces (Figure 51).

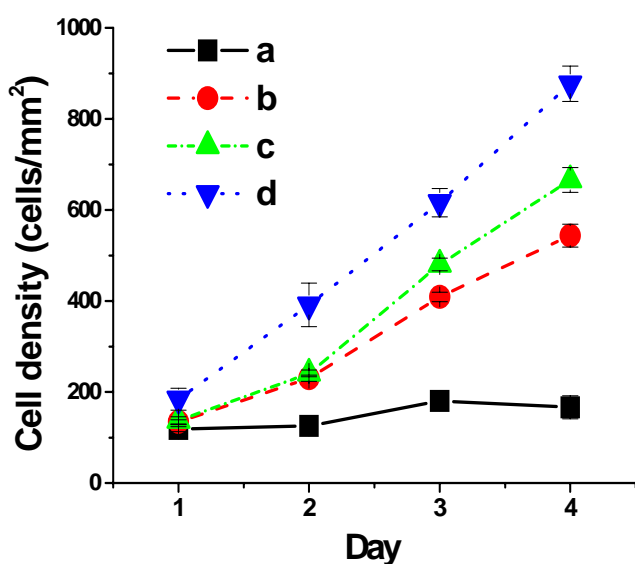


**Figure 51: Water contact angles of different surfaces.** The hydrophobicity of differently surfaces was determined by measuring the contact angle of water. Solid columns represent measurements performed on surfaces prior to incubation with cell culture media. Hollow columns represent water contact angles on surfaces after incubation with cell culture media under culturing conditions (37 °C, 5 % CO<sub>2</sub>) in the incubator for 24 hours. Prior to measuring the contact angles, surfaces were dried under a gentle stream of N<sub>2</sub>.

### Morphology and growth characteristics

The five different surfaces (Figure 51) were tested for biocompatibility by comparing cell morphology and growth characteristics. HeLa cells were seeded on the different surfaces and

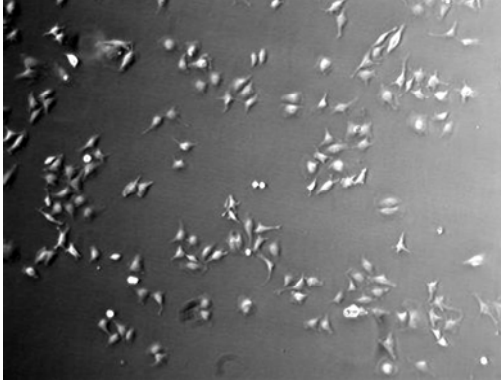
the cell density was determined throughout a four day period. Untreated SU-8 had a very low doubling time of  $147 \pm 56$  hours indicating an unusual slow growth compared to the reference cell culture flask that had a doubling time of  $32 \pm 0.9$  hours (Figure 52). The images suggested that the few cell attaching to untreated SU-8 were elongated compared to cell grown in the culture flask. Very few dividing cells were observed on untreated SU-8. The  $\text{HNO}_3$ -CAN modified SU-8 had a significantly higher cell density and lower generation time of  $36 \pm 0.7$  hours (Figure 52) than cells grown on untreated SU-8. Dividing cells were observed more frequently. By contrast, SU-8 surface treated with  $\text{HNO}_3$ -CAN and ethanolamine sustained cell growth rates that were indistinguishable from cell growth rates observed in cell culturing flask. Both surfaces resulted in cell doubling times of approximately 32 h.



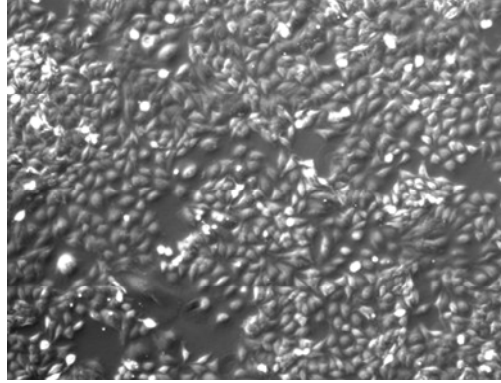
**Figure 52: Growth kinetics of HeLa cells on the differently modified SU-8 surfaces.** Samples of the differently modified SU-8 surfaces were immersed in standard cell culture media in separate cell culture flasks and seeded with equal amounts of HeLa cells. The cells were inspected every 24 hours and three to four representative pictures were grabbed from each surface on each occasion for cell manual counting. The entire culturing experiment was repeated twice. The label letters refer to the following different surfaces: (a). Untreated SU-8; (b).  $\text{HNO}_3$ -CAN treated SU-8; (c).  $\text{HNO}_3$ -CAN and ethanolamine treated SU-8; (d). Control culture flask surface. The error bars represent the standard deviation.

The morphologies of cells cultured on the  $\text{HNO}_3$ -CAN treated SU-8 closely resembled those of cells cultured on  $\text{HNO}_3$ -CAN and ethanolamine treated SU-8 surface and the culture flask surface. Cells cultured on untreated SU-8 however, displayed a more elongated morphology (Figure 53).

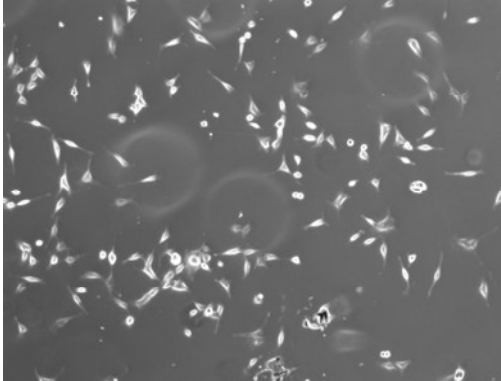
A: Culture flask, 24 h



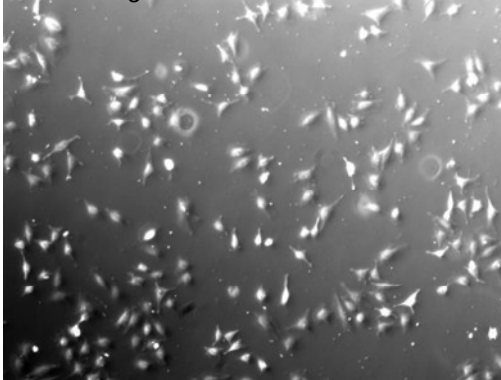
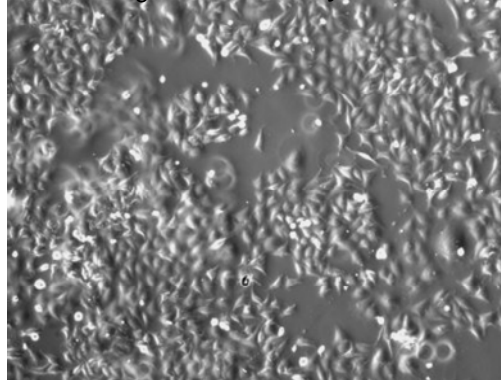
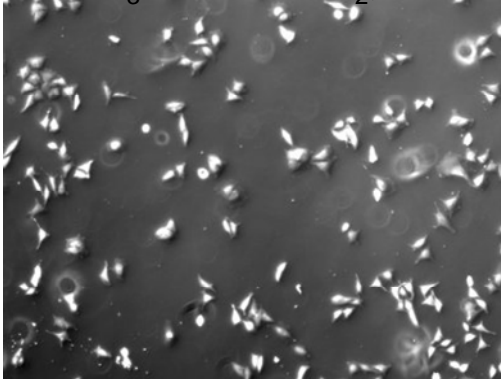
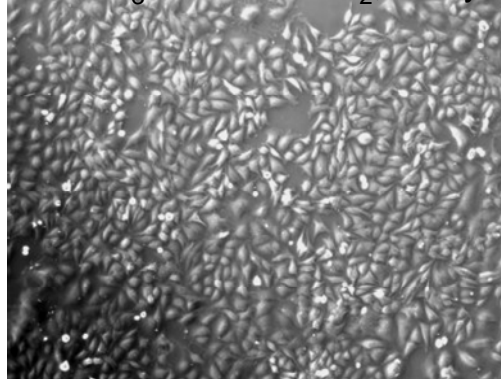
E: Culture flask, 4 days



B: Untreated SU-8, 24 h

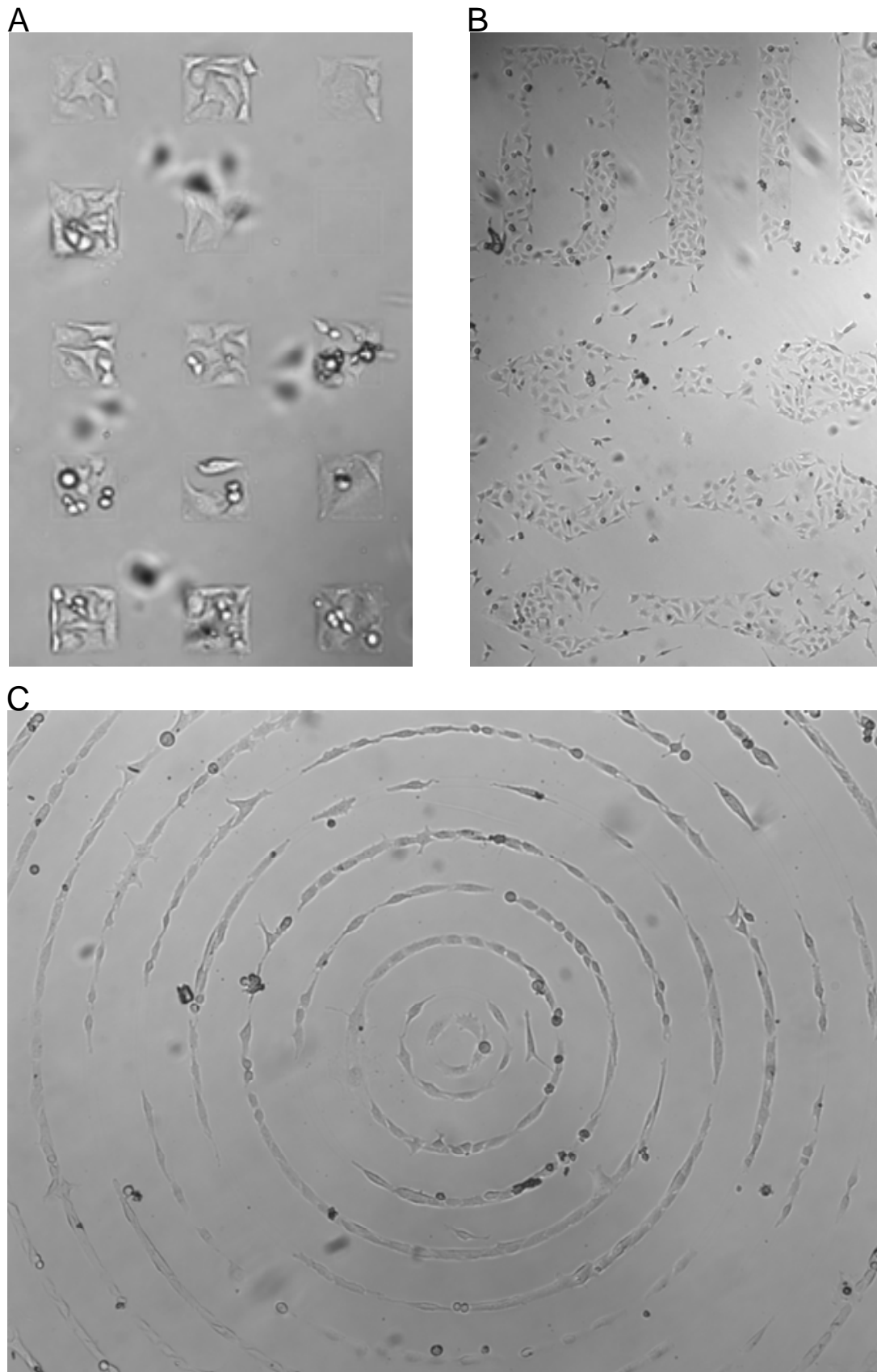


F: Untreated SU-8, 4 days

C: HNO<sub>3</sub>-CAN, 24 hG: HNO<sub>3</sub>-CAN, 4 daysD: HNO<sub>3</sub>-CAN + EtNH<sub>2</sub>, 24 hH: HNO<sub>3</sub>-CAN + EtNH<sub>2</sub>, 4 days

**Figure 53: HeLa cells cultured on differently treated SU-8 surfaces.** (A-D) Cells were cultured for 24 hours while in (E-H) the cells were cultured for four days. (A and E) is the reference culture flask. (B and F) is untreated SU-8. (C and G) represents HNO<sub>3</sub>-CAN treated SU-8 while (D and H) represents HNO<sub>3</sub>-CAN and ethanolamine (EtNH<sub>2</sub>) treated SU-8. All cells originated from the same culture and were cultured under identical conditions using the same media and culturing conditions.

Suspecting that soluble or diffusible factors might be responsible for the different growth kinetics as well as the differences in morphology observed, differently shaped patterns were created on the SU-8 surface by masking the SU-8 surface prior to treatment with HNO<sub>3</sub>-CAN and ethanolamine. The cells avoided areas that have not been exposed to HNO<sub>3</sub>-CAN and ethanolamine. Up to 18 cells were observed in 100 μm × 100 μm hydrophilic squares while no or few cells were observed on adjacent untreated surfaces (Figure 54 A). After cell division, cells on the patterned areas decreased in either size or attachment area rather than colonizing untreated SU-8. On the patterned 10 μm wide concentric circles, the cells appeared elongated and convex rather than circular, indicating the cells actively avoided the untreated SU-8 surface (Figure 54 B). Taken together these results demonstrate that SU-8 can be patterned with defined areas that sustain cell growth using the HNO<sub>3</sub>-CAN treatment. The results also suggest that diffusible factors/effectors are not causing the lack of growth on untreated SU-8 since cells separated by one or two μm displayed comparable morphologies and growth rates.



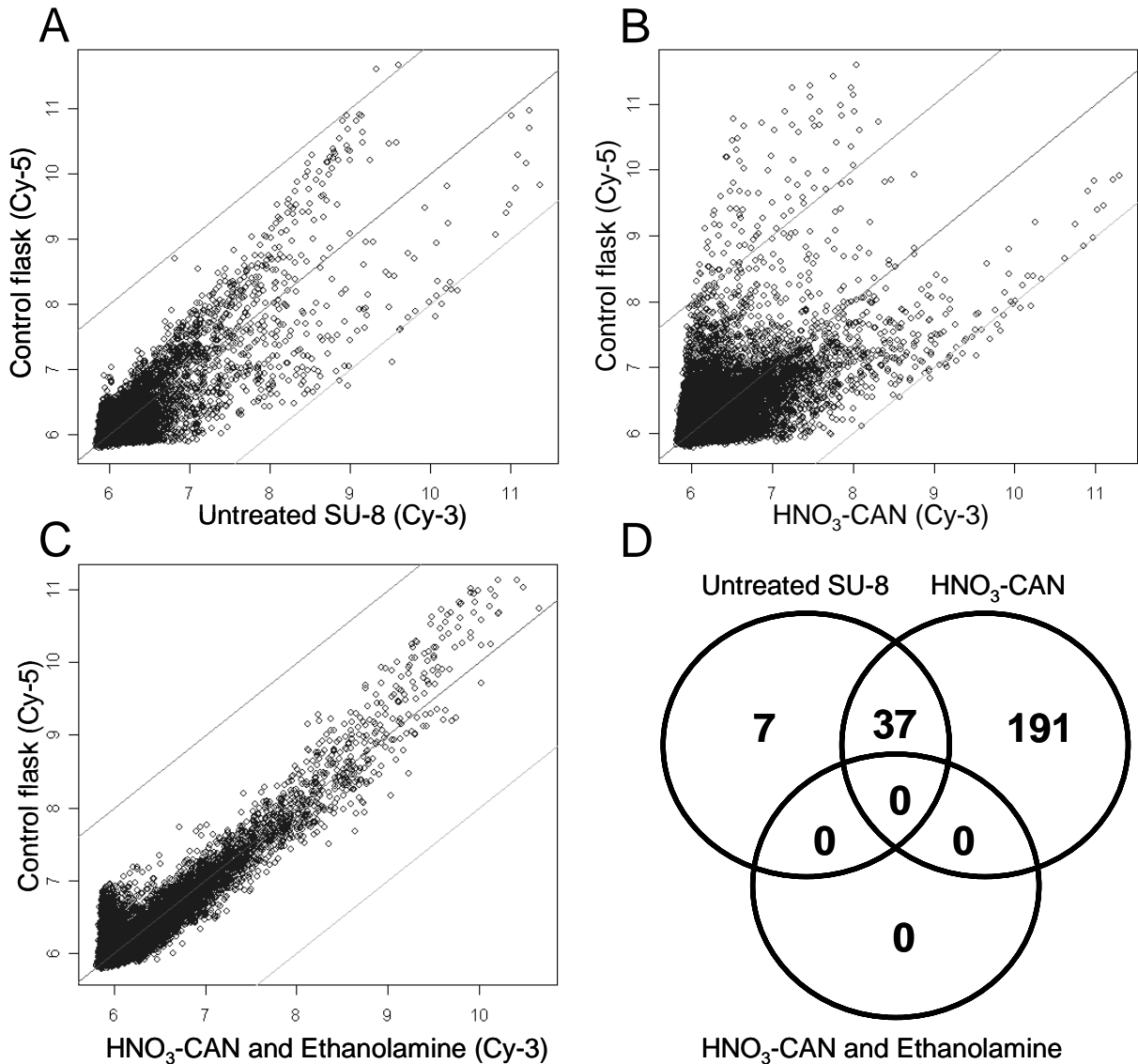
**Figure 54: HeLa cells cultured over night on SU-8 surfaces patterned with the HNO<sub>3</sub>-CAN ethanolamine treatment. (A)** HeLa cells grown on an array of 100 μm × 100 μm squares. The dark areas observed to be out of focus are cells adhering to the bottom of the culture flask below the pattern **(B)** HeLa cell cultured on the DTU logo. **(C)** HeLa cells cultured on 10 μm wide concentric circles. The cells appeared to change their morphologies to fit on to the HNO<sub>3</sub>-CAN ethanolamine treated patterns avoiding contact to the untreated SU-8.

---

**Whole genome expression profile comparison cells cultured on SU-8**

Following culturing of HeLa cells on the differently modified SU-8 surfaces, cells were collected and RNA was extracted. Following amplification, reverse transcription and labeling, the labeled cDNA was hybridized to whole genome DNA microarrays. Scatter plots of the resulting hybridization intensities (Figure 55 A-C) showed that cells grown on untreated SU-8 and HNO<sub>3</sub>-CAN treated SU-8 had significantly different gene expression profiles compared to cells grown in cell culture flasks (Figure 39 A-B). The whole genome expression profile of cells cultured on HNO<sub>3</sub>-CAN and ethanolamine treated SU-8 was indistinguishable from generated from cells cultured in the reference cell culture flask (Figure 39 A-B). Genes more than three fold regulated were considered significantly regulated. In cells cultured on untreated SU-8, 44 genes were found significantly regulated (Figure 55 D). Of the 44 significantly regulated genes, 37 were also regulated in cells cultured on HNO<sub>3</sub>-CAN treated SU-8. An additional 191 genes were also more than three fold regulated in cells cultured on HNO<sub>3</sub>-CAN treated SU-8 compared to cell growth in the culture flasks. All the regulated genes are found in Table 5 in Appendix. By contrast no genes were found more than three fold regulated relative to the culture flask, in cells cultured on SU-8 treated with HNO<sub>3</sub>-CAN and ethanolamine (Figure 55 C-D).

Despite the fact that incubation with cell culture medium reduced the contact angle to ~15 ° on all surfaces (Figure 51), it could not be excluded that the lack of biocompatibility of untreated SU-8 could be explained by its native hydrophobic properties. PMMA, another surface that was highly hydrophobic prior to incubation with cell culture medium (Figure 51), was previously investigated for biocompatibility and bio-comparability (Figure 39). PMMA has been used since 1960ies in orthopedic surgery<sup>145</sup>. More recently, PMMA has been used in  $\mu$ TAS for cell biology research<sup>6</sup> and as a substrate for DNA microarrays<sup>146,147</sup>. Cells cultured on PMMA showed no differences in cell morphology, growth kinetics or gene expression profiles compared to cell grown in TC-PS culture flasks (Figure 36, Figure 39 C-D and Figure 52).

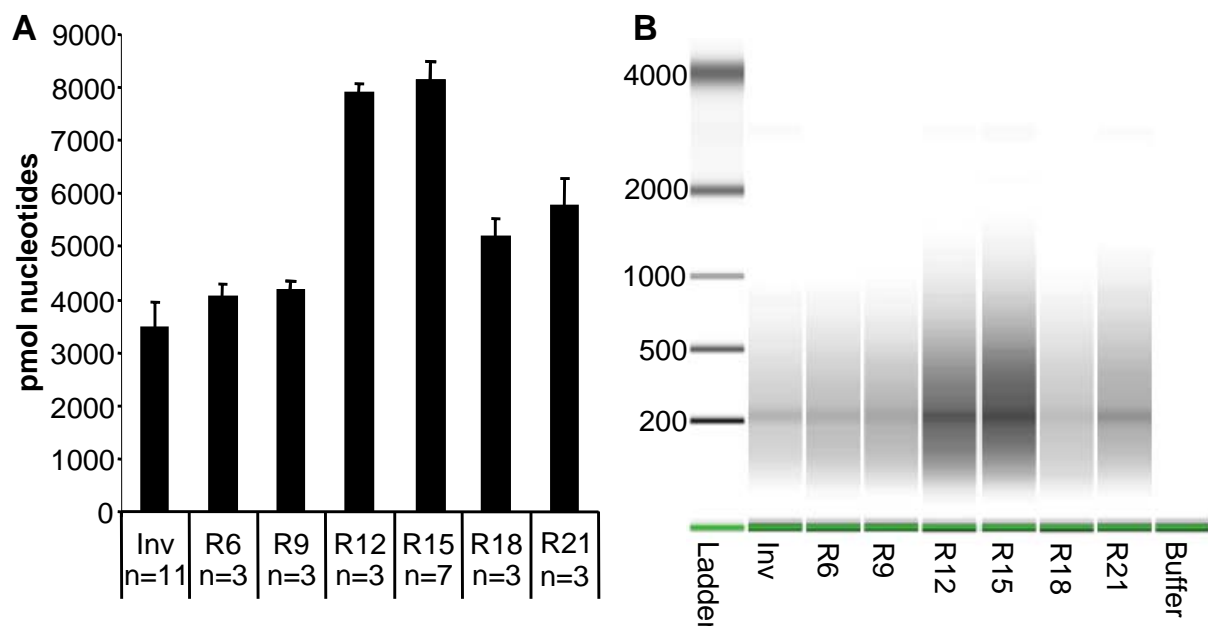


**Figure 55: Scatter plots of whole human genome expression profiles following four days culture on different surfaces.** Non-linear normalization of the raw data was performed using Qspline<sup>99</sup>. The central line is the median and the upper and lower line represent a fold change of 3 up and down, respectively. **(A)** Untreated SU-8. **(B)** HNO<sub>3</sub>-CAN treated SU-8. **(C)** HNO<sub>3</sub>-CAN and ethanolamine treated SU-8. **(D)** A Venn diagram was used to display the number of more than three fold regulated genes on the differently treated SU-8 surfaces relative to the reference cell culture flask. Each circle represents one culture surface and the number reflects the number of genes more than 3-fold regulated on that surface relative to the cell culture flask. The numbers in the overlapping region of the circles indicates the number of genes that were more than 3-fold regulated on both corresponding surfaces, while the number in the overlapping region of all three circles reflects the number of genes that were regulated on all three surfaces. The entire list of regulated gene names and ratios is available in Table 5 in the Appendix on page 186.

## ***Enhancement of the reverse transcription reaction for gene expression analysis***

### **cDNA yield of reverse transcription reactions**

To avoid 3' bias resulting from oligo(dT) priming, random priming was considered the method of choice. Conventional random priming method relies on the utilization of either random hexamers or random nonamers on poly(A) selected RNA. Some researchers claim that random nonamers perform better as the duplex formed between the RNA template and the primer is more stable. However, to the best of our knowledge, no systematic investigation of the effect of the random primer length on the resulting cDNA yield and quality has been performed. Seeking to elucidate if random nonamer primers was the optimal length, several random primers differing in length by 3 bases were investigated starting from hexamers ending at 21-mers. The initial experiment sought to find the random primer that resulted in the most cDNA starting from the same amount of template RNA. As control a commercial random primer formulation consisting primarily of random hexamers from Invitrogen (Inv) was included (Figure 56).

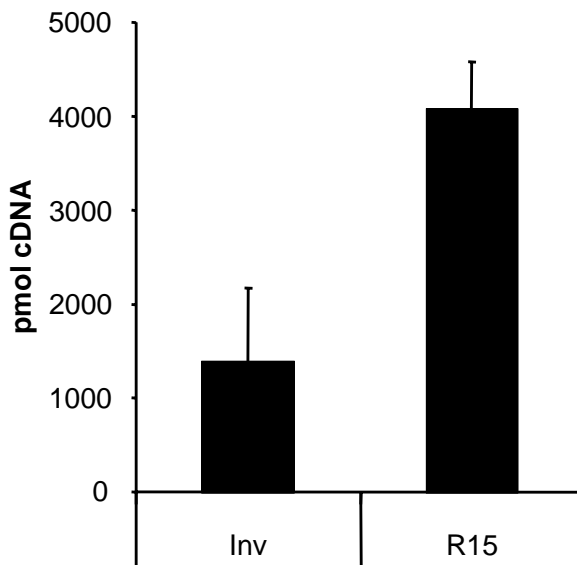


**Figure 56: Effect of random primer length on the yield of cDNA.** (A) cDNA yield obtained from reverse transcription of 3  $\mu$ g aRNA. Values are based on spectrophotometer measurements ( $A_{260}$ - $A_{310}$  nm). The random primers were obtained from an oligo vendor (Sigma-Genosys) ranging in length from 6 to 21 bases using a 3 base length increment (R6 to R21). (B) Size distribution of the generated cDNA using the Agilent Bioanalyzer and the RNA 6000 Nano LabChip<sup>®</sup>.



The results indicated that reverse transcription reaction initiated with either R12 or R15 yielded two-fold the amount of cDNA as did the commercial random primer formulation, R6 and R9 (Figure 56 A). It was also noted that both R6 and R9 obtained from an oligo vendor yielded more cDNA than did the commercial random primer formulation (Inv). Since the reactions were spiked with 3 µg T7 amplified RNA, the maximum yield is 10000 pmol synthesized nucleotides. Reactions initiated with R15 and R12 resulted in 80 % yield while R6 and R9 initiated reactions resulted in 40 % yield. However, cDNA concentration was measured spectroscopically after spin column purification steps which usually results in loss of DNA. It is therefore likely that R15 and R12 initiated reactions have yields close to 100 % indicating that almost the whole transcriptome was reverse transcribed using R15 and R12 primers. Seeking to validate the spectroscopically measured results the cDNA initiated with the various length random primers were analyzed using the Agilent bioanalyzer (Figure 56 B). The results indicate that the intensity of the R12 and R15 initiated reactions were roughly twice as intense as Inv, R6 and R9 initiated reactions. The R15 initiated reactions being slightly more intense than the R12 initiated reactions. While R18 and R21 initiated reaction were more intense than Inv, R6 and R9 initiated reactions but less intense than R12 and R15 corroborating the spectroscopically obtained findings.

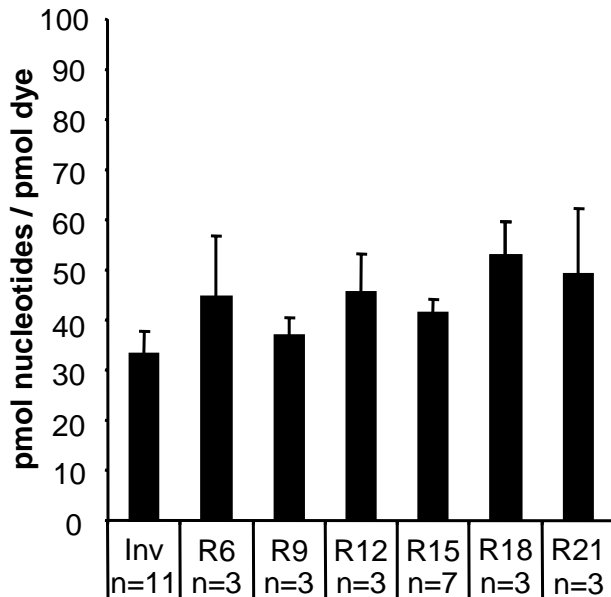
As mRNA also is frequently used as template for random primed reverse transcription reactions we wanted to test if the relationship in terms of cDNA yield between R15 and Inv initiated reactions was maintained when the template was mRNA rather than aRNA. The results (Figure 57) indicated that R15 initiated reactions yielded two-fold as much cDNA as did the Inv initiated reactions, confirming the findings from reactions relying on aRNA templates.



**Figure 57: Comparison of cDNA yield of the conversion of 1.5  $\mu$ g mRNA (non amplified RNA) into cDNA using Invitrogen R6 random primer and the R15. Each reaction was repeated three times using 6  $\mu$ g of primers in each reaction.**

The results also indicated that R15 initiated reactions transcribed almost 100 % of mRNA into cDNA which again was two-fold better than the Invitrogen random primer initiated reactions used as control (Figure 57) indicating that aRNA as well as mRNA templates were more efficiently transcribed using R15 primers than the Invitrogen random primer formulation.

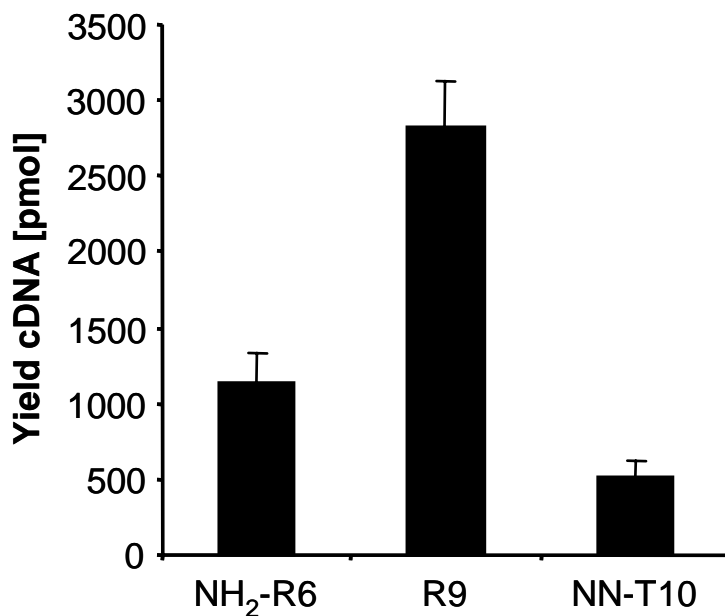
Seeking to elucidate if the different length primers influenced the labeling efficiency of the resulting cDNA, the ratio of nucleotides per dye (Nuc/Dye) was determined for the different primers tested. The results indicated that the length of the primer used to initiate the reaction had little if any effect on the amount of dye incorporated in the cDNA. For all reactions a ratio of nucleotides per dye (Nuc/Dye) was approximately  $40 \pm 15$  (Figure 58). This indicates that the incorporation efficiency of aminoallyl-dUTP was not affected by the different primers.



**Figure 58: The effect of the amount of dye incorporation with varying length of random oligonucleotides primers.**

The ratios were calculated based on spectroscopically measurements of the final labeled and purified cDNA.

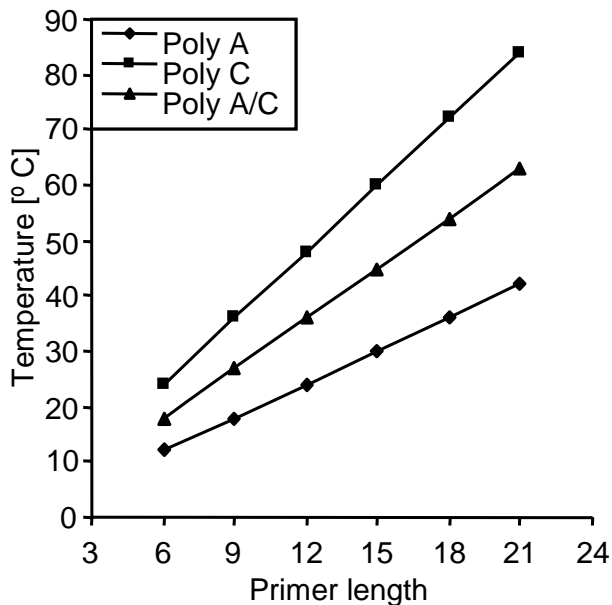
Seeking to elucidate the optimal priming method for the reverse transcription reaction, two random primers were compared to a twelve-mer primer having two wobble bases followed by a stretch of ten Ts. The idea of this primer was to bind to the poly(A) tail on mRNAs and initiate transcriptions from 3' end. In the literature suggestions has been put forward suggesting that random hexamer priming could be up to 10 fold enhanced if an amino liker was attached to the primer<sup>111</sup>. This effect was sought reproduced and compared to a random nonamers primer (Figure 59).



**Figure 59: Effect of priming method on the cDNA yield.** As template 100 µg total RNA selected for poly(A) by Dynabeads was used. All reactions were initiated using 3 µg of each primer. Each priming method was repeated four times.

The results indicated that R9 priming yielded almost three fold as much cDNA as did the amino linked R6. This suggests that the added amino group to the R6 primer may not positively influence the yield of the reaction. The results obtained from NN-T10 priming indicated that this method was inferior to random priming and was hence not tested further as it may also result in 3' bias.

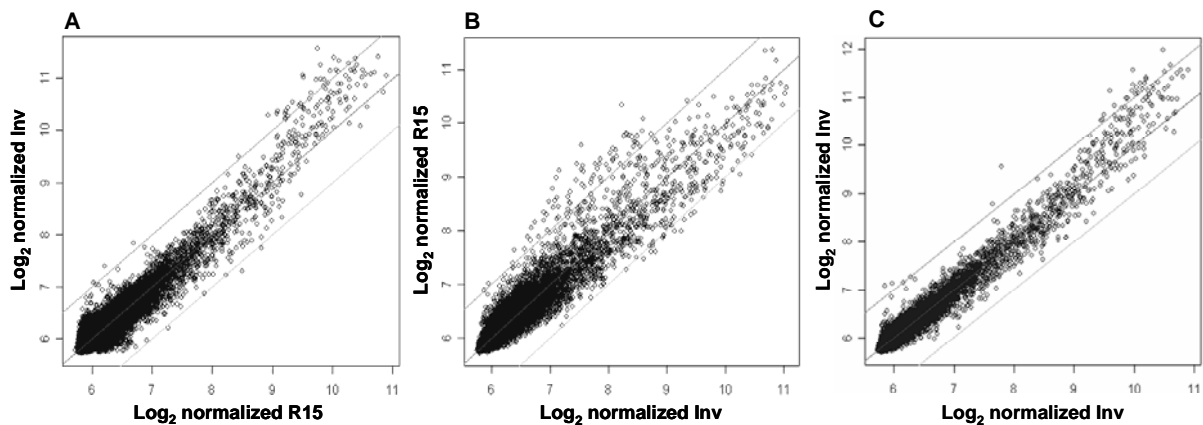
Random primers of varying length will have varying melting temperature. Analysis of the melting temperature as a function of random primer length suggests that short A/T rich random primers could have trouble initiating transcription at 42 °C since these primers most likely do not bind to RNA (Figure 60) at this temperature. Longer A/T rich primers have higher likelihood of initiating transcription due to their higher melting temperature.



**Figure 60: Melting curves of oligonucleotides with varying length and adenine, cytosine content.** The curves were generated by the theoretical melting temperature using oligonucleotides consisting solely of adenine (A), cytosine (C) or an equal amount of A and C. The reverse transcription reactions were performed at 42 °C.

## Effect of R15 priming on whole genome expression profiling

As oligo(dT) priming is known to introduce a bias towards the 3' end being transcribed more efficiently than the 5' end of transcripts we sought to elucidate if R15 priming resulted in an altered gene expression profile. Labeled cDNA was co-hybridized with equimolar amounts of incorporated Cy-dye to DNA microarray containing 44,000 probes covering the entire transcriptome. The resulting data was normalized using a non-linear normalization method<sup>111</sup>.



**Figure 61: Scatter plots of normalized data from hybridizations to whole human transcriptome arrays.** Non-linear normalization of the raw data was performed using Qspline<sup>111</sup>. Cy-5 labeled samples were always plotted on the y-axis. The central line is the median and the upper and lower lines correspond to a 2-fold change up or down respectively. Prior to hybridization, the differently labeled cDNA samples were pooled using equimolar amounts of each Cy-dye (200 pmol). Molar amounts mentioned in pmol in this figure refer to the amount of Cy-dye incorporated in the cDNA and not the amount of nucleotides of cDNA. **(A)** Normalized scatter plot of co-hybridization of 200 pmol Cy-5 labeled cDNA resulting from reactions initiated with Inv primes and 200 pmol Cy-3 labeled cDNA resulting from reactions initiated with R15 primers. **(B)** Repeating the experiment with the order of the dyes reversed. **(C)** Normalized scatter plot of co-hybridization of 200 pmol Cy-5 labeled cDNA and 200 pmol Cy-3 labeled cDNA both resulting from reactions initiated with Inv primers.

Genes were considered significantly different if the ratio exceeded two fold indicated by the upper and lower line on Figure 61 A-C. Repeating the experiments with the order of the dyes reversed enabled removal of non-significant noise and statistical analysis of the data. The results showed that, statistically, there were only three transcripts for genes that were found to differ between the R15 and Inv primed reactions (Table 4). In comparison, cDNA populations generated from four different Inv primed reactions differed statistically in two transcripts (Figure 61 C and Table 4).

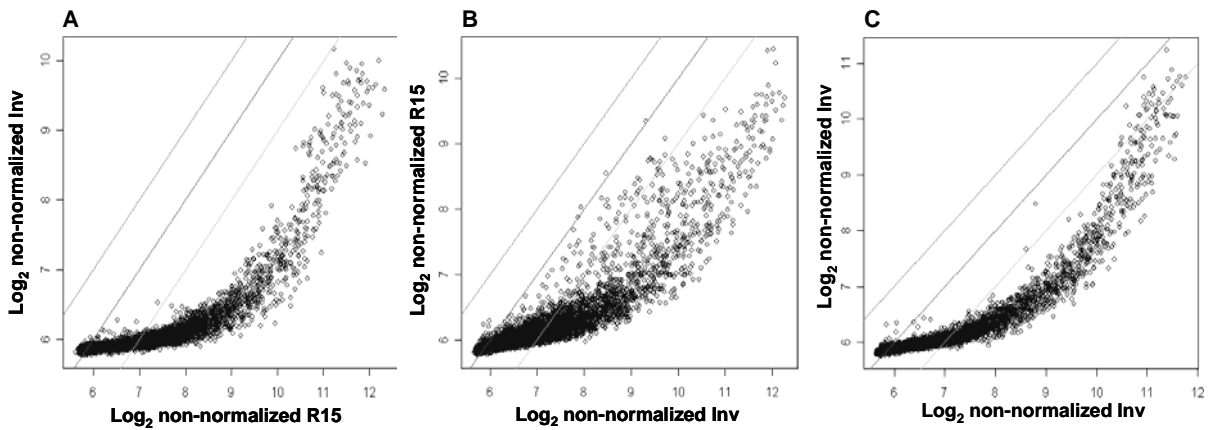
**Table 4: Genes showing significant changes in abundance in two cDNA populations.** The ratio of Inv R6 over R15 <sup>(a)</sup> was calculated for two slides and the values were averaged. The P values were calculated using the student T-test. Genes were considered significant if they were more than two fold regulated and the P value was less than 0.05. The Inv R6 over Inv R6 ratios were calculated by utilizing the Inv R6 values from three slides and averaging the ratios. Thus inherent slide to slide as well as experimental variations are contained in these values.

Probe name	Gene Name	Ratio	SD	% CV	P value	Probe Sequence
A_23_P355447	ZDHHC22	0.48 <sup>a)</sup>	0.01	1.86	0.0002	CAATGGGAGGGAGAGGGAGGAGGGG AAGATCTGGGCAATTTTGGCCTTGA CTCTTTCCTG
A_32_P158433	THC2001391	2.20 <sup>a)</sup>	0.29	13.37	0.029	CAGAAGTCGCTGGGCTCATAAGGCT CTTAGACGTGCTTGAGAGTGAGCCT TTCGAAGAGA
A_32_P187875	A_32_P187875	2.12 <sup>a)</sup>	0.15	6.93	0.0085	GAAGCATCGTATCACAGCAGGTTAC AACAACTTTGGGATAAAAAGGCAACT GGTAAACTGT
A_23_P87879	CD69	0.08 <sup>b)</sup>	0.04	48.58	0.00079	TGTGCAATATGTGATGTGGCAAATC TCTATTAGGAAATATTCTGTAATCT TCAGACCTAG
A_24_P694760	AK056312	2.26 <sup>b)</sup>	0.29	12.65	0.025	TCAACTTTGCCTTGATAATTATTGT AAACACTTTGTTTCATTTTTTCTTTT TTATTCACAA

<sup>a)</sup> Ratio refers to the ratio Inv R6 over R15.

<sup>b)</sup> Ratio refers to the average ratio values over three slides for Inv R6 signals.

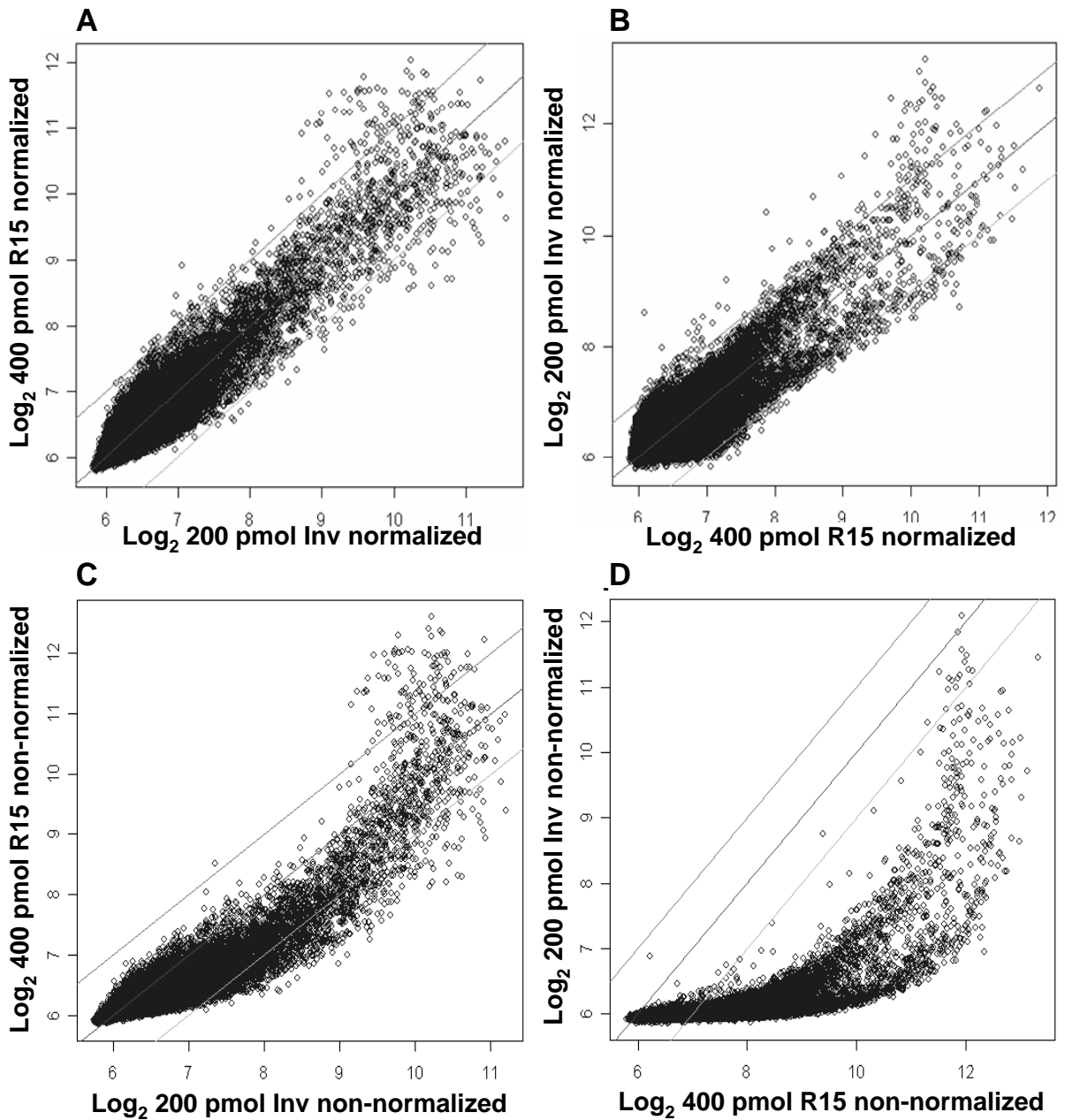
Inspecting the *non-normalized* microarray data (Figure 62 A-C) indicated a shift in the pattern of the scattered data plot indicating a shift of the data towards the R15 initiated cDNA. In Figure 62 A the shift is towards the Cy-3 channel containing R15 initiated cDNA when compared to the control (Figure 62 C). Repeating the experiment with the order of the dyes reversed the shift towards the Cy-5 channel containing the R15 initiated cDNA.



**Figure 62: Scatter plots of non-normalized hybridizations to whole human transcriptome arrays.** Cy-5 labeled samples were always plotted on the y-axis. The central line is the median and the upper and lower lines correspond to one log<sub>2</sub> fold change up or down respectively. (A-C) Non-normalized data from Figure 61.

The effect of increasing signals was highest in the Cy-5 channel (Figure 62 A-B) which can be explained by the fact that Cy-5 signals were generally weaker than Cy-3 signals. Normalization of the data removes the positive effect of R15 priming (Figure 61 A-B and Figure 62 A-B) which was expected since the algorithm<sup>111</sup> is designed to remove systematic variations.

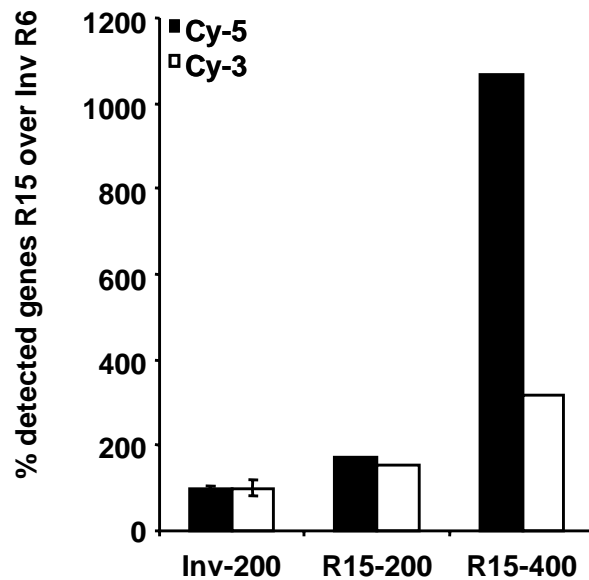
Reverse transcription reactions initiated with R15 routinely results in twice as much cDNA as do Inv/R6 priming (Figure 56 and Figure 57). The significance of that was illustrated by co-hybridization with twice the amount of Cy-dye incorporated R15 primed cDNA as Inv primed cDNA. Co-hybridizations were performed using R15 primed cDNA incorporated with 400 pmol and Inv primed cDNA incorporated with 200 pmol Cy-dye. The experiment was performed twice with the order of the dyes reversed (Figure 63).



**Figure 63: Co-hybridization with twice the amount of R15 primed cDNA than Inv primed cDNA.** Cy-5 labeled samples were always plotted on the y-axis. The central line is the median and the upper and lower lines correspond to a 2-fold change up or down respectively. (A-B) Normalized data. (C-D) Non-normalized data.

Seeking to elucidate if R15 priming resulted in an increase in the amount of detectable genes, the number of genes with intensities above background was calculated (Figure 64).





**Figure 64: Comparison of the amount of detectable genes with R15 and Inv priming.** A gene was considered detected if it displayed a signal that was 50 % more than the background signal calculated as the average of the 1000 weakest signals on the array.

The results showed that 55-72% more genes was detected using cDNA generated by R15 priming compared to cDNA generated by Inv priming when equimolar amounts of dye incorporated cDNA was utilized (Figure 64, two left-most bars). This result cannot be explained by differences in fluorescence or amount of target hybridized between the two populations since the amount of labeled cDNA was normalized to 200 pmol incorporated dye prior to hybridizations. Between 3 and 11-fold more genes were considered expressed on arrays hybridized with twice the amount of dye incorporated R15 primed cDNA compared to Inv primed cDNA (Figure 64, two right-most bars).

Taken together, the results showed that that R15 priming not only increases the amount of the resulting cDNA but also yields cDNA with better representation of the original mRNA population. As R15 priming does not result in any bias in the represented cDNA indicates that random hexamers and random nonamers can readily be substituted with R15 primers from a conventional oligo vendor to increase the yield and quality of the resulting cDNA in reverse transcription reactions.

## 5 Discussion

The aim of this project was the development of a low-cost polymeric chip that provides optimal conditions for mammalian cell culturing and which is optically transparent for on-line microscopic observation of the cultured cells. Conventional cell culturing is performed inside a CO<sub>2</sub> incubator providing a constant temperature of 37 °C and a CO<sub>2</sub> enriched atmosphere of usually 5 %. The culturing temperature confers with the temperature of our bodies and like us the cells are extremely sensitive to variations in temperature. By optimization of cell culture conditions long-term on-chip cell culturing with homogeneous environment throughout the cell culture chamber was achieved. Utilization of morphological observations, growth kinetics and whole genome expression profiling, the chamber was found to provide culture conditions indistinguishable from those of the cell culture flask in bench-top CO<sub>2</sub> incubators. This is important for collecting reproducible, high-quality data from real-time cell observations performed using the chip, and for the ability to compare and relate these results with conventional cell culture studies made in the past.

Basic physiological conditions necessary for cell growth were established by using an enclosed perfusion chamber design (Figure 1 and Figure 3). The enclosed perfusion chamber prevents evaporation and interaction of culture media with atmospheric air and therefore eliminates the need for CO<sub>2</sub> buffering and humidification of the surrounding atmosphere. Moreover, the enclosed system reduces risks of contamination of the culture, while hampering direct access to the cells. Continuous perfusion eliminates the periodic changes in cell culture conditions, such as altered concentration of nutrients and metabolic products caused by media exchange procedures when using standard cell culture techniques<sup>24</sup>. Continuous perfusion is not always advantageous; for example, maintaining cell cultures, that are strongly dependent on signaling and conditioning metabolites excreted by the cells themselves, requires perfusion involving periodic partial media exchange in the chamber instead of continuous flow<sup>148</sup>. However, cell culture chips with continuous perfusion can be a particularly valuable tool to identify such critical signaling factors since the perfusion constantly eliminates cell secreted factors within the chip and external factors can be added in a controlled manner. The  $\mu$ CCC is therefore highly suitable for studying effects on cell-to-cell communication by excreted factors or determining effects of pharmaceutical drugs in a highly controlled manner. Controlled addition of desired stimulating drugs or solutions to the media in the chip enables on-line monitoring of the kinetics of the cellular responses to these stimuli either in terms of

cell morphological or motility changes identifiable by optical microscopy or in terms of expression of fluorescently labeled proteins detectable by fluorescent microscopy. Additionally, on-line observations of changes in cell excreted factors due to changes in media formulation or addition/removal of selected growth factors might also be realized by perfusion of the outlet media through an antibody array if a labeled secondary antibody is added to the inlet media.

### **Material and fabrication**

Biocompatibility of the  $\mu$ CCC was a vital issue as cells cultured in the  $\mu$ CCC was desired to experience culturing conditions similar to the reference cell culture flask. Generally, PMMA is known as a biocompatible material and has been used since the 1960ies in orthopedic surgery<sup>145</sup>. More recent applications of PMMA include implantable intraocular lenses due to its excellent optical properties<sup>42,149</sup>, substrate for DNA microarrays<sup>146,147</sup> and  $\mu$ TAS systems as reviewed in<sup>6,150</sup>. PMMA was hence selected as material for realization of the  $\mu$ CCC. Cell morphology (Figure 36) and whole genome expression profiles of cells cultured on PMMA inside a cell culture flask was found indistinguishable from the reference cell culture flask (Figure 39) supporting previous findings that PMMA is biocompatible<sup>42,145,149</sup>. Furthermore, PMMA has been reported to have low autofluorescence<sup>151</sup> making it well suited for conventional light microscopy and fluorescence based assays. Three dimensional microstructures can be realized in PMMA by techniques such as injection molding<sup>152</sup>, hot-embossing<sup>153,154</sup> and laser ablation<sup>110,155</sup>. Depending on the use of the microstructure different sizes of microstructures may be required. The smallest feature sizes are attainable by injection molding or hot-embossing. However, these techniques are limited in their flexibility and especially hot-embossing using a stamp fabricated by lithography in *e.g.* silicon is highly labor intensive and expensive.

We found the dimensions of the flow equalizing barriers (Figure 6 and Figure 11) sufficient for equalizing the flow in the  $\mu$ CCC, while the height of the chamber (Figure 5) was used as a method of entrapping the cells. If more efficient cell traps are required in a microsystem, feature sizes smaller than the cell diameter (10  $\mu$ m) are required. Feature sizes down to 100  $\mu$ m are attainable with the IR-laser ablation technique<sup>110</sup>, while feature sizes less than 60  $\mu$ m are attainable using an excimer laser<sup>156</sup>. However, excimer laser ablation has been found to chemically modify the PMMA surface, which may influence the biocompatibility<sup>157</sup>. For smaller feature sizes hot-embossing or injection molding are required.

PDMS is a frequently used polymer as it can be used directly on a mold fabricated by lithography *i.e.* in SU-8, combining the small feature size of lithography with the ease of fabrication<sup>115</sup>. This makes it relatively simple to make several replicas of the same structure. PDMS is notorious to strongly adsorb molecules to the surface as well as being extremely hydrophobic making PDMS structures hard to fill with aqueous solutions<sup>9</sup> as well as it is highly gas permeable<sup>7,9,27,28</sup>. SU-8 itself may also be used as a cell culturing surface, provided the surface is modified (Figure 50, Figure 53-Figure 55)<sup>158</sup>. The modification was stable enough to sustain the lift-off process of photoresist. This enabled the formation of discrete biocompatible micropatterns on the bioincompatible SU-8 (Figure 54). If the PMMA culturing surface of the  $\mu$ CCC was replaced with SU-8 containing micropatterns of various shapes, on-line monitoring of *e.g.* cell-cell contact (Figure 23) could be studied on areas of confined space.

### Heating strategy

To ensure uniform heating of the  $\mu$ CCC we found ITO based heating ideal. Being optically transparent (Figure 3, Figure 9 and Figure 10) and electrically conductive, ITO film does not obscure illumination of the chamber and at the same time can generate Joule heat when electrical power is applied to it. Being able to continuously monitor the temperature inside the  $\mu$ CCC using a thermistor during culturing enabled fast responses to fluctuations in ambient temperature (Figure 20).

ITO-based heaters have also been integrated in some commercial glass micro-incubators instead of using peripheral heaters<sup>159,160</sup> as well as other cell culture devices<sup>16,24</sup>. However, there are challenges in coating polymeric materials with ITO, because standard thin film vapor-deposition systems melt polymeric targets due to high temperatures in the vicinity of the vapor sources, and alternative sol-gel nanoparticle deposition methods<sup>159,160</sup> give relatively poor quality and stability of the ITO coatings<sup>161,162</sup>. Therefore, specialized low-temperature sputter-deposition systems are typically required<sup>163</sup>. Due to the lack of direct access to such equipment, the ITO heater was incorporated into the PMMA structure of the chip by using commercially available ITO coated transparent PET films. These films were laminated in-between PMMA sheets during the thermal bonding procedure of chip fabrication (Figure 1 - Figure 3). Because PET has higher glass transition temperature than PMMA, it maintains the integrity of thin ITO coating during bonding at 110 °C under pressure. Such a configuration also increases the reliability of the ITO film during chip operation, because the

surrounding PMMA completely isolates the coating from culture media liquids and therefore protects the film from chemical and electrolytic erosion (Figure 1).

Various other solutions to the archival of a culturing temperature of 37 °C in culture chambers have been developed. The simplest being simply putting the culturing device inside the CO<sub>2</sub> incubator and relying on the incubator to provide the desired culturing temperature as well as CO<sub>2</sub> enriched atmosphere for buffering of media<sup>9,19,20,22,28,30</sup>. The practical usefulness of such a heating strategy seems limited as little improvement if any is attained over the conventional cell culture flask. Furthermore one are faced with the same problems as when culturing in the cell culture flasks – the lack of possibility of continuous visual inspection of the cell culture without affecting cell culture conditions. In other studies a microscope with CO<sub>2</sub> enriched stage environment<sup>4,5</sup> was utilized. Alternatively the temperature of the microscope stage was regulated<sup>18</sup>, or the chamber exterior is perfused with preheated medium<sup>7,26</sup>, or a resistive heating coil is used to heat the chip<sup>32</sup>.

If the effects of heat shock were to be studied, on-line temperature measurements and regulation could significantly increase the control of the actual temperature the cells were exposed, to as well as the time they were exposed to that temperature. If the  $\mu$ CCC were seeded with cells transformed with *e.g.* a green fluorescent protein (GFP) tagged heat shock protein (HSP) such as hsp90, the kinetics of translation of individual proteins of could be studied in real time and coupled with more accurate temperature readings. Resulting in the elucidation of the timing involved during the onset of heat shock and the involvement of selected proteins.

### **Phototoxicity**

When cells were cultured in the  $\mu$ CCC on the desktop, they were unlike the reference cells in the CO<sub>2</sub> incubator exposed to light. We found no indication of cell death when the power of the microscope bulb was set to minimal settings (Figure 18, Figure 19 and Figure 40) while cell death occurred within 48 hours when the power was raised above medium setting (Figure 29 and Figure 31-Figure 32). Phototoxic effects have previously been observed when exposing cells to light with wavelengths below 540 nm<sup>67</sup>. Spectral analysis of the light reaching the cells through the microchip showed that in accordance with Wien's displacement Law<sup>164</sup>, that cells grown in the  $\mu$ CCC were exposed to significant amounts of light with wavelengths below 540 nm if the power setting of the microscope light was set at one third or

above (Figure 33). This may indicate the existence of a correlation between perfusion rate, light intensity and the onset of phototoxic effects. The mechanism of phototoxicity is not clear but phototoxic effects of visible light results from photodecomposition of riboflavin/vitamin B<sub>2</sub><sup>69</sup>, tyrosine<sup>70</sup> and tryptophan<sup>71</sup> and the generation of <sup>1</sup>O<sub>2</sub> and ·OH<sup>69-71</sup>. Free radicals released due to photodecomposition of media components can induce serious cell damage and fibrogenesis as reviewed in<sup>74</sup>. Many of the photoeffects may be eliminated by addition of anti-oxidants<sup>69</sup>, indicating it to be advisable to add anti-oxidants to the medium if strong light sources are needed for an assay. Alternatively a system could be used that only expose cells to light during photographic recordings. Although we only have used white light microscopy, similar problems could occur using monochromatic light used for fluorescent assays.

### Shear stress

The  $\mu$ CCC was designed to expose the cultured cells to a minimum level of shear stress using flow equalizing barriers (Figure 5 - Figure 7). This design enabled on-line monitoring of cell cultured under conditions comparable to the cell culture flask (Figure 40 and Table 2). Shear stress has been considered in many studies<sup>4,5,14,15,19,26,30</sup>, but has been left unaddressed in others<sup>16,24,27-29,31,32</sup>. Culturing cells in confined channels or chambers during continuous perfusion of media may result in shear stress. Depending on the cell type cultured, this can have adverse effects on the cell. If a cell culturing device is to provide cell culturing conditions resembling the *in vivo* situation for *e.g.* epithelial cells, the dimensions of the chamber or microchannels or the flowrate, could be used to generate a level of shear stress resembling various sizes of blood vessels. Such devices could be useful for on-line studies of *e.g.* the effect of thrombosis on adjacent cells and could potentially be used to identify novel genetic markers for the early stages of thrombosis. The level of shear stress has previously been used to study the migration and orientation of smooth muscle cells<sup>165</sup> as well as the effect on gene expression of endothelial cells<sup>166</sup>.

### Biocompatibility

In the present study, HeLa cells cultured within the  $\mu$ CCC, showed comparable growth kinetics (Figure 19), cellular morphology (Figure 36) and whole genome expression profile (Figure 40) compared to cells grown in conventional culture flasks made of tissue culture quality polystyrene (TC-PS). Only two genes differed *significantly* in expression in all three experiments (Table 2), while a total of 119 genes was more than 3-fold regulated in all three

experiments. This indicates a substantial noise in gene expression analysis that could be due to subtle biological variances between each culture or inherent variances in the microarray assay (Figure 40 and Table 2-Table 3). One of the significantly regulated transcripts was Ataxin 10 (Atx-10). Atx-10 has previously been reported to be essential for the survival of cerebella neurons<sup>167</sup>. The significance of Atx-10 being down regulated in HeLa cells cultured in  $\mu$ CCC is at present unclear. Blast searches performed on the probe sequences failed to reveal further insight regarding the biological functions of the significantly regulated transcripts. The results strongly indicated that the cells grown in the  $\mu$ CCC are biologically comparable to cells grown in cell culture flask. The results also suggest that the PMMA surface of the  $\mu$ CCC is biocompatible (Figure 39), conferring with previous studies<sup>42,145,149</sup>. However, lower biocompatibility of osteosarcoma cells and endothelial cell (CPA-47) has been observed on untreated PMMA compared to TC-PS<sup>168</sup>. Interestingly, the biocompatibility of PMMA was significantly increased by radio-frequency plasma treatment, which is also a standard treatment of PS in order to reach TC-PS quality<sup>169</sup>. Changes in PMMA surface biocompatibility by plasma treatment, opens the possibility of systematically modifying surface properties, and with the use of the chip, direct on-line observations of cellular responses to these modifications could be performed.

For demanding cell cultures, biocompatibility of the chip might be improved by using TC-PS instead of PMMA as chamber material. Unfortunately, due its physical properties, PS cannot be ablated by IR-laser with the same resolution as PMMA, so PS can replace only those chamber parts that do not contain microfluidic channels or other microscale objects. Thus, in the presented design of the chip (Figure 1), the entire chamber lid and bottom, which basically are the only surfaces exposed for cell adhesion, can be replaced by TC-PS. The only difference in chip fabrication necessary for the combination of TC-PS and PMMA is that thermal bonding has to be performed at 95 °C due to the lower glass transition temperature of PS. A different and simpler way of modifying the biocompatibility of the PMMA surface was demonstrated. Coating of the  $\mu$ CCC or PMMA with either PLL or PEI resulted in significant improved biocompatibility for hNS1 and Bcl-X<sub>L</sub> stem cells (Figure 46 - Figure 49).

Our results showed no correlation between contact angle measurements of the dry material samples (Figure 51), growth kinetics (Figure 19 and Figure 52), morphology (Figure 36 and Figure 53) and whole genome expression profiles obtained from cells grown on them (Figure 39 and Figure 55). It has previously been speculated that a hydrophilic surface was important for cellular attachment<sup>43</sup> although other reports that hydrophobic surfaces yield better

biocompatibility<sup>36</sup>. It is noteworthy that pre-incubation the material samples with cell culture medium supplemented with 10 % FBS resulted in contact angles of 15 ° (Figure 51) suggesting that the surface the cells “see” is hydrophilic and if there was a correlation between hydrophobicity and biocompatibility, all surfaces would result in similar growth pattern and gene expression profiles. This was not observed (Figure 55). Most likely protein adsorption differs on the different surfaces. Adsorption and conformational changes of proteins to interfaces has previously been studied using atomic force microscopy (AFM)<sup>170</sup> and circular dichroism (CD)<sup>171,172</sup>. All studies indicate that the secondary structure of a protein changes when it is adsorbed to a surface. Structural changes was indicated by a decrease in the  $\alpha$ -helix content and an increase in the random fraction and/or  $\beta$ -sheet<sup>171,172</sup> and the formation of protein aggregates<sup>170</sup>. Different surfaces has also been shown to adsorb proteins differently, demonstrated by the differences in  $\alpha$ -helix content in BSA<sup>171</sup>, fibrinogen<sup>171,173</sup>, albumin and gamma globulin<sup>173</sup> adsorbed onto different surfaces, suggesting the importance of which functional groups reside on the surface. Other studies have reported that protein conformation and orientation is of greater importance than the total amount of adsorbed protein<sup>174,175</sup>. Hence it may not only be the coating of a surface by either a single protein like fibronectin<sup>30,46,47</sup> or a mixture of proteins like cell culture media supplemented with 10 % FBS that results in a biocompatible surface. Rather biocompatibility may arise from the orientation and conformation of the adsorbed protein(s).

As the molecular organization of adsorbed proteins is not likely to be detected by contact angle measurements (Figure 51) this method appears to be inappropriate for assessing biocompatibility. Comparing the whole genome expression profiles of cells cultured for several generations on a novel surface with identical cells cultured in the reference system may provide more insight into whether the cells can be regarded as biologically comparable to the reference cells and whether the surface or a micro system or an implant can be regarded as biocompatible (Figure 55). In principle, whole genome expression profiling utilizes more than 40,000 “sensors” to assess the actual metabolic state of a cell culture.

### **Bio-comparability**

As cells cultured on SU-8 treated with HNO<sub>3</sub>-CAN displayed similar proliferation rate (Figure 52) and morphology (Figure 53) when compared to cells cultured in the unperturbed culture flask, but showed a significantly different whole genome expression profile (Figure 55), led us to define a novel concept for comparing surfaces or environments used in cell



culturing. We defined bio-comparability as the degree of similarity in gene expression profiles between cells grown on two different surfaces. Surfaces or culturing conditions resulting in indistinguishable gene expression profiles were denoted bio-comparable. In the present study PMMA (Figure 39) and SU-8 treated with HNO<sub>3</sub>-CAN and ethanolamine (Figure 55) was found to be bio-comparable to the TC-PS culture flask. Furthermore the  $\mu$ CCC also gave rise to bio-comparable culture conditions (Figure 40). Similar growth kinetics (Figure 52) and morphology (Figure 53) was observed on SU-8 treated with HNO<sub>3</sub>-CAN, suggesting the surface to be biocompatible when compared to the culture flask. However, the whole genome expression profile indicated that the surface was not bio-comparable (Figure 55). Thus, biocompatibility does not infer bio-comparability.

It is possible that dissimilarities on the protein level could exist in cells growth on the four bio-comparable surfaces/environments (PMMA, cell culture flask,  $\mu$ CCC and SU-8 treated with HNO<sub>3</sub>-CAN and ethanol amine) which is not directly measured using DNA microarrays. This indicates that protein microarray may be better choice for analyzing bio-comparability in the future. Such protein microarray may also detect secondary modifications on proteins induced by surfaces. Current protein arrays are however less comprehensive than DNA microarrays<sup>109</sup> making protein arrays less ideal at the moment.

In the present study only the HeLa cell line was evaluated for bio-comparability in the  $\mu$ CCC. As different cell lines may respond differently to stimuli<sup>176,177</sup>, all cell lines should be evaluated for bio-comparability prior to making comparisons on assays performed in the  $\mu$ CCC with the culture flask.

### **Growth kinetics**

We found a flowrate of 0.1 mL/h (1.67  $\mu$ L/min) resulting in the theoretic exchange of media every hour suitable for the  $\mu$ CCC as the proliferation rate (Figure 19 and Figure 42) and the whole genome expression profile (Figure 40 and Table 2) were comparable to the cell culture flask. In another study utilizing an array of interconnected culture chambers, a slower flowrate (0.12  $\mu$ L/min resulting in exchange of media every 4.4 hours) was found optimal<sup>27,28</sup>. However the height of the chambers were only 40  $\mu$ m and it was not indicated which chamber in the array was used to establish the optimal growth rate. It could be speculated that the waste products generated in the first chambers would influence the growth rate in the following as spent media is perfused from chamber one through 10 in the array. However

growth rate comparisons between *i.e.* chamber one and ten in the chamber array were not included in the study. In the  $\mu$ CCC the media perfusion inlet was located more than 1 mm above the cell culturing surface and the total exchange of media components and waste products relied on diffusion. As the growth rates of both HeLa (Figure 19) and CACO 2 (Figure 42) cells observed in the  $\mu$ CCC corresponded to the growth rates of the control cells in the CO<sub>2</sub> incubator, and with values reported in the literature when a flowrate of 0.1 mL/h was used, we did not investigate the effect of flowrate further. However, when culturing hNS1 stem cells a growth rate of 25 hours was observed (Figure 46) which was roughly 15 hours faster than the growth rate reported in the literature<sup>178</sup>. This may result from the increased availability of the growth factors in the  $\mu$ CCC due to the continuous perfusion.

Determination of the generation time of COLO 205 cells was hampered by the extreme mobility of these cells in culture (Figure 44 - Figure 45) making it difficult to identify if the accumulation of cells were due to cellular migration or proliferation. The majority of cells migrated from the upper left to the lower right corner, indicating a preference for cell migration. However, cells were also observed to migrate in the opposite direction. These mobility observations of COLO 205 correlated well with the cell line were derived from a tumor that forms metastasis<sup>131</sup>, a trait which usually is associated with decreased adhesion and increased cell mobility<sup>179</sup>. If this increased migration rate was caused by protein movement similar to the actin-myosin movement in contracting muscles, the  $\mu$ CCC seems an ideal platform for on-line studying these proteins under culturing conditions similar to the reference cell culture flask.

### **Other cell culture chambers**

The  $\mu$ CCC presented in this thesis does unlike many other cell culture devices<sup>9,19,20,22,28,30</sup> not rely on the CO<sub>2</sub> incubator to supply heat, humidity and CO<sub>2</sub> for stabilizing the pH of the media. The  $\mu$ CCC has been proven to facilitate long term culturing (>2 weeks) of mammalian cells without contamination. The almost identical gene expression profile in cells grown on in the  $\mu$ CCC as compared with cells grown in the cell culture flask (Figure 40 and Table 2) strongly indicate that there is little if any difference between the two culturing conditions and the cells in the two systems could thus be directly compared to the HeLa cells. To our knowledge, this is the first cell culture chip for mammalian cells that has been validated down to the transcriptome level of the cultured cells. As DNA microarrays do not reveal information regarding protein abundance, stability, splice variations, post transcriptional

modifications etc. there is still the a small possibility that culture conditions provided by the  $\mu$ CCC might induce differences in terms of cellular responses when compared to the reference culture flask. Before conclusions are drawn based on biological assays performed in the  $\mu$ CCC relative to the reference culture flask, proper control experiments must be performed to elucidate if the assay conditions are comparable.

In contrast, in many microfluidic cell culture chamber designs, biocompatibility of cells in the chamber was either not considered or presented <sup>4,9,16,18,20,22,26,28</sup>. Other chambers were evaluated using crude viability assays <sup>8,21,30</sup> or morphological observations and growth kinetics <sup>19,32</sup>. Viability was also used to assess toxicity of the epoxy and UV curable glue in the present study (Figure 14), but viability assays only provides information on if the materials are associated with adverse effects. Such assays are not as sensitive as compared to gene expression arrays since the latter has the potential to find subtle changes not detected by cell growth kinetics or morphology studies. Cells displaying similar morphology may show differences in expression patterns <sup>180</sup> indicating that morphological comparison may not be sufficient for assessing biocompatibility. Gene expression profiling has been achieved on a single cell <sup>180,181</sup> enabling comparability verification to be performed on virtually all cell culture devices provided that the cell or cell RNA can be extracted.

In some studies individual cell culture chambers were arranged in arrays of interconnected chambers <sup>4,5,15,27,28</sup> in what could resemble a feeding line. Fresh media was perfused from the first chamber through all chambers in the feeding line prior to exiting to the waste. Feeding lines contained from 4 individual cell culture chambers <sup>15</sup> to 10 <sup>27,28</sup> and up to 16 chambers <sup>4,5</sup>. Depending of the flow rate utilized and the degree of cell confluence in the chambers, this may result a gradient of nutrients concentrations in the media. Furthermore, the feeding line may result in a gradient of the concentrations of both secreted waste products and growths factors from the first sub-chambers to the others. These gradients may result in different culturing conditions in the different culture chambers in the feeding line. However, no data was provided on *e.g.* differences growth kinetics in the different chambers.

### **Random priming**

Assessment of the bio-comparability of a novel surface or culture condition requires that the cDNA used is representative to the RNA pool. Whole genome expression profiling on DNA microarrays relies on the reverse transcription reaction to efficiently transcribe the entire

mRNA pool (transcriptome). The priming strategy in reverse transcription reactions may have large effects on the cDNA yield and quality<sup>89</sup>. Priming with random pentadecamers resulted in 80 % of the complex aRNA or mRNA population being reverse transcribed (Figure 56 and Figure 57). However, cDNA was measured spectroscopically *after* spin column purification steps, a purification method that usually results in loss of DNA. It is therefore likely that R15 and R12 primer primed reactions have yields close to 100 % indicating that almost the entire aRNA or mRNA pool (transcriptome) is reverse transcribed using R15 and R12 primers. The increased coverage of the transcription process using R15 primers may explain why 55-72 % more genes were considered expressed on microarrays hybridized with R15 primed cDNA compared to Inv primed cDNA (Figure 64). In comparison, up to eleven fold more genes were considered expressed on arrays hybridized with twice the amount of R15 primed cDNA compared to Inv primed cDNA (Figure 64). The latter result reflects the practical effect of the increased yield of cDNA synthesis using R15 primers (Figure 56 and Figure 57). The results strongly show that priming with random pentadecamers in cDNA synthesis results in better sensitivity in DNA microarray assays.

The largest effect on the number of genes detected using R15 primers in the cDNA synthesis was obtained in the Cy-5 channel. This is not surprising since we observed a non-linear relationship between the Cy-5 and Cy-3 channels with the Cy-5 channel consistently having lower signals (Figure 62). Increases in target concentration as result of using R15 as primers will therefore have larger effect on the number of genes detected since more genes were close to the background level when using Cy-5 as fluorochrome compared to Cy-3 (Figure 64).

Hybridization efficiencies of random primers to the RNA template may vary substantially due to sequence related secondary folding of the RNA template<sup>182</sup>. Increasing the annealing temperature in reverse transcription reactions increases the yield of the reaction by reducing the degree of secondary structures in the RNA template<sup>91,183</sup>. Random pentadecamers has previously been reported to be used as primers in pre-amplification steps in whole genome amplification (WGA)<sup>184</sup>. Presumably R15 primers were chosen because they would function in the PCR where annealing was done at 37 °C a temperature close to the 42 °C used in reverse transcriptions. Recently, reverse transcription polymerases operating at higher temperatures >50 °C has been introduced<sup>185,186</sup>. These enzymes should give better efficiency of reverse transcription reaction due to the fact that less secondary structures in the RNA are encountered during the transcription process<sup>186</sup>. It is likely that priming with longer primers could also have a large positive effect on reverse transcription reactions performed at 50 °C

since a larger fraction of the longer primers will be able to form duplexes with the RNA than the shorter primers.

During reverse transcription aminoallyl-dUTP are incorporated replacing dTTP. Following the reaction, fluorescent labels are conjugated to the aminoallyl groups enabling the detection of the cDNA on DNA microarrays. Hypothesizing that the aminoallyl-dUTP incorporation will take place more frequently in AT-rich regions this should in result in the detection of these regions on DNA microarray. However, if random hexamers are used as primers in the reverse transcription reaction at 42 °C, the majority of the primers may not remain hybridized to the RNA template long enough to ensure transcription as the melting temperature of AT-rich primers would be <15 °C (Figure 60). AT-rich R15 primers have a melting temperature slightly below 40 °C. This may explain the findings that R15 priming results in the identification of more genes (Figure 64) and suggest that random hexamer priming may not optimal for AT-rich templates.

The larger number of genes detected using non-normalized data (Figure 64) suggest initially that there would be significantly more genes that showed different expression pattern using normalized data. However, the normalization procedure is constructed to reduce systematic differences<sup>111</sup>. Normalization operates by assuming that no gene was regulated and as much as two fold more detected genes (using equimolar concentration of cDNA) may be considered a systematic change and is corrected for. This was also apparent when analyzing normalized data using different amount of targets (Figure 63 A-B) where essentially no difference was observed.

## 6 Conclusion

A low cost optically transparent polymeric micro cell culture chamber ( $\mu$ CCC) with integrated media perfusion microfluidics, temperature monitoring and regulation was developed. The fabrication process, which was based on laser micromachining and thermal bonding, offered a highly flexible design of the device, providing numerous lab-on-a-chip integration possibilities in the future. The  $\mu$ CCC was characterized by cell culturing of various cell lines and whole genome expression profiling. All tested cell lines could be cultured in the  $\mu$ CCC. The  $\mu$ CCC also supported resuscitation of cells from low temperature storage. Cells cultured in the  $\mu$ CCC revealed almost indistinguishable whole genome expression profiles to the reference cell culture flasks. No signs of photo induced effects, activation of DNA repair systems or shear stress was observed using whole human genome DNA microarrays. This suggests that the  $\mu$ CCC supports the culturing and on-line monitoring of mammalian cells under conditions indistinguishable from the reference cell culture flask in the CO<sub>2</sub> incubator. To the best of my knowledge the  $\mu$ CCC is the only micro cell culture chamber characterized using whole genome expression profiling.

A novel concept of bio-comparability was devised. Surfaces or culturing conditions resulting in similar whole genome expression profiles were defined as being bio-comparable. Bio-comparability should not be mistaken with biocompatibility. Two surfaces may be biocompatible *i.e.* no difference in cell morphology or cell growth kinetics may be observed, but significant differences gene expression profiles may be observed.

A novel random priming method was also developed and characterized in reverse transcription reactions. Not only was the yield increased at least two fold using both aRNA and mRNA templates up to 24-81 % more genes were considered expressed in the Cy-3 or Cy-5 channel respectively compared to a commercial random hexamer primer formulation.

## 7 Future outlook

The  $\mu$ CCC presented in the present thesis is capable of providing a culture environment which closely resembles the conventional culture flask and enables long term ( $> 2$  weeks) culturing of mammalian cells. The transparent nature of the polymers comprising the chamber enables on-line monitoring of the cell culture.

Initial experiments were performed with a modified design of the  $\mu$ CCC enabling the thermistor to be recycled reducing the cost price of the chambers. If the UV-curable and the epoxy glues used, were replaced with biocompatible versions of the same physical parameters, this chamber would be a significant improvement to the  $\mu$ CCC design.

The power of the  $\mu$ CCC could be further increased if the media outlet was passed over an antibody array containing *e.g.* immobilized antibodies directed against targeted secreted proteins, cytokines etc. and a secondary fluorescent labeled antibody was included in the media formulation on-line studies of protein expression was possible directly on a fluorescent microscope. The chamber comprising the antibody array could be heated using a similar ITO heater with thermistor based temperature monitoring and PID regulation. To avoid bleaching of the fluorescent labels a simple electronic switch should be designed capable of either turning on the microscope lamp or allowing the light to pass through to the chamber only when needed for obtaining the images.

Realization of a chamber holding a protein array would require a different bonding method as spotted proteins would not sustain the high temperatures required for bonding of PMMA. However bonding of PMMA sheets can be achieved using either acetone or dichloromethane without compromising either DNA-DNA or protein-protein interactions.

Media perfusion could also be simplified using the combination of gravity and capillary forces to drag fresh media through the chamber.

If the  $\mu$ CCC was redesigned using the suggestions regarding recycling the thermistor, commercialization of the system seem possible.

## 8 References

1. Gey, G. O., Coffman, W. D. & Kubicek, M. T. Tissue Culture Studies of the Proliferative Capacity of Cervical Carcinoma and Normal Epithelium. *Cancer Res* **12**, 264-265 (1952).
2. Dailey, M., Manders, E., Soll, D. & Terasaki, M. in *Handbook of Biological Confocal Microscopy* (ed. Pawley, J.) (Kluwer Academic Publishers, 2005).
3. Dailey, M., Marrs, G. & Kurpius, D. in *Imaging in Neuroscience and Development: A Laboratory Manual* (eds. Yuste, R. & Konnerth, A.) 1-8 (Cold Spring Harbor Lab Press, Cold Spring Harbor, NY., 2005).
4. Thompson, D. M. et al. Dynamic gene expression profiling using a microfabricated living cell array. *Anal Chem* **76**, 4098-103 (2004).
5. Wieder, K. J. et al. Optimization of Reporter Cells for Expression Profiling in a Microfluidic Device. *Biomed Microdevices* **7**, 213-222 (2005).
6. Fiorini, G. S. & Chiu, D. T. Disposable microfluidic devices: fabrication, function, and application. *Biotechniques* **38**, 429-46 (2005).
7. Ince, C., Beekman, R. E. & Verschragen, G. A micro-perfusion chamber for single-cell fluorescence measurements. *J Immunol Methods* **128**, 227-34 (1990).
8. Jager, E. W. H. et al. The Cell Clinic: Closable Microvials for Single Cell Studies. *Biomedical Microdevices* **4**, 177-187 (2002).
9. Prokop, A. et al. NanoLiterBioReactor: Long-Term Mammalian Cell Culture at Nanofabricated Scale. *Biomed Microdevices* **6**, 325-39 (2004).
10. Cooper, J. M. Towards electronic Petri dishes and picolitre-scale single-cell technologies. *Trends Biotechnol* **17**, 226-30 (1999).
11. Inoue, I., Wakamoto, Y., Moriguchi, H., Okano, K. & Yasuda, K. On-chip culture system for observation of isolated individual cells. *Lab Chip* **1**, 50-5 (2001).
12. Wakamoto, Y., Inoue, I., Moriguchi, H. & Yasuda, K. Analysis of single-cell differences by use of an on-chip microculture system and optical trapping. *Fresenius' Journal of Analytical Chemistry* **371**, 276-281 (2001).
13. Ince, C., van Dissel, J. T. & Diesselhoff, M. M. A teflon culture dish for high-magnification microscopy and measurements in single cells. *Pflugers Arch* **403**, 240-4 (1985).
14. Leclerc, E., Sakai, Y. & Fujii, T. Cell culture in 3-dimensional microfluidic structure of PDMS (polydimethylsiloxane). *Biomedical Microdevices* **5**, 109-114 (2003).
15. Leclerc, E., Sakai, Y. & Fujii, T. Microfluidic PDMS (polydimethylsiloxane) bioreactor for large-scale culture of hepatocytes. *Biotechnol Prog* **20**, 750-5 (2004).
16. Ho, C. L., Mou, T. Y., Chiang, P. S., Weng, C. L. & Chow, N. H. Mini chamber system for long-term maintenance and observation of cultured cells. *Biotechniques* **38**, 267-73 (2005).
17. Hofer, A. et al. A new perfusion cell chamber system for determination of heat shock effects by means of video-enhanced microscopy. *Med Biol Eng Comput* **37**, 667-9 (1999).
18. Moriguchi, H. et al. An agar-microchamber cell-cultivation system: flexible change of microchamber shapes during cultivation by photo-thermal etching. *Lab Chip* **2**, 125-32 (2002).
19. Tourovskaia, A., Figueroa-Masot, X. & Folch, A. Differentiation-on-a-chip: a microfluidic platform for long-term cell culture studies. *Lab Chip* **5**, 14-9 (2005).
20. Kojima, K., Kaneko, T. & Yasuda, K. A novel method of cultivating cardiac myocytes in agarose microchamber chips for studying cell synchronization. *J Nanobiotechnology* **2**, 9 (2004).



21. Li Jeon, N. et al. Neutrophil chemotaxis in linear and complex gradients of interleukin-8 formed in a microfabricated device. *Nat Biotechnol* **20**, 826-30 (2002).
22. Hediger, S., Fontannaz, J., Sayah, A., Hunziker, W. & Gijs, M. A. M. Biosystem for the culture and characterisation of epithelial cell tissues. *Sensors and Actuators B: Chemical* **63**, 63-73 (2000).
23. Hediger, S., Sayah, A., Horisberger, J. D. & Gijs, M. A. M. Modular microsystem for epithelial cell culture and electrical characterisation. *Biosensors and Bioelectronics* **16**, 689-694 (2001).
24. Blau, A. W. & Ziegler, C. M. Prototype of a novel autonomous perfusion chamber for long-term culturing and in situ investigation of various cell types. *J Biochem Biophys Methods* **50**, 15-27 (2001).
25. Lin, Y.-C., Jen, C.-M., Huang, M.-Y., Wu, C.-Y. & Lin, X.-Z. Electroporation microchips for continuous gene transfection. *Sensors and Actuators B: Chemical* **79**, 137-143 (2001).
26. Davidsson, R. et al. Developments toward a microfluidic system for long-term monitoring of dynamic cellular events in immobilized human cells. *Anal Chem* **76**, 4715-20 (2004).
27. Hung, P. J., Lee, P. J., Sabounchi, P., Lin, R. & Lee, L. P. Continuous perfusion microfluidic cell culture array for high-throughput cell-based assays. *Biotechnol Bioeng* **89**, 1-8 (2005).
28. Hung, P. J. et al. A novel high aspect ratio microfluidic design to provide a stable and uniform microenvironment for cell growth in a high throughput mammalian cell culture array. *Lab Chip* **5**, 44 - 48 (2005).
29. Viravaidya, K., Sin, A. & Shuler, M. L. Development of a microscale cell culture analog to probe naphthalene toxicity. *Biotechnol Prog* **20**, 316-23 (2004).
30. Sin, A. et al. The design and fabrication of three-chamber microscale cell culture analog devices with integrated dissolved oxygen sensors. *Biotechnol Prog* **20**, 338-45 (2004).
31. Viravaidya, K. & Shuler, M. L. Incorporation of 3T3-L1 cells to mimic bioaccumulation in a microscale cell culture analog device for toxicity studies. *Biotechnol Prog* **20**, 590-7 (2004).
32. Hing, W. A., Poole, C. A., Jensen, C. G. & Watson, M. An integrated environmental perfusion chamber and heating system for long-term, high resolution imaging of living cells. *J Microsc* **199** ( Pt 2), 90-5 (2000).
33. Kaplan, D., Bungay, P., Sullivan, J. & Zimmerberg, J. A rapid-flow perfusion chamber for high-resolution microscopy. *J Microsc* **181** ( Pt 3), 286-97 (1996).
34. Focht, D. C. Live-cell microscopy: environmental control for mammalian specimens. *Nat Biotechnol* **14**, 361-2 (1996).
35. Kirkpatrick, C. J. et al. Current trends in biocompatibility testing. *Proc Inst Mech Eng [H]* **212**, 75-84 (1998).
36. Wang, Y.-X., Robertson, J. L., Spillman, W. B. & Claus, R. O. Effects of the Chemical Structure and the Surface Properties of Polymeric Biomaterials on Their Biocompatibility. *Pharmaceutical Research* **21**, 1362-1373 (2004).
37. Dekker, A. et al. Quantitative methods for in vitro cytotoxicity testing of biomaterials. *Cells Mater. (USA)* **4**, 101-112 (1994).
38. Kirkpatrick, C. J. & Dekker, A. Quantitative evaluation of cell interaction with biomaterials in vitro. *Adv. Biomater.* **10**, 31 (1992).
39. Kooten, T. G. V. et al. From cytotoxicity to biocompatibility testing in vitro: cell adhesion molecule expression defines a new set of parameters. *Journal of Materials Science: Materials in Medicine* **8**, 835-841 (1997).
40. Dalby, M. J., Silvio, L. D., Harper, E. J. & Bonfield, W. In vitro adhesion and biocompatibility of osteoblast-like cells to poly(methylmethacrylate) and

- poly(ethylmethacrylate) bone cements. *Journal of Materials Science: Materials in Medicine* **13**, 311-314 (2002).
41. Kirkpatrick, C. J. et al. Quantitative scanning electron microscopy (SEM) to study the adhesion and spreading of human endothelial cells to surface-modified poly(carbonate urethane)s. *Cells and Mater.* **2**, 166-177 (1992).
  42. Geckeler, K. E., Wacker, R. & Aicher, W. K. Biocompatibility correlation of polymeric materials using human osteosarcoma cells. *Naturwissenschaften* **87**, 351-4 (2000).
  43. Allen, L. T. et al. Interaction of soft condensed materials with living cells: phenotype/transcriptome correlations for the hydrophobic effect. *Proc Natl Acad Sci U S A* **100**, 6331-6 (2003).
  44. Nicolau, D. V., Taguchi, T., Tanigawa, H. & Yoshikawa, S. Control of neuronal cell attachment by functionality manipulation of diazo-naphtho-quinone/novolac photoresist surface. *Biosens Bioelectron* **11**, 1237-1252 (1996).
  45. Irimia, D. & Karlsson, J. O. M. Development of a cell patterning technique using poly(ethylene glycol) disilane. *Biomedical Microdevices* **5**, 185-194 (2003).
  46. Gallant, N. D., Capadona, J. R., Frazier, A. B., Collard, D. M. & García, A. J. Micropatterned Surfaces to Engineer Focal Adhesions for Analysis of Cell Adhesion Strengthening. *Langmuir* **18**, 5579-5584 (2002).
  47. Charest, J. L., Bryant, L. E., Garcia, A. J. & King, W. P. Hot embossing for micropatterned cell substrates. *Biomaterials* **25**, 4767-75 (2004).
  48. Bouaidat, S. et al. Micro patterning of cell and protein non-adhesive plasma polymerized coatings for biochip applications. *Lab Chip* **4**, 632-7 (2004).
  49. Kato, K. et al. Immobilized culture of nonadherent cells on an oleyl poly(ethylene glycol) ether-modified surface. *Biotechniques* **35**, 1014-8, 1020-1 (2003).
  50. Pierschbacher, M. D. & Ruoslahti, E. Cell attachment activity of fibronectin can be duplicated by small synthetic fragments of the molecule. *Nature* **309**, 30-3 (1984).
  51. Hersel, U., Dahmen, C. & Kessler, H. RGD modified polymers: biomaterials for stimulated cell adhesion and beyond. *Biomaterials* **24**, 4385-4415 (2003).
  52. Kirkpatrick, C. J., Mohr, W. & Haferkamp, O. The effects of nickel ions on articular chondrocyte growth in monolayer culture. *Res Exp Med (Berl)* **181**, 259-64 (1982).
  53. Carinci, F. et al. Zirconium oxide: analysis of MG63 osteoblast-like cell response by means of a microarray technology. *Biomaterials* **25**, 215-28 (2004).
  54. Tsuda, Y. et al. The use of patterned dual thermoresponsive surfaces for the collective recovery as co-cultured cell sheets. *Biomaterials* **26**, 1885-93 (2005).
  55. Yamato, M. & Okano, T. Cell sheet engineering. *Materials Today* **7**, 42-47 (2004).
  56. Kapur, R. et al. Streamlining the Drug Discovery Process by Integrating Miniaturization, High Throughput Screening, High Content Screening, and Automation on the CellChip™ System. *Biomedical Microdevices* **2**, 99-109 (1999).
  57. Ito, Y. Surface micropatterning to regulate cell functions. *Biomaterials* **20**, 2333-42 (1999).
  58. McFarland, C. D., Thomas, C. H., DeFilippis, C., Steele, J. G. & Healy, K. E. Protein adsorption and cell attachment to patterned surfaces. *J Biomed Mater Res* **49**, 200-10 (2000).
  59. Bhatia, S. N., Yarmush, M. L. & Toner, M. Controlling cell interactions by micropatterning in co-cultures: hepatocytes and 3T3 fibroblasts. *J Biomed Mater Res* **34**, 189-99 (1997).
  60. Singhvi, R. et al. Engineering cell shape and function. *Science* **264**, 696-8 (1994).
  61. Mrksich, M., Dike, L. E., Tien, J., Ingber, D. E. & Whitesides, G. M. Using Microcontact Printing to Pattern the Attachment of Mammalian Cells to Self-Assembled Monolayers of Alkanethiolates on Transparent Films of Gold and Silver. *Experimental Cell Research* **235**, 305-313 (1997).

62. Chen, C. S., Mrksich, M., Huang, S., Whitesides, G. M. & Ingber, D. E. Geometric control of cell life and death. *Science* **276**, 1425-8 (1997).
63. Patel, N. et al. Spatially controlled cell engineering on biodegradable polymer surfaces. *FASEB Journal* **12**, 1447-1454 (1998).
64. Folch, A. & Toner, M. Cellular micropatterns on biocompatible materials. *Biotechnology Progress* **14**, 388-392 (1998).
65. Ostuni, E., Kane, R., Chen, C. S., Ingber, D. E. & Whitesides, G. M. Patterning mammalian cells using elastomeric membranes. *Langmuir* **16**, 7811-7819 (2000).
66. Folch, A., Jo, B.-H., Hurtado, O., Beebe, D. J. & Toner, M. Microfabricated elastomeric stencils for micropatterning cell cultures. *Journal of Biomedical Materials Research* **52**, 346-353 (2000).
67. Wang, R. J. Lethal effect of "daylight" fluorescent light on human cells in tissue-culture medium. *Photochem Photobiol* **21**, 373-5 (1975).
68. Zigler, J. S., Jr., Lepe-Zuniga, J. L., Vistica, B. & Gery, I. Analysis of the cytotoxic effects of light-exposed HEPES-containing culture medium. *In Vitro Cell Dev Biol* **21**, 282-7 (1985).
69. Lucius, R., Mentlein, R. & Sievers, J. Riboflavin-mediated axonal degeneration of postnatal retinal ganglion cells in vitro is related to the formation of free radicals. *Free Radic Biol Med* **24**, 798-808 (1998).
70. Stoen, J. D. & Wang, R. J. Effect of near-ultraviolet and visible light on mammalian cells in culture II. Formation of toxic photoproducts in tissue culture medium by blacklight. *Proc Natl Acad Sci U S A* **71**, 3961-5 (1974).
71. Edwards, A. M., Silva, E., Jofre, B., Becker, M. I. & De Ioannes, A. E. Visible light effects on tumoral cells in a culture medium enriched with tryptophan and riboflavin. *J Photochem Photobiol B* **24**, 179-86 (1994).
72. Siegel, W. & Pritchett, T. Tutorial: Examining the relationship between media and light. *Bio-pharm* **13**, 65-66 (2000).
73. Wang, R. J. Effect of room fluorescent light on the deterioration of tissue culture medium. *In Vitro* **12**, 19-22 (1976).
74. Poli, G. & Parola, M. Oxidative damage and fibrogenesis. *Free Radic Biol Med* **22**, 287-305 (1997).
75. Spierenburg, G. T., Oerlemans, F. T., van Laarhoven, J. P. & de Bruyn, C. H. Phototoxicity of N-2-hydroxyethylpiperazine-N'-2-ethanesulfonic acid-buffered culture media for human leukemic cell lines. *Cancer Res* **44**, 2253-4 (1984).
76. Lepe-Zuniga, J. L., Zigler, J. S., Jr. & Gery, I. Toxicity of light-exposed Hepes media. *J Immunol Methods* **103**, 145 (1987).
77. DeRisi, J. et al. Use of a cDNA microarray to analyse gene expression patterns in human cancer. *Nat Genet* **14**, 457-60 (1996).
78. Marton, M. J. et al. Drug target validation and identification of secondary drug target effects using DNA microarrays. *Nat Med* **4**, 1293-301 (1998).
79. Yang, Y. H. et al. Normalization for cDNA microarray data: a robust composite method addressing single and multiple slide systematic variation. *Nucl.Acids.Res.* **30**, e15 (2002).
80. Aslanian, A., Iaquinta, P. J., Verona, R. & Lees, J. A. Repression of the Arf tumor suppressor by E2F3 is required for normal cell cycle kinetics. *Genes Dev.* **18**, 1413-1422 (2004).
81. Maxfield, L. F., Fraize, C. D. & Coffin, J. M. From The Cover: Relationship between retroviral DNA-integration-site selection and host cell transcription. *PNAS* **102**, 1436-1441 (2005).
82. Hughes, T. P. et al. Frequency of Major Molecular Responses to Imatinib or Interferon Alfa plus Cytarabine in Newly Diagnosed Chronic Myeloid Leukemia. *N Engl J Med* **349**, 1423-1432 (2003).

83. Melo, J. V. et al. Reverse transcription/polymerase chain reaction (RT/PCR) amplification of very small numbers of transcripts: the risk in misinterpreting negative results. *Leukemia* **10**, 1217-21 (1996).
84. Suzuki, S., Asamoto, M., Tsujimura, K. & Shirai, T. Specific differences in gene expression profile revealed by cDNA microarray analysis of glutathione S-transferase placental form (GST-P) immunohistochemically positive rat liver foci and surrounding tissue. *Carcinogenesis* **25**, 439-443 (2004).
85. Mannhalter, C., Koizar, D. & Mitterbauer, G. Evaluation of RNA Isolation Methods and Reference Genes for RT-PCR Analyses of Rare Target RNA. *Clin Chem Lab Med* **38**, 171-177 (2000).
86. Li, X., Miyajima, M. & Arai, H. Analysis of TGF- $\beta$ 2 and TGF- $\beta$ 3 expression in the hydrocephalic H-Tx rat brain. *Child's Nervous System* **21**, 32-38 (2005).
87. Asnafi, V. et al. Analysis of TCR, pT $\alpha$ , and RAG-1 in T-acute lymphoblastic leukemias improves understanding of early human T-lymphoid lineage commitment. *Blood* **101**, 2693-2703 (2003).
88. Bustin, S. A. & Nolan, T. Pitfalls of Quantitative Real-Time Reverse-Transcription Polymerase Chain Reaction. *J Biomol Tech* **15**, 155-166 (2004).
89. Ståhlberg, A., Hakansson, J., Xian, X., Semb, H. & Kubista, M. Properties of the reverse transcription reaction in mRNA quantification. *Clin Chem* **50**, 509-15 (2004).
90. Michor, F. et al. Dynamics of chronic myeloid leukaemia. **435**, 1267-1270 (2005).
91. Brooks, E. M., Sheflin, L. G. & Spaulding, S. W. Secondary structure in the 3' UTR of EGF and the choice of reverse transcriptases affect the detection of message diversity by RT-PCR. *Biotechniques* **19**, 806-12, 814-5 (1995).
92. Brink, A. A. et al. Multiprimed cDNA synthesis followed by PCR is the most suitable method for Epstein-Barr virus transcript analysis in small lymphoma biopsies. *Mol Cell Probes* **11**, 39-47 (1997).
93. Iturriza-Gomara, M., Green, J., Brown, D. W., Desselberger, U. & Gray, J. J. Comparison of specific and random priming in the reverse transcriptase polymerase chain reaction for genotyping group A rotaviruses. *J Virol Methods* **78**, 93-103 (1999).
94. Schena, M., Shalon, D., Davis, R. W. & Brown, P. O. Quantitative monitoring of gene expression patterns with a complementary DNA microarray. *Science* **270**, 467-70 (1995).
95. Decraene, C., Reguigne-Arnould, I., Auffray, C. & Pietu, G. Reverse transcription in the presence of dideoxynucleotides to increase the sensitivity of expression monitoring with cDNA arrays. *Biotechniques* **27**, 962-6 (1999).
96. Yang, I. V. et al. Within the fold: assessing differential expression measures and reproducibility in microarray assays. *Genome Biol* **3**, research0062 (2002).
97. Sterrenburg, E., Turk, R., Boer, J. M., van Ommen, G. B. & den Dunnen, J. T. A common reference for cDNA microarray hybridizations. *Nucl.Acids.Res.* **30**, e116 (2002).
98. Luo, L. et al. Gene expression profiles of laser-captured adjacent neuronal subtypes. *Nat Med* **5**, 117-22 (1999).
99. Xiang, C. C. et al. Amine-modified random primers to label probes for DNA microarrays. *Nat Biotechnol* **20**, 738-742 (2002).
100. Kane, M. D. et al. Assessment of the sensitivity and specificity of oligonucleotide (50mer) microarrays. *Nucleic Acids Res* **28**, 4552-4557 (2000).
101. Schena, M. et al. Parallel human genome analysis: microarray-based expression monitoring of 1000 genes. *Proc Natl Acad Sci U S A* **93**, 10614-9 (1996).
102. Southern, E., Mir, K. & Shchepinov, M. Molecular interactions on microarrays. *Nat Genet* **21**, 5-9 (1999).
103. Duggan, D. J., Bittner, M., Chen, Y., Meltzer, P. & Trent, J. M. Expression profiling using cDNA microarrays. *Nat Genet* **21**, 10-4 (1999).

104. Lipshutz, R. J., Fodor, S. P., Gingeras, T. R. & Lockhart, D. J. High density synthetic oligonucleotide arrays. *Nat Genet* **21**, 20-4 (1999).
105. Cheung, V. G. et al. Making and reading microarrays. *Nat Genet* **21**, 15-9 (1999).
106. Zhang, L. et al. Gene Expression Profiles in Normal and Cancer Cells. *Science* **276**, 1268-1272 (1997).
107. Alizadeh, A. A. et al. Distinct types of diffuse large B-cell lymphoma identified by gene expression profiling. *Nature* **403**, 503-11 (2000).
108. Ma, X. J. et al. Gene expression profiles of human breast cancer progression. *Proc Natl Acad Sci U S A* **100**, 5974-9 (2003).
109. Dufva, M. & Christensen, C. B. Diagnostic and analytical applications of protein microarrays. *Expert Rev Proteomics* **2**, 41-8 (2005).
110. Klank, H., Kutter, J. P. & Geschke, O. CO<sub>2</sub>-laser micromachining and back-end processing for rapid production of PMMA-based microfluidic systems. *Lab Chip* **2**, 242-6 (2002).
111. Workman, C. et al. A new non-linear normalization method for reducing variability in DNA microarray experiments. *Genome Biol* **3**, research0048 (2002).
112. Rafael A. Irizarry et al. (2005).
113. Gentleman, R. C. et al. Bioconductor: open software development for computational biology and bioinformatics. *Genome Biol* **5**, R80 (2004).
114. R\_Development\_Core\_Team. (R Foundation for Statistical Computing, Vienna, Austria, 2005).
115. Hu, S. et al. Surface modification of poly(dimethylsiloxane) microfluidic devices by ultraviolet polymer grafting. *Anal Chem* **74**, 4117-23 (2002).
116. Charati, S. G. & Stern, S. A. Diffusion of Gases in Silicone Polymers: Molecular Dynamics Simulations. *Macromolecules* **31**, 5529-5535 (1998).
117. T. C. Merkel, V. I. B., K. Nagai, B. D. Freeman, I. Pinnau., Gas sorption, diffusion, and permeation in poly(dimethylsiloxane). *Journal of Polymer Science Part B: Polymer Physics* **38**, 415-434 (2000).
118. De Bo, I. et al. Investigation of the permeability and selectivity of gases and volatile organic compounds for polydimethylsiloxane membranes. *Journal of Membrane Science* **215**, 303-319 (2003).
119. Dufva, M., Stangegaard, M. & Christensen, C. in *μTAS 276-278* (Malmö, Sweden, 2004).
120. Zieger, M. A., Glogfcheski, D. J., Lepock, J. R. & Kruuv, J. Factors influencing survival of mammalian cells exposed to hypothermia. V. Effects of hepes, free radicals, and H<sub>2</sub>O<sub>2</sub> under light and dark conditions. *Cryobiology* **28**, 8-17 (1991).
121. Cho, R. J. et al. A genome-wide transcriptional analysis of the mitotic cell cycle. *Mol Cell* **2**, 65-73 (1998).
122. Spellman, P. T. et al. Comprehensive identification of cell cycle-regulated genes of the yeast *Saccharomyces cerevisiae* by microarray hybridization. *Mol Biol Cell* **9**, 3273-97 (1998).
123. Iyer, V. R. et al. The transcriptional program in the response of human fibroblasts to serum. *Science* **283**, 83-7 (1999).
124. Tusher, V. G., Tibshirani, R. & Chu, G. Significance analysis of microarrays applied to the ionizing radiation response. *Proc Natl Acad Sci U S A* **98**, 5116-21 (2001).
125. Dhanasekaran, S. M. et al. Delineation of prognostic biomarkers in prostate cancer. *Nature* **412**, 822-6 (2001).
126. Golub, T. R. et al. Molecular classification of cancer: class discovery and class prediction by gene expression monitoring. *Science* **286**, 531-7 (1999).
127. Hughes, T. R. et al. Expression profiling using microarrays fabricated by an ink-jet oligonucleotide synthesizer. *Nat Biotechnol* **19**, 342-347 (2001).

128. Fogh, J., Wright, W. C. & Loveless, J. D. Absence of HeLa cell contamination in 169 cell lines derived from human tumors. *J Natl Cancer Inst* **58**, 209-14 (1977).
129. Stangegaard, M., Dufva, I. H. & Dufva, M. Reverse transcription using random pentadecamer primers increases yield and quality of resulting cDNA. *Biotechniques* **40** (5), 649-657 (2006).
130. Chantret, I. et al. Differential expression of sucrase-isomaltase in clones isolated from early and late passages of the cell line Caco-2: evidence for glucose-dependent negative regulation. *J Cell Sci* **107** ( Pt 1), 213-25 (1994).
131. Semple, T. U., Quinn, L. A., Woods, L. K. & Moore, G. E. Tumor and lymphoid cell lines from a patient with carcinoma of the colon for a cytotoxicity model. *Cancer Res* **38**, 1345-55 (1978).
132. Liste, I., Garcia-Garcia, E. & Martinez-Serrano, A. The generation of dopaminergic neurons by human neural stem cells is enhanced by Bcl-XL, both in vitro and in vivo. *J Neurosci* **24**, 10786-95 (2004).
133. Villa, A., Snyder, E. Y., Vescovi, A. & Martinez-Serrano, A. Establishment and properties of a growth factor-dependent, perpetual neural stem cell line from the human CNS. *Exp Neurol* **161**, 67-84 (2000).
134. Manz, A., Graber, N. & Widmer, H. M. Miniaturized total chemical analysis systems: A novel concept for chemical sensing. *Sensors and Actuators B: Chemical* **1**, 244-248 (1990).
135. Lorenz, H. et al. SU-8: a low-cost negative resist for MEMS. *J. Micromech. Microeng.* **7**, 121-124 (1997).
136. Mogensen, K. B., El-Ali, J., Wolff, A. & Kutter, J. P. Integration of polymer waveguides for optical detection in microfabricated chemical analysis systems. *Applied Optics* **42**, 4072-4079 (2003).
137. Wang, Z. et al. Measurements of scattered light on a microchip flow cytometer with integrated polymer based optical elements. *Lab on a Chip* **4**, 372-377 (2004).
138. Hsieh, J., Weng, C. J., Yin, H. L., Lin, H. H. & Chou, H. Y. Realization and characterization of SU-8 micro cylindrical lenses for in-plane micro optical systems. *Microsystem Technologies* **11**, 429-437 (2005).
139. Mappes, T., Achenbach, S., Last, A., Mohr, J. & R., T. Evaluation of optical qualities of a LIGA-spectrometer in SU-8. *Microsystem Technologies* **10**, 560-563 (2004).
140. Zhang, J., Tan, K. L. & Gong, H. Q. Characterization of the polymerization of SU-8 photoresist and its applications in micro-electro-mechanical systems (MEMS). *Polymer Testing* **20**, 693-701 (2001).
141. Kotzar, G. et al. Evaluation of MEMS materials of construction for implantable medical devices. *Biomaterials* **23**, 2737-2750 (2002).
142. El-Ali, J. et al. Simulation and experimental validation of a SU-8 based PCR thermocycler chip with integrated heaters and temperature sensor. *Sensors and Actuators A-Physical* **110**, 3-10 (2004).
143. Iranpoor, N. & Salehi, P. Ceric Ammonium Nitrate: a Mild and Efficient Reagent for Conversion of Epoxides to beta-Nitrato Alcohols. *Tetrahedron* **51**, 909-912 (1995).
144. Nordström, M., Marie, R., Calleja, M. & Boisen, A. Rendering SU-8 hydrophilic to facilitate use in micro channel fabrication. *J. Micromech. Microeng.* **14**, 1614-1617 (2004).
145. Charnley, J. Anchorage of the femoral head prosthesis to the shaft of the femur. *J Bone Joint Surg Br* **42-B**, 28-30 (1960).
146. Fixe, F., Dufva, M., Telleman, P. & Christensen, C. B. Functionalization of poly(methyl methacrylate) (PMMA) as a substrate for DNA microarrays. *Nucleic Acids Res* **32**, e9 (2004).

147. Fixe, F., Dufva, M., Telleman, P. & Christensen, C. B. One-step immobilization of aminated and thiolated DNA onto poly(methylmethacrylate) (PMMA) substrates. *Lab Chip* **4**, 191-5 (2004).
148. Manz, A., Graber, N. & Widmer, H. M. Miniaturized Total Chemical-Analysis Systems - a Novel Concept for Chemical Sensing. *Sensors and Actuators B-Chemical* **1**, 244-248 (1990).
149. Visser, S. A., Hergenrother, R. W. & Cooper, S. L. in *Biomaterials science: An introduction to materials in medicine* (eds. Ratner, B. D., Hoffman, A. S., Schoen, F. J. & Lemons, L. E.) 50-64 (Academic Press, San Diego, 1996).
150. Becker, H. & Gartner, C. Polymer microfabrication methods for microfluidic analytical applications. *Electrophoresis* **21**, 12-26 (2000).
151. Piruska, A. et al. The autofluorescence of plastic materials and chips measured under laser irradiation. *Lab Chip* **5**, 1348-54 (2005).
152. McCormick, R. M., Nelson, R. J., Alonso-Amigo, M. G., Benvegna, D. J. & Hooper, H. H. Microchannel electrophoretic separations of DNA in injection-molded plastic substrates. *Anal Chem* **69**, 2626-30 (1997).
153. Xu, J., Locascio, L., Gaitan, M. & Lee, C. S. Room-temperature imprinting method for plastic microchannel fabrication. *Anal Chem* **72**, 1930-3 (2000).
154. Martynova, L. et al. Fabrication of plastic microfluid channels by imprinting methods. *Anal Chem* **69**, 4783-9 (1997).
155. Petronis, S., Stangegaard, M., Christensen, C. B. V. & Dufva, M. Transparent polymeric cell culture chip with integrated temperature control and uniform media perfusion. *Biotechniques* **40** (3), 368-375 (2006).
156. Johnson, T. J., Waddell, E. A., Kramer, G. W. & Locascio, L. E. Chemical mapping of hot-embossed and UV-laser-ablated microchannels in poly(methyl methacrylate) using carboxylate specific fluorescent probes. *Applied Surface Science* **181**, 149-159 (2001).
157. Srinivasan, R. Controlled degradation and ablation of polymer surfaces by ultraviolet laser radiation. *Polymer Degradation and Stability* **17**, 193-203 (1987).
158. Stangegaard, M., Wang, Z., Kutter, J. P., Dufva, M. & Wolff, A. Whole genome expression profiling using DNA microarray for determining biocompatibility of polymeric surfaces. *Molecular Biosystems* **2**, 421-428 (2006).
159. Aegerter, M. A. & Al-Dahoudi, N. Wet-Chemical Processing of Transparent and Antiglare Conducting ITO Coating on Plastic Substrates. *Journal of Sol-Gel Science and Technology* **27**, 81-9 (2003).
160. Al-Dahoudi, N., Bisht, H., Gobbert, C., Krajewski, T. & Aegerter, M. A. Transparent conducting, anti-static and anti-static-anti-glare coatings on plastic substrates. *Thin Solid Films* **392**, 299-304 (2001).
161. Ederth, J., Heszler, P., Hultaker, A., Niklasson, G. A. & Granqvist, C. G. Indium tin oxide films made from nanoparticles: models for the optical and electrical properties. *Thin Solid Films* **445**, 199-206 (2002).
162. Ederth, J. et al. Electrical and optical properties of thin films prepared by spin coating a dispersion. *Smart Materials and Structures* **11**, 675-78 (2002).
163. Herrero, J. & Guillen, C. Transparent films on polymers for photovoltaic applications. *Vacuum* **67**, 611-16 (2002).
164. Bransden, B. H. & Joachain, C. J. in *Physics of atoms and molecules* page 10 (Longman Scientific & Technical, Essex, England, 1994).
165. Liu, S. Q. & Goldman, J. Role of blood shear stress in the regulation of vascular smooth muscle cell migration. *IEEE Trans Biomed Eng* **48**, 474-83 (2001).
166. Chen, B. P. C. et al. DNA microarray analysis of gene expression in endothelial cells in response to 24-h shear stress. *Physiol. Genomics* **7**, 55-63 (2001).

167. Marz, P. et al. Ataxin-10, the Spinocerebellar Ataxia Type 10 Neurodegenerative Disorder Protein, Is Essential for Survival of Cerebellar Neurons. *J. Biol. Chem.* **279**, 35542-35550 (2004).
168. Balaban, N. Q. et al. Force and focal adhesion assembly: a close relationship studied using elastic micropatterned substrates. *Nat Cell Biol* **3**, 466-72 (2001).
169. Risbud, M. V., Dabhade, R., Gangal, S. & Bhonde, R. R. Radio-frequency plasma treatment improves the growth and attachment of endothelial cells on poly(methyl methacrylate) substrates: implications in tissue engineering. *Journal of Biomaterials Science, Polymer Edition* **13**, 1067-1080 (2002).
170. Kim, D. T., Blanch, H. W. & Radke, C. J. Direct Imaging of Lysozyme Adsorption onto Mica by Atomic Force Microscopy. *Langmuir* **18**, 5841-5850 (2002).
171. Tanaka, M. et al. Blood compatible aspects of poly(2-methoxyethylacrylate) (PMEA)-relationship between protein adsorption and platelet adhesion on PMEA surface. *Biomaterials* **21**, 1471-81 (2000).
172. Giacomelli, C. E. & Norde, W. The Adsorption-Desorption Cycle. Reversibility of the BSA-Silica System. *Journal of Colloid and Interface Science* **233**, 234-240 (2001).
173. Dong Keun Han, K. D. P., Gyu Ha Ryu, Un Young Kim, Byoung Goo Min, Young Ha Kim. Plasma protein adsorption to sulfonated poly(ethylene oxide)-grafted polyurethane surface. *Journal of Biomedical Materials Research* **30**, 23-30 (1996).
174. Tsai, W. B., Grunkemeier, J. M. & Horbett, T. A. Human plasma fibrinogen adsorption and platelet adhesion to polystyrene. *J Biomed Mater Res* **44**, 130-9 (1999).
175. Balasubramanian, V., Grusin, N. K., Bucher, R. W., Turitto, V. T. & Slack, S. M. Residence-time dependent changes in fibrinogen adsorbed to polymeric biomaterials. *J Biomed Mater Res* **44**, 253-60 (1999).
176. Soares, R. et al. Vascular Endothelial Growth Factor, Transforming Growth Factor- $\{\alpha\}$ , and Estrogen Receptors: Possible Cross-Talks and Interactions. *Am J Pathol* **160**, 381-383 (2002).
177. Lim, Y.-C. et al. Heterogeneity of Endothelial Cells from Different Organ Sites in T-Cell Subset Recruitment. *Am J Pathol* **162**, 1591-1601 (2003).
178. Villa, A. et al. Long-term molecular and cellular stability of human neural stem cell lines. *Exp Cell Res* **294**, 559-70 (2004).
179. Zheng, H. C. et al. Growth, invasion, metastasis, differentiation, angiogenesis and apoptosis of gastric cancer regulated by expression of PTEN encoding products. *World J Gastroenterol* **9**, 1662-6 (2003).
180. Eberwine, J. et al. Analysis of Gene Expression in Single Live Neurons. *PNAS* **89**, 3010-3014 (1992).
181. Luo, L. et al. Gene expression profiles of laser-captured adjacent neuronal subtypes. *Nat Med* **5**, 117-22 (1999).
182. Mir, K. U. & Southern, E. M. Determining the influence of structure on hybridization using oligonucleotide arrays. *Nat Biotechnol* **17**, 788-92 (1999).
183. Kuo, K. W., Leung, M. F. & Leung, W. C. Intrinsic secondary structure of human TNFR-I mRNA influences the determination of gene expression by RT-PCR. *Mol Cell Biochem* **177**, 1-6 (1997).
184. Zhang, L. et al. Whole genome amplification from a single cell: implications for genetic analysis. *Proc Natl Acad Sci U S A* **89**, 5847-51 (1992).
185. Kawano, M., Reynolds, A. A., Miranda-Rios, J. & Storz, G. Detection of 5'- and 3'-UTR-derived small RNAs and cis-encoded antisense RNAs in Escherichia coli. *Nucl. Acids Res.* **33**, 1040-1050 (2005).
186. Zhang, Y. J., Pan, H. Y. & Gao, S. J. Reverse transcription slippage over the mRNA secondary structure of the LIP1 gene. *Biotechniques* **31**, 1286, 1288, 1290, passim (2001).



## 9 Publications and manuscripts

Paper 1: S. Petronis, **M. Stangegaard**, C. B. V. Christensen and M. Dufva, "*Transparent polymeric cell culture chip with integrated temperature control and uniform media perfusion*". *Biotechniques* **40** (3), 368-375 (2006).

Paper 2: **M. Stangegaard**, S. Petronis, A. M. Jørgensen, C. B. V. Christensen and M. Dufva, "*A biocompatible micro cell culture chamber for the culturing and on-line monitoring of Eukaryote cells*". *Lab on a Chip*, **6** (8), 1045-1051 (2006).

Paper 3: **M. Stangegaard**, Z. Wang, J. P. Kutter, M. Dufva and A. Wolff, "*Whole genome expression profiling using DNA microarrays for determining biocompatibility of polymeric surfaces*". *Molecular Biosystems* **2** (9), 421-428 (2006).

Paper 4: **M. Stangegaard**, I. H. Dufva and M. Dufva, "*Reverse transcription using random pentadecamer primers increases yield and quality of resulting cDNA*". *Biotechniques* **40** (5), 649-657 (2006).

***Paper 1: Transparent polymeric cell culture chip with integrated temperature control and uniform media perfusion***

# Transparent polymeric cell culture chip with integrated temperature control and uniform media perfusion

Sarunas Petronis, Michael Stangegaard, Claus Bo Vöge Christensen, and Martin Dufva

*BioTechniques* 40:368-376 (March 2006)  
doi 10.2144/000112122

*Modern microfabrication and microfluidic technologies offer new opportunities in the design and fabrication of miniaturized cell culture systems for online monitoring of living cells. We used laser micromachining and thermal bonding to fabricate an optically transparent, low-cost polymeric chip for long-term online cell culture observation under controlled conditions. The chip incorporated a microfluidic flow equalization system, assuring uniform perfusion of the cell culture media throughout the cell culture chamber. The integrated indium-tin-oxide heater and miniature temperature probe linked to an electronic feedback system created steady and spatially uniform thermal conditions with minimal interference to the optical transparency of the chip. The fluidic and thermal performance of the chip was verified by finite element modeling and by operation tests under fluctuating ambient temperature conditions. HeLa cells were cultured for up to 2 weeks within the cell culture chip and monitored using a time-lapse video recording microscopy setup. Cell attachment and spreading was observed during the first 10–20 h (lag phase). After approximately 20 h, cell growth gained exponential character with an estimated doubling time of about 32 h, which is identical to the observed doubling time of cells grown in standard cell culture flasks in a CO<sub>2</sub> incubator.*

## INTRODUCTION

Cell culturing is a core method in biological science and clinical research as well as in many biotechnological and biomedical engineering areas. Typically, mammalian cells are grown in a nutrient buffer in plastic culture flasks or multiwell plates, which are placed in a standard benchtop incubator. The incubator maintains the physiological conditions necessary for cell growth, such as sterility, proper temperature, pH, and osmotic pressure. Standard cell culturing is reliable and is used in the majority of cell culture-based experiments. However, it has limitations when dynamic processes of the cells have to be investigated. The cells can be taken out of the incubator for a brief observation and then returned to the incubator until the next observation, but this does not allow for continuous online monitoring of the cellular processes.

For the continuous real-time observation of cells, the incubator has to be: (i) enlarged to the size of a room to

accommodate all observation instruments as well as the operator; (ii) modified to enclose the observation instrument and provide the instrument controls to the outside operator; or (iii) reduced to fit into the instrument; for example, on the stage of a microscope. The first option is usually chosen when running many parallel online experiments on a regular basis, but it requires a large investment and running costs. Furthermore, to allow the operator to breathe normally, the atmosphere is not enriched for CO<sub>2</sub>, which requires special cell culture media and thus limits the range of cell types that can be investigated. Moreover, the operator working with the incubator might contaminate cell cultures. Enclosing the investigation instruments—typically a microscope—by the incubator is less costly and provides better sterility than a room incubator because it isolates the operator from the cell culture and the instrument. However, in this case, physical accessibility to the instrument is significantly reduced, and therefore it has to be equipped with remote controls

and handling tools. Miniaturized cell culture incubators not only enable the growth and online observation of cells directly on the stage of an optical microscope, but they also provide the whole list of benefits intrinsic to microsystems, including low consumption of power and reagents as well as fast response due to the small mass and volume of the devices. In addition, this type of setup provides opportunities for parallel operation for high-throughput analysis and integration of multiple sensors for monitoring environmental parameters. Finally, the microsystems can be designed as single-use disposable devices due to the low costs, which are a consequence of the requirement for only a small amount of raw material and the potential for mass production using a batch-type fabrication (1).

The opportunities offered by microfabrication and microfluidic technologies in design and fabrication of miniaturized cell culture systems are being explored by researchers (2). One trend is the development of

Technical University of Denmark, Lyngby, Denmark

extremely small cell culture chambers intended for the study of single/few cell-related biological phenomena (3–7). Alternatively, microchambers are designed to provide and/or investigate effects of unique physiological cell culture conditions in terms of culture media composition, pressure, shear stress, and chemical and geometrical microenvironments (8–17).

Commercially available miniaturized cell culture systems are primarily developed for live-cell microscopy, sometimes including options for mechanical cell micromanipulations and electrophysiology. Typically, they consist of two parallel glass coverslips, defining the top and the bottom of the chamber, and a sealing spacer, providing the walls of the chamber (18). For long-term cultures, such systems contain inlets for continuous media perfusion, which provides fresh nutrients and removes metabolic wastes (19,20). The perfusion is typically driven by gravity or by peristaltic/syringe pumps. The temperature required for cell growth is maintained by a heated airstream directed to the chamber, by heated water flow in the channels surrounding the chamber, or by integrated electric heaters consisting of resistance wires, thin films, or thermoelectric (Peltier elements), all controlled via an electronic feedback loop (20,21).

Several modifications of these setups exist, such as open chamber systems containing a cleaned oil layer on top of the culture media instead of a glass coverslip, which prevents fluid evaporation without hindering direct access to the cells by manipulation or probing tools (22,23). Some devices do not contain an integrated cell chamber but accommodate a standard cell culture dish and interface it with media perfusion and temperature control systems (Open Perfusion Microincubators; Harvard Apparatus, Holliston, MA, USA).

The thin dimensions and material properties of the glass coverslips used in the described systems provide a very good optical setup for high-magnification microscopy. Unfortunately, commercial cell culture microincubators are expensive and available in a limited number of designs (24). Moreover, many commercial chambers provide uneven environmental conditions for cells and therefore might contribute to artifacts or irreproducibility in the experimental data recorded from cells (16,21). For example, cells experience different temperatures in the central part of the chamber compared with peripheral parts when the heat is induced by heaters that are designed as a ring surrounding the cell chamber. Moreover, the perfusion of the media in most commercial

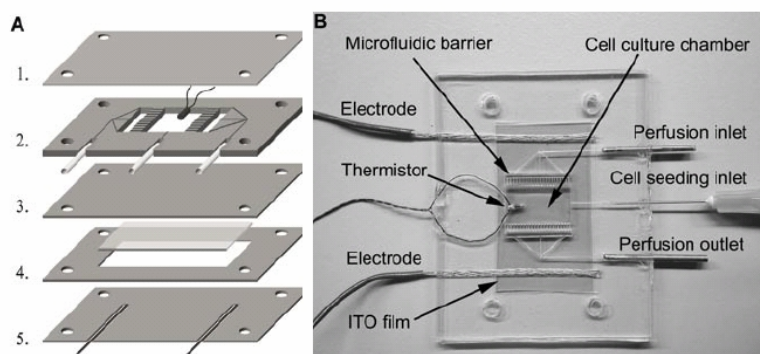
chambers is carried out via localized inlet apertures, which induces high flow velocities in the vicinity of the inlet or outlet apertures and low velocities in the remote chamber parts. This causes uneven shear stress and supply of the nutrients to the cells in different parts of the chamber. Although many of these problems can now be eliminated by using more advanced designs and technologies (10,21), only a few improvements have been implemented in commercially available cell culture chambers. The added sophistication significantly increases the cost of these devices.

Our approach is to utilize the advantages of modern microfabrication and microfluidics technologies in order to develop a novel disposable polymeric chip containing a fully transparent perfusion chamber that enables reliable, long-term cell culture and is compatible with all types of microscopy (upright/inverted, reflective/transmission).

## MATERIALS AND METHODS

### Fabrication

The cell culture chip was composed of five poly(methyl methacrylate) (PMMA) sheets (Figure 1A), which were separately cut and micromachined by laser ablation and assembled into a functional structure by a thermal bonding technique previously described by Klank et al. (25). Briefly, an infrared laser ablation system (50W Synrad F48 laser equipped with an FHIW 30-200 marking head; Synrad, Mukilteo, WA, USA) was run using 500–800 mm/s beam movement velocity, 28–32 W laser power, and 1000 dpi exposure resolution to induce chip contours, alignment holes, chamber and heater spacers, and microfluidic channels on 1.5- and 0.25-mm thickness PMMA sheets (type 99530; Röhm GmbH & Co. KG, Darmstadt, Germany). Prior to the bonding processes, the micromachined PMMA parts were annealed at 80°C temperature for at least 30 min in order to avoid stress cracks in the structure. After annealing, the parts were wiped with 96% ethanol, aligned, and exposed to the 110°C heat treatment under mechanical pressure for 1 h, which



**Figure 1. Construction of the cell culture chip.** (A) Structure of the chip consisting of five transparent PMMA sheets. The uppermost layer serves as the chamber lid. The second layer defines the cell culture chamber, microfluidic channels, inlets for perfusion, and cell seeding, as well as incorporates the temperature probe. The third layer separates the chamber from the heater, which consists of an ITO-coated PET film integrated in the fourth layer. The fifth layer contains alignment grooves for electrodes to the heater and protects the heater from the environment. Each layer contains four alignment holes. (B) Layout of the fabricated cell culture chip with the functional parts labeled. PMMA, poly(methyl methacrylate); ITO, indium tin oxide; PET, polyethylene terephthalate.

## RESEARCH REPORT

**Table 1. Material Properties Used in 2-D Finite Element Modeling of Fluid and Heat Transfer Within the Cell Culture Chip**

Physical Properties	Value
PMMA density	1180 kg/m <sup>3</sup>
PMMA heat capacity	1500 J/(kg•K)
PMMA thermal conductivity	0.18 W/(m•K)
Buffer density	1007 kg/m <sup>3</sup>
Buffer dynamic viscosity (37°C)	0.0007 N•s/m <sup>2</sup>
Buffer heat capacity (37°C)	4000 J/(kg•K)
Buffer thermal conductivity (37°C)	0.62 W/(m•K)
Heat dissipation to ambient	20 W/(m <sup>2</sup> •K)

2-D, two-dimensional; PMMA, poly(methyl methacrylate).

caused an irreversible bonding of the structured PMMA parts.

The integrated heater was made from indium tin oxide (ITO)-coated polyethylene terephthalate (PET) film (Sigma-Aldrich, St. Louis, MO, USA) embedded in the chip below the cell culture chamber bottom. The electrodes were made from standard copper wires and attached to ITO film by conductive epoxy-based glue (CircuitWorks<sup>®</sup>; Chemtronics, Kennesaw, GA, USA). The resistance of the ITO film was used as a measure of the connection quality. Only chambers with a resistance lower than 17  $\Omega$  were used.

Inlets and outlets of the chip consisted of 18 gauge blunt-end stainless steel needles (Becton Dickinson, Drogheda, Ireland) that were abraded on the surface for better interlock with the polymer structure of the chip. The needles were fixed and sealed to the structure with epoxy glue (5-Min. Epoxy; R&G GmbH, Waldenbuch, Germany).

### Temperature Control

The temperature inside the cell culture chamber was controlled by a proportional-integral-derivative (PID) feedback loop that was implemented using LabView<sup>™</sup> v7.0 software (National Instruments, Austin, TX, USA). The computer program controlled the voltage applied to the ITO film-based heater depending on the temperature readings from the model TS67-170 micro-thermistor (Oven Industries, Mechanicsburg, PA, USA) located within the cell culture chamber. A USB-based multifunction data

370 BioTechniques

input/output board (LabJack<sup>™</sup> U12; LabJack, Lakewood, CO, USA) and two homemade electronic circuits (see Supplementary Figure S1) were used to connect the heater and the thermistor to the computer and the external power source (9 V, 500 mA, AC/DC converter type OTC 910801; Otron Electronics, Hong Kong). One electronic circuit controlled the electrical power provided to the heater, depending on the voltage level in the analogic output (AO) port of the LabJack board. The voltage applied to the heater followed the AO voltage but with much higher current supplied from the external power source. The second electronic circuit kept constant current (50  $\mu$ A) passing through the thermistor, and therefore converted temperature-dependant resistance changes of the thermistor into voltage signals that were registered by the analogic input (AI) port of the LabJack board. The voltage signal was further converted into temperature values and logged into the computer memory by the same LabView code.

### Physical Modeling

Two-dimensional (2-D) finite element modeling was performed to evaluate the fluidic and thermal properties of the chip. Modeling was made using fluid dynamics and heat transfer modules of FEMLAB<sup>™</sup> v3.1b software (COMSOL<sup>™</sup> A/S, Kgs. Lyngby, Denmark). The physical parameters of the materials used in simulations are listed in Table 1.

First, the incompressible Navier-Stokes equations were solved to simulate the steady-state velocity

field of the culture media perfusion. No-slip boundary conditions were applied to the walls of the channels and the chamber, a parabolic velocity profile with an average speed corresponding to 0.1 mL/h perfusion rate was used at the inlet, and zero pressure conditions were set at the outlet.

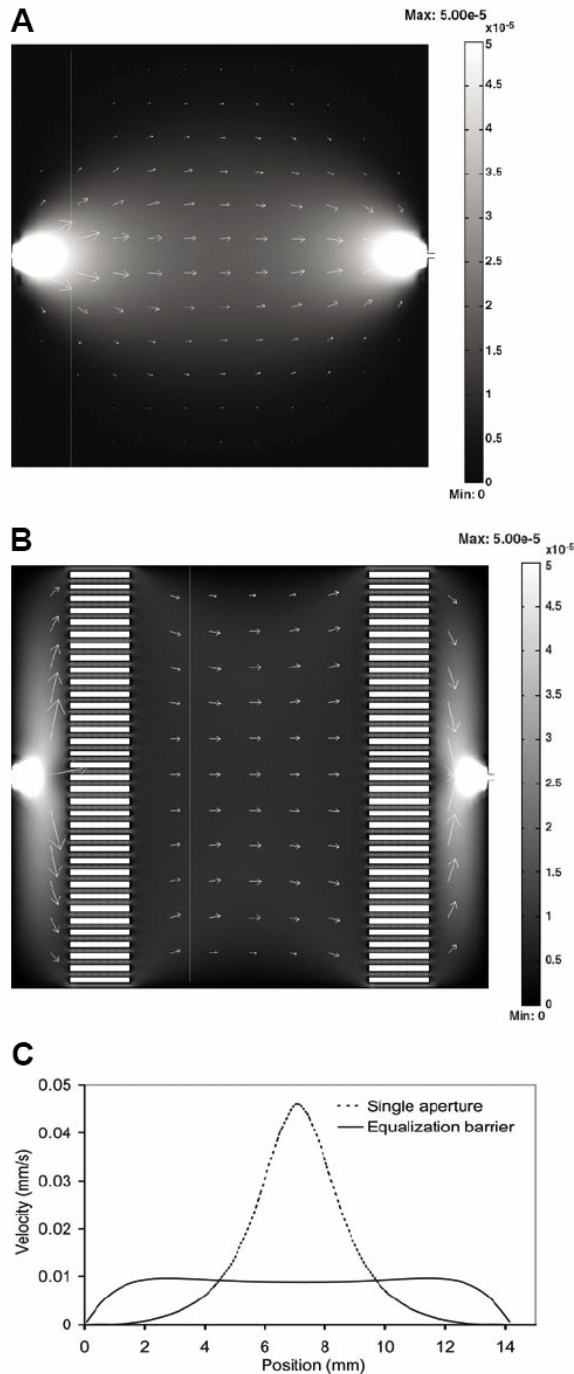
In the second step, the obtained flow velocity field was used to compute heat transfer by convection and conduction of heat energy. It was assumed that the liquid, which is continuously entering the chip, is initially at room temperature. The heat from the heater was induced at the same power across the entire surface of the chip. Heat dissipation to the ambient at 20 W/(m<sup>2</sup>•C) was also taken into account in the model.

### Cell Culture and Time-Lapse Microscopy

The human carcinoma cell line HeLa was maintained in 75 cm<sup>2</sup> culture flasks (EasyFlask; Nalge Nunc International, Rochester, NY, USA) in 25 mL RPMI 1640 media supplemented with 10% fetal bovine serum (FBS), 1000 U/mL penicillin, and 1 mg/mL streptomycin (all components from Sigma-Aldrich). The alkalinity of the media was inspected by a miniLab<sup>™</sup> IQ125 pH meter (IQ Scientific Instruments, Carlsbad, CA, USA). Cells were routinely cultured in a benchtop incubator (Assab; Don Whitley Scientific Ltd., Shipley, West Yorkshire, UK) providing 37°C and a 5% CO<sub>2</sub>-enriched atmosphere. Seeding of the cells was performed with a density of 6667 cells per cm<sup>2</sup> and the cells were subcultured every 3 to 4 days when approximately 90% confluence was reached. For cell growth doubling time estimation, two independent cell culture experiments, each lasting 4 days, were carried out. Cell counting was performed using microscopic images of the cell culture taken by temporarily removing the cell culture flasks from the CO<sub>2</sub> incubator and placing them on the stage of the inverted microscope. Three to four images were grabbed from each culture flask every day over a 4-day period and counting was performed (27 counts in total).

For on-chip cell culture experi-

Vol. 40, No. 3 (2006)



**Figure 2. Modeling of the flow within the chamber.** (A) FEMLAB-modeled flow when the perfusion media enter the chamber via the single aperture of the inlet and (B) results when the media enter via the multiple apertures of the equalization barriers. Velocity field intensity is indicated by a grayscale color code. The arrows visualize flow direction and intensity. (C) For comparison, the flow velocity profiles 2 mm away from the cell chamber entrances (indicated by the straight gray lines) are plotted.

ments, the perfusion inlet of the chip was connected to a 20-mL sterile syringe (Becton Dickinson) by polytetrafluoroethylene (PTFE) tubing (inner diameter: 0.8 mm; Böhler GmbH, Grünsfeld, Germany), which was attached by flexible polydimethylsiloxane (PDMS) connectors. The syringe was loaded with cell culture media that was preheated to 37°C to minimize bubble formation inside the syringe. Continuous media perfusion was done using a syringe pump (Model 22; Harvard Apparatus), generating a flow rate of 0.1 mL/h (1.67  $\mu$ L/min).

The chip was mounted on a microscope stage of a standard phase-contrast microscope (Alpha Phot 2 YS2; Nikon, Tokyo, Japan). Injection of cells was performed through a 25-gauge needle attached to a 1-mL syringe. Cells were seeded at a density of 10–100 cells within the field of view of the  $\times 10$  magnification objective. Cell culture images were digitally recorded using a Coolpix 990 camera attached to the microscope via a Coolpix MDC lens and equipped with an MC-EUI remote control unit (all from Nikon) operating in time-lapse mode, typically with a 5-min period. The images were converted into AVI movie format and time-stamped using Scion Image v.4.0.2 freeware (Scion, Frederick, MD, USA) and home-written macros.

Cell growth doubling time in on-chip culture was estimated from two independent experiments that lasted 50 and 120 h. Cell counting was performed using time-lapse microscopy image sequence. Cell counts were made on the images taken every 10 h, making 20 counts in total.

## RESULTS

The composite layers and the resulting complete fabricated chip are shown in Figure 1. The basic design of the chip incorporates a single  $7.6 \times 13.0$  mm<sup>2</sup> cell culture chamber, which contains an inlet and outlet for media perfusion and an additional inlet for cell seeding. All channels have a Gaussian cross-section (25) that is 400  $\mu$ m wide and 500  $\mu$ m high. The microfluidic barriers, which consist of a series of microchannels on both sides

## RESEARCH REPORT

of the cell chamber, establish uniform media flow during perfusion and cell entrapment during the seeding process. The microchannels are 1.5 mm long and are distributed with 0.6 mm pitch along the barriers. The channels have a Gaussian cross-section that is 300  $\mu\text{m}$  wide and 350  $\mu\text{m}$  high. The integrated thin-film heater entirely covers the bottom or top of the cell chamber (depending on whether an upright or inverted microscope is used) and part of the microfluidic channels, which helps to preheat the perfusion media before it enters the cell chamber. The temperature probe is incorporated directly into the chamber to ensure on-site readings of the temperature.

The homogeneity of the cell culture environment was significantly improved by flow equalization barriers and an integrated heater, which regulate media supply distribution, shear stress, and thermal conditions within the chamber. As can be seen from the two-dimensional numerical modeling results (Figure 2), the equalization barriers are predicted to cause a uniform flow velocity field over the majority of the cell chamber area:  $\pm 10\%$  variation over 70% of the chamber area compared with  $\pm 90\%$  variation in the same area with direct inlet/outlet configuration. The modeling was also performed on the chamber configuration containing three inlet and outlet channels (Supplementary Figure S2). Such configuration significantly improves flow distribution in the chamber without equalization barriers ( $\pm 60\%$  variation over 70% of the chamber area). However, in this case, the flow profile is very sensitive to clogging of one or more of the channels and is still less uniform than in the chamber containing microfluidic flow equalization barriers. In the chip itself, the effectiveness of the barriers was confirmed by observing dye flow in the chamber (see Supplementary Movies S1 and S2). A similar configuration was proven to be effective on a smaller scale by Hung et al. (10,11), while Focht (21) used “T” shaped grooves as inlet and outlet for laminar media perfusion.

Results of 2-D temperature distribution modeling are shown in Figure 3. Temperature variation along the cell

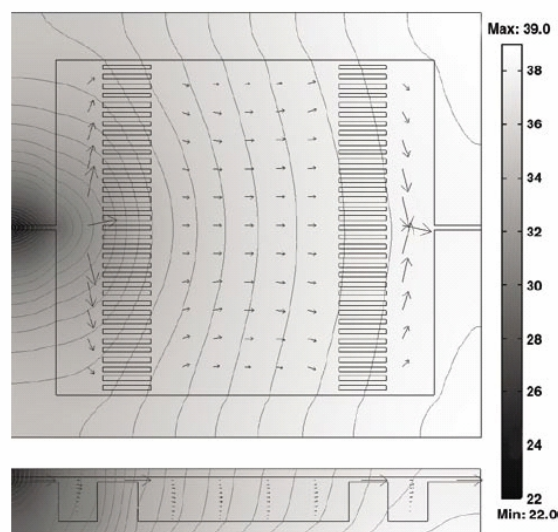
culture chamber is predicted to be up to 3°C when a steady state of 37°C is achieved in the middle part of the chamber. Bottom-to-top variation is modeled to be less than 0.6°C. The temperature gradients are mainly caused by the infusion of room temperature cell culture media. In the functional device, the entering media has more time to be preheated in the inlet channels lying above the heater. Assuming that the media reaches 28°C in the inlet channels, we estimate the temperature variation within the chamber is less than 1.5°C.

To test the chip for thermal control stability over long time periods, temperature was recorded during operation for 1 week (Figure 4). Despite significant fluctuations in ambient temperature (18.0°–24.3°C) caused by the day-night cycle, the temperature in the chamber was maintained unperturbed (37.00°  $\pm$  0.26°C) by PC-controlled feedback, which continuously adapted the voltage amplitude applied to the heater (2.2–2.9 V).

No changes in the pH of the perfused media were observed, indicating that the enclosed perfusion system efficiently eliminated the need for CO<sub>2</sub> buffering of the media.

HeLa cell culture experiments indicated normal growth and morphology of the cells during the online observations lasting up to 2 weeks. Contamination of the cell culture was efficiently eliminated by dry sterilization (100°C, 1 h) of the chip and wet autoclaving (140°C, 15 min) of the connection tubing prior to media infusion and seeding of cells.

Time-lapse microscopy was used to evaluate cell attachment and growth kinetics inside the chamber of the

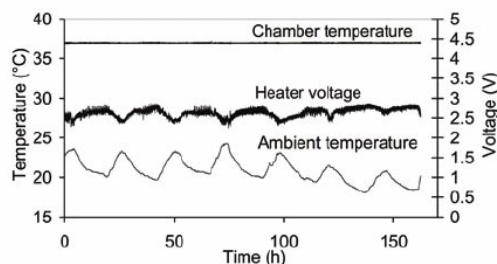


**Figure 3. Modeling of the heat distribution within cell culture chip.** The FEMLAB modeling is performed in the two-dimensional space using top-view and side-view projections of the chip. Temperature is indicated by a grayscale color code. The arrows show cell culture media flow direction and intensity.

cell culture chip. Cell attachment and spreading was observed during the first 10–20 h (lag phase). After approximately 4–6 h, the cells started to divide. After approximately 20 h, cell growth became exponential, with an estimated doubling time of 32 h with 6 h standard deviation (Figure 5). The doubling rate of the reference cells cultured in standard culture flasks in a benchtop incubator was 32 h with 1 h standard deviation. A movie of a 141 h culture experiment is available as Supplementary Movie S3.

## DISCUSSION

The goal of this study was to develop a low-cost polymeric chip that provides optimal conditions for cell culturing and that is optically transparent for online microscopic observation of the cultured cells. By optimization of cell culture conditions, we aim to achieve long-term on-chip cell culturing with a homogeneous environment throughout the cell culture chamber and with expressed cell biological behavior, identical to the cell cultures grown in benchtop incubators and standard cell culture flasks. This is important for



**Figure 4.** Thermal performance of the cell culture chip during 1-week operation under 0.1 mL/h perfusion conditions.

collecting reproducible, high-quality data from real-time cell observations performed using the chip and for the ability to compare and relate these results with previous standard cell culture studies. The time-lapse microscopic observation of HeLa cells allowed us to follow cell attachment and spreading right after the seeding (Figure 5) as well as the growth kinetics of the culture for up to 2 weeks. This indicates that cells can be successfully cultured outside a benchtop incubator with on-chip thermoregulation and continuous flow of cell culture medium.

Basic physiological conditions necessary for cell growth were established by using an enclosed perfusion chamber design. The enclosed perfusion

chamber prevents the evaporation and interaction of the culture media with atmospheric air and therefore eliminates the need for CO<sub>2</sub> buffering and humidification of surrounding atmosphere. Moreover, the enclosed system reduces the risks of infection or contamination of the culture. Unlike standard

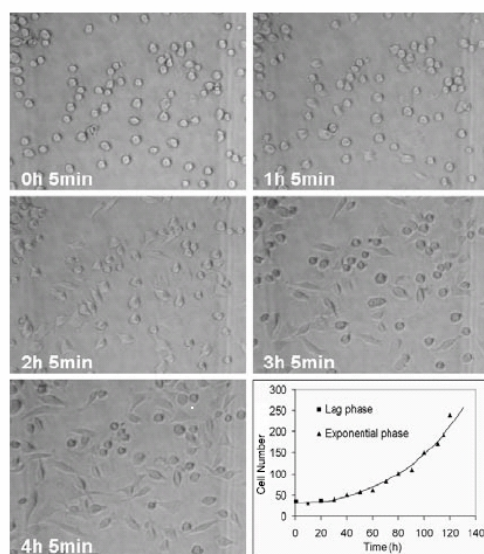
cell culturing, where the medium is replaced every third or fourth day, continuous perfusion of the chamber with fresh culture media provides a constant supply of nutrients and metabolic waste removal. Continuous perfusion eliminates the periodic changes in cell culture conditions, such as altered concentration of nutrients and metabolic products caused by media exchange procedures when using standard cell culture techniques (17). Continuous perfusion is not always advantageous; for example, maintaining cell cultures that are strongly dependent on signaling and conditioning metabolites excreted by the cells themselves requires perfusion involving periodic partial media exchange in the chamber

instead of continuous flow (26). However, cell culture chips with continuous perfusion can be a particularly valuable tool to identify such critical signaling factors because perfusion constantly eliminates cell-secreted factors within the chip, and external factors can be added in a controlled manner. The chip is therefore highly suitable for studying effects on cell-to-cell communication by excreted factors or determining effects of pharmaceutical drugs in a highly controlled manner. Controlled addition of desired stimulating drugs or solutions to the media in the chip enables online monitoring of the kinetics of the cellular responses to these stimuli either in terms of cell morphological or

motility changes identifiable by optical microscopy or in terms of expression of fluorescently labeled proteins detectable by fluorescent microscopy.

Additionally, online observations of changes in cell-excreted factors due to changes in media formulation or addition/removal of selected growth factors might also be realized by perfusion of the outlet media through an antibody array if a labeled antibody is added to the inlet media. Indeed, autofluorescence measurements of the chip materials in Cy<sup>TM</sup>3 and Cy5 fluorescence channels using a microarray laser scanner (ScanArray<sup>®</sup> Lite; Packard Biochip Technologies, Billerica, MA, USA) showed that fluorescence studies of the cultured cells are completely possible in the Cy3 channel. However, the ITO-coated PET sheet was found to autofluoresce in the Cy5 channel (data not shown), which limits the range of fluorescence dyes that can be used for cell staining or protein/antibody labeling.

In this study, polymers have been chosen as a base material of the cell culture chip because they offer an attractive combination of functional and processing properties. First of all, polymers, especially polystyrene (PS), are known to be biocompatible with the majority of cell cultures (27). Additionally, many polymers are transparent to the light and therefore allow online microscopy of the cells and optical readout of integrated probes/sensors. From the fabrication point of view, polymers are inexpensive materials and have well-established techniques for large-scale microreplication and production (e.g., hot embossing, injection molding) (28). This provides the possibility of producing inexpensive, easy-to-use disposable biochips, ensuring a sterile environment for the cells and high-quality bioanalysis (1). The combination of polymer micro-machining techniques used in this study—computer-controlled laser microablation and thermal bonding of polymers—allows rapid production of prototype microsystems, giving the opportunity for easy modification and optimization of the chip during the development phase (25,29). Laser micromachining combined with thermal



**Figure 5.** Cell growth kinetics in the cell culture chip. The time-lapse sequence of phase-contrast images shows initial cell attachment and spreading on the chamber bottom during the first 4 h, and the plot demonstrates the growth of the cell population during 120 h of cell culturing in the chip.



## RESEARCH REPORT

bonding is a technique used to make general lab-on-a-chip systems (25), so the cell culture chamber of the chip can be integrated with microfluidic components such as pumps, valves, mixers, or with complete sample pretreatment and analysis microsystems. Microfluidic drug concentration gradients for high-throughput drug screening (10,11), optical sensors for metabolism analysis (30), and on-chip staining and flow cytometry (31) are a few integration options that we plan to add to the cell culture chip in the future. In comparison, such structures are complicated to do in glass or silicon because it requires a lot of specialized machinery and clean room facilities (10,11).

To ensure uniform heating, ITO-based heaters have been integrated in some commercial glass microincubators instead of using peripheral heaters (21). Being optically transparent and electrically conductive, ITO film does not obscure illumination of the chamber and, at the same time, can generate Joule heat when electrical power is applied to it. However, there are challenges in coating polymeric materials with ITO because standard thin-film vapor-deposition systems melt polymeric targets due to high temperatures in the vicinity of the vapor sources, and alternative sol-gel nanoparticle deposition methods (32,33) give relatively poor quality and stability of the ITO coatings (34,35). Therefore, specialized low-temperature sputter-deposition systems are typically required (36). Due to the lack of direct access to such equipment, the ITO heater was incorporated into the PMMA structure of the chip by using commercially available ITO-coated transparent PET films. These films were laminated in between PMMA sheets during the thermal bonding procedure of chip fabrication (Figure 1). Because PET has a higher glass transition temperature than PMMA, it maintains the integrity of thin ITO coating during the bonding at 110°C under pressure. Such a configuration also increases the reliability of the ITO film during chip operation because the surrounding PMMA completely isolates the coating from culture media liquids and therefore protects the film

from chemical and electrolytic erosion (Figure 1A).

Biocompatibility of the chip materials is an important issue for the long-term culture of healthy cells. Generally, PMMA is known as a biocompatible material and is widely used as implantable intraocular lenses due to its excellent optical properties (27). In our study, HeLa cells cultured within the PMMA chip showed identical morphology and doubling times (Figure 5) compared with cells grown in commercial culture flasks made of tissue culture-quality polystyrene (TC-PS). However, lower biocompatibility of osteosarcoma cells and endothelial cells (CPA-47) has been observed on untreated PMMA compared with TC-PS (37,38). Interestingly, the biocompatibility of PMMA was significantly increased by radiofrequency plasma treatment, which is also a standard treatment of PS, in order to reach TC-PS quality (38). Changes in PMMA surface biocompatibility by plasma treatment allow the possibility of systematically modifying surface properties and, with the use of the chip, directly observing cell culture responses to these modifications. For demanding cell cultures, biocompatibility of the chip might be improved by using TC-PS instead of PMMA as chamber material. Unfortunately, due to its physical properties, PS cannot be ablated by infrared laser with the same resolution as PMMA, so PS can replace only those chamber parts that do not contain microfluidic channels or other microscale objects. Thus, in the presented design of the chip, the entire chamber lid and bottom, which basically are the only surfaces exposed for cell adhesion, can be replaced by TC-PS. The only difference in chip fabrication necessary for the combination of TC-PS and PMMA is that thermal bonding has to be performed at 95°C due to the lower glass transition temperature of PS.

In conclusion, we have developed a low-cost optically transparent polymeric chip with integrated perfusion microfluidics and thermoregulation for long-term cell culture under controlled conditions. The fabrication process, which is based on laser micromachining and thermal bonding,

offers the flexible design of the chip, providing numerous lab-on-a-chip integration possibilities in the future.

## ACKNOWLEDGMENTS

*The study was supported by the Medicon Valley BIO+IT program and by The Danish Research Council [grant no. 2014-00-0003, Danish Biotechnology Instrument Center (DABIC)]. The HeLa cell line was kindly donated by Peter Thomsen, Scandinavian Micro Biodevices (SMB), Farum, Denmark.*

## COMPETING INTERESTS STATEMENT

*The authors declare no competing interests.*

## REFERENCES

1. Fiorini, G.S. and D.T. Chiu. 2005. Disposable microfluidic devices: fabrication, function, and application. *BioTechniques* 38:429-446.
2. Park, T.H. and M.L. Shuler. 2003. Integration of cell culture and microfabrication technology. *Biotechnol. Prog.* 19:243-253.
3. Prokop, A., Z. Prokop, D. Schaffer, E. Kozlov, J. Wikswo, D. Cliffler, and F. Baudenbacher. 2004. NanoLiterBioReactor: long-term mammalian cell culture at nanofabricated scale. *Biomed. Microdevices* 6:325-339.
4. Jager, E.W.H., C. Immerstrand, K.H. Peterson, K.-E. Magnusson, I. Lundström, and O. Inganäs. 2002. The cell clinic: closable microvials for single cell studies. *Biomed. Microdevices* 4:177-187.
5. Cooper, J.M. 1999. Towards electronic Petri dishes and picolitre-scale single-cell technologies. *Trends Biotechnol.* 17:226-230.
6. Inoue, I., Y. Wakamoto, H. Moriguchi, K. Okano, and K. Yasuda. 2001. On-chip culture system for observation of isolated individual cells. *Lab Chip.* 1:50-55.
7. Wakamoto, Y., I. Inoue, H. Moriguchi, and K. Yasuda. 2001. Analysis of single-cell differences by use of an on-chip microculture system and optical trapping. *Fresenius J. Anal. Chem.* 371:276-281.
8. Walker, G.M., H.C. Zeringue, and D.J. Beebe. 2004. Microenvironment design considerations for cellular scale studies. *Lab Chip.* 4:91-97.
9. Leclerc, E., Y. Sakai, and T. Fujii. 2004. Microfluidic PDMS (polydimethylsiloxane) bioreactor for large-scale culture of hepatocytes. *Biotechnol. Prog.* 20:750-755.
10. Hung, P.J., P.J. Lee, P. Sabouchi, N. Aghdam, R. Lin, and L.P. Lee. 2005. A novel high aspect ratio microfluidic design to provide a stable and uniform microenvironment for cell growth in a high throughput mammalian cell culture array. *Lab Chip.* 5:44-48.
11. Hung, P.J., P.J. Lee, P. Sabouchi, R. Lin, and L.P. Lee. 2005. Continuous perfusion

- microfluidic cell culture array for high-throughput cell-based assays. *Biotechnol. Bioeng.* 89:1-8.
12. Moriguchi, H., Y. Wakamoto, Y. Sugio, K. Takahashi, I. Inoue, and K. Yasuda. 2002. An agar-microchamber cell-cultivation system: flexible change of microchamber shapes during cultivation by photo-thermal etching. *Lab Chip* 2:125-132.
  13. Li Jeon, N., H. Baskaran, S.K. Dertinger, G.M. Whitesides, L. Van de Water, and M. Toner. 2002. Neutrophil chemotaxis in linear and complex gradients of interleukin-8 formed in a microfabricated device. *Nat. Biotechnol.* 20:826-830.
  14. Borenstein, J.T., H. Terai, K.R. King, E.J. Weinberg, M.R. Kaazempur-Mofrad, and J.P. Vacanti. 2002. Microfabrication technology for vascularized tissue engineering. *Biomed. Microdevices* 4:167-175.
  15. Khamis, R. 2005. Labs on a chip: meet the stripped down rat. *Nature* 435:12-13.
  16. Chen, C.S., X. Jiang and G.M. Whitesides. 2005. Microengineering the environment of mammalian cells in culture. *MRS Bulletin—Materials Research Society* 30:194-201.
  17. Davidsson, R., A. Boketoff, J. Bristuff, K. Kotarsky, B. Olde, C. Owman, M. Bengtsson, T. Laurell, and J. Emneus. 2004. Developments toward a microfluidic system for long-term monitoring of dynamic cellular events in immobilized human cells. *Anal. Chem.* 76:4715-4720.
  18. Sykes, J.A. and E.B. Moore. 1960. A simple tissue culture chamber. *Tex. Rep. Biol. Med.* 18:288-297.
  19. Dvorak, J.A. and W.F. Stotler. 1971. A controlled-environment culture system for high resolution light microscopy. *Exp. Cell Res.* 68:144-148.
  20. McKenna, N.M. and Y.L. Wang. 1989. Culturing cells on the microscope stage. *Methods Cell Biol.* 29:195-205.
  21. Focht, D.C. 1996. Live-cell microscopy: environmental control for mammalian specimens. *Nat. Biotechnol.* 14:361-362.
  22. Ince, C., D.L. Ypey, M.M. Diesselhoff-Den Dulk, J.A. Visser, A. De Vos, and R. Van Furth. 1983. Micro-CO<sub>2</sub>-incubator for use on a microscope. *J. Immunol. Methods* 60:269-275.
  23. Ince, C., J.T. van Dissel, and M.M. Diesselhoff. 1985. A teflon culture dish for high-magnification microscopy and measurements in single cells. *Pflügers Arch.* 403:240-244.
  24. Heidemann, S.R., P. Lamoureux, K. Ngo, M. Reynolds, and R.E. Buxbaum. 2003. Open-dish incubator for live cell imaging with an inverted microscope. *BioTechniques* 35:708-716.
  25. Klank, H., J.P. Kutter and O. Geschke. 2002. CO<sub>2</sub>-laser micromachining and back-end processing for rapid production of PMMA-based microfluidic systems. *Lab Chip* 2:242-246.
  26. Blau, A.W. and C.M. Ziegler. 2001. Prototype of a novel autonomous perfusion chamber for long-term culturing and in situ investigation of various cell types. *J. Biochem. Biophys. Methods* 50:15-27.
  27. Visser, S.A., R.W. Hergenrother, and S.L. Cooper. 1996. Polymers, p. 50-64. *In* B.D. Ratner, A.S. Hoffman, F.J. Schoen, and J.E. Lemons (Eds.), *Biomaterials Science: An Introduction to Materials in Medicine*. Academic Press, San Diego.
  28. Becker, H. and C. Gartner. 2000. Polymer microfabrication methods for microfluidic analytical applications. *Electrophoresis* 21:12-26.
  29. Jensen, M.F., J.E. McCormack, B. Helbo, L.H. Christensen, T.R. Christensen, and O. Geschke. 2004. Rapid prototyping of polymer microsystems via excimer laser ablation of polymeric moulds. *Lab Chip* 4:391-395.
  30. Zanzotto, A., N. Szita, P. Boccazzi, P. Lessard, A.J. Sinskey, and K.F. Jensen. 2004. Membrane-aerated microreactor for high-throughput bioprocessing. *Biotechnol. Bioeng.* 87:243-254.
  31. Buhlmann, C., T. Preckel, S. Chan, G. Luedke, and M. Valer. 2003. A new tool for routine testing of cellular protein expression: integration of cell staining and analysis of protein expression on a microfluidic chip-based system. *J. Biomol. Tech.* 14:119-127.
  32. Aegerter, M.A. and N. Al-Dahoudi. 2003. Wet-chemical processing of transparent and antiglare conducting ITO coating on plastic substrates. *J. Sol-Gel Sci. Technol.* 27:81-89.
  33. Al-Dahoudi, N., H. Bisht, C. Gobbert, T. Krajewski, and M.A. Aegerter. 2001. Transparent conducting, anti-static and anti-static-anti-glare coatings on plastic substrates. *Thin Sol. Films* 392:299-304.
  34. Ederth, J., P. Heszler, A. Hultaker, G.A. Niklasson, and C.G. Granqvist. 2003. Indium tin oxide films made from nanoparticles: models for the optical and electrical properties. *Thin Sol. Films* 445:199-206.
  35. Ederth, J., A. Hultaker, P. Heszler, G.A. Niklasson, C.G. Granqvist, A. van Doorn, C. van Haag, M.J. Jongerius, and D. Burgard. 2002. Electrical and optical properties of thin films prepared by spin coating a dispersion of nano-sized tin-doped indium oxide particles. *Smart Mater. Struct.* 11:675-678.
  36. Herrero, J. and C. Guillen. 2002. Transparent films on polymers for photovoltaic applications. *Vacuum* 67:611-616.
  37. Geckeler, K.E., R. Wacker, and W.K. Aicher. 2000. Biocompatibility correlation of polymeric materials using human osteosarcoma cells. *Naturwissenschaften* 87:351-354.
  38. Risbud, M.V., R. Dabhade, S. Gangal, and R.R. Bhonde. 2002. Radio-frequency plasma treatment improves the growth and attachment of endothelial cells on poly(methyl methacrylate) substrates: implications in tissue engineering. *J. Biomater. Sci. Polym. Ed.* 13:1067-1080.

Received 17 August 2005; accepted 19 December 2005.

**Address correspondence to:**

Martin Dufva  
 Department of Micro and Nanotechnology  
 Technical University of Denmark  
 Ørstedts Plads 345 East  
 DK-2800 Kgs. Lyngby, Denmark  
 e-mail: mdu@mic.dtu.dk

***Paper 2: A Biocompatible Micro Cell Culture Chamber ( $\mu$ CCC) for the Culturing and On-line Monitoring of Eukaryote Cells***

## A biocompatible micro cell culture chamber ( $\mu$ CCC) for the culturing and on-line monitoring of eukaryote cells†

Michael Stangegaard,<sup>a</sup> S. Petronis,<sup>b</sup> A. M. Jørgensen,<sup>a</sup> C. B. V. Christensen<sup>c</sup> and M. Dufva<sup>\*a</sup>

Received 8th March 2006, Accepted 30th May 2006

First published as an Advance Article on the web 15th June 2006

DOI: 10.1039/b603379b

We have previously shown that a polymeric (PMMA) chip with medium perfusion and integrated heat regulation provides sufficiently precise heat regulation, pH-control and medium exchange to support cell growth for weeks. However, it was unclear how closely the cells cultured in the chip resembled cells cultured in the culture flask. In the current study, gene expression profiles of cells cultured in the chip were compared with gene expression profiles of cells cultured in culture flasks. The results showed that there were only two genes that were differently expressed in cells grown in the cell culture chip compared to cell culture flasks. The cell culture chip could without further modification support cell growth of two other cell lines. Light coming from the microscope lamp during optical recordings of the cells was the only external factor identified, that could have a negative effect on cell survival. Low grade light exposure was however compatible with optical recordings as well as cell viability. These results strongly indicate that a cell culture chip could be constructed that allowed for on-line optical recording of cellular events without affecting the cell culturing condition compared to cell cultured in culture flasks incubated in a dark and CO<sub>2</sub> conditioned incubator.

### Introduction

The advances in microfabrication and polymer technologies and the opportunities offered in terms of design and fabrication of miniaturized cell culture systems<sup>1</sup> has led to the development of several cell culture chambers for various purposes. Some chambers focus on single cell observations over long periods of time.<sup>2–4</sup> Another group of micro chambers holds a larger amount of cells and is used for the study of wound healing processes,<sup>5</sup> cell–cell interactions,<sup>6</sup> differentiation,<sup>7</sup> myocyte synchronization,<sup>8</sup> chemotaxis,<sup>9</sup> electrical characterization,<sup>10,11</sup> and cell stress levels.<sup>12</sup> Other studies rely on arrays of interconnected cell culture chambers for online gene expression monitoring<sup>13</sup> or potential drug screening.<sup>14</sup> More advanced chambers have interconnected chambers each holding different cell lines representing the different organs and their interconnective metabolism<sup>15</sup> and these cell culture systems are used for determining the

toxicological and pharmacological profiles of chemicals and pharmaceuticals. It is thus clear that micro-fabricated cell culture chips provide a range of advantages, but these chips have to ensure proper temperature, medium and CO<sub>2</sub> conditioning of the cells, and prevent external factors such as the light used for microscopy from influencing the cells, and that physical and chemical factors of the chip, *e.g.* material choice and miniaturization, do not influence the cells in any way. If these factors are not controlled properly they can influence the quality of the data obtained from biochips.<sup>16</sup>

Maintaining the desired culture temperature within a narrow range of *e.g.*  $\pm 0.1$  °C can be a challenge even for commercial CO<sub>2</sub> incubators. Several of the above mentioned chambers rely on a conventional incubator to supply heat and CO<sub>2</sub> for maintaining physiological pH<sup>4,7,8,10,14,15</sup> or a microscope with CO<sub>2</sub> enriched stage environment.<sup>13</sup> Alternatively the temperature of the microscope stage is regulated,<sup>6</sup> the chamber exterior is perfused with preheated medium,<sup>2,12</sup> or a resistive heat coil is used to heat the chip.<sup>17</sup> Most advanced is the use of indium tin oxide (ITO) coated glass to supply heat to the chamber bottom and heating of the chamber exterior walls<sup>5,11</sup> in response to an internal temperature sensor. Temperature sensors controlling heating located within the cell culture chambers can compensate for day to day variances in temperature<sup>18</sup> which is important for long term studies.

Minimizing the effect of the culture environment on the cells requires the use of biocompatible surroundings. The term biocompatible surface refers to a surface devoid of both cytotoxic and positive effects in the sense of biofunctionality *i.e.* promotion or obstruction of biological processes compared to the reference surface.<sup>19,20</sup> Bio-incompatible surfaces such as SU-8,<sup>3</sup> silicon,<sup>12</sup> polylysine coated silicon,<sup>15</sup> alkanethiol self-assembled monolayers,<sup>21</sup> polyimide,<sup>22</sup> plasma polymerized

<sup>a</sup>Department of Micro and Nanotechnology, Technical University of Denmark, Ørstedes Plads 345 east, DK-2800 Kgs. Lyngby, Denmark. E-mail: mdu@mic.dtu.dk; Fax: +45 4588 7762; Tel: +45 4525 6324

<sup>b</sup>Dept. of Applied Physics, Fysikgården 4, Chalmers University of Technology, SE-412 96 Göteborg, Sweden

<sup>c</sup>Coloplast, Høltedam 1, DK-3050 Humlebæk, Denmark

† Electronic supplementary information (ESI) available: Movie 1: Culturing of Caco-2 cells. Images were obtained using a 15 min increment over a 110 h culturing period; movie 2: Culturing of Colo-205 cells. Images were obtained using a 5 min increment over a 50 h culturing period; movie 3: Resuscitation of HeLa cells in the  $\mu$ CCC. Cells were taken directly from the  $-80$  °C freezer, gently brought to room temperature and seeded in the  $\mu$ CCC. Fig. S1: Resuscitation of HeLa cells in the  $\mu$ CCC. Cell counts were performed at selected time intervals and plotted. The points from 20 h could be fitted to an exponential function ( $R^2 = 0.9946$ ) corresponding to a growth rate of approximately 45 h. See DOI: 10.1039/b603379b

hexene,<sup>23</sup> and bovine serum albumin (BSA) coated glass<sup>24</sup> have been rendered biocompatible by coating with fibronectin,<sup>15,21,22</sup> poly-D-lysine and laminin,<sup>11</sup> poly-L-lysine followed by O<sub>2</sub> plasma treatment,<sup>3</sup> poly-L-lysine,<sup>12</sup> hydrophilic polymer materials<sup>23</sup> and a specially designed anchor molecule<sup>24</sup> to allow culture of cells.

Biocompatibility is usually determined by viability assays,<sup>3,9,15</sup> morphology,<sup>17</sup> and growth rate kinetic comparisons<sup>7,25</sup> and these methods can be used to validate a chip. These methods for determining biocompatibility measure relatively large changes in cellular function and may miss subtle changes in the cells. Gene expression profiling using transcriptome DNA microarrays will therefore provide a far better picture of whether or not the cell culture chip provides comparable conditions to the reference system since gene expression profiling determines, comprehensively, the physiological state of the cell by measuring the levels of ~40000 different mRNA species in the cells. Gene expression profiling has for instance been used to classify cancers that otherwise are difficult to classify by morphology and other methods.<sup>26</sup> In this report we show that it is possible to construct a polymeric microfluidic chip with integrated heater which provides cell culture conditions indistinguishable from cell culture flasks in terms of cell growth rate, morphology and gene expression patterns.

## Results and discussion

The intension of this work was to clarify if a micro cell culture chamber ( $\mu$ CCC) previously described<sup>18</sup> was capable of sustaining culturing of eukaryote cells with on-line monitoring under conditions similar to the reference cell culture flask in the CO<sub>2</sub> incubator. The cell culture chip was composed of five PMMA sheets, which were separately cut and micromachined by laser ablation and assembled into a functional structure by thermal bonding.<sup>27</sup> The total size of the chip was 5.1 by 4.1 cm while the culturing area was 7.6 by 13.0 mm. The cell culture chip was designed to rely on continuous perfusion of the medium which circumvented the requirement for CO<sub>2</sub> buffering of the medium. Perfusion barriers were used to evenly distribute media over the cell culture area.<sup>18</sup> Shear stress was presumably eliminated by locating media inlets and outlets more than 1 mm above the culturing surface. Heating of the cell culture chamber was obtained with an integrated heater made from indium tin oxide (ITO)-coated polyethylene terephthalate film integrated in one of the PMMA layers of the chip. The temperature during culture was monitored by a thermistor located inside the culture chamber. The temperature inside the cell culture chamber was controlled by a proportional-integral-derivative (PID) feedback loop. In such cell culture chips, the temperature regulation is precise ( $37 \pm 0.2$  °C) with heat and fresh medium distributed relatively evenly within the culture area during perfusion.

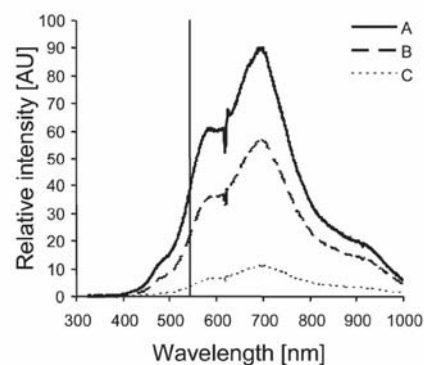
### Light effect

Initial observations indicated that cell death occurred within 48 h when the power of the microscope lamp used for monitoring cell growth in the  $\mu$ CCC was set above a certain threshold (data not shown). Phototoxic effects have previously

been observed when exposing cells to light with wavelengths below 540 nm.<sup>28</sup> Spectral analysis of the light reaching the cells through the microchip showed that the cells grown in the  $\mu$ CCC were exposed to significant amounts of light with wavelengths below 540 nm if the power setting of the microscope light was set at one third or above (Fig. 1). Extensive cell death was observed when cell were grown with the microscope light set to medium power. Possible effects of sun light as well as ceiling light were minimized by darkening the room during culture. There was little amount of light with wavelength below 540 nm reaching the cells when the power of the microscope lamp was reduced to the minimal setting (Fig. 1C). No significant cell death was observed using this light condition and cells could routinely be cultured for weeks. In conclusion, the results showed that light was inducing cell death. The mechanism is not clear but phototoxic effects of visible light results from photodecomposition of riboflavin/vitamin B<sub>2</sub>,<sup>29</sup> tyrosine<sup>30</sup> and tryptophan<sup>31</sup> and the generation of <sup>1</sup>O<sub>2</sub> and ·OH.<sup>29–32</sup> Free radicals released due to photodecomposition of media components can induce serious cell damage and fibrogenesis as reviewed in.<sup>33</sup> Many of the photo-effects may be eliminated by addition of anti-oxidants,<sup>29</sup> indicating it to be advisable to add anti-oxidants to the medium if strong light sources are needed for an assay. Alternatively, a system could be used that only expose cells to light during photographic recordings. Although we only have used white light microscopy, similar problems could be encountered using monochromatic light used for fluorescent assays.

### Cell growth rate in $\mu$ CCC

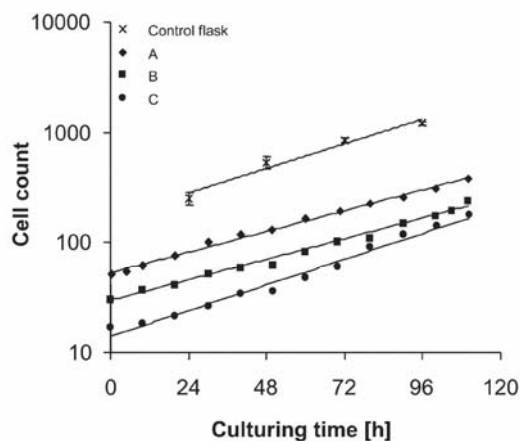
As the  $\mu$ CCC relies on constant perfusion of fresh media one possible effect could be a decrease in growth kinetics due to enhanced dilution of cellular secreted growth stimulating factors. Conversely, this effect may be counter balanced by the simultaneous dilution of growth inhibiting waste products. To determine if the  $\mu$ CCC gave rise to altered growth kinetics



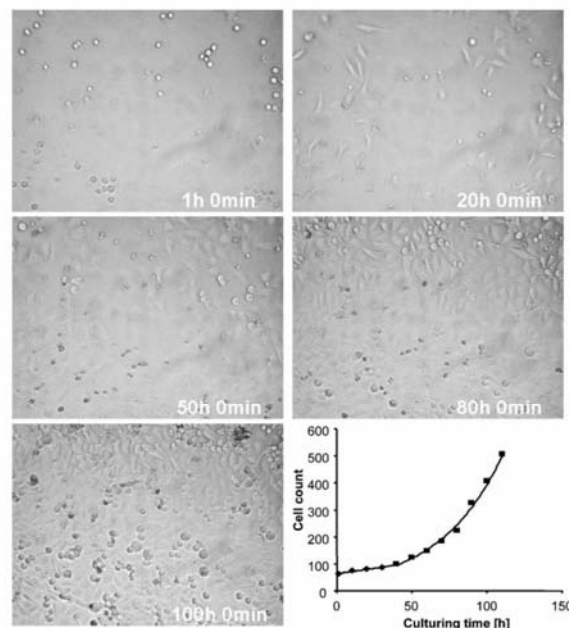
**Fig. 1** Light spectra obtained at different intensity settings. Each measurement was obtained ten times and the plotted values are average values of these measurements. All values were corrected for background by subtracting measurements obtained in complete darkness. (A) Spectra recorded with half the possible light intensity. (B) Spectra recorded with one third of the possible light intensity. (C) Spectra recorded with minimal light intensity. The black vertical line indicates 540 nm.

relative to the culture flask, HeLa cells were cultured in three different  $\mu$ CCCs for more than 100 h. Cell counts at representative time intervals were obtained by manual counting. For comparison, cells seeded in two reference culture flasks were inspected every 24 h and three to four representative images were obtained at each inspection. The doubling times of HeLa cells cultured in the  $\mu$ CCC were between 32.6 and 37.9 h while cells in the control flasks averaged to 32.0 h indicating slightly reduced growth in some culture experiments and comparable growth kinetics in others (Fig. 2).

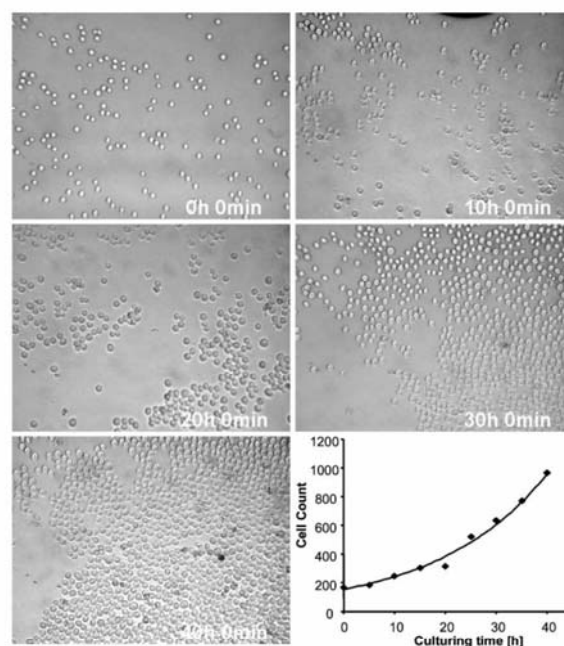
The generality of the  $\mu$ CCC for supporting cell growth was tested by culture of Colo-205, a colorectal adenocarcinoma cell line, and Caco-2 cells (Caucasian colon adenocarcinoma cell line). Caco-2 cells were cultured for more than 110 h (Fig. 3) with a doubling time of  $29.7 \pm 2.5$  h. This is in accordance with figures reported in the literature<sup>34,35</sup> where doubling times between 24 and 34 h were observed. This indicated that culture of Caco-2 cells in the  $\mu$ CCC does not significantly influence the doubling time. A movie of the culture is provided as ESI (movie 1).<sup>†</sup> Colo-205 cells behaved differently from Caco-2 cells in the culture. Colo-205 cells reached confluence after 50 h of culture but the proliferation continued until the culture experiment was stopped 115 h post seeding (Fig. 4). Colo-205 cells were extremely mobile and seemed to aggregate during cell culture making it difficult to estimate cell division rate since accumulation of cells could be partly due to cell division and partly due to cell migration (movie 2).<sup>†</sup> The majority of cells migrated from the upper left corner to the lower right corner indicating a preference for cell migration. However, cells were also observed to migrate in the opposite direction indicating a directed movement governed by presumably chemotaxis. Interestingly, Colo-205 cells are derived from a



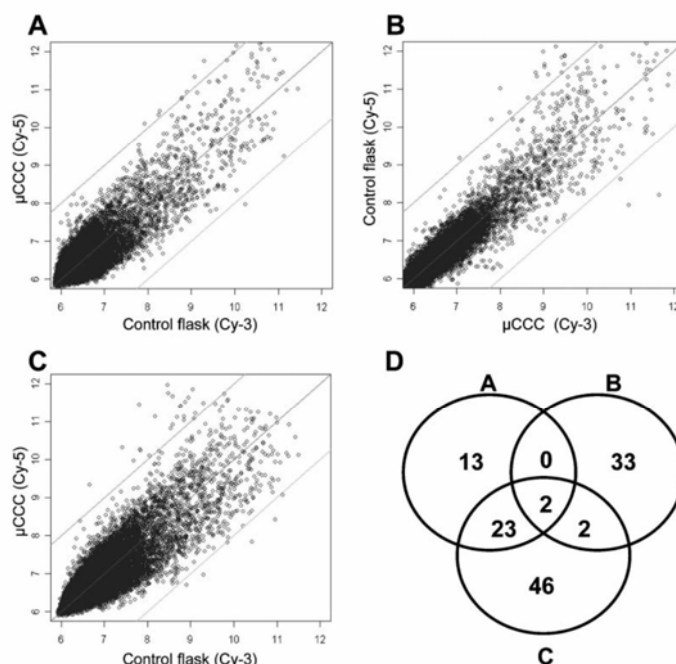
**Fig. 2** Growth kinetics of HeLa cells. Three long term culturing experiments were performed in the  $\mu$ CCC. Cell counts at selected time intervals were obtained and compared to cell counts from the culture flask. All cell counts were plotted and fitted with an exponential regression indicated with the line. The error bars on the cell counts from the culture flask represent the standard error of the mean (SEM). The doubling times for the control flask was 32.0 h, while doubling times of the three  $\mu$ CCCs were 37.9 h, 36.7 h and 32.6 h, respectively as derived from the slopes of the fitted lines.



**Fig. 3** Culturing of Caco-2 cells in the  $\mu$ CCC. Cell counts were performed at selected time intervals and plotted. Following roughly 40 h of lag time (♦) exponential growth (■) commenced. The data was fitted to an exponential regression line ( $R^2 = 0.9926$ ). During exponential growth, the doubling time was  $29.7 \pm 2.5$  h.



**Fig. 4** Culturing of Colo-205 cells in the  $\mu$ CCC. Cell counts were performed at selected time intervals and plotted. An exponential regression line ( $R^2 = 0.9837$ ) was fitted through the points. Ignoring accumulation of cells due to migration, the doubling time was estimated to be 15 h.



**Fig. 5** Comparison of gene expression profiles of cells grown in the  $\mu$ CCC with cells grown in culture flasks. Normalized scatter plots of gene expression profiles were obtained from three independent culture experiments in the  $\mu$ CCC and the culture flask. The central line is the median, and the upper and lower lines represent a fold change of three up or down, respectively. In two of the experiments, the cDNA deriving from cells grown in  $\mu$ CCC was labeled with Cy-5 and the cDNA deriving from the cell grown in control flasks with Cy-3 (A and C). In order to avoid systematic errors due to the respective dye, the order of colors was reversed in one experiment (B). (D) Venn diagram of the three independent experiments. Each array is depicted as a circle enclosing the number representing more than three fold regulated genes (up and down) relative to the culture flask. The number of genes similarly regulated on more than one array was placed in the overlapping region of the corresponding circle(s).

metastasis forming tumor, which may explain the high migration rate of these cells.

#### Resuscitation in the $\mu$ CCC

Cells are extremely fragile and sensitive to shear stress during resuscitation. To evaluate if the  $\mu$ CCC was capable of resuscitating cells without subjecting them to lethal stress, cells were taken directly from the  $-80\text{ }^{\circ}\text{C}$  freezer, gently brought to room temperature and seeded in the  $\mu$ CCC. Relying on continuous perfusion resulted in the dilution of the cryo-protective agent (DMSO) to non-cytotoxic levels (Fig. S1 and movie 3†). The generation time was found to be 45 h indicating a slower growth rate than HeLa cells that has been cultured in cell culture flasks for a few passages. Following two to three sub-cultures of the resuscitated cells, the growth rate decreased to around 32 h. This was observed both when cells were resuscitated in the cell culture chip and in the culture flask (data not shown). The results showed that the  $\mu$ CCC sustained resuscitation of HeLa cells indicating that also fragile cells could be cultured in the cell culture chamber.

#### Whole genome expression profiling of cells grown in the $\mu$ CCC

The gene expression profile of HeLa cells growing in the  $\mu$ CCC was compared to the gene expression profile of HeLa cells grown in cell culture flasks. Total RNA was extracted from

three separate culture experiments each culture lasting more than 100 h (Fig. 2C, culture A–C). Whole genome expression profiles were generated in three replicates utilizing DNA microarrays with 60 base long oligo probes directed against the entire human transcriptome (44 290 probes in total). Genes regulated more than three fold were considered significant. Scatter plots of the resulting hybridization intensities (Fig. 5 A–C) indicated that some transcripts were more than three-fold regulated. However, only two genes differed significantly in expression in all three experiments indicating a substantial noise in gene expression analysis that could be due to subtle biological variances between each culture or inherent variances in the microarray assay (Fig. 5D and Table 1). Ataxin 10 (Atx-10) has previously been reported to be essential for survival of cerebella neurons.<sup>36</sup> However, it is likely that

**Table 1** The two genes regulated more than three fold on all three arrays. The average fold change was computed as the average of the intensities derived from  $\mu$ CCC cultured cells divided by the control flask cultured cells. The *P*-values were computed based on *t*-test statistics

Probe name	Gene name	Average fold change	<i>P</i> -value
A_32_P162760	BI003432 (ATXN10: Ataxin 10)	0.25	$2.28 \times 10^{-5}$
A_23_P141785	A_23_P141785	5.02	0.0422

Ataxin 10 does not have a similar critical role for survival of HeLa cells because no decrease in cell viability was observed in cell grown in the cell culture chip compared with cells grown in cell culture flasks.<sup>18</sup> Blast homology searches using the probe sequences of the significantly regulated transcripts (Table 1 and Fig. 5D) failed to provide further clues to the biological functions of these transcripts. Therefore, we cannot, currently, explain why Ataxin 10 and *A\_23\_P141785* were observed to be regulated in cells cultured in the cell culture chip. Taken together, the results strongly indicated that the cells grown in the  $\mu$ CCC are biologically *comparable* to cells grown in a cell culture flask.

The goal was to construct a chip for optical on-line monitoring of cell behavior and in the process eliminate factors that affected cell growth and function. It is however very important that the cells grown in the chips are as similar as possible as cells grown in the reference systems to be able to compare data or to use cells grown in the  $\mu$ CCC as models. The almost identical gene expression profile in cells grown in the  $\mu$ CCC as compared with cells grown in the cell culture flask strongly indicate that there is little if any difference between the two culture conditions and the cells in the two systems could thus be directly compared. To our knowledge, this is the first cell culture chip for mammalian cells that has been validated down to the transcriptome level of the cultured cells. In contrast, in many microfluidic cell culture chamber designs, biocompatibility of cells in the chamber was either not considered or presented.<sup>4–6,8,10,12–14</sup> Other chambers were evaluated using viability assays<sup>3,9,15</sup> or morphological observations and growth kinetics.<sup>7,17</sup> Such assays are not as sensitive as whole genome expression profiling, since the latter has the potential to find subtle changes not detected by cell growth kinetics or morphology studies. Gene expression profiling has been achieved on a single cell<sup>37,38</sup> enabling comparability verification to be performed on virtually all cell culture devices provided that the cell or cell RNA can be extracted.

## Experimental

### Fabrication of $\mu$ CCC

The individual layers of the  $\mu$ CCC were fabricated by laser ablation of polymethyl methacrylate (PMMA) sheets (type 99530 Röhm GmbH & Co. KG, Darmstadt, Germany) either 1.5 mm or 0.25 mm thick with a CO<sub>2</sub> laser (Synrad Inc., Mukilteo, WA, USA).<sup>27</sup> The individual layers of the chamber were wiped with 96% ethanol (Merck KGaA, Darmstadt, Germany) assembled and bonded between two glass bonding blocks (Gustav Sørensen & Son, Rødovre, Denmark) at 110 °C for 1 h with a pressure of 100 N cm set with a 40–200 N cm torque screwdriver (Lindstrom, Orange, CA, USA) in a Memmert oven (Memmert, Schwabach, Germany). After bonding, the bonding blocks with  $\mu$ CCC were allowed to cool to room temperature before the pressure was gently released. Electrical connection to the Indium Tin Oxide (ITO) coated film (Sigma) was made with copper wires and conductive epoxy based glue (Circuitworks, Chemtronics, Kennesaw, GA, USA). The resistance through the ITO-film was used as a measure of the connection quality. Only chambers with a resistance lower than 17  $\Omega$  were used. Inlet tubes were realized

from blunt end 25-gauge stainless steel needles (Becton Dickinson, Drogheda, Ireland) that were divided in two by a metal saw and scratched on the surface for better attachment to the structure. Attachment to the structure was performed with epoxy glue (R&G GmbH, Waldenbuch, Germany).

Electronics design, blueprints and Labview programming is described/available elsewhere.<sup>18</sup>

### Cell culture in CO<sub>2</sub> incubator

Human carcinoma cells (HeLa) were cultured in 75 cm<sup>2</sup> culture flasks (Easyflask, Nalge Nunc International Rochester, NY, USA) in 25 mL media (RPMI 1640 media (Sigma) supplemented with 10% Fetal Bovine Serum (FBS) (Sigma), penicillin (100 U mL<sup>-1</sup>) and streptomycin (100  $\mu$ g mL<sup>-1</sup>) (Sigma)). Cells were cultured at 37 °C in an atmosphere containing 5% CO<sub>2</sub> (AGA, Copenhagen, Denmark) in a CO<sub>2</sub> incubator (Assab, Don Whitley Scientific Ltd., Shipley, West Yorkshire, UK). The cells were seeded at density of 6660 cells per cm<sup>2</sup> and the cells were passaged every three to four days when around 90% confluence was reached. Sub-culturing was performed by trypsinisation (Sigma). For cell growth doubling time estimation, two independent cell culture experiments, each lasting 4 days, were carried out. Cell counting was performed using microscopic images of the cell culture taken by temporarily removing the cell culture flasks from the CO<sub>2</sub> incubator and placing them on the stage of the inverted microscope. Three to four images were grabbed from each culture flask every day over a 4 day period and counting was performed (27 counts in total).

### Cells cultured in the $\mu$ CCC

For cell culture experiments in the  $\mu$ CCC, the perfusion inlet of the chip was connected to a 20 mL sterile syringe (Becton Dickinson) by polytetrafluoroethylene (PTFE) tubing (inner diameter: 0.8 mm, Bohlender GmbH, Grünsfeld, Germany), which was attached by flexible polydimethylsiloxane (PDMS) connectors. The syringe was pre-filled with cell culture media (RPMI 1640 media (Sigma) supplemented with 10% Fetal Bovine Serum (FBS) (Sigma), penicillin (100 U mL<sup>-1</sup>) and streptomycin (100  $\mu$ g mL<sup>-1</sup>) (Sigma)) preheated to 37 °C prior to loading in the syringe to minimize bubble formation inside the syringe. Continuous media perfusion was realized with a stepper pump (Harvard Apparatus 22, Holliston, MA, USA) generating a perfusion rate of 0.1 mL h<sup>-1</sup> (1.67  $\mu$ L min<sup>-1</sup>).

The  $\mu$ CCC was mounted on a microscope stage of a standard phase-contrast microscope (Nikon model Alphashot 2 YS2; Nikon, Tokyo, Japan). The cells were injected through a blunt end 25-gauge needle (Becton Dickinson) attached to a 1 mL syringe (Becton Dickinson). Cells were seeded in a density of 10–100 cells visible in the microscope (Nikon Coolpix 990) viewed at 10 $\times$  magnification by manually adjusting the seeding volume. The camera was attached to the microscope *via* a Nikon Coolpix MDC lens and equipped with a Nikon MC-EUI remote control unit operating in time-lapse mode, typically with a five-minute period, and was used to digitally record cell culture images at defined time intervals. The images were time-stamped using ScionImage v.4.0.2 freeware (Scion Corp., USA) and home-written macros.



### RNA isolation and amplification

Total RNA was isolated by RNeasy RNA purification kit (Qiagen, Valencia, CA, USA). Total RNA was quantified in an Ultraspec 3000 spectrophotometer (Pharmacia Biotech, Cambridge, UK) and the RNA integrity was validated by capillary electrophoresis (Agilent 2100 Bioanalyzer, Agilent Technologies, Palo Alto, CA, USA). Amplification was performed with the Riboamp T7-based RNA amplification kit (Areturus Engineering, Mountain View, CA, USA) according to the manufacturer's instructions using 2 µg total RNA as starting material yielding 35–40 µg aRNA after one round of amplification. For each labeling reaction, 3 µg of aRNA was used.

### cDNA synthesis

The cDNA was synthesized as described elsewhere,<sup>39</sup> with modifications described below. In brief: each reaction was primed with 3.35 nmol random 15-mer primers (Sigma-Genosys, Haverhill, UK) as described in ref. 40 in 18.5 µL reactions by incubation at 70 °C for 10 min, snap cooling on ice for at least one minute and incubating at room temperature for 2–5 min. Reverse transcription of the RNA was performed in the presence of 500 µM each of dATP, dCTP, and dGTP, 300 µM dTTP (Larova Biochemie GMBH, Teltow, Germany), 200 µM 5-aminoallyl-dUTP (Sigma), 40 U RNasin (Promega, Mannheim, Germany), 1× first-strand buffer (Invitrogen), 10 mM dithiothreitol (DTT) (Invitrogen), and 400 U Superscript II (Invitrogen) in 31 µL reactions at 42 °C for 5 h. Reactions were quenched by addition of 10 µL of 0.5 M EDTA (Sigma) and RNA hydrolyzed by the addition of 10 µL of 1 M NaOH followed by incubation at 65 °C for 15 min. The reactions were neutralized by addition of 10 µL 1 M HCl, and cDNA was purified on QIAquick columns (Qiagen, Valencia, CA, USA) according to the manufacturer's instructions but substituting phosphate wash buffer (5 mM potassium phosphate pH 8.0, 80% ethanol) for buffer PE, and phosphate elution buffer (4 mM potassium phosphate pH 8.5) for buffer EB.

cDNA was lyophilized to dryness and resuspended in 4.5 µL of 0.1 M sodium carbonate pH 9.0 buffer. NHS ester (4.5 µL) of Cy-3 or Cy-5 dye (GE Healthcare) in dimethyl sulfoxide (DMSO) (dye from one tube was dissolved in 73 µL of DMSO) was added and reactions were incubated at room temperature in the dark for 1 h. Coupling reactions were quenched by the addition of 35 µL of 0.1 M sodium acetate pH 5.2, and unincorporated dye was removed using QIAquick columns according to the manufacturer's instructions. Labeling efficiency was determined by analyzing the undiluted sample in a spectrophotometer using a 50 µL micro-cuvette (Hellma, Müllheim, Germany).

### Microarray hybridization

Labelled cDNA was hybridized to whole human genome microarrays containing 44 290 probes (Agilent Technologies, Palo Alto, CA, USA) according to supplier's instructions. In brief, 200 pmol Cy-5 labeled cDNA was mixed with 200 pmol Cy-3 labeled cDNA in 200 µL milliQ water and denatured at

98 °C for 3 min followed by incubation at room temperature for 2–3 min and addition of 50 µL 10× control solution (Agilent) and 250 µL 2× hybridization buffer (Agilent). Hybridization was performed in a hybridization chamber (Agilent) mounted on a rotation device placed in a Hybaid Shake 'n' Stack hybridization oven (Thermo Electron Corporation, San Diego, CA, USA) for 17 h at 60 °C with the lowest rotation setting (~4 rpm). Following hybridization the gasket slide was removed while the slides were submerged in washing solution 1 (6× SSC (AppliChem, Darmstadt, Germany), 0.005% Triton-X-102 (Agilent)) and the slides were washed for 10 min at room temperature (RT) in wash solution 1 followed by 5 min in wash solution 2 (0.1× SSC (AppliChem), 0.005% Triton-X-102 (Agilent)) at 4 °C. Scanning and quantification was performed in an ArrayWoRx microarray scanner (Applied Precision, Issaquah, WA, USA). The data was normalized using the non-linear method Qspline<sup>41</sup> and further processed in Excel.

### Spectral analysis

The spectrum of the light emitted by the microscope halogen lamp was measured using an AvaSpec2048 spectrometer (Avantes, Netherlands). The spectrometer was connected to a step index optical fiber with a core diameter of 50 µm and a numerical aperture of 0.22. This fiber was mounted on the microscope fixture and aligned with the collimated illumination light. The spectrum was measured both in the dark and for several settings of the microscope light intensity using integration times between 2 and 20 ms. The measurements were scaled to an integration time of 20 ms and the dark spectrum was subtracted. Each measurement was obtained ten times and the plotted values are average values of these measurements.

### Conclusion

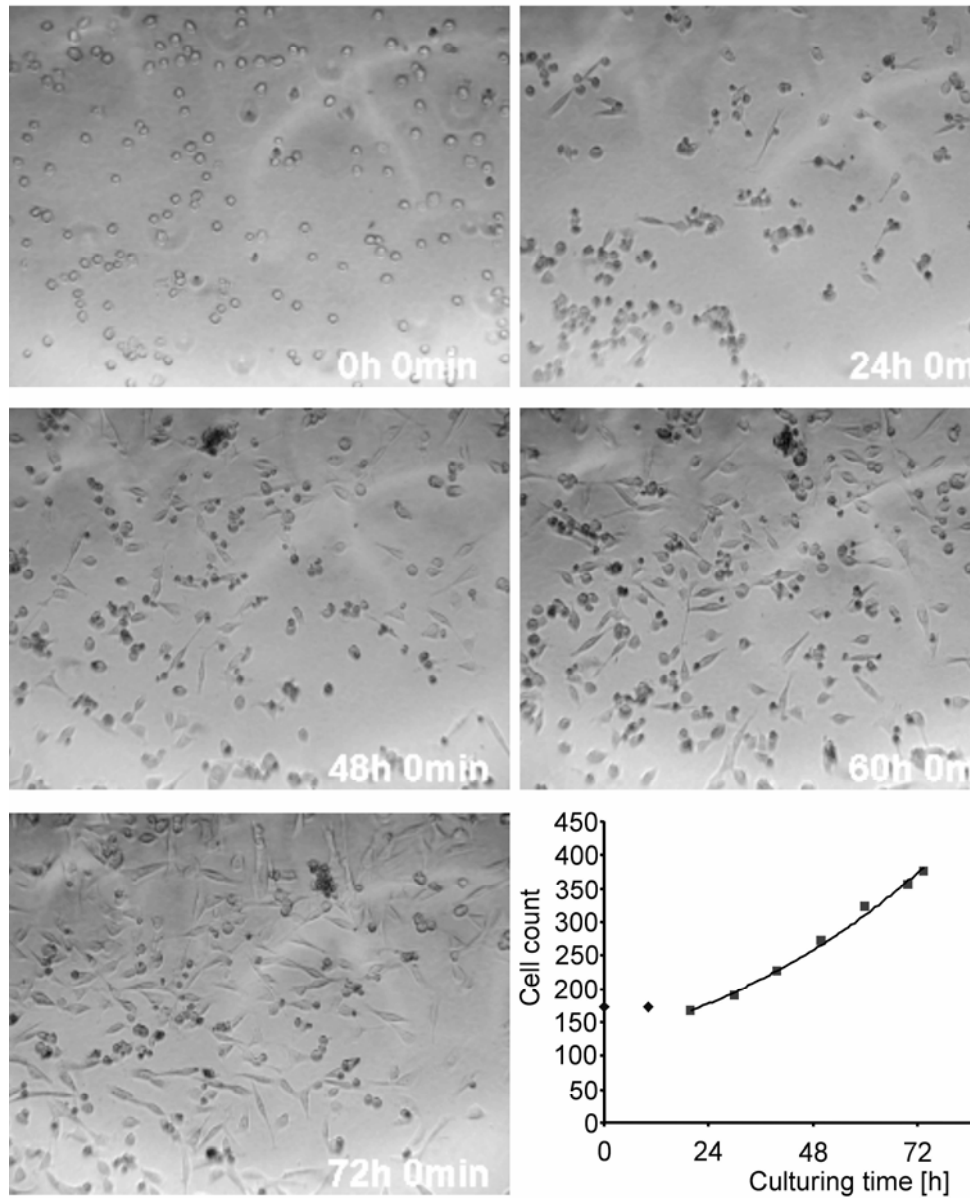
A micro cell culture chamber was characterized by cell culture of various cell lines and gene expression profiling. All tested cell lines could be cultured in the chamber with similar growth rates as cells grown in cell culture flasks. Cells cultured in the chamber revealed almost indistinguishable gene expression profiles to the cells cultured in cell culture flasks. No signs of photo induced effects, activation of DNA repair systems or shear stress was observed using whole human genome DNA microarrays. This suggests that the µCCC supports culturing and on-line monitoring of mammalian cells under conditions indistinguishable from the reference cell culture flask in the CO<sub>2</sub> incubator.

### Acknowledgements

This work was supported by The Danish Research Council (grant #2014-00-0003, DABIC) and by Medicon Valley Academy BIO+IT program. The HeLa cell line was kindly donated by Dr Peter Thomsen, Scandinavian Micro Biodevices (SMB), Farum, Denmark. The Colo-205 and Caco-2 cell lines were kindly donated by Dr Duang D. Bang, Department of Poultry, Fish and Fur Animals, Danish Veterinary Institute, Aarhus, Denmark.

## References

- 1 G. S. Fiorini and D. T. Chiu, *Biotechniques*, 2005, **38**, 429–446.
- 2 C. Ince, R. E. Beekman and G. Verschragen, *J. Immunol. Methods*, 1990, **128**, 227–234.
- 3 E. W. H. Jager, C. Immerstrand, K. H. Peterson, K.-E. Magnusson, I. Lundström and O. Inganäs, *Biomed. Microdevices*, 2002, **4**, 177–187.
- 4 A. Prokop, Z. Prokop, D. Schaffer, E. Kozlov, J. Wikswo, D. Clifflé and F. Baudenbacher, *Biomed. Microdevices*, 2004, **6**, 325–339.
- 5 C. L. Ho, T. Y. Mou, P. S. Chiang, C. L. Weng and N. H. Chow, *Biotechniques*, 2005, **38**, 267–273.
- 6 H. Moriguchi, Y. Wakamoto, Y. Sugio, K. Takahashi, I. Inoue and K. Yasuda, *Lab Chip*, 2002, **2**, 125–132.
- 7 A. Tourouvskaia, X. Figueroa-Masot and A. Folch, *Lab Chip*, 2005, **5**, 14–19.
- 8 K. Kojima, T. Kaneko and K. Yasuda, *J. Nanobiotechnology*, 2004, **2**, 9.
- 9 N. L. Jeon, H. Baskaran, S. K. Dertinger, G. M. Whitesides, L. Van de Water and M. Toner, *Nat. Biotechnol.*, 2002, **20**, 826–830.
- 10 S. Hediger, J. Fontannaz, A. Sayah, W. Hunziker and M. A. M. Gijs, *Sens. Actuators, B*, 2000, **63**, 63–73.
- 11 A. W. Blau and C. M. Ziegler, *J. Biochem. Biophys. Methods*, 2001, **50**, 15–27.
- 12 R. Davidsson, A. Boketoft, J. Bristulf, K. Kotarsky, B. Olde, C. Owman, M. Bengtsson, T. Laurell and J. Emneus, *Anal. Chem.*, 2004, **76**, 4715–4720.
- 13 D. M. Thompson, K. R. King, K. J. Wieder, M. Toner, M. L. Yarmush and A. Jayaraman, *Anal. Chem.*, 2004, **76**, 4098–4103.
- 14 P. J. Hung, P. J. Lee, P. Sabouchi, N. Aghdam, R. Lin and L. P. Lee, *Lab Chip*, 2005, **5**, 44–48.
- 15 A. Sin, K. C. Chin, M. F. Jamil, Y. Kostov, G. Rao and M. L. Shuler, *Biotechnol. Prog.*, 2004, **20**, 338–345.
- 16 D. C. Focht, *Nat. Biotechnol.*, 1996, **14**, 361–362.
- 17 W. A. Hing, C. A. Poole, C. G. Jensen and M. Watson, *J. Microsc.*, 2000, **199**, Pt 2, 90–95.
- 18 S. Petronis, M. Stangegaard, C. B. V. Christensen and M. Dufva, *Biotechniques*, 2006, **40**, 368–375.
- 19 C. J. Kirkpatrick, F. Bittinger, M. Wagner, H. Kohler, T. G. van Kooten, C. L. Klein and M. Otto, *Proc. Inst. Mech. Eng. [H]*, 1998, **212**, 75–84.
- 20 Y.-X. Wang, J. L. Robertson, W. B. Spillman and R. O. Claus, *Pharm. Res.*, 2004, **21**, 1362–1373.
- 21 N. D. Gallant, J. R. Capadona, A. B. Frazier, D. M. Collard and A. J. Garcia, *Langmuir*, 2002, **18**, 5579–5584.
- 22 J. L. Charest, L. E. Bryant, A. J. Garcia and W. P. King, *Biomaterials*, 2004, **25**, 4767–4775.
- 23 S. Bouaidat, C. Berendsen, P. Thomsen, S. G. Petersen, A. Wolff and J. Jonsmann, *Lab Chip*, 2004, **4**, 632–637.
- 24 K. Kato, K. Umezawa, D. P. Funeriu, M. Miyake, J. Miyake and T. Nagamune, *Biotechniques*, 2003, **35**, 1014–1018, 1020–1011.
- 25 Y. M. Kong, C. J. Bae, S. H. Lee, H. W. Kim and H. E. Kim, *Biomaterials*, 2005, **26**, 509–517.
- 26 A. A. Alizadeh, M. B. Eisen, R. E. Davis, C. Ma, I. S. Lossos, A. Rosenwald, J. C. Boldrick, H. Sabet, T. Tran, X. Yu, J. I. Powell, L. Yang, G. E. Marti, T. Moore, J. Hudson, Jr., L. Lu, D. B. Lewis, R. Tibshirani, G. Sherlock, W. C. Chan, T. C. Greiner, D. D. Weisenburger, J. O. Armitage, R. Warnke, R. Levy, W. Wilson, M. R. Grever, J. C. Byrd, D. Botstein, P. O. Brown and L. M. Staudt, *Nature*, 2000, **403**, 503–511.
- 27 H. Klank, J. P. Kutter and O. Geschke, *Lab Chip*, 2002, **2**, 242–246.
- 28 R. J. Wang, *Photochem. Photobiol.*, 1975, **21**, 373–375.
- 29 R. Lucius, R. Mentlein and J. Sievers, *Free Radical Biol. Med.*, 1998, **24**, 798–808.
- 30 J. D. Stoen and R. J. Wang, *Proc. Natl. Acad. Sci. U. S. A.*, 1974, **71**, 3961–3965.
- 31 A. M. Edwards, E. Silva, B. Jofre, M. I. Becker and A. E. De Ioannes, *J. Photochem. Photobiol., B*, 1994, **24**, 179–186.
- 32 R. J. Wang, J. D. Stoen and F. Landa, *Nature*, 1974, **247**, 43–45.
- 33 G. Poli and M. Parola, *Free Radic. Biol. Med.*, 1997, **22**, 287–305.
- 34 M.-C. Grès, B. Julian, M. Bourrié, V. Meunier, C. Roques, M. Berger, X. Boulenc, Y. Berger and G. Fabre, *Pharm. Res.*, 1998, **15**, 726–733.
- 35 I. Chantret, A. Rodolosse, A. Barbat, E. Dussaulx, E. Brot-Laroche, A. Zweibaum and M. Rousset, *J. Cell Sci.*, 1994, **107**, Pt 1, 213–225.
- 36 P. Marz, A. Probst, S. Lang, M. Schwager, S. Rose-John, U. Otten and S. Ozbek, *J. Biol. Chem.*, 2004, **279**, 35542–35550.
- 37 J. Eberwine, H. Yeh, K. Miyashiro, Y. Cao, S. Nair, R. Finnell, M. Zettel and P. Coleman, *Proc. Natl. Acad. Sci. U. S. A.*, 1992, **89**, 3010–3014.
- 38 L. Luo, R. C. Salunga, H. Guo, A. Bittner, K. C. Joy, J. E. Galindo, H. Xiao, K. E. Rogers, J. S. Wan, M. R. Jackson and M. G. Erlander, *Nat. Med.*, 1999, **5**, 117–122.
- 39 I. V. Yang, E. Chen, J. P. Hasseman, W. Liang, B. C. Frank, S. Wang, V. Sharov, A. I. Saeed, J. White, J. Li, N. H. Lee, T. J. Yeatman and J. Quackenbush, *Genome Biol.*, 2002, **3**, research0062.
- 40 M. Stangegaard, I. H. Dufva and M. Dufva, *Biotechniques*, 2006, **40**, 649–657.
- 41 C. Workman, L. J. Jensen, H. Jarmer, R. Berka, L. Gautier, H. B. Nielsen, H. H. Saxild, C. Nielsen, S. Brunak and S. Knudsen, *Genome Biol.*, 2002, **3**, research0048.



**Fig S1:** Resuscitation of HeLa cells in the  $\mu$ CCC. Cell counts were performed at selected time intervals and plotted. The points from 20 h could be fitted to an exponential function ( $R^2 = 0.9946$ ) corresponding to a growth rate of approximately 45 h.

*Paper 3: Whole genome expression profiling using DNA microarray for determining biocompatibility of polymeric surfaces*

# Whole genome expression profiling using DNA microarray for determining biocompatibility of polymeric surfaces†

Michael Stangegaard,‡ Z. Wang,‡ J. P. Kutter, M. Dufva\* and A. Wolff

Received 12th June 2006, Accepted 13th July 2006

First published as an Advance Article on the web 26th July 2006

DOI: 10.1039/b608239d

There is an ever increasing need to find surfaces that are biocompatible for applications like medical implants and microfluidics-based cell culture systems. The biocompatibility of five different surfaces with different hydrophobicity was determined using gene expression profiling as well as more conventional methods to determine biocompatibility such as cellular growth rate, morphology and the hydrophobicity of the surfaces. HeLa cells grown on polymethylmethacrylate (PMMA) or a SU-8 surface treated with HNO<sub>3</sub>-ceric ammonium nitrate (HNO<sub>3</sub>-CAN) and ethanolamine showed no differences in growth rate, morphology or gene expression profiles as compared to HeLa cells grown in cell culture flasks. Cells grown on SU-8 treated with only HNO<sub>3</sub>-CAN showed almost the same growth rate ( $36 \pm 1$  h) and similar morphology as cells grown in cell culture flasks ( $32 \pm 1$  h), indicating good biocompatibility. However, more than 200 genes showed different expression levels in cells grown on SU-8 treated with HNO<sub>3</sub>-CAN compared to cells grown in cell culture flasks. This shows that gene expression profiling is a simple and precise method for determining differences in cells grown on different surfaces that are otherwise difficult to find using conventional methods. It is particularly noteworthy that no correlation was found between surface hydrophobicity and biocompatibility.

## Introduction

Polymeric materials (e.g., polymethylmethacrylate (PMMA)) have been used since the 1960s in orthopedic surgery.<sup>1</sup> More recently, polymer materials have been used in micro-total analysis systems ( $\mu$ TAS) for cell biology research.<sup>2–4</sup> Culturing cells *in vitro* requires biocompatible surfaces.<sup>5</sup> A biocompatible surface is a surface without both negative (cytotoxic) and positive effects with regard to biofunctionality, i.e., the promotion or obstruction of biological processes compared to a reference surface.<sup>6–8</sup> Surfaces can be rendered biocompatible for tissue and cell culturing studies by coating them with fibronectin<sup>9–11</sup> or hydrophilic polymer materials,<sup>12</sup> or treating them with O<sub>2</sub> plasma.<sup>13</sup> However, those coating processes can be laborious and expensive, and the coating may prove unstable over time.

Cytotoxicity determination is an important aspect of biomaterial testing standards such as those proposed by the International Organization for Standardization (ISO) and the American Society for Testing and Materials (ASTM). However, the absence of cytotoxicity as, for example, measured by the 3-(4,5-dimethylthiazol-2-yl)-2,5-diphenyl-tetrazolium bromide (MTT) test<sup>14</sup> or the fluorescent membrane integrity test (FMIT),<sup>15</sup> does not necessarily imply that a

biomaterial is biocompatible. For each application, tests have to be conducted in settings reflecting the natural environment and the demands posed on the application to elucidate the biocompatibility of the biomaterial. The biocompatibility of a material has been related to cellular functions like adhesion<sup>15–17</sup> and spreading<sup>18</sup> on the surface, proliferation rate,<sup>17</sup> metabolic activity,<sup>17</sup> surface inhomogeneity and moderate wettability.<sup>19</sup> However, as evident in some reports, increasing the surface wettability does not necessarily correspond to an increased biocompatibility.<sup>20,21</sup>

As an epoxy-based negative constructional photoresist, SU-8 is widely used for fabricating microstructures in various  $\mu$ TAS devices because of its excellent chemical stability, optical properties and fast fabrication process.<sup>22–27</sup> However, the SU-8 epoxy surface is not biocompatible.<sup>28</sup> Coating of the SU-8 surface with polymers<sup>29,30</sup> have been reported to result in temporary biocompatibility. Chemical treatments have the potential to modify the SU-8 surface properties for extended periods of time, and can easily be combined with other micro-fabrication processes. The epoxy moieties on the SU-8 surface are generally not reactive with standard corrodents (e.g., THF, HCl or HNO<sub>3</sub>),<sup>31,32</sup> reflecting the pronounced chemical stability of SU-8. However, with the catalyst ceric ammonium nitrate (CAN, (NH<sub>4</sub>)<sub>2</sub>Ce(NO<sub>3</sub>)<sub>6</sub>), the epoxy rings were reported to open under the reaction with HNO<sub>3</sub><sup>33</sup> or acetic acid.<sup>34</sup> Recently, such reaction mechanisms were applied to render SU-8 hydrophilic for use in micro-channel fabrication.<sup>34</sup>

Gene expression profiling using DNA microarrays has been widely used in the past 10 years to unravel molecular events within cell cycle regulation,<sup>35,36</sup> response to growth factors<sup>37</sup> and cellular responses to irradiation.<sup>38</sup> DNA microarrays are used as cancer classifiers<sup>39–42</sup> because there is strong evidence

MIC-Department of Micro and Nanotechnology, Technical University of Denmark, Ørstedts Plads 345 East, DK-2800, Kgs. Lyngby, Denmark. E-mail: mdu@mic.dtu.dk; Fax: +45 4588 7762; Tel: +45 4525 6324

† Electronic supplementary information (ESI) available: HeLa cells cultured on differently treated SU-8 surfaces (Figs S1 and S2) and list of significantly regulated genes on cells cultured on SU-8 HNO<sub>3</sub>-CAN (SU-8 CAN) and SU-8 surfaces relative to cells cultured in the culture flask (Table S1). See DOI: 10.1039/b608239d

‡ Both authors contributed equally to the work.

that the gene expression profile differs in cancer cells compared to their “normal” counterparts. The DNA microarrays normally used consist of DNA probes that are complementary to about 40 000 genes or possible genes. In one batch process, the expression level of these 40 000 genes in a particular cell can be monitored and compared to a reference cell. Culturing cells on a surface that is not biocompatible will most likely induce changes in the mRNA expression profile of a cell.<sup>43</sup> This became apparent when studying changes in gene expression in MG63 osteoblast-like cells grown on zirconium oxide,<sup>44</sup> where genes involved in immunity, cell cycle, and vesicular transport showed significant changes compared to the reference system.

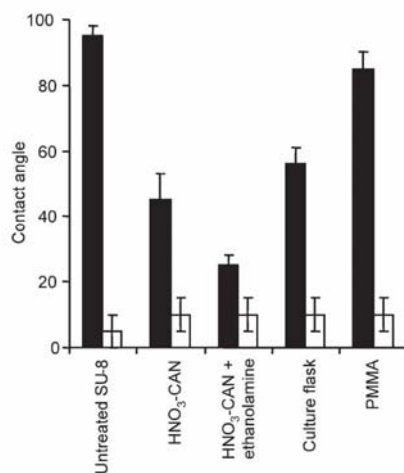
In this report, we compare different methods to determine biocompatibility such as contact angle measurements and aspects of mammalian cell culturing (including morphology and growth kinetics) and whole genome expression profiling. The biocompatibility methods were tested using cells grown on modified and unmodified SU-8 as well as on unmodified PMMA.

## Results and discussion

### Surface modifications

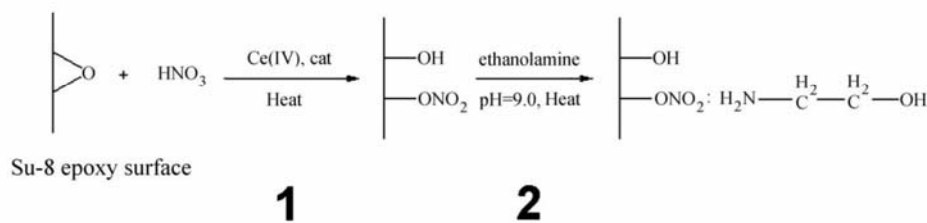
Because SU-8 and PMMA are popular materials for building microfluidics structures,<sup>22</sup> these materials were evaluated in biocompatibility tests and compared to polystyrene (PS) cell culture flasks. SU-8 as well as PMMA are highly hydrophobic, suggesting that they may be less suitable for cell growth.<sup>7</sup> Therefore, a method was developed to modulate the hydrophobicity of SU-8. A simple two-step chemical surface treatment resulted in a hydrophilic SU-8 surface. The assumed chemical reaction mechanism of the protocol is shown in Fig. 1: the HNO<sub>3</sub>-CAN treatment opens the SU-8 epoxy groups and converts them to nitro groups.<sup>33</sup> This surface can subsequently be modified with ethanolamine (Fig. 1).<sup>34</sup>

The water contact angle was measured on the differently modified SU-8 surfaces, on PMMA and on PS cell culturing flasks. Treatment of SU-8 with HNO<sub>3</sub>-CAN decreased the contact angle from 95° to 45° (Fig. 2). The contact angle of SU-8 could be further decreased to 25° by treating SU-8 first with HNO<sub>3</sub>-CAN and then with ethanolamine. Ethanolamine had no effect on the contact angle without the initial HNO<sub>3</sub>-CAN treatment. The contact angle of SU-8 treated with HNO<sub>3</sub>-CAN and ethanolamine changed back to about 50° after storage at room temperature for two months. In contrast,



**Fig. 2** Water contact angles of different surfaces. The hydrophobicity of different surfaces was determined by measuring the contact angle of water. Solid bars represent measurements performed on surfaces prior to incubation with cell culture media. Open bars represent water contact angles on surfaces after incubation with cell culture media under culturing conditions (37 °C, 5% CO<sub>2</sub>) in the incubator for 24 h. Prior to measuring the contact angles, surfaces were dried under a gentle stream of N<sub>2</sub>.

the surface of SU-8 treated with HNO<sub>3</sub>-CAN was chemically stable over time as determined by contact angle measurements. Furthermore, it also tolerated the ultrasonic agitation lift-off process of photoresist in acetone. The contact angle of a PMMA sheet was measured to be 85° and the PS cell culturing flask was determined to be 56° (Fig. 2). These two surfaces served as control surfaces for the study of the differently treated SU-8 surfaces. As contact angles measured on a dry surface hardly reflect the environment encountered by the cells during culturing, the different surfaces were exposed to cell culture media and incubated for 24 h under cell culturing conditions. After drying under a gentle stream of N<sub>2</sub>, all surfaces had a contact angle with water which was less than 15° (Fig. 2). The reduction of the contact angle to approximately 15° was most likely caused by adsorption of proteins to the respective surfaces. Protein binding has indirectly been observed on untreated PMMA and SU-8 because PCR microchips made in SU-8 and PMMA require at least two-fold more enzyme to sustain PCR reactions.<sup>30,45</sup> Furthermore, both SU-8 and PMMA can directly form covalent bonds with



**Fig. 1** Proposed reaction scheme of the two-step SU-8 surface modification. **1:** The epoxy ring on the SU-8 surface is believed to be opened by treatment with HNO<sub>3</sub>-CAN. **2:** The nitro radical on the modified SU-8 surface reacts with the amino group of ethanolamine.

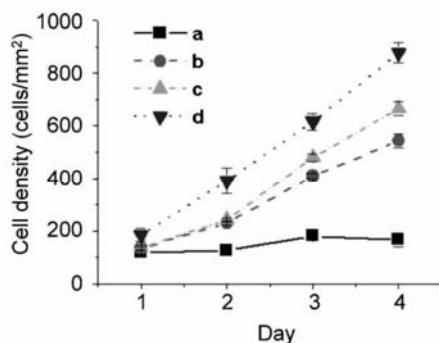
single stranded amino modified DNA,<sup>46,47</sup> indicating that these surfaces are reactive to amine-containing biomolecules such as DNA and proteins.

#### Morphology and growth kinetics

Five different surfaces (Fig. 2) were tested for biocompatibility by comparing cell morphology and growth characteristics. HeLa cells were seeded on the different surfaces and the cell density was determined throughout a four day period. Untreated SU-8 had a very high generation time of  $147 \pm 56$  h, indicating unusually slow growth compared to the reference cell culture flask, which had a generation time of  $32 \pm 1$  h (Fig. 3). The images show that the few cells attached to untreated SU-8 were elongated compared to cells grown in the culture flask. Very few dividing cells were observed on untreated SU-8. Treatment of SU-8 with HNO<sub>3</sub>-CAN resulted in a surface that supported HeLa cell growth with a generation time of  $36 \pm 1$  h (Fig. 3). By contrast, SU-8 surfaces treated with HNO<sub>3</sub>-CAN and ethanolamine sustained cell growth rates, indistinguishable from cell growth rates in a cell culture flask. Both surfaces resulted in a cell generation time of approximately 32 h. The morphology of cells cultured on the SU-8 surface treated with HNO<sub>3</sub>-CAN closely resembled the morphology of cells cultured on the SU-8 surface treated with HNO<sub>3</sub>-CAN and ethanolamine, and the culture flask surface (see Fig. S1 and S2 in ESI†). Similar to cells grown on SU-8 treated with HNO<sub>3</sub>-CAN and ethanolamine, cells grown on PMMA showed no differences in morphology or growth rate compared to cells grown in cell culture flasks. These results show that the growth rate does not correlate with the hydrophobicity of the investigated surfaces. PMMA had, for

instance, a higher initial hydrophobicity than SU-8 treated with HNO<sub>3</sub>-CAN and ethanolamine (Fig. 2). Incubating the surfaces with cell culturing medium resulted in a similar hydrophobicity (15°) for all the surfaces, suggesting that all surfaces should sustain growth with similar efficiency. However, this was not observed.

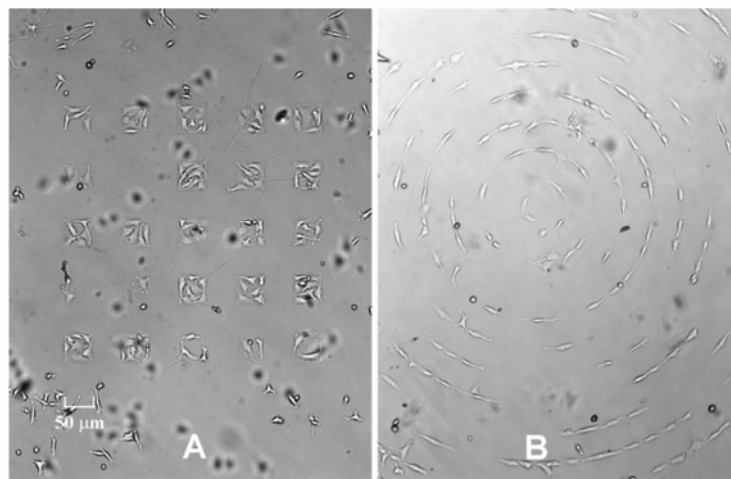
SU-8 might be releasing chemical factors such as residual solvents or monomers from the polymerization and lithographical processes. Such factors might be responsible for the different growth kinetics as well as the differences in morphology observed on the different SU-8 surfaces tested. The existence of such factors was tested by growing cells on SU-8 samples that were patterned chemically so that the samples contained small checkerboard or circular areas that were biocompatible. Such patterns were created on the SU-8 surface by masking the SU-8 surface prior to treatment with HNO<sub>3</sub>-CAN and ethanolamine. The cells avoided areas that had not been exposed to HNO<sub>3</sub>-CAN and ethanolamine. Two or three cells were observed in  $50 \mu\text{m} \times 50 \mu\text{m}$  patterned squares, while no or few cells were observed on adjacent untreated surfaces (Fig. 4A). After cell division, cells on the patterned areas decreased in either size or attachment area, rather than colonizing on untreated SU-8. On the  $5 \mu\text{m}$  wide concentric circles, the cells appeared elongated and convex rather than round, indicating that the cells actively avoided the untreated SU-8 surface (Fig. 4B). Taken together these results demonstrate that SU-8 can be patterned with defined areas that sustain cell growth using the suggested novel method and that chemicals diffusing out of the bulk material are not causing the lack of growth on untreated SU-8 since cells separated by only one or two  $\mu\text{m}$  displayed different morphologies and growth rates.



**Fig. 3** Growth kinetics of HeLa cells on the differently modified SU-8 surfaces. Samples of the differently modified SU-8 surfaces were immersed in standard cell culture media in separate cell culture flasks and seeded with equal amounts of HeLa cells. The samples were incubated for 4 days in the incubator. The cells were inspected every 24 h and three to four representative pictures were taken on each surface on each occasion for cell counting. The entire culturing experiment was repeated twice and the cell counts were averaged. The error bars represent the standard deviation. The number of attached cells was manually counted for calculation of the cell densities. The label letters refer to the following different surfaces: (a) untreated SU-8; (b) SU-8 treated with HNO<sub>3</sub>-CAN; (c) SU-8 treated with HNO<sub>3</sub>-CAN and ethanolamine; (d) control culture flask surface.

#### Whole genome expression profile comparison of cells grown on different surfaces

DNA microarray analysis was used to determine the differences in gene expression profile on cells cultured on various surfaces. Therefore, the gene expression profiles of cells cultured on PMMA, SU-8, SU-8 treated with HNO<sub>3</sub>-CAN, and SU-8 treated with HNO<sub>3</sub>-CAN and ethanolamine were determined and compared with the gene expression profiles of cells cultured on PS cell culturing flasks. Whole genome expression profiles were generated using DNA microarrays carrying 60 base-long oligo probes directed against the entire human transcriptome (44290 probes in total). To estimate the amount of noise, two self-self hybridizations were performed using cDNA generated only from cells cultured in culture flasks. The results showed that 40 genes had more than a two-fold difference in expression level. However, no genes showed more than three fold difference in expression level (Fig. 5 A–B), and a cut-off of three fold was therefore used for detection of significant up- or down regulation. Scatter plots of the resulting hybridization intensities indicated that cells grown on untreated SU-8 and HNO<sub>3</sub>-CAN treated SU-8 (Fig. 5 C–D) had significantly different gene expression profiles (*i.e.*, genes with more than three-fold higher or lower expression levels) compared to cells grown in cell culture flasks (Fig. 5 A–B). Thirty-one genes were up-regulated in cells



**Fig. 4** HeLa cells cultured overnight on SU-8 surfaces patterned with the HNO<sub>3</sub>-CAN ethanolamine treatment. **A:** HeLa cells grown on an array of 50 μm × 50 μm squares. The dark areas observed to be out of focus are cells adhering to the bottom of the culture flask below the pattern. **B:** HeLa cells grown on the 5 μm wide concentric circles. The cells appeared to change their morphologies to fit on to the HNO<sub>3</sub>-CAN and ethanolamine treated patterns, avoiding contact with the untreated SU-8.

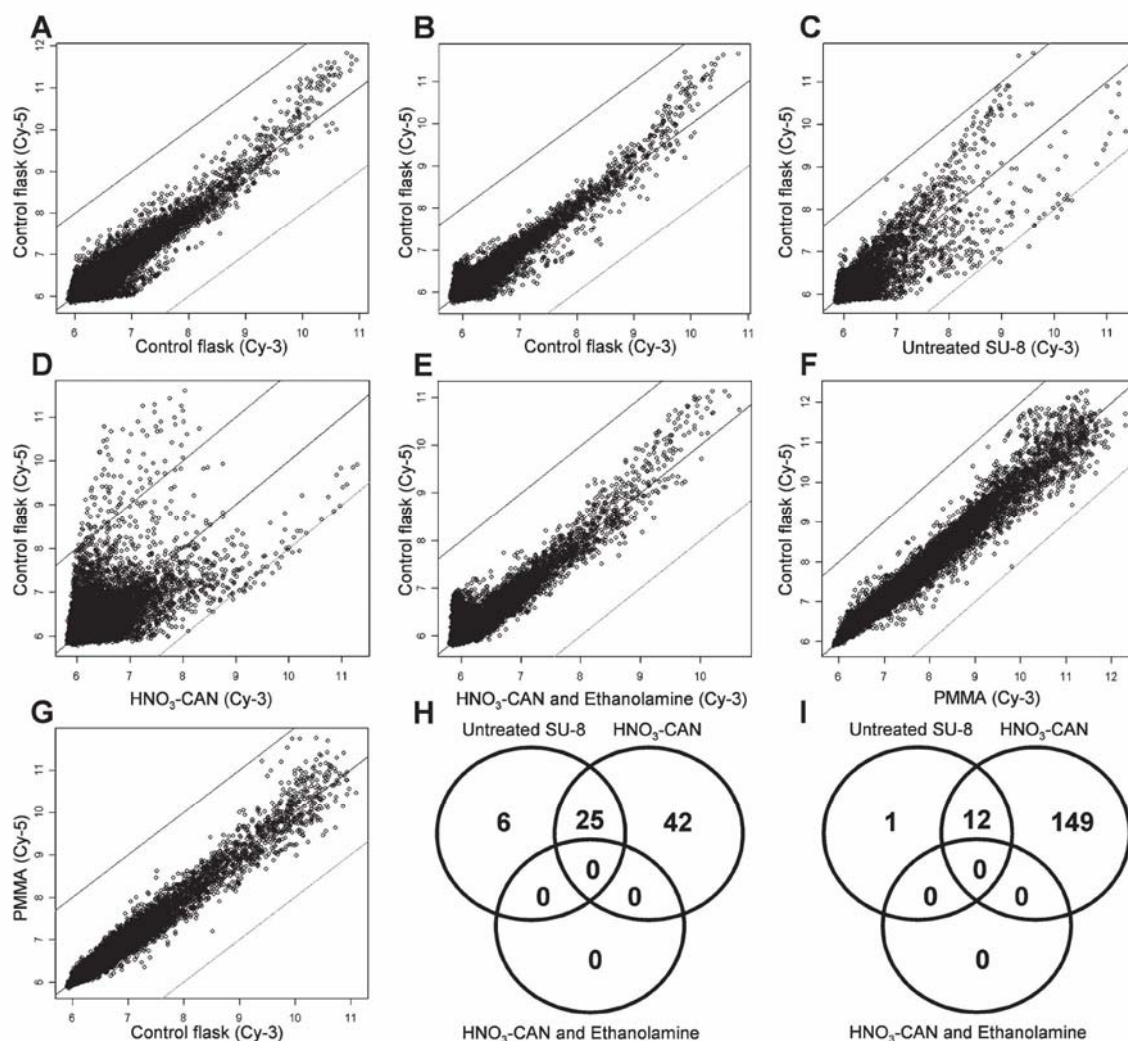
cultured on untreated SU-8 (Fig. 5 H), while 13 were down-regulated (Fig. 5 I). Of the 31 up-regulated genes, 25 were also up-regulated in cells cultured on HNO<sub>3</sub>-CAN treated SU-8, while 12 of the 13 down-regulated genes were also down-regulated in cells grown on SU-8 treated with HNO<sub>3</sub>-CAN. In addition, 42 genes were up-regulated and 149 genes were down-regulated in cells cultured on SU-8 treated with HNO<sub>3</sub>-CAN compared to cells grown on the culture flask surface. In contrast, none of the genes in cells cultured on SU-8 treated with HNO<sub>3</sub>-CAN and ethanolamine were significantly up- or down-regulated (Fig. 5 E). Similar to cells grown on SU-8 treated with HNO<sub>3</sub>-CAN and ethanolamine, cells grown on PMMA showed no change in gene expression compared to cells grown in cell culture flasks (Fig. 5 F–G). This observation is consistent with previous findings where a cell culture chip fabricated in PMMA<sup>3</sup> was found to result in culture conditions indistinguishable from the culture flasks.<sup>4</sup> All the regulated genes are summarized in Table S1 in the ESI.†

Although both the cell morphology and growth kinetics of HeLa cells cultured on a HNO<sub>3</sub>-CAN treated SU-8 surface were similar to the reference cell culture flask surface, the whole genome expression profile indicates significant differences. The differences may arise from the different chemical functional groups on the surfaces (*i.e.* nitrate radicals) or differences in surface charge densities.<sup>7</sup> Cells grown on SU-8 treated with HNO<sub>3</sub>-CAN showed up-regulation of Rho guanine nucleotide exchange factor 15 (ARHGEF15) which encodes a specific guanine nucleotide exchange factor for RhoA. Because RhoA is inhibiting cellular spreading,<sup>48</sup> this up-regulation indicates that cell spreading and migration might be down-regulated on HNO<sub>3</sub>-CAN treated SU-8 relative to the culture flask. Furthermore histone deacetylase 4 (HDAC4) was found up-regulated indicating changes in transcriptional regulation or cell cycle progression as histone deacetylation is a mechanism for epigenetic repression.

Various DNA binding proteins was found up-regulated as well as the anti-apoptotic junD proto-oncogene (JUND) indicating an increased stress stimuli.<sup>49</sup> Among the down regulated genes in cells cultured on HNO<sub>3</sub>-CAN treated SU-8 were the transcription factor BTF3 required for initiation of transcription,<sup>50</sup> beta actin, tubulin alpha chain and a dynamin like protein involved in the microtubule formation. This is consistent with the observed reduced growth kinetics. Interestingly, both tubulin and alpha actin was also found to be down-regulated in HeLa cells cultured on co-polymer films with contact angle between 53 and 57° compared to the cell culture flask.<sup>43</sup> We measured the contact angle of cell culture flasks to 57° indicating that *chemistry* more than *hydrophobicity* determines gene expression in cells.

Ideally, the effect of foreign surfaces on the cells cultured on them should be minimal or preferably zero. In the case of medical implants, changes in cellular gene expression can result in cells responding differently to stimuli than normal cells, which can lead to cancer or other undesired side effects. In *in vitro* systems, it is advantageous to find environments that closely reflect the *in vivo* situation. The *in vitro* cultured cells should be functionally comparable to the corresponding cells grown *in vivo*.<sup>8</sup> Our results show that gene expression profiling is better than conventional functional studies like cell growth and morphology to determine biocompatibility. This is illustrated by the fact that cells grown on a test surface can show similar cell attachment, morphology and cell growth rate as cells grown on a reference surface, but still show significant differences in terms of gene expression. Without doubt, the cells grown on SU-8 surfaces treated only with HNO<sub>3</sub>-CAN had a similar morphology and almost equal growth rate to cells grown on PMMA, cell culture flask material, and SU-8 treated with HNO<sub>3</sub>-CAN and ethanolamine. Based on growth rate and morphology it is therefore difficult to rule out SU-8 treated with only HNO<sub>3</sub>-CAN as a surface suitable for cell





**Fig. 5** Scatter plots of whole human genome expression profiles following four days of culture on different surfaces. In all scatter plots the central line is the median and the upper and lower lines represent a three-fold change up and down, respectively. Data originating from the Cy-5 channel were always plotted on the y-axis while the corresponding Cy-3 data were plotted on the x-axis. **A** and **B**: Self-self hybridization control experiments. **C**: Untreated SU-8. **D**: HNO<sub>3</sub>-CAN treated SU-8. **E**: HNO<sub>3</sub>-CAN and ethanolamine treated SU-8. **F** and **G**: PMMA. **H**: The figure displays the number of more than three-fold up-regulated genes on the differently treated SU-8 surfaces relative to the reference cell culture flask. The numbers in the overlapping region of the circles indicate the number of genes that were up-regulated on both corresponding surfaces, while the number in the overlapping region of all three circles reflects the number of genes that were up-regulated on all three surfaces. All fold changes were measured relative to the reference cell culture flask. **I**: Same as **H** but for down regulated genes. The entire list of regulated gene names and descriptions is available in Table S1 in the ESI.†

studies. Gene expression profiling, however, strongly showed that SU-8 treated with only HNO<sub>3</sub>-CAN results in surfaces that affect cells so much as to render them significantly different in terms of gene expression from cells grown on either PMMA, cell culture flask material or SU-8 treated with HNO<sub>3</sub>-CAN and ethanolamine. In contrast, cells grown on the three latter surfaces are very similar in terms of growth rate and morphology and also in terms of gene expression profiles. These three surfaces apparently provide comparable culturing conditions for the cells. It is, however, still possible that

differences on the *protein level* exist in cells grown on PMMA, cell culture flask material and SU-8 treated with HNO<sub>3</sub>-CAN and ethanolamine. This cannot directly be determined using DNA microarrays, indicating that protein microarrays may be an even better choice for analyzing biocompatibility in the future. Such protein microarrays may also detect secondary modifications on proteins induced by surfaces. Protein arrays are, however, less comprehensive than DNA microarrays,<sup>51</sup> making DNA microarrays the best analysis tool currently.

## Experimental

### Preparation of modified SU-8 surface

A 5  $\mu\text{m}$  thin layer of SU-8 XP2005 negative photoresist (Microchem, Switzerland) was spin-coated on a 4" 500  $\mu\text{m}$  thick Pyrex wafer (Schott Corporation, Germany). The SU-8 layer was fully cross-linked by a 10 s UV flood exposure ( $9\text{ mW cm}^{-2}$  at 365 nm) and a post-bake process (on a 95  $^{\circ}\text{C}$  hotplate for 10 min with a 10 min ramp). The SU-8 surface was modified by reaction with 1 M nitric acid (Fluka, Germany), catalyzed by 0.1 M ceric ammonium nitrate ( $\text{CAN}$ ,  $(\text{NH}_4)_2\text{Ce}(\text{NO}_3)_6$ ) (Sigma, USA) at 50  $^{\circ}\text{C}$  for 1 h and subsequently washed with MilliQ water. The material samples were dried and, optionally, treated with 0.1 M ethanolamine (Fluka, Germany) in 0.1 M sodium phosphate (Sigma, USA) buffer (pH 9.0) for 20 min at 50  $^{\circ}\text{C}$ . Finally, the material samples were washed with MilliQ water and dried.

### Water contact angle measurements

Contact angles between the different surfaces and MilliQ water were measured by a commercial contact angle measurement instrument DSA 10 MK2 (Krüss GMBH, Germany).

### Patterning on SU-8 surface

A two-step photolithography process was established to create the hydrophilic patterns on an otherwise hydrophobic SU-8 surface for the cell patterning experiments. A 1.5  $\mu\text{m}$  layer of AZ5214e photoresist (Honeywell, USA) film was deposited on a fully developed 5  $\mu\text{m}$  SU-8 layer by spin coating. The patterns on the AZ5214e photoresist were defined by standard UV lithography, and developed. Then, the whole wafer was dipped into the  $\text{HNO}_3$ -CAN solution for the first step of the surface treatment. After the  $\text{HNO}_3$ -CAN treatment, the AZ5214e photoresist layer was lifted off in acetone (Fluka, Germany), with 4 min of ultrasonic agitation. Finally, the whole wafer was dipped into the ethanolamine solution to finish the second step of the surface treatment. Incubation of untreated SU-8 with ethanolamine did not change the contact angle. The contact angle was only observed to decrease upon prior reaction with  $\text{HNO}_3$ -CAN. Thus, on the SU-8 surface, patterned areas were rendered hydrophilic for cell attachment while the remaining areas kept their original hydrophobic character.

### Cell culture

Human carcinoma cells (HeLa) were cultured in 75  $\text{cm}^2$  culture flasks (Easyflask, Nalge Nunc International Rochester, USA) in 25 mL media (RPMI 1640 media (Sigma, USA)) supplemented with 10% Fetal Bovine Serum (FBS) (Sigma, USA), penicillin ( $100\text{ U mL}^{-1}$ ) and streptomycin ( $100\text{ }\mu\text{g mL}^{-1}$ ) (Sigma, USA). Cells were cultured at 37  $^{\circ}\text{C}$  in an atmosphere containing 5%  $\text{CO}_2$  in a  $\text{CO}_2$  incubator. Seeding of the cells was performed with a density of 6700 cells per  $\text{cm}^2$  and the cells were passaged every three to four days when around 90% confluence was reached, by trypsinization.

### Target cDNA preparation

Total RNA was isolated with the RNeasy total RNA isolation kit (Qiagen, USA). Quantification of total RNA was performed using an Ultraspec 3000 spectrophotometer (Pharmacia Biotech, U.K.) and validation of RNA quality was performed using an Agilent 2100 Bioanalyzer (Agilent Technologies, USA). Amplification was performed with the Riboamp T7-based RNA amplification kit (Arcturus Engineering, USA) according to the manufacturer's instructions using 2  $\mu\text{g}$  total RNA as starting material yielding 35–40  $\mu\text{g}$  amplified RNA (aRNA) after one round of amplification. Synthesis of cDNA was performed as described elsewhere,<sup>52</sup> using random nonamer as primers.

### Microarray hybridization

Slides containing 44 290 sixty-base-long oligos directed against the human genome were obtained (Agilent Technologies, USA). Hybridization was performed according to the supplier's instructions using 200 pmol of each of the differently Cy-labeled cDNA in a hybridization chamber (Agilent) containing a total of 490  $\mu\text{L}$  hybridization solution (Agilent). The hybridization chamber was mounted on a rotation device and placed in a Hybaid Shake 'n' Stack hybridization oven (Thermo Electron Corporation, USA) for 17 h at 60  $^{\circ}\text{C}$  with rotation ( $\sim 4\text{ rpm}$ ).

Following hybridization, the slides were washed in washing solution 1 ( $6\times\text{SSC}$  (AppliChem, Germany), 0.005% Triton-X-102 (Agilent)) for 10 min at room temperature followed by 5 min wash in wash solution 2 ( $0.1\times\text{SSC}$  (AppliChem, Germany), 0.005% Triton-X-102 (Agilent)) at 4  $^{\circ}\text{C}$ . All the washing steps were performed in an in-house fabricated microarray washing station. The slides were dried by centrifugation followed by scanning and quantification performed in an ArrayWoRx microarray scanner (Applied Precision, USA).

### Data analysis

The data was normalized using the non-linear method Qspline<sup>53</sup> included in the affy software package (version 1.6.7)<sup>54</sup> in Bioconductor software extension package version 1.6<sup>55</sup> run under the freeware statistical program R (version 2.1.1).<sup>56</sup> Scatter plots of the co-hybridizations were constructed with the  $\log_2$  values of the Cy-3 labeled cDNA hybridization intensities on the  $x$ -axis and the  $\log_2$  values of the Cy-5 labeled cDNA on the  $y$ -axis.

### Conclusion

Examination of biocompatibility of the different SU-8 surfaces and PMMA showed that contact angle measurements, morphological studies and growth kinetics might not be sufficient parameters for assessing the effect of the surfaces on cell functions. A surface, such as SU-8 treated with  $\text{HNO}_3$ -CAN, can be biocompatible with respect to cell growth, morphology, and cell adhesion, while still inducing differences in gene expression in cells grown on this substrate compared to a reference substrate. Thus, comparing the whole genome expression profiles of cells cultured for several generations on a

novel surface with identical cells cultured on a reference surface gives a better indication whether the cells can be regarded as biologically comparable to the reference cells. Furthermore, gene expression profiling can be used to determine if microfluidic systems intended to simulate a particular environment *in vivo* (e.g. a blood vessel) indeed provides conditions for the cells that result in gene expression profiles that are identical to the gene expression profiles in cells in their natural environment.

### Acknowledgements

We thank Jin Ulrik Louw Andersen for his testing and optimizing of the treatment protocol and Maria Nordström at MIC, DTU for her kind information regarding the SU-8 treatment protocol. The research was supported by the Danish Research Council (Grant no.2014-00-0003, DABIC) and the Danish Technical Research Council (Grant no. 26-02-0307, STVF).

### References

- J. Charnley, *J. Bone Jt Surg. Br.*, 1960, **42-B**, 28–30.
- G. S. Fiorini and D. T. Chiu, *Biotechniques*, 2005, **38**, 429–446.
- S. Petronis, M. Stangegaard, C. B. V. Christensen and M. Dufva, *Biotechniques*, 2006, **40**, 368–375.
- M. Stangegaard, S. Petronis, A. Jørgensen, C. Christensen and M. Dufva, *Lab Chip*, 2006, **6**, 1045–1051.
- C. S. Chen, X. Jiang and G. M. Whitesides, *MRS Bull.*, 2005, **30**, 194–201.
- C. J. Kirkpatrick, F. Bittinger, M. Wagner, H. Kohler, T. G. van Kooten, C. L. Klein and M. Otto, *Proc. Inst. Mech. Eng. Part H*, 1998, **212**, 75–84.
- Y.-X. Wang, J. L. Robertson, W. B. Spillman and R. O. Claus, *Pharm. Res.*, 2004, **21**, 1362–1373.
- D. Williams, *Med. Device Technol.*, 2003, **14**, 10–13.
- N. D. Gallant, J. R. Capadona, A. B. Frazier, D. M. Collard and A. J. Garcia, *Langmuir*, 2002, **18**, 5579–5584.
- A. Sin, K. C. Chin, M. F. Jamil, Y. Kostov, G. Rao and M. L. Shuler, *Biotechnol. Prog.*, 2004, **20**, 338–345.
- J. L. Charest, L. E. Bryant, A. J. Garcia and W. P. King, *Biomaterials*, 2004, **25**, 4767–4775.
- S. Bouaidat, B. Winther-Jensen, S. F. Christensen and J. Jonsmann, *Sens. Actuators, A*, 2004, **110**, 390–394.
- E. W. H. Jager, C. Immerstrand, K. H. Peterson, K.-E. Magnusson, I. Lundström and O. Inganäs, *Biomed. Microdevices*, 2002, **4**, 177–187.
- A. Dekker, C. Panfil, M. Valdor, G. Pennartz, H. Richter, C. H. Mittermayer and C. J. Kirkpatrick, *Cells Mater. (USA)*, 1994, **4**, 101–112.
- C. J. Kirkpatrick and A. Dekker, *Adv. Biomater.*, 1992, **10**, 31.
- T. G. V. Kooten, C. L. Klein, H. Kohler, C. J. Kirkpatrick, D. F. Williams and R. Eloy, *J. Mater. Sci.: Mater. Med.*, 1997, **8**, 835–841.
- M. J. Dalby, L. D. Silvio, E. J. Harper and W. Bonfield, *J. Mater. Sci.: Mater. Med.*, 2002, **13**, 311–314.
- C. J. Kirkpatrick, t. Otterbach, d. Anderheiden, j. Schiefer, H. Richter, H. Höcker, C. H. Mittermayer and A. Dekker, *Cells Mater.*, 1992, **2**, 166–177.
- K. E. Geckeler, R. Wacker and W. K. Aicher, *Naturwissenschaften*, 2000, **87**, 351–354.
- D. V. Nicolau, T. Taguchi, H. Tanigawa and S. Yoshikawa, *Biosens. Bioelectron.*, 1996, **11**, 1237–1252.
- D. Irimia and J. O. M. Karlsson, *Biomed. Microdevices*, 2003, **5**, 185–194.
- H. Lorenz, M. Despont, N. Fahrni, N. LaBianca, P. Renaud and P. Vettiger, *J. Microelectromech. Syst.*, 1997, **7**, 121–124.
- K. B. Mogensen, J. El-Ali, A. Wolff and J. P. Kutter, *Appl. Opt.*, 2003, **42**, 4072–4079.
- Z. Wang, J. El-Ali, I. R. P. Nielsen, K. B. Mogensen, D. Snakenborg, J. P. Kutter and A. Wolff, *Lab Chip*, 2004, **4**, 372–377.
- J. Hsieh, C. J. Weng, H. L. Yin, H. H. Lin and H. Y. Chou, *Microsyst. Technol.*, 2005, **11**, 429–437.
- T. Mappes, S. Achenbach, A. Last, J. Mohr and R. Truckenmüller, *Microsyst. Technol.*, 2004, **10**, 560–563.
- J. Zhang, K. L. Tan and H. Q. Gong, *Polym. Test.*, 2001, **20**, 693–701.
- G. Kotzar, M. Freas, P. Abel, A. Fleischman, S. Roy, C. Zorman, J. M. Moran and J. Melzak, *Biomaterials*, 2002, **23**, 2737–2750.
- S. Bouaidat, C. Berendsen, P. Thomsen, S. G. Petersen, A. Wolff and J. Jonsmann, *Lab Chip*, 2004, **4**, 632–637.
- J. El-Ali, I. R. Perch-Nielsen, C. R. Poulsen, D. D. Bang, P. Telleman and A. Wolff, *Sens. Actuators, A*, 2004, **110**, 3–10.
- N. Zhang, J. Xie, M. Guers and V. K. Varadan, *Smart Mater. Struct.*, 2003, **12**, 260–263.
- Y. Song, C. S. S. R. Kumar and J. Hormes, *J. Micromech. Microeng.*, 2004, **14**, 932–940.
- N. Iranpoor and P. Salchi, *Tetrahedron*, 1995, **51**, 909–912.
- M. Nordström, R. Marie, M. Calleja and A. Boisen, *J. Micromech. Microeng.*, 2004, **14**, 1614–1617.
- R. J. Cho, M. J. Campbell, E. A. Winzeler, L. Steinmetz, A. Conway, L. Wodicka, T. G. Wolfsberg, A. E. Gabrielian, D. Landsman, D. J. Lockhart and R. W. Davis, *Mol. Cell*, 1998, **2**, 65–73.
- P. T. Spellman, G. Sherlock, M. Q. Zhang, V. R. Iyer, K. Anders, M. B. Eisen, P. O. Brown, D. Botstein and B. Futcher, *Mol. Biol. Cell*, 1998, **9**, 3273–3297.
- V. R. Iyer, M. B. Eisen, D. T. Ross, G. Schuler, T. Moore, J. C. Lee, J. M. Trent, L. M. Staudt, J. Hudson, Jr., M. S. Boguski, D. Lashkari, D. Shalon, D. Botstein and P. O. Brown, *Science*, 1999, **283**, 83–87.
- V. G. Tusher, R. Tibshirani and G. Chu, *Proc. Natl. Acad. Sci. U. S. A.*, 2001, **98**, 5116–5121.
- S. M. Dhanasekaran, T. R. Barrette, D. Ghosh, R. Shah, S. Varambally, K. Kurachi, K. J. Pienta, M. A. Rubin and A. M. Chinnaiyan, *Nature*, 2001, **412**, 822–826.
- S. A. Ahrendt, S. Halachmi, J. T. Chow, L. Wu, N. Halachmi, S. C. Yang, S. Wehage, J. Jen and D. Sidransky, *Proc. Natl. Acad. Sci. U. S. A.*, 1999, **96**, 7382–7387.
- A. A. Alizadeh, M. B. Eisen, R. E. Davis, C. Ma, I. S. Lossos, A. Rosenwald, J. C. Boldrick, H. Sabet, T. Tran, X. Yu, J. I. Powell, L. Yang, G. E. Marti, T. Moore, J. Hudson, Jr., L. Lu, D. B. Lewis, R. Tibshirani, G. Sherlock, W. C. Chan, T. C. Greiner, D. D. Weisenburger, J. O. Armitage, R. Warnke and L. M. Staudt, *Nature*, 2000, **403**, 503–511.
- T. R. Golub, D. K. Slonim, P. Tamayo, C. Huard, M. Gaasenbeek, J. P. Mesirov, H. Coller, M. L. Loh, J. R. Downing, M. A. Caligiuri, C. D. Bloomfield and E. S. Lander, *Science*, 1999, **286**, 531–537.
- L. T. Allen, E. J. Fox, I. Blute, Z. D. Kelly, Y. Rochev, A. K. Keenan, K. A. Dawson and W. M. Gallagher, *Proc. Natl. Acad. Sci. U. S. A.*, 2003, **100**, 6331–6336.
- F. Carinci, F. Pezzetti, S. Volinia, F. Francioso, D. Arcelli, E. Farina and A. Piattelli, *Biomaterials*, 2004, **25**, 215–228.
- C. R. Poulsen, J. El-Ali, I. R. Perch-Nielsen, D. D. Bang, P. Telleman and A. Wolff, *J. Rapid Methods Autom. Microbiol.*, 2005, **13**, 111–126.
- F. Fixe, M. Dufva, P. Telleman and C. B. Christensen, *Lab Chip*, 2004, **4**, 191–195.
- R. Marie, S. Schmid, A. Johansson, L. Ejsing, M. Nordström, D. Häfliger, C. Christensen, A. Boisen and M. Dufva, *Biosens. Bioelectron.*, 2006, **21**, 1327–1332.
- L. A. Roberts, H. Glenn, C. S. Hahn and B. S. Jacobson, *J. Cell Physiol.*, 2003, **196**, 196–205.
- J. B. Weitzman, L. Fiette, K. Matsuo and M. Yaniv, *Mol. Cell*, 2000, **6**, 1109–1119.
- X. M. Zheng, D. Black, P. Chambon and J. M. Egly, *Nature*, 1990, **344**, 556–559.
- M. Dufva and C. Christensen, *Expert Rev. Proteomics*, 2005, **2**, 41–48.
- I. V. Yang, E. Chen, J. P. Hasseman, W. Liang, B. C. Frank, S. Wang, V. Sharov, A. I. Saeed, J. White, J. Li, N. H. Lee, T. J. Yeatman and J. Quackenbush, *Genome Biol.*, 2002, **3**, R62.

- 53 C. Workman, L. J. Jensen, H. Jarmer, R. Berka, L. Gautier, H. B. Nielsen, H. H. Saxild, C. Nielsen, S. Brunak and S. Knudsen, *Genome Biol.*, 2002, 3, R48.
- 54 A. Irizarry Rafael, Laurent Gautier, Benjamin Milo Bolstad, Crispin Miller, M. Astrand, Leslie M. Cope, Robert Gentleman, Jeff Gentry, Conrad Halling, Wolfgang Huber, James MacDonald, Benjamin I. P. Rubinstein, C. Workman and J. Zhang, *affy: Methods for Affymetrix Oligonucleotide Arrays. R package.*, 2005.
- 55 R. C. Gentleman, V. J. Carey, D. M. Bates, B. Bolstad, M. Dettling, S. Dudoit, B. Ellis, L. Gautier, Y. Ge, J. Gentry, K. Hornik, T. Hothorn, W. Huber, S. Iacus, R. Irizarry, F. Leisch, C. Li, M. Maechler, A. J. Rossini, G. Sawitzki, C. Smith, G. Smyth, L. Tierney, J. Y. Yang and J. Zhang, *Genome Biology*, 2004, 5, R80.
- 56 R\_Development\_Core\_Team, *R: A language and environment for statistical computing*, R Foundation for Statistical Computing, Vienna, Austria, 2005.

# Chemical Biology

An exciting news supplement providing a snapshot of the latest developments in chemical biology



Free online and in print issues of selected RSC journals!\*

**Research Highlights** – newsworthy articles and significant scientific advances

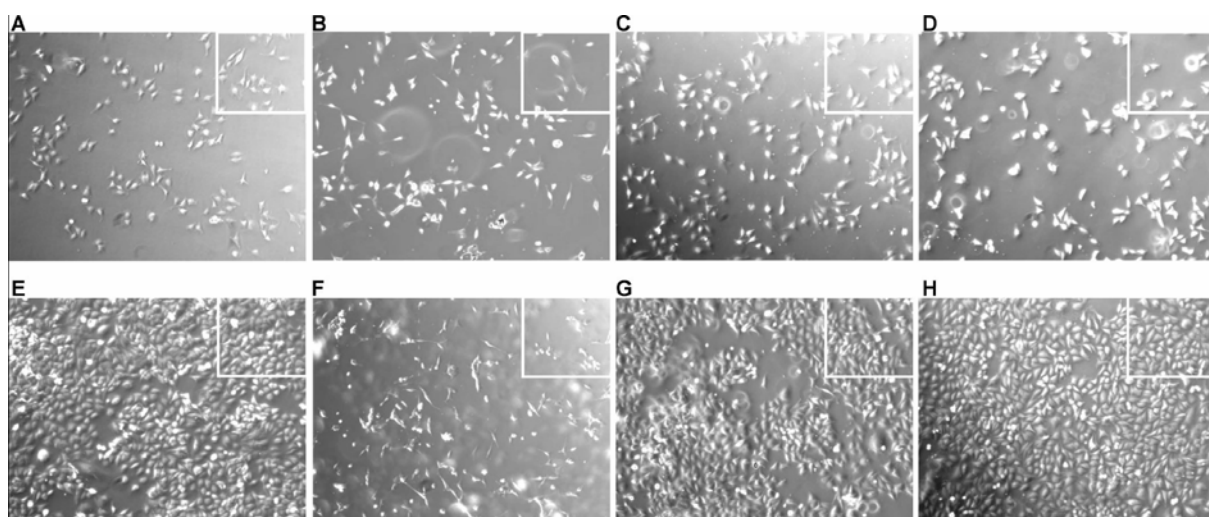
**Essential Elements** – latest developments from RSC publications

**Free links** to the full research paper from every online article during month of publication

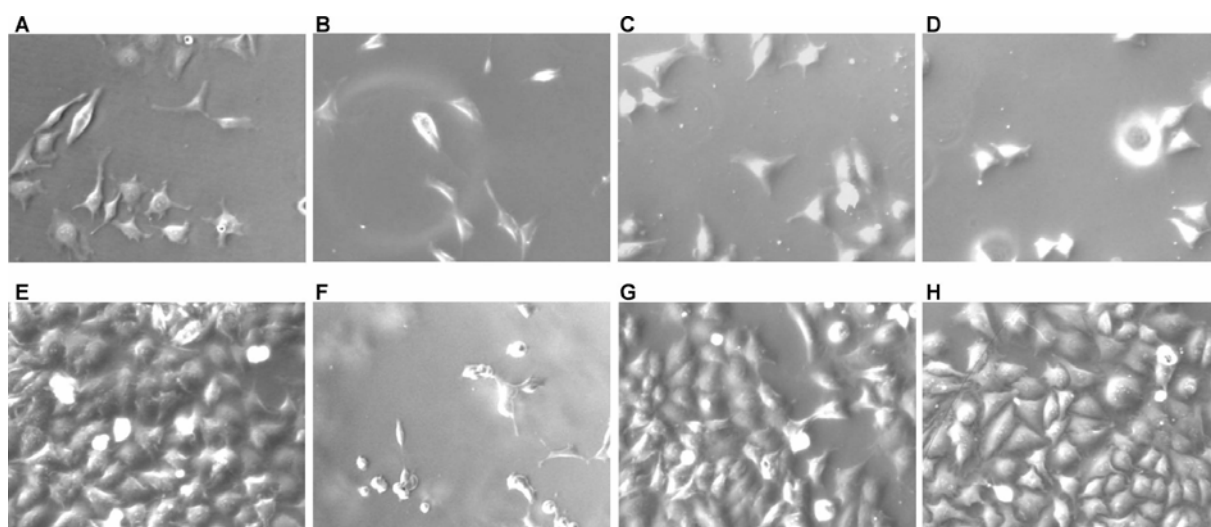
\*A separately issued print subscription is also available

RSC Publishing

[www.rsc.org/chemicalbiology](http://www.rsc.org/chemicalbiology)



**Supplementary Figure 1:** HeLa cells cultured on differently treated SU-8 surfaces. In **A-D** the cells were cultured for 24 hours while in **E-H** the cells were cultured for four days. **A** and **E** are the reference culture flask. **B** and **F** are untreated SU-8. **C** and **G** represent SU-8 treated with HNO<sub>3</sub>-CAN, while **D** and **H** represent SU-8 treated with HNO<sub>3</sub>-CAN and ethanolamine. All cells originated from the same culture and were cultured under identical culture conditions using the same media formulation. The white rectangle indicates the area magnified in Supplementary Figure 2.



**Supplementary Figure 2:** Magnification of the region indicated with a white rectangle in Supplementary Figure 1.

Supplementary Table 1

Name	Class	Description	SU-8 CAN	SU-8
AF144054	Apoptosis	Homo sapiens apoptosis related protein APR-4 mRNA, partial cds. [AF144054]	3,300	
BM023129	Cell cycle	BM023129 ie79h07.x1 Melton Normalized Human Islet 4 N4-HIS 1 Homo sapiens cDNA clone IMAGE:5673444 3' similar to SW:BUB3_MOUSE_Q9WVA3 MITOTIC CHECKPOINT PROTEIN BUB3 ;, mRNA sequence [BM023129]	0.332	
TAGLN2	Differentiation	Homo sapiens transgelin 2 (TAGLN2), mRNA [NM_003564]	3.349	
HSPC065	Heat shock	Homo sapiens HSPC065 protein (HSPC065), mRNA [NM_014157]	3.102	
CCL19	Ligand	Homo sapiens chemokine (C-C motif) ligand 19 (CCL19), mRNA [NM_006274]	3.800	
THC2045396	Membrane	O00429 (O00429) Dynamin-like protein, partial (16%) [THC2045396]	0.131	
AW075437	Metabolism	AW075437 xb23c01.x1 NCI_CGAP_Kid13 Homo sapiens cDNA clone IMAGE:2577120 3' similar to WP:C17G10.8 CE16861 FAT-3: ALCOHOL DEHYDROGENASE ;, mRNA sequence [AW075437]	0.314	
HAAO	Metabolism	Homo sapiens 3-hydroxyanthranilate 3,4-dioxygenase (HAAO), mRNA [NM_012205]	4.733	3.885
ABHD9	Metabolism	Homo sapiens abhydrolase domain containing 9 (ABHD9), mRNA [NM_024794]	3.689	
NPEPL1	Metabolism	Homo sapiens aminopeptidase-like 1 (NPEPL1), mRNA [NM_024663]	3.837	4.054
PNPO	Metabolism	Homo sapiens pyridoxine 5'-phosphate oxidase (PNPO), mRNA [NM_018129]	3.978	
SLC27A1	Metabolism	Homo sapiens solute carrier family 27 (fatty acid transporter), member 1 (SLC27A1), mRNA [NM_198580]	3.066	
THC2159243	Metabolism	RIB2_HUMAN (P04844) Dolichyl-diphosphooligosaccharide--protein glycosyltransferase 63 kDa subunit precursor (Ribophorin II) (RPN-II) (RIBIIR) , partial (25%) [THC2159243]	0.311	
THC2200192	Metabolism	THU1_HUMAN (Q9NXG2) THUMP domain containing protein 1, partial (69%) [THC2200192]	0.155	
AI918632	Metabolism	ts32h01.x1 NCI_CGAP_Ut4 Homo sapiens cDNA clone IMAGE:2230321 3' similar to gb:X60221 ATP SYNTHASE B CHAIN, MITOCHONDRIAL PRECURSOR (HUMAN);, mRNA sequence [AI918632]	0.118	
AI267511	Mitochondria	AI267511 aq65g08.x1 Stanley Frontal SN pool 2 Homo sapiens cDNA clone IMAGE:2035838 similar to gb:X16560 CYTOCHROME C OXIDASE POLYPEPTIDE VIIC PRECURSOR (HUMAN);, mRNA sequence [AI267511]	0.294	
AI961400	Mitochondria	AI961400 wt22a12.x1 NCI_CGAP_Ut1 Homo sapiens cDNA clone IMAGE:2508190 3' similar to gb:X60036 MITOCHONDRIAL PHOSPHATE CARRIER PROTEIN PRECURSOR (HUMAN);, mRNA sequence [AI961400]	0.070	
THC2200745	Mitochondria	DAAMTTGRG Damaliscus dorcas mitochondrial 12S and 16S ribosomal RNA genes, and Phe-, Val-, and Leu-tRNA genes, partial (5%) [THC2200745]	0.074	
AI278811	Oncogene	AI278811 qo50a11.x1 NCI_CGAP_Co8 Homo sapiens cDNA clone IMAGE:1911932 3' similar to gb:K02276 MYC PROTO-ONCOGENE PROTEIN (HUMAN);, mRNA sequence [AI278811]	0.164	
THC2134410	Oncogene	AI732190 ae38f11.x5 Gessler Wilms tumor Homo sapiens cDNA clone IMAGE:898125 3', mRNA sequence [AI732190]	4.095	
AY117690	Oncogene	Homo sapiens lung cancer oncogene 5 (HLC5) mRNA, complete cds. [AY117690]	0.312	
TMEFF2	Oncogene	Homo sapiens mRNA for tomeregulin, complete cds. [AB004064]	0.305	0.104

AY170823	Oncogene	Homo sapiens transformation-related protein 2 mRNA, complete cds. [AY170823]	0.303	
AI457687	Other	AI457687 tJ48g10.x1 Soares NSF_F8_9W_OT_PA_P_S1 Homo sapiens cDNA clone IMAGE:2144802 3' similar to TR:O22899 O22899 RNA HELICASE ISOLOG. ;, mRNA sequence [AI457687]	0.276	
AI937689	Other	AI937689 wp82d09.x1 NCI_CGAP_Brn25 Homo sapiens cDNA clone IMAGE:2468273 3' similar to gb:M32886 SORCIN (HUMAN);, mRNA sequence [AI937689]	0.275	
ADM	Other	Homo sapiens adrenomedullin (ADM), mRNA [NM_001124]	3.745	
AF271776	Other	Homo sapiens DC48 mRNA, complete cds. [AF271776]	0.227	
DPYSL3	Other	Homo sapiens dihydropyrimidinase-like 3 (DPYSL3), mRNA [NM_001387]	3.949	
FTH1	Other	Homo sapiens ferritin, heavy polypeptide 1, mRNA (cDNA clone IMAGE:3874046). [BC032091]	0.084	
FTHL7	Other	Homo sapiens ferritin, heavy polypeptide-like 7 (FTHL7) on chromosome 13 [NR_002202]	0.075	
XTP7	Other	Homo sapiens protein 7 transactivated by hepatitis B virus X antigen (HBxAg) (XTP7), mRNA [NM_138568]	3.777	4.126
SDK2	Other	Homo sapiens sidekick homolog 2 (chicken) (SDK2), mRNA [NM_019064]	4.410	3.912
AF187554	Other	Homo sapiens sperm antigen-36 mRNA, complete cds. [AF187554]	0.182	
THC2182978	Other	TTR320199 immunoglobulin mu heavy chain [Tursiops truncatus] , partial (10%) [THC2182978]	4.322	
AD7C-NTP	Other	Homo sapiens neuronal thread protein AD7c-NTP (AD7C-NTP), mRNA [NM_014486]	3.823	3.404
DUB3	Protease	Homo sapiens deubiquitinating enzyme 3 (DUB3), mRNA [NM_201402]	3.069	
THC2202467	Protease	PSA7_HUMAN (O14818) Proteasome subunit alpha type 7 (Proteasome subunit RC6-1) (Proteasome subunit XAPC7) , partial (22%) [THC2202467]	0.235	
AI567808	Receptor	AI567808 tr62h05.x1 NCI_CGAP_Pan1 Homo sapiens cDNA clone IMAGE:2222937 3' similar to gb:M14043 ANNEXIN II (HUMAN);, mRNA sequence [AI567808]	0.314	0.081
THC2174183	Receptor	BC012448 thyroid hormone receptor interactor 4 [Homo sapiens] , partial (75%) [THC2174183]	0.261	
DKFZp564K142	Receptor	Homo sapiens implantation-associated protein (DKFZp564K142), mRNA [NM_032121]	3.093	
LENG8	Receptor	Homo sapiens leukocyte receptor cluster (LRC) member 8 (LENG8), mRNA [NM_052925]	3.086	
KCNK7	Receptor	Homo sapiens potassium channel, subfamily K, member 7 (KCNK7), transcript variant C, mRNA [NM_005714]	3.679	3.157
AA780485	Ribosome	ac65f02.s1 Stratagene fetal retina 937202 Homo sapiens cDNA clone IMAGE:867483 3' similar to gb:X69392 60S RIBOSOMAL PROTEIN L26 (HUMAN);, mRNA sequence [AA780485]	0.296	0.114
AI613259	Ribosome	AI613259 ty35c04.x1 NCI_CGAP_Ut2 Homo sapiens cDNA clone IMAGE:2281062 3' similar to gb:X69391 60S RIBOSOMAL PROTEIN L6 (HUMAN);, mRNA sequence [AI613259]	0.265	0.071
BQ614035	Ribosome	BQ614035 il02g06.x1 Human insulinoma Homo sapiens cDNA clone IMAGE:6028979 3' similar to SW:RS11_HUMAN P04643 40S RIBOSOMAL PROTEIN S11. [1] ;, mRNA sequence [BQ614035]	0.219	
RPS15A	Ribosome	H.sapiens mRNA for ribosomal protein (homologous to yeast S24). [X62691]	0.113	
RPS15A	Ribosome	H.sapiens mRNA for ribosomal protein (homologous to yeast S24). [X62691]	0.137	
THC2194550	Ribosome	HUMCH13C3A ribosomal protein small subunit [Homo sapiens] , partial (27%) [THC2194550]	0.067	
N75321	Ribosome	N75321 za79f05.s1 Soares_fetal_lung_NbHL19W Homo sapiens cDNA clone IMAGE:298785 3' similar to SW:RL24_HUMAN P38663 60S RIBOSOMAL PROTEIN L24. [2] PIR:JN0549 ;, mRNA sequence [N75321]	0.192	
THC2166330	Ribosome	RL35_HUMAN (P42766) 60S ribosomal protein L35, partial (67%) [THC2166330]	0.299	

THC2044542	Ribosome	RS10_HUMAN (P46783) 40S ribosomal protein S10, partial (93%) [THC2044542]	0.193	
THC2162618	Ribosome	RS3A_HUMAN (P61247) 40S ribosomal protein S3a, partial (81%) [THC2162618]	0.208	0.085
AA300289	Ribosome	AA300289 EST13009 Uterus tumor I Homo sapiens cDNA 3' end similar to similar to ribosomal protein YL10, mRNA sequence [AA300289]	0.121	
HNRPH1	RNA metabolism	Homo sapiens heterogeneous nuclear ribonucleoprotein H1 (H) (HNRPH1), mRNA [NM_005520]	0.299	
THC2084699	RNA metabolism	HSEXPORT1 Exportin(tRNA) [Homo sapiens] , partial (13%) [THC2084699]	0.204	
THC2083654	RNA metabolism	PR18_HUMAN (Q99633) Pre-mRNA splicing factor 18 (PRP18 homolog) (hPRP18), partial (31%) [THC2083654]	0.286	
AI608782	Skeleton	AI608782 tw94g05.x1 NCI_CGAP_HN6 Homo sapiens cDNA clone IMAGE:2267384 3' similar to gb:K00558 TUBULIN ALPHA-1 CHAIN (HUMAN);, mRNA sequence [AI608782]	0.244	
ACTB	Skeleton	Homo sapiens actin, beta (ACTB), mRNA [NM_001101]	0.160	
RASD1	Skeleton	Homo sapiens RAS, dexamethasone-induced 1 (RASD1), mRNA [NM_016084]	4.053	
TNNI1	Skeleton	Homo sapiens troponin I, skeletal, slow (TNNI1), mRNA [NM_003281]	3.623	3.911
THC2087016	Skeleton	HUMMYLCC smooth muscle myosin light chain {Homo sapiens} , partial (22%) [THC2087016]	0.295	0.129
THC2045155	Skeleton	MLRM_HUMAN (P19105) Myosin regulatory light chain 2, nonsarcomeric (Myosin RLC), complete [THC2045155]	0.269	
THC2200669	Signal	HNT1_HUMAN (P49773) Histidine triad nucleotide-binding protein 1 (Adenosine 5'-monophosphoramidase) (Protein kinase C inhibitor 1) (Protein kinase C-interacting protein 1) (PKCI-1), partial (51%) [THC2200669]	0.136	
ASB16	Signal	Homo sapiens ankyrin repeat and SOCS box-containing 16 (ASB16), mRNA [NM_080863]	4.027	
CDKAL1	Signal	Homo sapiens CDK5 regulatory subunit associated protein 1-like 1 (CDKAL1), mRNA [NM_017774]	3.116	
FAM19A4	Signal	Homo sapiens family with sequence similarity 19 (chemokine (C-C motif)-like), member A4 (FAM19A4), transcript variant 1, mRNA [NM_182522]	3.351	
FLJ90024	Signal	Homo sapiens fasting-inducible integral membrane protein TM6P1 (FLJ90024), mRNA [NM_153342]	4.265	
ARHGEF15	Signal	Homo sapiens Rho guanine nucleotide exchange factor (GEF) 15 (ARHGEF15), mRNA [NM_173728]	3.727	
SLA	Signal	Homo sapiens Src-like-adaptor (SLA), mRNA [NM_006748]	3.607	4.085
TRH	Signal	Homo sapiens thyrotropin-releasing hormone (TRH), mRNA [NM_007117]	3.015	
TRAF4	Signal	Homo sapiens TNF receptor-associated factor 4 (TRAF4), transcript variant 1, mRNA [NM_004295]	0.323	
THC2128887	Signal	WSB1_HUMAN (Q9Y6I7) WD repeat and SOCS box containing protein 1 (WSB-1) (SOCS box-containing WD protein SWiP-1), partial (55%) [THC2128887]	0.268	0.142
THC2162031	Structure	TCPH_HUMAN (Q99832) T-complex protein 1, eta subunit (TCP-1-eta) (CCT-eta) (HIV-1 Nef interacting protein), partial (80%) [THC2162031]	0.261	
HDAC4	Transcription	Homo sapiens histone deacetylase 4 (HDAC4), mRNA [NM_006037]	3.066	
JUND	Transcription	Homo sapiens jun D proto-oncogene (JUND), mRNA [NM_005354]	3.342	
TIP120A	Transcription	Homo sapiens TBP-interacting protein (TIP120A), mRNA [NM_018448]	3.298	
TCF15	Transcription	Homo sapiens transcription factor 15 (basic helix-loop-helix) (TCF15), mRNA [NM_004609]	4.081	
ZNF403	Transcription	Homo sapiens zinc finger protein 403 (ZNF403), mRNA [NM_024835]	3.413	
MKRN4	Transcription	Makrin 4 (Zinc finger protein 127-Xp) (ZNF127-Xp). [Source:Uniprot/SWISSPROT;Acc:Q13434] [ENST00000355859]	3.056	
THC2203017	Transcription	Q08243 (Q08243) CCAAT-binding protein (Fragment), partial (32%) [THC2203017]	0.295	
W45382	Transcription	W45382 zc80e10.s1 Pancreatic Islet Homo sapiens cDNA clone IMAGE:328650 3' similar to gb:D13748 EUKARYOTIC INITIATION FACTOR 4A-I (HUMAN);, mRNA sequence [W45382]	0.218	
THC2022176	Transcription	AA601920 np02d02.s1 NCI_CGAP_Pr2 Homo sapiens cDNA clone IMAGE:1115139 similar to gb:M90356_cds1 TRANSCRIPTION FACTOR BTF3 (HUMAN);, mRNA sequence [AA601920]	0.185	0.142
GLTSCR1	Tumor sup	Homo sapiens glioma tumor suppressor candidate region gene 1 (GLTSCR1), mRNA [NM_015711]	3.986	



*Paper 4: Reverse transcription using random pentadecamer primers increases yield and quality of resulting cDNA*

# Reverse transcription using random pentadecamer primers increases yield and quality of resulting cDNA

Michael Stangegaard<sup>1</sup>, Inge Høgh Dufva<sup>2</sup>, and Martin Dufva<sup>1</sup>

*BioTechniques* 40:649-657 (May 2006)  
doi 10.2144/000112153

*Reverse transcription of RNA is an invaluable method for gene expression analysis by real-time PCR or microarray methods. Random primers of varying lengths were compared with respect to their efficiency of priming reverse transcription reactions. The results showed that 15-nucleotide-long random oligonucleotides (pentadecamers) consistently yielded at least 2-fold as much cDNA as did random hexamers using either poly(A) RNA or an amplified version of messenger RNA (aRNA) as a template. The cDNA generated using pentadecamers did not differ in size distribution or the amount of incorporated label compared with cDNA generated with random hexamers. The increased efficiency of priming using random pentadecamers resulted in reverse transcription of >80% of the template aRNA, while random hexamers induced reverse transcription of only 40% of the template aRNA. This suggests a better coverage of the transcriptome when using random pentadecamers over random hexamers. Using the same amount of aRNA as starting material, random pentadecamer-primed reactions resulted in 11-fold more genes being detected in whole transcriptome DNA microarray experiments than random hexamer-primed reactions. The results indicate that random pentadecamers can replace random hexamers in reverse transcription reactions on both poly(A) RNA and amplified RNA, resulting in higher cDNA yields and quality.*

## INTRODUCTION

Reverse transcription of RNA into cDNA is a core method for analysis of gene expression using DNA microarray or real-time PCR (1–5). The reverse transcription should result in a cDNA population that reflects the original messenger RNA (mRNA) population in terms of transcript abundance and complexity. Furthermore, the reverse transcription reaction should be as efficient as possible to give maximum sensitivity in the final assay. Sensitivity is often problematic in microarray analysis of unamplified mRNA. Sensitivity is also an issue when following fusion gene markers in cancer patients where, for instance, it is desired to detect a single cancer cell expressing the BCR/ABL fusion transcripts in a background of 100,000 normal cells in chronic myeloid leukemia (CML) patients (6,7). This suggests that improvements in reverse

transcription could have large impact in assay results.

RNA quality (8–12), priming strategy (13), and enzyme efficiency (14,15) are important parameters for obtaining high yield cDNA of good quality. Less studied is the impact of different primers in the reaction. Reverse transcription reactions can be primed using specific primers (16,17) if relatively few mRNA species are targeted. This approach is not practical for whole transcriptome analysis using microarray, because it would require synthesis and mixing of thousands of specific primers. In those cases, the reverse transcription reaction is primed with oligo(dT) (18,19) random hexamers (18,20–23) or random nonamers (23,24). Oligo(dT) priming has the virtue of producing cDNA from the 3' end of poly(A) mRNA, allowing total RNA to be used as a template. The drawback is that oligo(dT) priming often results in a 3' bias compared with

random priming (14). Poly(A)-selected RNA like an isolated mRNA fraction or amplified RNA (aRNA) are preferably reverse transcribed with random primers, because random priming is less likely to give a 3' end bias in the resulting cDNA.

Here we report a novel priming method for reverse transcription reactions and a study of the implication of random primer length in reverse transcription reactions on the yield of the resulting cDNA and the influence on the amount of detectable genes on oligonucleotide microarrays.

## MATERIALS AND METHODS

### Cells

Human carcinoma cells (HeLa) were cultured in 75 cm<sup>2</sup> culture flasks (EasyFlask™; Nalge Nunc International, Rochester, NY, USA) in

<sup>1</sup>Technical University of Denmark, Lyngby and <sup>2</sup>University of Copenhagen, Herlev, Denmark

## RESEARCH REPORT

25 mL RPMI 1640 media supplemented with 10% fetal bovine serum (FBS), penicillin (100 U/mL), and streptomycin (100 µg/mL; all from Sigma, St. Louis, MO, USA). Cells were cultured at 37°C in an atmosphere containing 5% CO<sub>2</sub> (AGA, Copenhagen, Denmark) in a CO<sub>2</sub> incubator (Assab; Don Whitley Scientific Ltd., Shipley, West Yorkshire, UK). The cells were seeded at a density of 6667 cells/cm<sup>2</sup>, and the cells were subcultured every 3 to 4 days when approximately 90% confluence was reached.

### RNA Isolation and Amplification

Total RNA was isolated by using RNeasy® Mini Kit spin columns (Qiagen, Valencia, CA, USA). Quantification of total RNA was performed in an Ultraspec 3000 spectrophotometer (Pharmacia Biotech, Cambridge, UK), and validation of RNA quality was performed by using the RNA 6000 Nano Assay on an Agilent 2100 Bioanalyzer (Agilent Technologies, Palo Alto, CA, USA). Amplification was performed with the RiboAmp® T7-based RNA amplification kit (Arcturus Engineering, Mountain View, CA, USA) according to the manufacturer's instructions using 2 µg total RNA as a starting material, yielding 35–40 µg aRNA after one round of amplification. For each labeling reaction, 3 µg aRNA were used unless otherwise mentioned. The mRNA fraction was isolated from 100 µg total RNA using oligo(dT)<sub>25</sub> Dynabeads® (Dyna, Oslo, Norway) according to the manufacturer's instructions. The mRNA (2–3 µg) was eluted in 20 µL buffer (10 mM Tris-HCl, pH 7.5).

### cDNA Synthesis

Synthesis of cDNA was performed as described elsewhere (23), with the following modifications. In brief, 2–3 µg aRNA were mixed with 3.35 nmol random primers (Sigma-Genosys, Haverhill, UK or Invitrogen, Paisley, UK), unless otherwise mentioned, in a total volume of 18.5 µL. The mixture was heated at 70°C for 10 min and snap-cooled on ice for at least 1 min. Reverse transcription

reaction mixture lacking enzyme was added to a final concentration of 500 µM each dATP, dCTP, and dGTP, 300 µM dTTP (Larova Biochemie GMBH, Teltow, Germany), 200 µM 5-aminoallyl-dUTP (Sigma-Aldrich, Steinheim, Germany), 40 U RNasin® (Promega, Mannheim, Germany), 1× first-strand buffer (Invitrogen), 10 mM dithiothreitol (DTT; Invitrogen) in a final volume of 29 µL. The reaction mixture was incubated for 3–5 min at room temperature to let the primers anneal. SuperScript™ II (400 U, 2 µL; Invitrogen) were added, and the mixture was incubated at 42°C for 5 h. Avian myeloblastosis virus (AMV)-catalyzed reactions were performed in 100-µL reactions containing 3 µg aRNA, 1× reaction buffer, 6 µg either Inv or R15 primer, 60 U RNasin, 50 µg/mL BSA, 500 µM each dATP, dCTP, and dGTP, 300 µM dTTP, 200 µM 5-aminoallyl-dUTP, and 40 U AMV enzyme (USB, Cleveland, Ohio, USA). Moloney murine leukemia virus (MmLV)-catalyzed reactions were performed in 50-µL reactions containing 3 µg aRNA, 6 µg either Inv or R15 primer, 1× reaction buffer, 40 U RNasin, 500 µM each dATP, dCTP, and dGTP, 300 µM dTTP, 200 µM 5-aminoallyl-dUTP, and 500 U MmLV enzyme (USB). Annealing of primers was performed identically to SuperScript II-catalyzed reactions, and the enzymes were added last to all reactions.

Reactions were terminated by the addition of 10 µL 0.5 M EDTA (Sigma), and the RNA was hydrolyzed by the addition of 10 µL 1 M NaOH (Sigma) followed by heating at 65°C for 15 min. Reactions were neutralized by adding 10 µL 1 M HCl (Sigma). The cDNA was subsequently purified on QIAquick® PCR Purification kit spin columns (Qiagen) according to the manufacturer's instructions, but substituting phosphate wash buffer [5 mM potassium phosphate (Sigma), pH 8.0, 80% ethanol] for buffer PE and phosphate elution buffer (4 mM potassium phosphate, pH 8.5) for buffer EB.

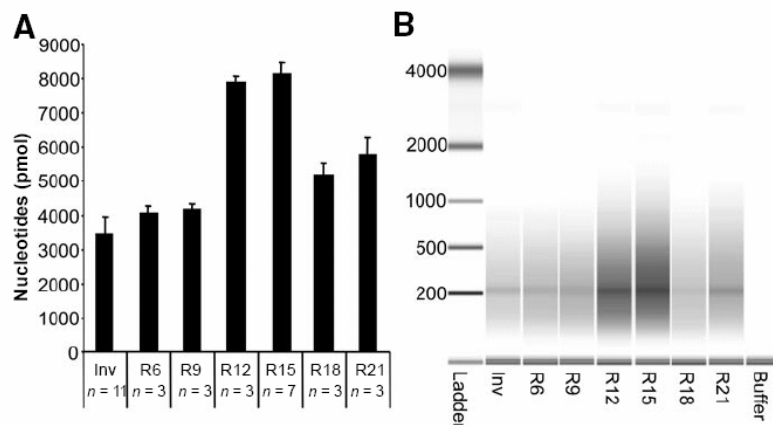
The cDNA was lysophilized and resuspended in 4.5 µL 0.1 M fresh sodium carbonate buffer, pH 9.0. N-hydroxysuccinimide (NHS) esters (4.5 µL) of Cy<sup>TM</sup>3 or Cy5 dye (Amersham

Biosciences, Piscataway, NJ, USA) in dimethylsulfoxide (DMSO, lysophilized dye from one tube was dissolved in 73 µL DMSO; Sigma) were added, and reactions were incubated at room temperature in the dark for 1 h. Coupling reactions were quenched by the addition of 35 µL 0.1 M sodium acetate (Sigma), pH 5.2, and unincorporated dye was removed using QIAquick PCR Purification kit spin columns according to the manufacturer's instructions. Labeling efficiency was determined by analyzing the whole undiluted sample in a spectrophotometer using a 50-µL microcuvette (Hellma, Müllheim, Germany).

### Microarray

Slides prespotted with 44,290 60-nucleotide-long oligonucleotides directed against the human transcriptome were obtained (Agilent Technologies), and hybridizations were performed according to supplier's instructions. In brief, unless otherwise mentioned, 200 pmol of each of the differently Cy-labeled cDNA reactions were combined in 200 µL Milli-Q® water (Millipore, Billerica, MA, USA) and denatured at 98°C for 3 min followed by incubation at room temperature for 2–3 min. Fifty microliters 10× control (Agilent) and 250 µL 2× hybridization buffer (Agilent) were then added to the cDNA mixture. Four hundred ninety microliters were applied to a gasket slide (Agilent) placed in a hybridization chamber (Agilent). The slide containing the microarray was mounted on top of the gasket slide containing the hybridization solution, and the hybridization chamber was then closed and inspected for bubble formation. Stationary bubbles were dislodged by gentle tapping. The hybridization chamber was mounted on a rotation device and placed in a Hybaid Shake 'n' Stack hybridization oven (Thermo Electron Corporation, San Diego, CA, USA) for 17 h at 60°C with the lowest rotation setting (approximately 4 rpm).

Following hybridization, the gasket slide was removed from the slide containing the array while submerged in washing solution 1 [6× standard saline



**Figure 1.** Effect of random primer length on the amount of generated cDNA. (A) cDNA yield obtained from reverse transcription of 3  $\mu$ g amplified RNA (aRNA). Values are based on spectrophotometer measurements ( $A_{260}$ – $A_{310}$  nm). A commercial random primer formulation primarily consisting of random hexamers from Invitrogen (Inv) was included as a control. Random primers were obtained from Sigma Genosys ranging in length from 6 to 21 bases using a 3 base length increment (R6 to R21). (B) Size distribution of the generated cDNA using the 2100 Bioanalyzer and the RNA 6000 Nano LabChip<sup>®</sup> (Agilent).

citrate (SSC; AppliChem, Darmstadt, Germany), 0.005% Triton<sup>®</sup>X-102 (Agilent)]. The slides were washed for 10 min at room temperature in washing solution 1 followed by 5 min in wash solution 2 (0.1 $\times$  SSC, 0.005% Triton X-102) at 4 $^{\circ}$ C in an in-house fabricated microarray washing station. The slides were dried by centrifugation at 100 $\times$  g and scanned in an arrayWoRx<sup>™</sup> microarray scanner (Applied Precision, Issaquah, WA, USA). Quantification was performed in the quantification software accompanying the arrayWoRx scanner.

#### Data Analysis

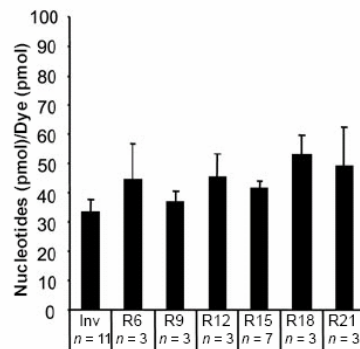
The data was normalized using the Qspline normalization method (25), and further analysis was performed using Excel<sup>®</sup>.

## RESULTS

### Yield of cDNA Synthesis Using Different Primers

cDNA reactions (23) were primed with random primers, ranging from 6 bases to 21 bases in length, to evaluate the effect of primer length on the yield and quality of the resulting cDNA. As control, the Invitrogen random primer

formulation (referred to subsequently as Inv) was utilized and compared with primers synthesized at an oligonucleotide house. The Invitrogen formulation consists primarily of random hexamers. Reverse transcription reactions initiated with either random 15-mer (R15) or R12 primers resulted in 100% more cDNA, while R18- and R21-primed reactions resulted in 40%–50% more cDNA compared with cDNA yield using the shorter R6 and R9 primers (Figure 1A). The results also suggests that cDNA synthesis initiated with



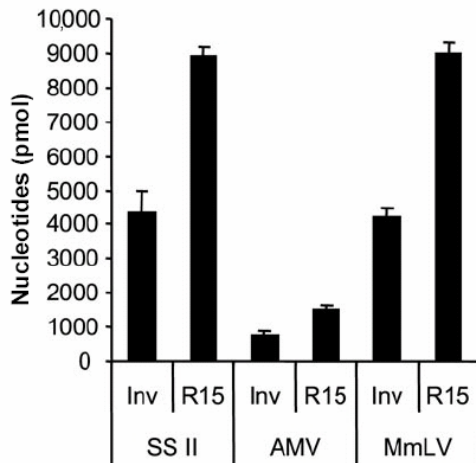
**Figure 2.** Amount of dye incorporated in cDNA produced with different primers. The incorporation efficiencies were determined as the ratio of the amount of cDNA (Figure 1) and the amount of Cy3 or Cy5 determined by spectroscopic analysis (550 and 650 nm, respectively).

R6 and R9 primers obtained from an oligonucleotide vendor results in cDNA yields comparable to reactions initiated with the commercial random primer formulation, Inv. Because the reactions were spiked with 3  $\mu$ g T7-amplified RNA, the maximum yield was 10,000 pmol synthesized nucleotides of cDNA. Reactions initiated with R15 and R12 resulted in 80%–90% yield, while R6- and R9-initiated reactions resulted in 40% yield. The relative yield between different priming methods was verified by electrophoresis, where R15 primers gave significantly more cDNA than the other primers (Figure 1B). The gel image also suggests that all unused primers were removed during purification and therefore did not contribute to the resulting cDNA yields measured by spectroscopy. There was no difference in size distributions of the respective cDNA populations produced by different primers. Synthesis initiated using different primers did not affect the amount of aminoallyl-dUTP incorporated in the cDNA, as all cDNA had a ratio of nucleotides per dye (Nuc/Dye) that was approximately  $40 \pm 15$  (Figure 2).

Reverse transcription of mRNA was investigated, and the results showed that R15 primer-initiated reactions yielded 2-fold more cDNA than reactions initiated with Inv primers, confirming the findings from reactions with aRNA as the template (Figure 1). The results also showed that R15-initiated reactions reverse transcribed almost 80% of mRNA, which was 2-fold better than the Invitrogen random primer-initiated reactions used as control.

Adding a C6dT modification to random hexamer primers has previously been shown to increase the sensitivity of microarray assay 10-fold (22). However, in our hands, a random hexamer primer modified with a primary amine attached by a C6 linker to the 5' end did not give more cDNA in reverse transcription of mRNA compared with corresponding unmodified primers. No positive effect in the amount of incorporated dye in the cDNA was observed using amino-modified random hexamers compared with unmodified primers (data not shown).

RESEARCH REPORT



**Figure 3. Yield of cDNA synthesis using different reverse transcriptase enzymes.** All reactions were initiated with 6 µg primer and 3 µg amplified RNA (aRNA) originating from the same pool. All reactions were performed at 42°C for 5 h. SS II, SuperScript II; AMV, avian myeloblastosis virus; MmLV, Moloney murine leukemia virus.

**Yield of cDNA Using Different Polymerases**

The effect of different reverse transcription polymerases on the yield of cDNA was investigated and showed that for all three enzymes used, a 2-fold increase in yield was obtained using random pentadecamer primers compared with reactions primed with random hexamer primers (Figure 3). The SuperScript II and the MmLV were found to have close to identical yields (about 90%), while the AMV

polymerase had a significantly lower yield.

**Microarray Analysis of cDNA Populations**

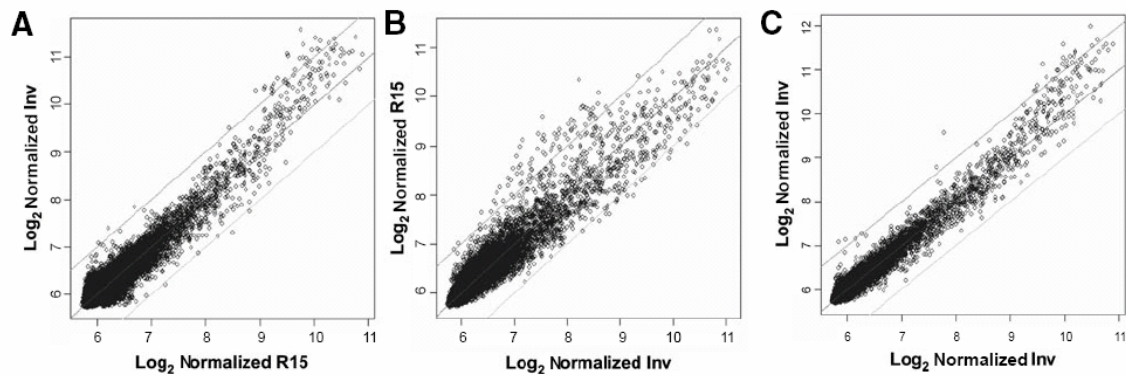
The R15 primer-generated cDNA populations were compared with cDNA populations generated by Inv priming by co-hybridization of the respective cDNA populations to DNA microarrays of 44,000 probes. All cDNA populations were generated using equal amounts of the same aRNA pool as template. Genes were considered to be differently expressed significantly if the ratio between the R15- and Inv-primed cDNA exceeded 2-fold as indicated by the upper and lower line on Figure 4, A–C. Repeating the experiments with the order of the dyes reversed enabled removal of nonsignificant noise and statistical analysis of the data. The results showed that, statistically, there were only three gene transcripts that were found to differ between the R15- and Inv-primed reactions (Figure 4, A and B, and Table 1). In comparison, cDNA populations generated from four different Inv-primed reactions differed statistically in two transcripts (Figure 4C and Table 1).

Inspecting the non-normalized microarray data showed that 55%–72% more genes were detected using cDNA generated by R15 priming compared with cDNA generated by Inv priming (see Figure 5, A, B, and F, two leftmost bars). This result cannot be explained by differences in fluorescence or amount of target hybridized between the two populations because the amount of dye was normalized to 200 pmol dye prior to hybridization. The effect of increasing signals was highest in the Cy5 channel (Figure 5F), which can be explained by the fact that Cy5 signals were generally weaker than Cy3 signals. Normalization of the data removed the positive effect of R15 priming (Figure 4, A and B, and Supplementary Figure S1 available online at [www.BioTechniques.com](http://www.BioTechniques.com)), which is expected because the algorithm (25) is designed to remove systematic variations. We routinely obtain twice as much cDNA during reverse transcription with R15 priming over Inv/R6 priming (Figure 1). The significance of that was illustrated by co-hybridizing microarrays with twice the amount of R15-primed cDNA as Inv-primed cDNA. Between 3- and 11-fold more genes were considered expressed on arrays hybridized with twice the amount of R15-primed cDNA compared with Inv-primed cDNA (Figure 5, C, D, and F). This means that from the same amount of starting material, cDNA generated by R15 priming results in more genes being

**Table 1. Genes Showing Differences in Expression in cDNA Populations Primed with Either R15 or Inv Primers**

Probe	Gene	Ratio	SD	CV (%)	P Value	Sequence
A_23_P355447	ZDHHC22	0.48 <sup>a</sup>	0.01	1.86	0.0002	5'-CAATGGGAGGGAGAGGGAGGGGAAGA-3' 5'-TCTGGGCAATTTTGGCCTTGACTCTTTCCTG-3'
A_32_P158433	THC2001391	2.20 <sup>a</sup>	0.29	13.37	0.029	5'-CAGAAGTCGCTGGGCTCATAAGGCTCTTAG-3' 5'-ACGTGCTTGAGAGTGAGCCTTTCGAAGAGA-3'
A_32_P187875	A_32_P187875	2.12 <sup>a</sup>	0.15	6.93	0.0085	5'-GAAGCATCGTATCACAGCAGGTTACAACAA-3' 5'-CTTTGGGATAAAAAGCAACTGGTAAACTGT-3'
A_23_P87879	CD69	0.08 <sup>b</sup>	0.04	48.58	0.00079	5'-TGTGCAATATGTGATGTGGCAAATCTCTATT-3' 5'-AGGAAATATTCTGTAATCTTCAGACCTAG-3'
A_24_P694760	AK056312	2.26 <sup>b</sup>	0.29	12.65	0.025	5'-TCAACTTTGCCTTGATAATTATTGTAACAC-3' 5'-TTTGTTCATTTTTCTTTTTATTACAA-3'

Genes showing significant differences in expression in cDNA populations primed with either R15 or Inv primers using equal amounts of the same amplified RNA (aRNA) pool as template (Figure 4, A–B). The ratio of Inv R6 over R15 (<sup>a</sup>) was calculated for two slides, and the values were averaged. The P values were calculated using the Student's *t*-test. Genes were considered significantly regulated if the fold-change exceeded 2-fold and the P value was less than 0.05. The Inv R6 over Inv R6 ratios were calculated by utilizing the Inv R6 values from three slides and averaging the ratios. Thus, inherent slide-to-slide as well as experimental variations are contained in these values.  
<sup>a</sup>Ratio refers to the ratio Inv R6 over R15.  
<sup>b</sup>Ratio refers to the average ratio values over three slides for Inv R6 signals.



**Figure 4.** Scatter plots of normalized data from hybridizations to whole human transcriptome arrays. Cy5-labeled samples were always plotted on the y-axis. Prior to hybridization, the differently labeled cDNA samples were pooled using equimolar amounts of each Cy dye (200 pmol). Molar amounts mentioned in pmol in this figure refer to the amount of Cy dye incorporated in the cDNA and not the amount of nucleotides of cDNA. (A) Normalized scatter plot of co-hybridization of 200 pmol Cy5-labeled cDNA resulting from reactions initiated with Inv primers and 200 pmol Cy3-labeled cDNA resulting from reactions initiated with R15 primers. (B) Repeating the experiment with the order of the dyes reversed. (C) Normalized scatter plot of co-hybridization of 200 pmol Cy5-labeled cDNA and 200 pmol Cy3-labeled cDNA, both resulting from reactions initiated with Inv primers. The central line is the median, and the upper and lower lines correspond to one  $\log_2$ -fold change up or down, respectively. Nonlinear normalization of the raw data was performed using Qspline (25).

detected on microarrays compared with cDNA generated by Inv/R6 priming.

Taken together, the results showed that R15 priming increases the amount of the resulting cDNA, but also yields cDNA with better representation of the original mRNA population. Although cDNA populations were generated for analysis with DNA microarrays as shown in this study, R15 primers could also be applied to single-cell real-time PCR with similar efficiency to Inv primers (data not shown), indicating that Inv primers can generally be substituted with R15 primers in other applications.

## DISCUSSION

cDNA synthesis from RNA is a critical step in gene expression analysis, and the choice of priming can have large effects on the cDNA yield and quality as shown in this report. Priming with random pentadecamers resulted in 80%–90% of the complex aRNA or mRNA population being reverse transcribed. However, cDNA was measured spectroscopically after spin column purifications, a purification method that is not suitable for aRNA. **Circle Reader Service No. 179** and R12 primer-initiated reactions have yields close to 100%, indicating that almost the entire aRNA or mRNA pool (transcriptome) is reverse transcribed

using R15 and R12 primers. The increased coverage of the transcription process using R15 primers may explain why 55%–72% more genes were considered expressed using microarrays hybridized with R15-primed cDNA compared with Inv-primed cDNA.

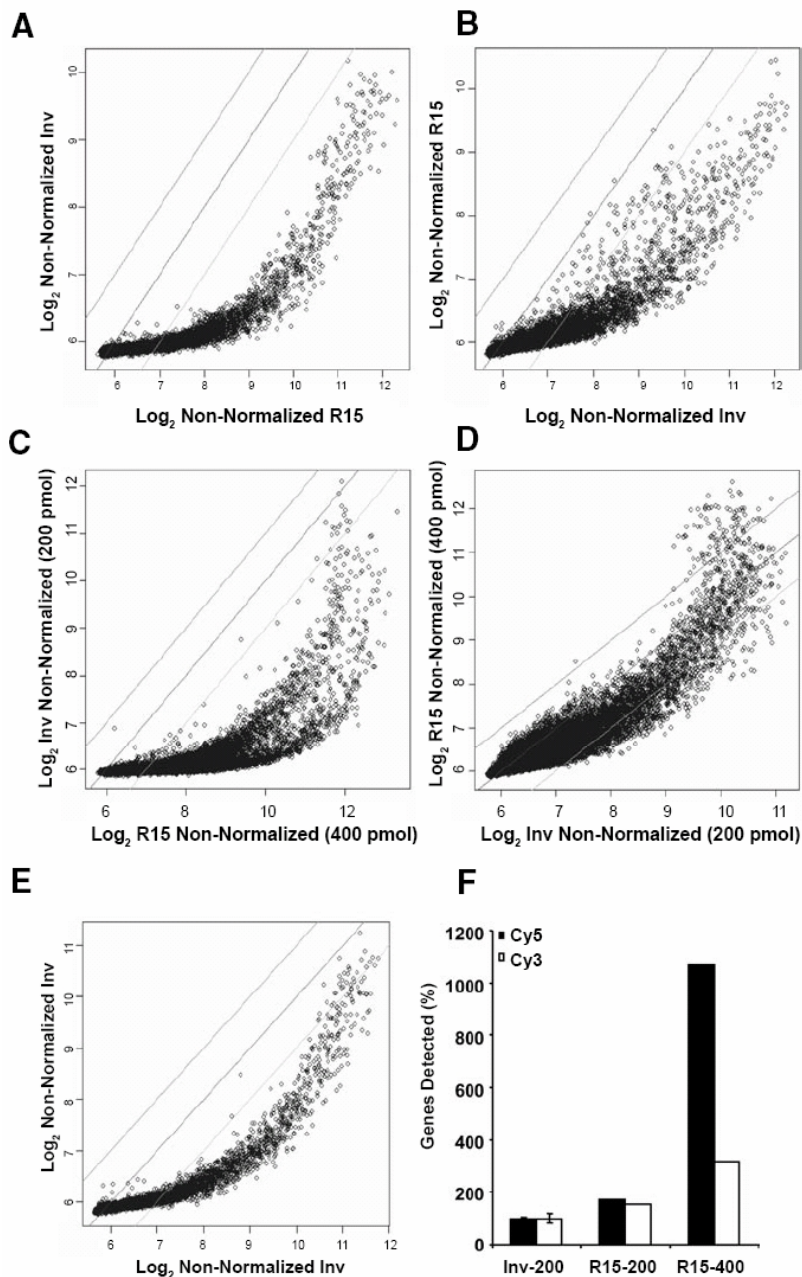
Amplified RNA was used in these studies to have enough of a complex RNA population for all experiments and to avoid bias between the different cDNA pools (26). Because aRNA reactions are primed with poly(dT) primers, it is likely that this RNA population has a 3' bias compared with mRNA, meaning that the aRNA is less complex than mRNA. The effect of using different length of primers was however similar if mRNA was used as template instead of aRNA (Figure 1A). In both cases, random pentadecamer priming resulted in close to 100% reverse transcription of the complex RNA sample, if losses during purification were accounted for. This indicates that the positive effects in hybridization reactions by using the R15 as primers in the cDNA synthesis on aRNA template most likely also apply to mRNA as template.

It is not clear why the use of R15 primers results in an increased yield of cDNA compared with R6 primers. One possible reason could be that shorter primers have difficulty annealing during the reverse transcription process. This can be deduced from calculating the

melting temperature of random primers with different lengths and GC content (Supplementary Figure S2). It is likely that the R6 primers as well as the R15 primers hybridize during cooling on ice (see the Materials and Methods section for the procedure). However, preincubation at 20°C would induce the melting of AT-rich R6 primers, while AT-rich R15 primers will not melt (Supplementary Figure S2). It is less likely that R6 primers anneal to the RNA during synthesis at 42°C, while annealing of GC-rich R15 primers can occur at 42°C. It is therefore likely that R15 or longer primers will bind better to AT-rich sequences than R6 primers during the reverse transcription procedure, indicating a mechanism for the observed increase in transcriptome coverage using longer primers. The lower yields obtained using random primers that were 18 nucleotides or longer can be the result of secondary structure formation or increased specificity resulting in fewer binding sites for the primers. This may indicate an optimum in terms of the length of random primers that is balanced between melting temperature of the primer-template duplex and the increased specificity originating from the increasing length.

Random pentadecamers have previously been reported to be used as primers in a preamplification step in whole genome amplification (WGA) (27). Presumably R15 primers were

## RESEARCH REPORT



**Figure 5.** Scatter plots of non-normalized hybridizations to whole human transcriptome arrays. Cy5-labeled samples were always plotted on the y-axis. Molar amounts mentioned in pmol in this figure refer to the amount of Cy dye incorporated in the cDNA and not the amount of nucleotides of cDNA. (A, B, and E) Non-normalized data from Figure 4. (C) Repeating the experiment in panel A with twice the amount of labeled cDNA originating from R15-initiated reactions (400 pmol Cy dye-labeled cDNA) than Inv-initiated reactions (200 pmol Cy dye-labeled cDNA). (D) Repeating the experiment in panel C with the order of the dyes reversed. (F) Comparison of the amount of detectable genes with R15 and Inv priming. The data was normalized to the average amount of genes detected with 200 pmol of labeled cDNA primed with Inv primers in two independent hybridization reactions. To be able to compare the effects in the respective fluorescent channels each average, Cy3 and Cy5, respectively, was set to 100%. A gene was considered detected if it displayed a signal that was 50% more than the background signal, calculated as the average of the 1000 weakest signals on the array.

chosen because they would function in the PCR where annealing was done at 37°C, a temperature close to the 42°C used in reverse transcription reactions. Recently, reverse transcription polymerases operating at higher temperatures (>50°C) have been introduced (28,29). These enzymes should give better efficiency of reverse transcription reactions due to the fact that fewer secondary structures in the RNA template are encountered during the transcription process (29). It is likely that priming with longer primers could also have a greater positive effect on reverse transcription reactions performed at 50°C, because a larger fraction of the longer primers will be able to form duplexes with the RNA template than the shorter primers.

It has previously been found that the requirement for an mRNA template can be reduced by a factor of 10 by using amino C6dT-modified random hexamers (22). It was speculated that the effect is most likely due to the increased incorporation of dyes in the target, because more amine groups are available on the target for the Cy dye esters to react with. However, if we assume that the cDNA is 400 nucleotides long on average, and the Nuc/Dye ratio is 40, there are 10 dyes per cDNA copy. An additional dye from the C6dT-modified hexamer would only increase the dye content by 10% if the coupling efficiency is assumed to be 100%. The relatively small gain in fluorescent signal that an amine group would give, according to this reasoning, was confirmed by our results in which an amino moiety linked to a C6 linker to R6 primers did not perform better than unmodified primers.

Techniques like laser capture microdissection (LCM) enable the isolation of single cells (30). Comparing the gene expression profiles of single cells captured by LCM requires amplification (20), as the amount of mRNA in a single cell is limited. Linear amplification of RNA is usually performed utilizing a T7-based method (31). However, subsequent rounds of RNA amplification may include random hexamer or nonamer priming (20,32). This technique yields only minute and highly precious amounts of genetic material. If the random hexamers

or nonamers in these reactions were replaced with random pentadecamers, we believe, based on data presented in this work, that higher yields and quality of aRNA and subsequently better cDNA could be obtained. Other critical assays, like probing exon-arrays (33,34) would also benefit from using R15 primers in reverse transcription, because a bias introduced by the patchy R6 priming could, in the worst case, significantly underestimate exon usage in cells.

In conclusion, a simple substitution of random hexamers with random pentadecamers in the reverse transcription reaction has many advantages, such as better genome coverage and a better yield. The effect is that better sensitivity is obtained using random pentadecamers as primers, which should be an advantage for gene expression analysis using microarrays or real-time PCR in general.

#### ACKNOWLEDGMENTS

The study was supported by The Danish Research Council [grant no. 2014-00-0003, Danish Biototechnology Instrument Center (DABIC)]. The HeLa cell line was kindly donated by Dr. Peter Thomsen, Scandinavian Micro Biodevices (SMB), Farum, Denmark. We thank Jesper Petersen for critical reading of the manuscript.

#### COMPETING INTERESTS STATEMENT

The authors declare no competing interests.

#### REFERENCES

- Aslanian, A., P.J. Iaquinta, R. Verona, and J.A. Lees. 2004. Repression of the Arf tumor suppressor by E2F3 is required for normal cell cycle kinetics. *Genes Dev.* 18:1413-1422.
- DeRisi, J., L. Penland, P.O. Brown, M.L. Bittner, P.S. Meltzer, M. Ray, Y. Chen, Y.A. Su, and J.M. Trent. 1996. Use of a cDNA microarray to analyse gene expression patterns in human cancer. *Nat. Genet.* 14:457-460.
- Marton, M.J., J.L. DeRisi, H.A. Bennett, V.R. Iyer, M.R. Meyer, C.J. Roberts, R. Stoughton, J. Burchard, et al. 1998. Drug target validation and identification of secondary drug target effects using DNA microarrays. *Nat. Med.* 4:1293-1301.
- Maxfield, L.F., C.D. Fraize, and J.M. Coffin. 2005. From the cover: relationship between retroviral DNA-integration-site selection and host cell transcription. *Proc. Natl. Acad. Sci. USA* 102:1436-1441.
- Yang, Y.H., S. Dudoit, P. Luu, D.M. Lin, V. Peng, J. Ngai, and T.P. Speed. 2002. Normalization for cDNA microarray data: a robust composite method addressing single and multiple slide systematic variation. *Nucleic Acids Res.* 30:e15.
- Hughes, T.P., J. Kaeda, S. Branford, Z. Rudzki, A. Hochhaus, M.L. Hensley, I. Gathmann, A.E. Bolton, et al. 2003. Frequency of major molecular responses to imatinib or interferon alfa plus cytarabine in newly diagnosed chronic myeloid leukemia. *N. Engl. J. Med.* 349:1423-1432.
- Melo, J.V., X.H. Yan, J. Diamond, F. Lin, N.C. Cross, and J.M. Goldman. 1996. Reverse transcription/polymerase chain reaction (RT/PCR) amplification of very small numbers of transcripts: the risk in misinterpreting negative results. *Leukemia* 10:1217-1221.
- Asnafi, V., K. Beldjord, E. Boulanger, B. Comba, P. Le Tuteur, M.-H. Estienne, F. Davi, J. Landman-Parker, et al. 2003. Analysis of TCR, pT $\alpha$ , and RAG-1 in T-acute lymphoblastic leukemias improves understanding of early human T-lymphoid lineage commitment. *Blood* 101:2693-2703.
- Bustin, S.A., and T. Nolan. 2004. Pitfalls of quantitative real-time reverse-transcription polymerase chain reaction. *J. Biomol. Tech.* 15:155-166.
- Li, X., M. Miyajima, and H. Aral. 2005. Analysis of TGF- $\beta$ 2 and TGF- $\beta$ 3 expression in the hydrocephalic H-Tx rat brain. *Childs Nerv. Syst.* 21:32-38.
- Mannhalter, C., D. Koizar, and G. Mitterbauer. 2000. Evaluation of RNA isolation methods and reference genes for RT-PCR analyses of rare target RNA. *Clin. Chem. Lab. Med.* 38:171-177.
- Suzuki, S., M. Asamoto, K. Tsujimura, and T. Shirai. 2004. Specific differences in gene expression profile revealed by cDNA microarray analysis of glutathione S-transferase placental form (GST-P) immunohistochemically positive rat liver foci and surrounding tissue. *Carcinogenesis* 25:439-443.
- Ståhlberg, A., J. Hakansson, X. Xian, H. Semb, and M. Kubista. 2004. Properties of the reverse transcription reaction in mRNA quantification. *Clin. Chem.* 50:509-515.
- Brooks, E.M., L.G. Sheflin, and S.W. Spaulding. 1995. Secondary structure in the 3' UTR of EGF and the choice of reverse transcriptases affect the detection of message diversity by RT-PCR. *BioTechniques* 19:806-815.
- Michor, F., T.P. Hughes, Y. Iwasa, S. Branford, N.P. Shah, C.L. Sawyers, and M.A. Nowak. 2005. Dynamics of chronic myeloid leukaemia. *Nature* 435:1267-1270.
- Brink, A.A., J.J. Oudejans, M. Jiwa, J.M. Walboomers, C.J. Meijer, and A.J. van den Brule. 1997. Multiplexed cDNA synthesis followed by PCR is the most suitable method for Epstein-Barr virus transcript analysis in small lymphoma biopsies. *Mol. Cell. Probes* 11:39-47.
- Iturriza-Gomara, M., J. Green, D.W. Brown, U. Desselberger, and J.J. Gray. 1999. Comparison of specific and random priming in the reverse transcriptase polymerase chain reaction for genotyping group A rotaviruses. *J. Virol. Methods* 78:93-103.
- Decraene, C., I. Reguigne-Arnould, C. Auffray, and G. Pietu. 1999. Reverse transcription in the presence of dideoxynucleotides to increase the sensitivity of expression monitoring with cDNA arrays. *BioTechniques* 27:962-966.
- Schena, M., D. Shalon, R.W. Davis, and P.O. Brown. 1995. Quantitative monitoring of gene expression patterns with a complementary DNA microarray. *Science* 270:467-470.
- Luo, L., R.C. Salunga, H. Guo, A. Bittner, K.C. Joy, J.E. Galindo, H. Xiao, K.E. Rogers, et al. 1999. Gene expression profiles of laser-captured adjacent neuronal subtypes. *Nat. Med.* 5:117-122.
- Sterrenburg, E., R. Turk, J.M. Boer, G.B. van Ommen, and J.T. den Dunnen. 2002. A common reference for cDNA microarray hybridizations. *Nucleic Acids Res.* 30:e116.
- Xiang, C.C., O.A. Kozhich, M. Chen, J.M. Inman, Q.N. Phan, Y. Chen, and M.J. Brownstein. 2002. Amine-modified random primers to label probes for DNA microarrays. *Nat. Biotechnol.* 20:738-742.
- Yang, I.V., E. Chen, J.P. Hasseman, W. Liang, B.C. Frank, S. Wang, V. Sharov, A.I. Saeed, et al. 2002. Within the fold: assessing differential expression measures and reproducibility in microarray assays. *Genome Biol.* 3:research0062.
- Kane, M.D., T.A. Jatkoe, C.R. Stumpf, J. Lu, J.D. Thomas, and S.J. Madore. 2000. Assessment of the sensitivity and specificity of oligonucleotide (50mer) microarrays. *Nucleic Acids Res.* 28:4552-4557.
- Workman, C., L.J. Jensen, H. Jarmer, R. Berka, L. Gautier, H.B. Nielsen, H.H. Saxild, C. Nielsen, et al. 2002. A new non-linear normalization method for reducing variability in DNA microarray experiments. *Genome Biol.* 3:research0048.
- Li, Y., T. Li, S. Liu, M. Qiu, Z. Han, Z. Jiang, R. Li, K. Ying, et al. 2004. Systematic comparison of the fidelity of aRNA, mRNA and T-RNA on gene expression profiling using cDNA microarray. *J. Biotechnol.* 107:19-28.
- Zhang, L., X. Cui, K. Schmitt, R. Hubert, W. Navidi, and N. Arnheim. 1992. Whole genome amplification from a single cell: implications for genetic analysis. *Proc. Natl. Acad. Sci. USA* 89:5847-5851.
- Kawano, M., A.A. Reynolds, J. Miranda-Rios, and G. Storz. 2005. Detection of 5' and 3'-UTR-derived small RNAs and cis-encoded antisense RNAs in *Escherichia coli*. *Nucleic Acids Res.* 33:1040-1050.
- Zhang, Y.J., H.Y. Pan, and S.J. Gao. 2001. Reverse transcription slippage over the mRNA secondary structure of the LIP1 gene. *BioTechniques* 31:1286-1294.
- Emmert-Buck, M.R., R.F. Bonner, P.D. Smith, R.F. Chuaiqui, Z. Zhuang, S.R. Goldstein, R.A. Weiss, and L.A. Liotta. 1996. Laser capture microdissection. *Science* 274:998-1001.
- Van Gelder, R.N., M.E. von Zastrow, A. Yool, W.C. Dement, J.D. Barchas, and J.H. Eberwine. 1990. Amplified RNA synthesized from limited quantities of heterogeneous cDNA. *Proc. Natl. Acad. Sci. USA* 87:1663-1667.



RESEARCH REPORT

---

32. Xiang, C.C., M. Chen, L. Ma, Q.N. Phan, J.M. Inman, O.A. Kozhich, and M.J. Brownstein. 2003. A new strategy to amplify degraded RNA from small tissue samples for microarray studies. *Nucleic Acids Res.* 31:e53.
33. Dhami, P., A.J. Coffey, S. Abbs, J.R. Vermeesch, J.P. Dumanski, K.J. Woodward, R.M. Andrews, C. Langford, and D. Vetric. 2005. Exon array CGH: detection of copy-number changes at the resolution of individual exons in the human genome. *Am. J. Hum. Genet.* 76:750-762.
34. Pinkel, D. and D.G. Albertson. 2005. Array comparative genomic hybridization and its applications in cancer. *Nat. Genet.* 37(Suppl): S11-S17.

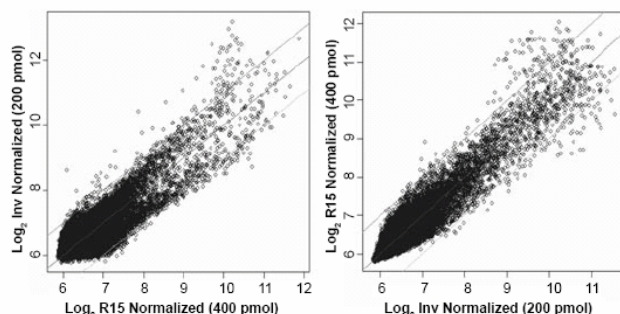
Received 2 December 2006; accepted  
15 February 2006.

**Address correspondence to:**

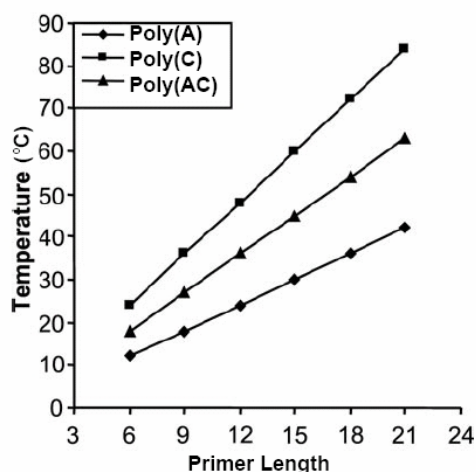
Martin Dufva  
*Department of Micro and Nanotechnology  
Technical University of Denmark  
Ørsted's Plads 345 east  
DK-2800 Kgs. Lyngby, Denmark  
e-mail: mdu@mic.dtu.dk*

SUPPLEMENTARY MATERIAL FOR:

# Reverse transcription using random pentadecamer primers increases yield and quality of resulting cDNA

Michael Stangegaard<sup>1</sup>, Inge Høgh Dufva<sup>2</sup>, and Martin Dufva<sup>1</sup>*BioTechniques 40:649-657 (May 2006)*

**Supplementary Figure S1.** Normalized scatter plots of Figure 5, C and D. The central line is the median, and the upper and lower lines correspond to one log<sub>2</sub> fold-change up or down, respectively. Nonlinear normalization of the raw data was performed using Qspline (28).



**Supplementary Figure S2.** Melting curves of oligonucleotides with varying length and adenine, cytosine content. The curves were generated by the theoretical melting temperature using oligonucleotides consisting solely of adenine (A), cytosine (C), or an equal amount of A and C. The reverse transcription reactions were performed at 42°C.

<sup>1</sup>Technical University of Denmark, Lyngby and <sup>2</sup>University of Copenhagen, Herlev, Denmark

Vol. 40, No. 5 (2006)

BioTechniques 1

## 10 Conference proceedings

### Peer reviewed conference proceedings:

Poster 1: M. Dufva, **M. Stangegaard**, and C. B. V. Christensen, “*Simple bonding of PMMA microstructures to modified glass surfaces preprinted with DNA and protein microarrays*”. Miniaturized Systems for Chemistry and Life Sciences ( $\mu$ TAS 2004)

Poster 2: Z. Wang, **M. Stangegaard**, M. Dufva, J. P. Kutter, and A. Wolff, “*A simple hydrophilic treatment of SU-8 surfaces for cell culturing and cell patterning*”. Miniaturized Systems for Chemistry and Life Sciences ( $\mu$ TAS 2005)

### Conference proceedings:

Poster 3: **M. Stangegaard**, S. Petronis, C. B. V. Christensen, and M. Dufva, “*A micro cell culture chamber ( $\mu$ CCC) for the culturing and study of eukaryotic cells*”. Screening Europe 2005

Poster 4: **M. Stangegaard**, I. H. Dufva, V. Wohlgehagen and M. Dufva, “*Significance of the length of random oligo primers on the yield of cDNA during reverse transcription*”. Advances in Microarray Technologies (AMT 2005)

Poster 5: S. Petronis, **M. Stangegaard**, and M. Dufva, “*Micromachined Polymeric Cell Culture Chamber with Uniform Media Perfusion and Integrated Temperature Control*”. Life Matters Conversations 2005

## ***Poster 1: Simple bonding OF PMMA microstructures to modified glass surfaces preprinted with DNA and protein microarrays***

**Martin Dufva, Michael Stangegaard and Claus BV Christensen**

Department of Micro- and Nano Technology, technical University of Denmark, Ørsteds plads 345 east, DK-2800, Kgs Lyngby

**Keywords:** Protein, DNA, microarray, PMMA, agarose film

### **Introduction**

Protein and DNA microarrays are usually produced with glass or polymer slides. Enclosing a microarray in a microstructure puts several demands on the bonding technique. It is of highest importance that the biological activity of the microarray is not compromised by the procedure, which for instance exclude high temperatures. Here we describe a very simple and fast method to enclose protein or DNA micro arrays printed on glass slides in microstructures made in PMMA by flushing the microstructure with dichloromethane.

### **Materials**

Agarose coated microscope slides was prepared according to the method by Afanassiev et al. [1] Approximately 1 nL sample containing oligonucleotides or proteins was deposited onto the slide using a Qarray robot (Genetix, UK).

The microstructures were produced in Polymethylmethacrylate (PMMA) by laser ablation using an 150 W CO<sub>2</sub> IR laser (Synrad, Mukilteo, WA, USA). A hybridization chamber 4.5 mm in diameter was connected with channels (an inlet and an outlet) that where either 1000, 500 or 200 µm wide. At the ends of each channel holes were cut through the PMMA sheet to allow loading of the samples. The structure holds approximately 15 µL of sample. The structures were bonded to substrates by flushing approximately 30 µL dichloromethane through the channels. During re-polymerization, the channels were kept open with a gentle stream of air or N<sub>2</sub>.

The microstructures covering the DNA microarray were flushed with 150 µL 0.1 X SSC and blocked with 10% BSA in 0.1 X SSC for 5 minutes. The DNA microarrays where hybridized with a mixture of 0.5-50 nM targets dissolved in 3 X SSC, 0.3 % sodium dodecyl sulphate and 10 g/L salmon sperm DNA. Un-hybridized DNA was removed by flushing the channels with 0.1 X SSC. Prior to scanning the structures was removed with a scalpel if not mentioned otherwise. All liquid handling was made using an ordinary pipette.

## Results and discussion

The objective of the present work was to find a simple procedure to attach a microstructure over a protein or DNA microarray immobilized on a glass or polymer slide. It was desirable that the bonding technique did not include heat, since it would potentially destroy the activity of biomolecules, particularly proteins. The approach is based on dissolving the surface of the plastic a little with a solvent and, upon re-polymerization, the microstructure is bound to the glass slide. The strength of the bond between glass and the attached PMMA structure was tested by filling the hybridization chamber with 0.1X.SSC and incubating the structure at 37 °C or 50 °C. The stability of the bond was challenged at certain time intervals by emptying and filling the structure again and then continues incubating the structure. Several different microarray substrates was tested and the results showed that the bond between PMMA and agarose film coated film slides could withstand at least four challenges and 210 minutes incubation time at both 37 °C or 50 °C. This is sufficient for genetic analysis and small molecules measurements using microarrays printed on agarose film coated substrates [2, 3]. It is possible that the strong bond between PMMA and agarose film is caused by the structure of agarose which is 10-fold rougher than glass [2]. However aldehyde and amine surfaces could withstand three challenges and 150 minutes incubation times suggesting that the bonding technique also could be used with other microarray substrates. Although the bonding technique relies on dissolving PMMA, which deforms the microstructure (**Fig 1A**), functional hybridization chambers that were 4.5 mm long, 5 mm in width and only 100 µm in height could efficiently be bonded to the agarose film.

To test if the flushing bonding technique is compatible with protein activity, a small protein array was printed on agarose slides. The array consisted of an anti-mouse antibody, the pesticide metabolite BAM conjugated to BSA, FITC conjugated strepavidin and BSA. The protein microarray was enclosed in a microstructure bonded by the flushing technique and the reactivity of anti-mouse and the BAM-BSA conjugate was tested by filling the structure with a solution of mouse anti BAM antibody conjugated with the Cy5 fluochrome. The antibody reactions showed that the BAM-BSA conjugate on the microarray retained activity after the dichloromethane flushing (**Fig 1**). The microstructure supported the reaction between the anti-mouse antibody and the mouse anti BAM antibody was much better than the same reaction carried out under a coverslip or without any coverage of the antibody solution. The reason for this is not clear.

We next tested if the bonding technique was compatible with DNA microarray hybridization assay. The results showed that the microstructures did not interfere with the hybridization reaction (**Fig 2**). If anything, the microstructure could in some instances enhance hybridization efficiency up to 100 %. We calculated the CV to be around 15% for arrays hybridized with or without microstructures.

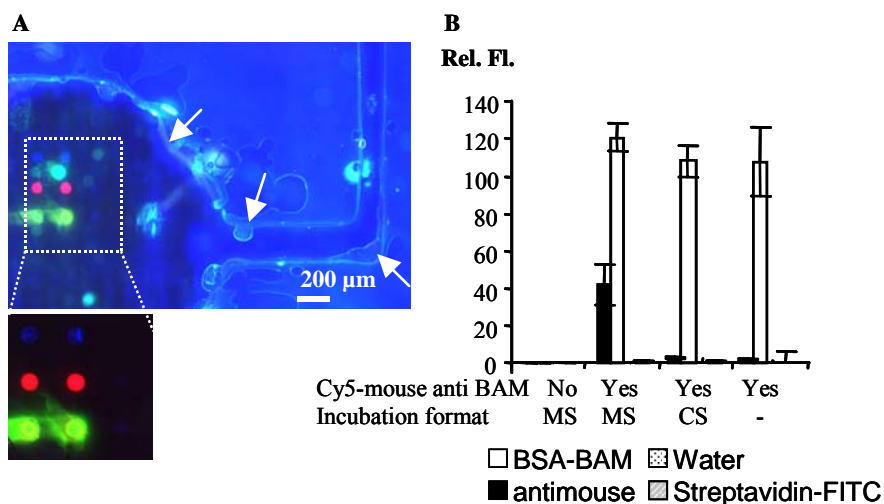
### **Conclusions**

We describe a simple, fast biocompatible way to attach microstructures made in PMMA to microarray substrates preprinted with protein or DNA microarrays. Since the technique relies on dissolving PMMA with dichloromethane, the microstructures are deformed by the process. However, for simple application like a hybridization chambers the deformation has no practical consequence. The bond is stable enough for most genetic and protein analysis using DNA microarrays. The microstructure could easily be removed enabling the use of standard microarray scanners which usually only accept microscope slides. The bonding technique did not inhibit the molecular functions of DNA or protein microarrays and conveniently enables the attachment of a microfluidic system over a microarray, which simplified the liquid handling of multistep assays like colorimetric detection of hybridization.

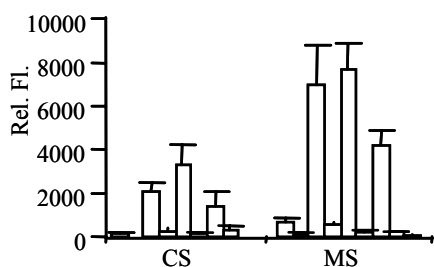
### **References**

1. Afanassiev, V., V. Hanemann, and S. Wolfl, *Preparation of DNA and protein micro arrays on glass slides coated with an agarose film*. Nucleic Acids Res. **28**(12): p. E66.2000.
2. Dufva, M., S. Petronis, L. Bjerremann Jensen, C. Krag, and C. Christensen, *Characterization of an inexpensive, non-toxic and highly sensitive microarray substrate*. Accepted Biotechniques.
3. Belleville, E., M. Dufva, J. Aamand, L. Bruun, and C. Christensen, *Quantitative Assessment of Factors affecting the Sensitivity of a Competitive Immuno-Microarray for Pesticide Detection*. Biotechniques. **35**: p. 1044-1051.2003.

Figures



**Figure 1.** Comparison of an antibody reaction performed in a microarray of immobilized molecules. Scans of microarrays incubated with Cy5 mouse anti BAM before (upper panel) and after (lower panel) removal of the microstructure. B. Comparison of signals of microarrays incubated with Cy5-mouse anti BAM using a microstructure (MS), coverslip (CS) and open air (-). The bars represents the signal obtained from different protein spots in the microarray. Arrows indicate clear deformations of the microstructure.



**Figure 2.** Hybridization signals from microarrays hybridized with either coverslip (CS) or microstructure (MS). Three different Cy3-labelled targets were hybridized to a microarray consisting of eight different probes of which three are complementary to the targets.

# DTU Simple bonding of PMMA microstructures to modified glass surfaces preprinted with DNA and protein microarrays



Martin Dufva, Michael Stangegaard and Claus BV Christensen

Department of Micro- and Nano Technology, Technical University of Denmark, Ørstedssplads 345 east, DK-2800, Kgs Lyngby

## Introduction

Protein and DNA microarrays are usually produced with glass or polymer slides. Enclosing a microarray in a microstructure puts several demands on the bonding technique. It is of highest importance that the biological activity of the microarray is not compromised by the procedure, which for instance exclude high temperatures.

## Material and methods.

Protein and DNA microarrays were spotted onto agarose film coated slides. PMMA structures was bonded to the slides by flushing the structures with dichloromethane.

## Results

The described approach is based on dissolving the surface of the plastic using a solvent and, upon re-polymerisation, bonding the microstructure to the glass slide. The bond between PMMA and agarose film coated film slides could withstand at least four challenges and 210 minutes incubation time at both 37 °C or 50 °C. This is regarded as sufficient for genetic analysis and small molecules measurements using microarrays printed on agarose film coated substrates [2, 3].

Although the bonding technique relies on dissolving PMMA, which deforms the microstructure (Fig 1A), functional hybridisation chambers that were 4.5 mm long, 5 mm in width and only 100 µm in height could efficiently be bonded to the agarose film (data not shown).

Antibody reactions towards a protein array of antigens showed that dichloromethane bonding did not affect the antigens on the microarray (Fig 1)

The bonding technique also was compatible with DNA microarray hybridisation assay (Fig 2). If anything, the microstructure could in some instances enhance hybridisation efficiency up to 100 %. We calculated the CV to be around 15% for arrays hybridised with or without microstructures.

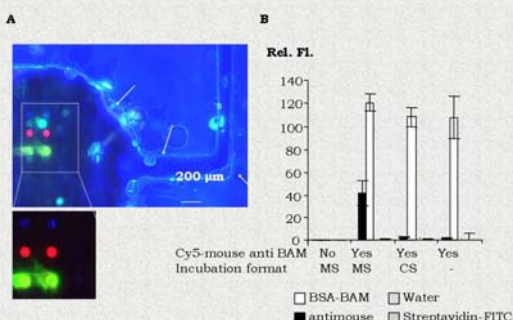
## Conclusions

We describe a simple, fast biocompatible method to attach microstructures made in PMMA to microarray substrates preprinted with protein or DNA microarrays.

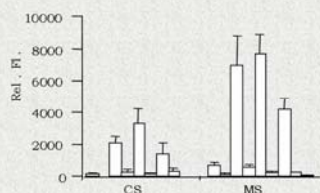
The bond is stable enough for most genetic and protein analysis using DNA/protein microarrays.

The microstructure could easily be removed enabling the use of standard microarray scanners which usually only accept microscope slides.

The bonding technique did not inhibit the molecular functions of DNA or protein microarrays and conveniently enables the attachment of a microfluidic system over a microarray.



**Figure 1.** Comparison of an antibody reaction performed in a microarray of immobilised molecules. Scans of microarrays incubated with Cy5 mouse anti BAM before (upper panel) and after (lower panel) removal of the microstructure. B. Comparison of signals of microarrays incubated with Cy5-mouse anti BAM using a microstructure (MS), coverslip (CS) and open air (-). The bars represents the signal obtained from different protein spots in the microarray. Arrows indicate clear deformations of the microstructure.



**Figure 2.** Hybridisation signals from microarrays hybridised with either coverslip (CS) or microstructure (MS). Three different Cy3-labelled targets were hybridised to a microarray consisting of eight different probes of which three are complementary to the targets.

## References.

1. Afanassiev, V., V. Hanemann, and S. Wolff, *Preparation of DNA and protein micro arrays on glass slides coated with an agarose film*. *Nucleic Acids Res.* **28**(12): p. E66.2000.
2. Dufva, M., S. Petronis, L. Bjerremann Jensen, C. Krag, and C. Christensen, *Characterization of an inexpensive, non-toxic and highly sensitive microarray substrate*. *Biotechniques.* **37**:p. 286-296. 2004
3. Belleville, E., M. Dufva, J. Aamand, L. Bruun, and C. Christensen, *Quantitative Assessment of Factors affecting the Sensitivity of a Competitive Immuno-Microarray for Pesticide Detection*. *Biotechniques.* **35**: p. 1044-1051.2003.



## ***Poster 2: A simple hydrophilic treatment of SU-8 surfaces for cell culturing and cell patterning***

Category: (4.1 Surface Modification)

Zhenyu Wang, Michael Stangegaard, Martin Dufva, Jörg P. Kutter, and Anders Wolff

MIC - Department of Micro and Nanotechnology, DTU Building 345 east, Kgs. Lyngby, DK2800, Denmark

Phone: +45 4525 6319, Fax: +45 4588 7762 Contact E-MAIL: zw@mic.dtu.dk

SU-8, an epoxy-based negative photoresist, is widely used for fabricating microstructures in various  $\mu$ TAS devices because of its excellent chemical stability and optical properties. However, since the SU-8 surface is hydrophobic, cell adhesion and culturing is hampered in SU-8 based microsystems. Here, we report a simple, cheap and robust method to render a SU-8 surface hydrophilic. The treated SU-8 surface could efficiently sustain the growth of human cells while the corresponding untreated surface was not compatible with cell growth.

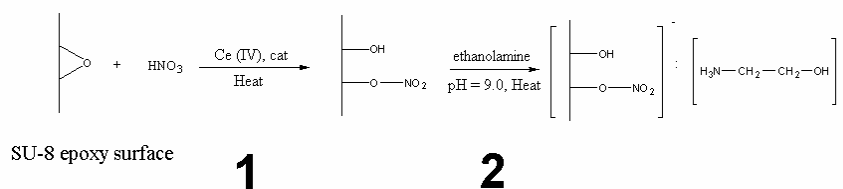
Human epithelial cells, such as HeLa cells [1], preferably adhere and grow on hydrophilic surfaces [2]. Hydrophilic surfaces can be generated by coating SU-8 surfaces with fibronectin [3] or hydrophilic polymer materials [2] to allow culturing of cells. However, such dynamic coatings may not be stable over time. Chemical treatments, on the other hand, have the potential to modify the SU-8 surface properties for extended periods [4].

Normally, the epoxy moieties on the SU-8 surface are hard to react using classical epoxy opening chemicals (e.g., HCl or HNO<sub>3</sub>), because of the chemical stability of SU-8. However, with the catalyst ceric ammonium nitrate (CAN, (NH<sub>4</sub>)<sub>2</sub>Ce(NO<sub>3</sub>)<sub>6</sub>), the epoxy rings can be opened and reacted with HNO<sub>3</sub> [5] (Figure 1). After this first CAN-HNO<sub>3</sub> treatment, the nitrate radicals on the opened epoxy ring can react further with the amino group of ethanolamine. The contact angle of water on the differently treated SU-8 surfaces was used to represent the changes in hydrophobicity (Figure 2A). The contact angle on the SU-8 surface was reduced from 95° to 45° by the CAN-HNO<sub>3</sub> treatment. This indicates that hydroxyl groups were formed on the SU-8 surface. After the second (ethanolamine) treatment, the contact angle on the SU-8 surface was further reduced to 25°. However, the second treatment is an ionic reaction, and hence reversible: after 2 months of storage, a contact angle of 50° was observed.

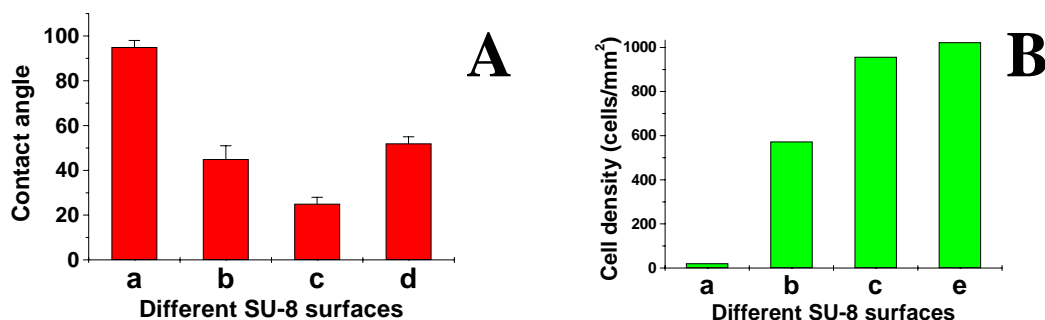
For testing the biocompatibility, HeLa cells were grown on differently treated SU-8 surfaces for one week. The differently modified SU-8 surfaces showed different attached cell densities (Figure 2B). Untreated SU-8 had a very low cell density (21 cells/mm<sup>2</sup>). CAN-HNO<sub>3</sub> treated SU-8 had a significantly higher cell density (573 cells/mm<sup>2</sup>). After the second treatment (ethanolamine), the cell

density was further increased (957 cells/mm<sup>2</sup>), close to that on the control culture flask (1023 cells/mm<sup>2</sup>). The results indicate that as the hydrophobicity of SU-8 decreases the cell density increases. Finally, HeLa cells were cultured on untreated SU-8 surfaces with hydrophilic patterns (Figure 3). The images show that HeLa cells changed their morphologies to fit onto the hydrophilic SU-8 patterns, suggesting that HeLa cells actively avoided hydrophobic surfaces.

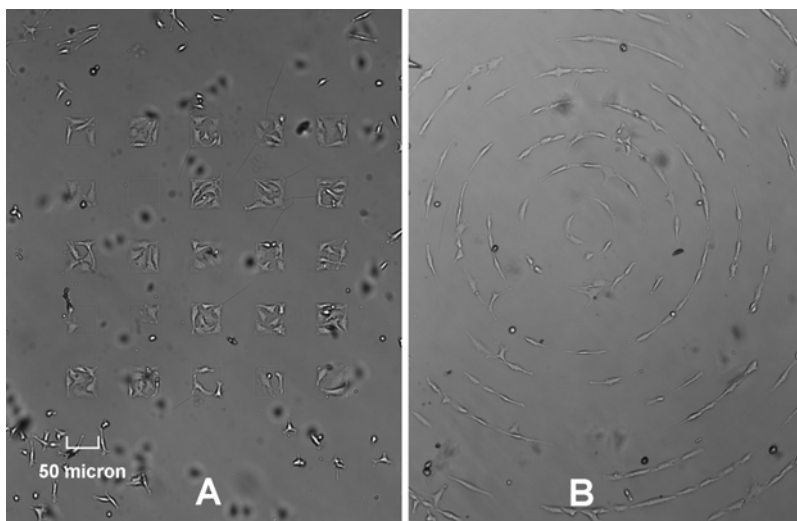
In conclusion, a two-step chemical treatment for modification of SU-8 surfaces was developed. The treated SU-8 surface shows good biocompatibility for cell culturing, and indicates a possible route to integrate cell culture functionalities in SU-8 based  $\mu$ TAS devices. The treatment can be used to create hydrophilic patterns on the SU-8 surface for defining localized cell growth.



**Figure 1.** Reaction scheme of the two-step SU-8 surface modification: **1:** The epoxy ring on the SU-8 surface was opened by treatment with 1 M HNO<sub>3</sub>, catalyzed by 0.1 M CAN at 50°C for 1 hour; **2:** The nitrate radical on the modified SU-8 surface was then reacted with the amino group of ethanolamine (0.1 M) in 0.1 M sodium phosphate buffer (pH = 9.0) for 20 minutes at 50°C.



**Figure 2.** Contact angle (**A**) and biocompatibility (**B**) of different SU-8 surfaces. The letters on the x-axis refer to the following SU-8 surfaces: (**a**). Untreated; (**b**). Treated with CAN-HNO<sub>3</sub>; (**c**). Treated with CAN-HNO<sub>3</sub> and ethanolamine; (**d**). Treated with CAN-HNO<sub>3</sub> and ethanolamine and then stored for 2 months. **A:** The hydrophobicity of differently treated SU-8 surfaces was determined by measuring the contact angle of water. **B:** For the biocompatibility test, differently treated SU-8 surfaces were immersed in culture flasks and seeded with HeLa cells. The samples were incubated for one week at 37°C in an atmosphere containing 5% CO<sub>2</sub>. The attached cell densities on different surfaces were counted to give an indication of the biocompatibility of the different surface. The cell density on the control culture flask surface (**e**) was 1023 cells/mm<sup>2</sup>.



**Figure 3.** HeLa cells cultured over night on SU-8 surfaces with hydrophilic patterns. The hydrophilic patterns were created by standard photolithography of AZ5214e photoresist on top of a 5  $\mu\text{m}$  SU-8 layer. Then, the whole glass wafer was dipped into  $\text{HNO}_3$  with CAN for the treatment. Finally, the photoresist was lifted off in acetone (4 minutes ultrasonic agitation.) **A:** HeLa cells growing on an array of  $50\mu\text{m} \times 50\mu\text{m}$  squares; **B:** HeLa cells growing on concentric circles. A change in the cell morphology was observed during culturing. It appeared as though the cells would change their morphologies to fit on to the hydrophilic SU-8 patterns rather than display their normal morphologies and hence be in contact with the untreated SU-8.

## References

- [1]. "Tissue culture studies of the proliferative capacity of cervical carcinoma and corneal Epithelium," G. O. Gey, W. D. Coffman, and M. T. Kubicek, *Cancer Research*, **12**, 264-265, 1952.
- [2]. "Micro scale patterning of cell and protein non-adhesive pco-like coatings, deposited by low frequency AC plasma polymerization," S. Bouaidat, C. Berendsen, P. Thomsen, S.G. Pederson, A. Wolff, and J. Jonsmann,  *$\mu\text{TAS}2004$* , **2**, 106-108, 2004.
- [3]. "Micropatterned surfaces to engineer focal adhesions for analysis of cell adhesion strengthening," N. D. Gallant, J. R. Capadona, A. B. Frazier, D. M. Collard, and A. J. Garcia, *Langmuir*, **18**, 5579-5584, 2002.
- [4]. "Rendering SU-8 hydrophilic to facilitate use in micro channel fabrication," M. Nordstrom, R. Marie, M. Calleja and A. Boisen, *J. Micromech. Microeng.* **14**, 1614-1617, 2004.
- [5]. "Ceric ammonium nitrate: a mild and efficient reagent for conversion of epoxides to  $\beta$ -nitrate alcohols," N. Iranpoor, P. Salehi, *Tetrahedron*, **51**, 909-912, 1995.



# A SIMPLE HYDROPHILIC TREATMENT OF SU-8 SURFACES FOR CELL CULTURING AND CELL PATTERNING



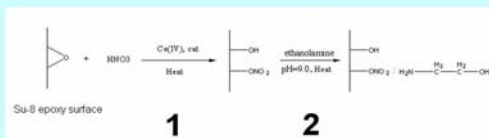
Zhenyu Wang, Michael Stangegaard, Martin Dufva, Jörg P. Kutter, and Anders Wolff

MIC - Department of Micro and Nanotechnology, Technical University of Denmark, Building 345 east, Denmark  
Phone: +45 4525 6319; Email: zw@mic.dtu.dk

## 1. Introduction

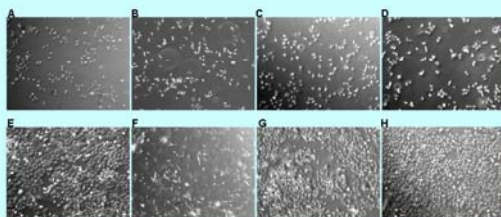
As an epoxy negative photoresist, SU-8 has been widely used as a construction polymer material. The surface properties of SU-8 result in low adhesion of mammalian cells. In this poster, we present a simple, moderate and robust chemical treatment protocol to render a SU-8 surface hydrophilic. The treated SU-8 surface is suitable for cell culturing and patterning. The whole genome expression profiles of cells cultured on different surfaces were compared to evaluate the surface biocompatibility.

## 2. Chemical treatment protocol



Reaction scheme of the two-step SU-8 surface modification: 1: The epoxy ring on the SU-8 surface is opened by treatment with HNO<sub>3</sub>-CAN [1]; 2: The nitro radical on the modified SU-8 surface is then reacted with the amino group of ethanolamine. During this two-step protocol, the contact angle of SU-8 surface decreased from 95° to 45° after the first step, and then to 25° after the second step.

## 3. Cell culturing

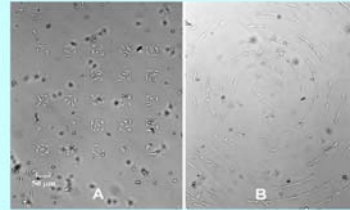


HeLa cells cultured on differently treated SU-8 surfaces. In **A-D** the cells were cultured for 24 hours while in **E-H** the cells were cultured for four days. **A** and **E**: reference culture flask; **B** and **F**: untreated SU-8; **C** and **G**: HNO<sub>3</sub>-CAN treated SU-8; **D** and **H**: HNO<sub>3</sub>-CAN and ethanolamine treated SU-8.

### Reference:

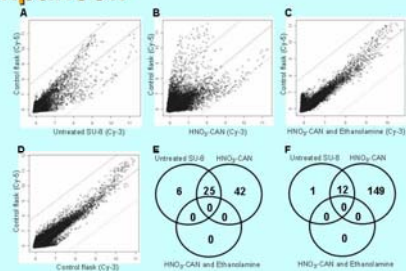
[1] N. Iranpoor, P. Salehi, Tetrahedron, 51, 909-912, 1995.

## 4. Cell patterning



HeLa cells cultured over night on SU-8 surfaces with HNO<sub>3</sub>-CAN and ethanolamine treatment patterns. **A**: HeLa cells grown on an array of 50 μm × 50 μm squares; **B**: HeLa cells grown on 5 μm wide concentric circles.

## 5. Whole genome expression comparison



Whole genome expression comparison of the incubated HeLa cells on different surfaces by microarray. **A**: Untreated SU-8; **B**: HNO<sub>3</sub>-CAN treated SU-8; **C**: HNO<sub>3</sub>-CAN and ethanolamine treated SU-8; **D**: self-self hybridization control experiment; **E**: The number of more than three-fold up-regulated genes on the different surfaces relative to the reference cell culture flask; **F**: Same as **E** but for down-regulated genes.

## 6. Conclusion

In conclusion, a two-step chemical treatment protocol for modification of SU-8 surfaces was developed. The modified SU-8 surface shows excellent biocompatibility for cell culturing and patterning. The whole genome expression comparison provides more detailed information on the surface biocompatibility than growth rate and cell morphology alone.

Poster 3



# A MICRO CELL CULTURE CHAMBER ( $\mu$ CCC) FOR THE CULTURING AND STUDY OF EUKARYOTIC CELLS

Michael Stangegaard, Sarunas Petronis, Claus B. V. Christensen, Martin Dufva

Dept. of Micro and Nanotechnology, Technical University of Denmark, Ørsteds Plads 345 east, DK-2800 Kgs. Lyngby, Denmark

**Introduction:**

Culturing and direct online morphological observation of human cells<sup>1</sup> is important in several biomedical research areas, including drug screening, stem cell research, zygote research and biomaterials science. We have realized a micro cell culture chip that meets the fastidious demands of human cell culturing<sup>2</sup>. The transparency of the chip and implementation of continuous media perfusion enabled long term cell culturing and real time morphological observations directly on the microscope stage.

**Chip Design and Fabrication:**

The individual parts of the cell culture chip were produced by laser ablation of poly (methyl methacrylate) (PMMA) and thermally bonded<sup>3</sup> (Fig. 1) eliminating the need for lithography<sup>4</sup>. The total size of the chip was 51 mm by 41 mm and 2.7 mm high, offering 1 sq. cm of culture area. A sheet of indium tin oxide (ITO) covered polyethylene terephthalate (PET) film was used to generate heating when a low current (< 3 V) was applied.

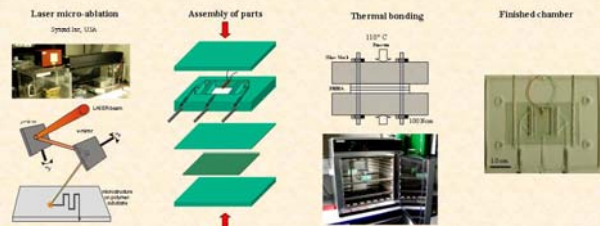


Figure 1: Fabrication of the  $\mu$ CCC.

**Simulations:**

2D Fluid flow was simulated in Femlab v. 3.0a with and without flow-equalizing barriers (Fig. 2). Flow equalizing barriers created uniform flow profiles as seen in the liquid flow profile below. 2D Heat distribution simulations indicated that the maximum heat difference across the chip was 2 °C.

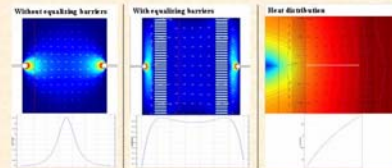


Figure 2: 2D Femlab simulations of liquid flow and heat distribution.

**Results:**

Proportional integrative and differentiative (PID) regulation<sup>5</sup> of the applied voltage to the cell culture chip enabled the temperature to be kept at 37 °C  $\pm$  0.2 °C (Fig. 3).

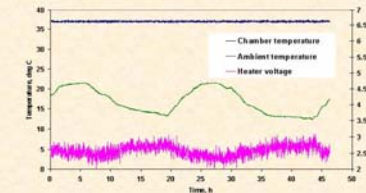


Figure 3: Temperature stability of the  $\mu$ CCC.

The first signs of cell attachment were visible after 20 minutes of incubation. After 2 hours, most cells showed signs of attachment. After 10 hours, many cells were in the process of dividing, identified by the formation of larger round cells. Cells doubling time was estimated to be around 32 hours, consistent with culturing in culture flasks (Fig. 4).

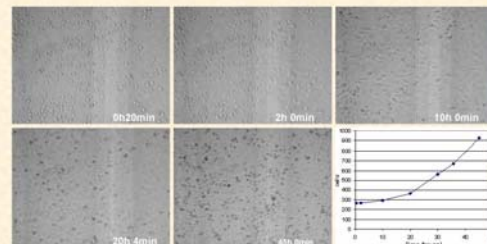


Figure 4: Time lap series of HeLa cells grown in the  $\mu$ CCC.

**References:**

- [1] G. O. Gey, W. D. Coffman, and M. T. Kubicek, "Tissue Culture Studies of the Proliferative Capacity of Cervical Carcinoma and Normal Epithelium," *Cancer Research*, vol. 12, pp. 264-265, 1952.
- [2] N. M. McKenna and Y. L. Wang, "Culturing cells on the microscope stage," *Methods Cell Biol.*, vol. 29, pp. 195-205, 1989.
- [3] H. Klank, J. P. Kutter, and O. Geschke, "CO<sub>2</sub>-laser micromachining and back-end processing for rapid production of PMMA-based microfluidic systems," *Lab Chip*, vol. 2, pp. 242-6, 2002.
- [4] P. J. Hung, P. J. Lee, P. Sabounchi, N. Aghdam, R. Lin, and L. P. Lee, "A novel high aspect ratio microfluidic design to provide a stable and uniform microenvironment for cell growth in a high throughput mammalian cell culture array," *Lab Chip*, vol. 5, pp. 44 - 48, 2005.
- [5] J. Essick, in *Advanced LabVIEW Labs*. Upper Saddle River N.J.: Prentice Hall, 1999, pp. 397.

**Acknowledgments:**

This work was supported by The Danish Research Council (grant #2014-00-0003, DABIC) and by Medicion Valley Academy BIO+IT program and Otto Monstedts fond for travel and conference contribution

Poster 4

# SIGNIFICANCE OF THE LENGTH OF RANDOM OLIGO PRIMERS ON THE YIELD OF cDNA DURING REVERSE TRANSCRIPTION

Michael Stangegaard<sup>1</sup>, Inge Høgh Dufva<sup>2</sup>, Vibeke Wohlgelegen<sup>2</sup> and Martin Dufva<sup>1</sup>

<sup>1</sup>Department of Micro and Nanotechnology, Technical University of Denmark, Ørstedss Plads 345 east, DK-2800 Kgs. Lyngby, Denmark. Tel: +45 4525 6324; Fax: +45 4588 7762; E-mail: mdh@mie.dtu.dk

<sup>2</sup>Department of Haematology, Herlev Hospital, University of Copenhagen, Herlev Ringvej 75, DK-2730 Herlev, Denmark

**Introduction:**

Gene expression studies rely on largely on reverse transcription of RNA into cDNA which subsequently can be analyzed by real time PCR or using microarrays. An efficient synthesis step is necessary for a sensitive analysis. Furthermore, the resulting cDNA should reflect the mRNA population.

**Results:**

Random primers of different lengths were compared (Figure 1 and 2) using reverse transcription [1] and the results showed that 15bp long random oligonucleotides (pentadecimers) from an oligo vendor gave a cDNA yield corresponding to almost 100 % conversion of the RNA while random hexamers induced conversion of only 50%. The results suggest that random pentadecimers primers result in cDNA that covers close to the whole transcriptome. The reason for the higher efficiency of random pentadecimers primers in cDNA synthesis can be its higher melting temperature (Figure 3). This leads to a more stable duplex formation between the random pentadecimers primers and the RNA compared to random hexamer primers. Microarray analysis using co-hybridizations to 44 290 element 60bp commercial oligo arrays covering the entire transcriptome showed that no bias was introduced using random pentadecimers compared to random hexamers indicating that random pentadecimers results in more cDNA that is qualitatively similar to cDNA from random hexamer primers (Figure 4).

**Conclusion:**

Our results suggest that random hexamers can readily be substituted with random pentadecimers available from an oligo vendor to get higher yields while not introducing bias.

**References:**

- [1] Wang J. V. et al. Within the fold: assessing differential expression measures and reproducibility of microarray assays. *Genome Biol* 3, research0062 (2002).
- [2] Van Gelder, R. S. et al. Amplified RNA synthesized from limited quantities of heterogeneous cDNA. *Proc Natl Acad Sci U S A*, vol. 87, pp. 1663-7, 1990
- [3] Workalem, C. et al. A new non-linear normalization method for reducing variability in DNA microarray experiments. *Genome Biol* 3, research0048 (2002).

**Acknowledgments:**  
This work was supported by The Danish Research Council (grant #2014-00-0003, DABIC)

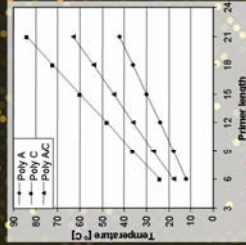


Figure 3: Melting curves of oligonucleotides with varying length. The curves were generated by the theoretical melting temperature using oligonucleotides consisting solely of adenines, cytosines or an equal amount of guanines and cytosines.

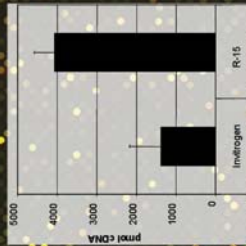


Figure 2: Effect of random primer length on the amount of generated cDNA using 1.5 µg mRNA as template

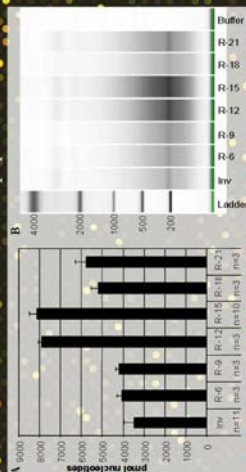


Figure 1: Effect of random primer length on the amount of generated cDNA. (A) cDNA yield obtained from reverse transcription of 3 µg 17 amplified RNA (mRNA) [2]. A commercial random primer formulation from Invitrogen (INV) was included as a control. Random primers were obtained from Sigma-Genosys ranging in length from 6 to 21 bases using a 3 base length increment (R-6 to R-21). (B) Size distribution of the generated cDNA using the Agilent Bioanalyzer and the RNA 6000 Nano Lab-Chip kit.

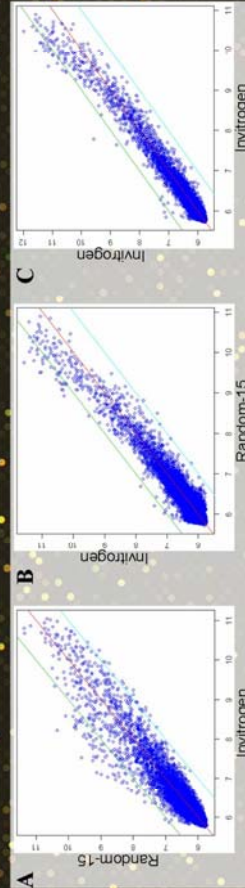



Figure 4: Scatter plots of log<sub>2</sub> transformed hybridizations for whole human genome arrays. (A and B) Dye-swap co-hybridizations of cDNA generated from Invitrogen random hexamers and Random-15mers. The green and blue line represent a 2-fold regulation relative to the mean indicated by the red line. The cDNA was normalized to 200 pmol of each type prior to hybridizations. (C) Self-seq hybridization control. Non-linear normalization of the raw data was performed using Qspline [3].

Poster 5



# Micromachined Polymeric Cell Culture Chamber with Uniform Media Perfusion and Integrated Temperature Control

**Sarunas Petronis\*, Michael Stangegaard, Martin Dufva**  
 Department of Micro and Nanotechnology, Technical University of Denmark, DK-2800 Lyngby, Denmark  
 \*Current affiliation: Applied Physics, Chalmers University of Technology, SE-41296 Göteborg, Sweden

### 1. Background

Long-term culturing and real-time observation of the mammalian cells is important in several biomedical research areas, including drug screening and biomaterials science.

Major environmental conditions for successful in vitro cell culture are:

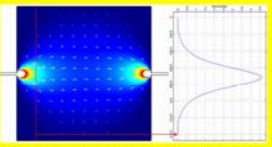
- constant temperature (37°C),
- alkalinity (pH 7.2-7.4),
- osmolality (right concentration of media components)
- supply of nutrients in cell culture buffer.

**Our aim** is to utilize advantages of modern microfabrication and microfluidics technologies in order to develop a novel disposable polymeric chip containing a fully-transparent perfusion chamber which enables reliable, long-term cell culture and is compatible with all types of microscopy (upright/inverted, reflective/transmission) as well as optical tweezers for cell manipulation.

### 3. Simulations and Testing of Physical Performance

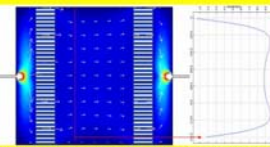
FEMLAB flow dynamics simulations:

Without equalizing barrier



±90 % flow rate variation over 70 % of the chamber area

With equalizing barrier

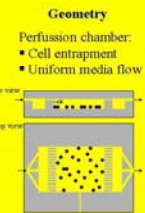


±10 % flow rate variation over 70 % of the chamber area

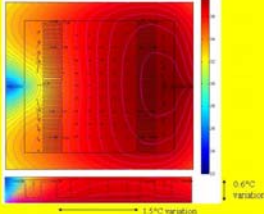
### 2. Design and Fabrication

**Design considerations:**

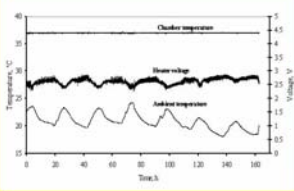
Materials	Geometry	Temperature control
Poly-methyl-methacrylate (PMMA): • Biocompatible • Transparent • Low thermal conductivity • Inexpensive • Mask-free micromachining using laser ablation • Well-established techniques for large-scale replication	Perfusion chamber: • Cell entrapment • Uniform media flow	Integrated heater: • ITO transparent thin film Temperature probe: • thermistor Control electronics and software: • Resistance-to-voltage converter • USB I/O card • Noise filtering • Temperature logging • P-I-D control algorithm • Power amplifier



FEMLAB simulations of conductive and convective heat distribution:

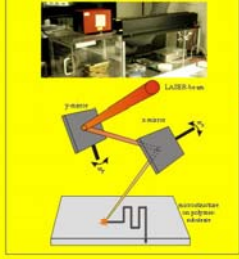


Thermal performance of cell culture chip during one week operation:



**Major fabrication steps:**

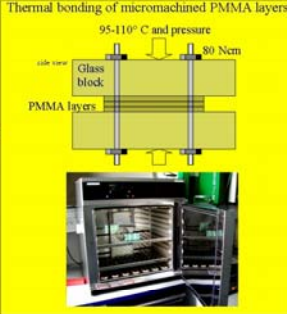
Laser micromachining of PMMA  
Synrad Inc, USA



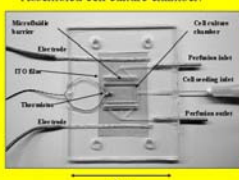
Structural layers of the chamber:

- Lid of the chamber
- Chamber, thermistor, microfluidic channels and inlets
- Bottom of the chamber
- ITO heater film
- Electrodes to the heater

Thermal bonding of micromachined PMMA layers


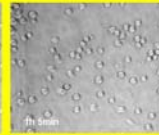
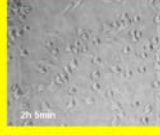
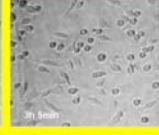
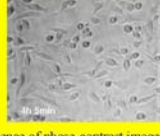
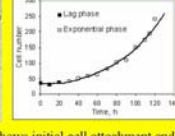


Assembled cell culture chamber:



### 4. Biological Experiments

Time-lapse microscopy of HeLa cells:

The time-lapse sequence of phase-contrast images shows initial cell attachment and spreading on the chamber bottom during the first 4 hours, and the plot demonstrates growth of cell population during 120 hours of cell culturing in the chip. The observed doubling time of 32 hours is identical to the doubling of the reference cells cultured in standard culture flasks in a bench-top incubator.

### 5. Conclusions

- A low-cost optically transparent polymeric cell culture chamber is developed for long-term cell culturing and real-time microscopy
- Integrated perfusion microfluidics and thermoregulation provides highly uniform environmental conditions in the chamber
- HeLa cells cultured in the chamber express the same biological activity in terms of doubling times as in standard culture flasks in bench-top incubator.
- The fabrication process based on laser micromachining and thermal bonding offers flexible design of the chip, providing numerous lab-on-a-chip integration possibilities in the future.

### 6. Acknowledgements

We kindly acknowledge support from Medicion Valley Academy via Bio+IT program, Nanobiotechnology project.



Poster 6



# A Biocompatible Micro Cell Culture Chamber ( $\mu$ CCC) for Culturing and On-line Monitoring of Mammalian Cells

Michael Stangegaard<sup>1</sup>, Šarūnas Petronis<sup>2</sup>, Claus Bo Vøge Christensen<sup>3</sup>, Martin Dufva<sup>1</sup>

<sup>1</sup>Department of Micro and Nanotechnology, Technical University of Denmark, Ørstedes Plads 345 east, DK-2800 Kgs. Lyngby, Denmark. Tel: +45 4525 6324; Fax: +45 4588 7762; E-mail: mdu@mic.dtu.dk  
<sup>2</sup>Dept. of Applied Physics, Fysikgården 4, Chalmers University of Technology, SE-412 96 Göteborg, Sweden.  
<sup>3</sup>Coloplast, Holteham 1, DK-3050 Humlebæk, Denmark.

**Introduction:**

Culturing and direct on-line morphological observation of human cells<sup>1</sup> is important in several biomedical research areas, including drug screening, stem cell research, zygote research and biomaterials science. Vital for comparison of results is that the culturing environment is comparable to the reference culture flask.

We have realized a micro cell culture chip that meets the fastidious demands of human cell culturing<sup>2</sup>. The transparency of the chip and implementation of continuous media perfusion enabled long term cell culturing and real time morphological observations directly on the microscope stage.

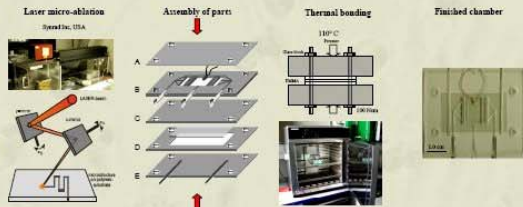


Figure 1: Fabrication of the chip.

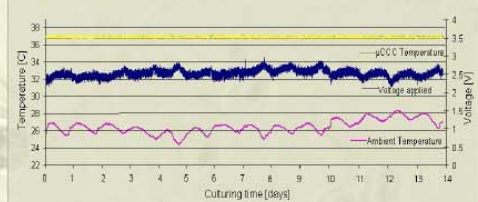


Figure 2: Thermal performance of the  $\mu$ CCC.

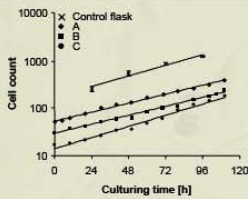


Figure 3: Growth kinetics of HeLa cells in the  $\mu$ CCC.

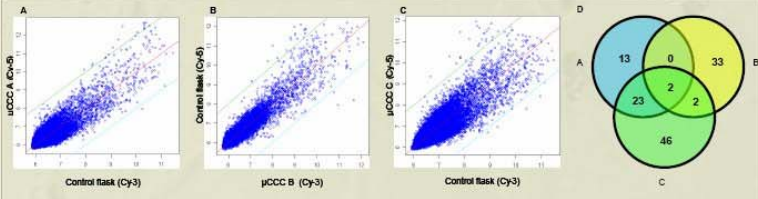


Figure 4: Biocompatibility of the  $\mu$ CCC.

**Chip Design and Fabrication:**

The individual parts of the cell culture chip were produced by laser ablation of poly (methyl methacrylate) (PMMA) and thermally bonded<sup>3</sup> (Fig. 1). A sheet of indium tin oxide (ITO) covered polyethylene terephthalate (PET) film was used to generate heating when a low current (< 3 V) was applied.

**Results:**

Proportional integrative and differentiative (PID) regulation<sup>4</sup> of the applied voltage to the  $\mu$ CCC enabled the temperature to be kept at 37 °C  $\pm$  0.2 °C despite significant fluctuations in ambient temperature (Fig. 2)<sup>2</sup>. Cell doubling time was estimated to 32 hours, consistent with the reference cell culture flasks (Fig. 3).

**References:**

- [1] G. O. Gey, W. D. Coffman, and M. T. Kubicek, "Tissue Culture Studies of the Proliferative Capacity of Cervical Carcinoma and Normal Epithelium," *Cancer Research*, vol. 12, pp. 264-265, 1952.
- [2] S. Petronis, M. Stangegaard, C. B. V. Christensen, and M. Dufva, "Transparent polymeric cell culture chip with integrated temperature control and uniform media perfusion," *Biotechniques*, in press, 2006.
- [3] H. Klank, J. P. Kutter, and O. Geschke, "CO<sub>2</sub>-laser micromachining and back-end processing for rapid production of PMMA-based microfluidic systems," *Lab Chip*, vol. 2, pp. 242-6, 2002.
- [4] J. Essick, in *Advanced LabVIEW Labs*. Upper Saddle River N.J.: Prentice Hall, 1999, pp. 397.

**Acknowledgments:**

This work was supported by The Danish Research Council (grant #2014-00-0003, DABIC).

The biocompatibility of the  $\mu$ CCC was assessed by whole genome expression profiling on 44 K DNA microarrays carrying 60 nt long probes (Fig. 4). Only two genes were differently regulated in cells grown in  $\mu$ CCC compared to cells grown in cell culture flasks (Fig. 4).

**Conclusion:**

The  $\mu$ CCC provides the possibility of studying cellular processes in real time under conditions indistinguishable from the cell culture flask in the CO<sub>2</sub> incubator.



## 11 Acknowledgment

Above all I would like to express my sincere gratitude to my supervisors Martin Dufva, Claus BV Christensen and Pieter Telleman for the introduction to the field of microfabrication and molecular biology in microdevices, for their constant guidance, support and professional advice.

A lot of people influenced the realization of this project. Most significantly was the assistance of Šarūnas Petronis for his invaluable help and support designing the  $\mu$ CCC, realizing temperature monitoring and regulation in the  $\mu$ CCC, setting up the Labview program, writing of macros for Scion Image and much much more.

All the other present and former members of the Bio-Array now Microarray Technology group at MIC.

Furthermore, I wish to thank Anders Michael Jørgensen for help obtaining spectral analysis and light intensity measurements in the  $\mu$ CCC. Zenyu Wang for his help and regarding photolithography techniques and SU-8 surface modifications. Rest of MIC. May the MIC spirit be with you.

I also wish to thank Jenny Emnéus, Christer Spégel, Arto Heiskanen and Linda Leoni Joelson (Department of Analytical Chemistry at Lund University, Sweden) and Jan Tønnesen (Section of Restorative Neurology, Wallenberg Neuroscience Center, University Hospital, Lund, Sweden) for their support with arranging and carrying out stem cell experiments.

Peter Thomsen (Scandinavian Micro Biodevices, Farum, Denmark) for kindly donating the HeLa cells and assistance with inaugurating cell culturing at MIC. Dang Duong Bang (Danish Institute for Food and Veterinary Research, Århus, Denmark) for donating the COLO 205 and CACO 2 cells. Alberto Martinez Serrano (Center of Molecular Biology “Severo Ochoa”, Autonomous University of Madrid, Spain) and Merab Kokaia (Section of Restorative Neurology, Wallenberg Neuroscience Center, University Hospital, Lund, Sweden) for allowing the culturing of the Bcl-X<sub>L</sub> and hNS1 stem cells.

This work has been financially supported by the Danish Biotechnology Instrument Center (DABIC) project no. 2014-00-0003, which is gratefully acknowledged.

Last but not least - my family, especially my wife, Lene. Without her ever present support and tolerance for my physical and mental absence, my completion of this project would not have been possible.

Den der tror han er færdiguddannet er ikke uddannet men færdig

## 12 Appendix

**Table 5: Table of regulated genes from HeLa cells cultured on modified SU-8 surfaces relative to the cell culture flask.** The ratio refers to the ratio between the modified surface and the reference cell culture flask. Where gene names were not available relevant accession numbers or the Agilent probe numbers are provided.

Gene Name	CAN-HNO <sub>3</sub>	Untreated SU-8	Gene Name	CAN-HNO <sub>3</sub>	Untreated SU-8
RPLP0	0,052	0,330	BC014322	3,336	3,045
AI567808	0,081	0,314	A_32_P172002	4,016	3,071
BQ007298	0,159	0,311	A_23_P119407	3,439	3,178
TMEFF2	0,104	0,305	A_23_P136296	3,907	3,327
BE962960	0,093	0,300	LOC284542	3,413	3,342
AA780485	0,114	0,296	AK000809	3,325	3,448
THC2087016	0,129	0,295	BC032064	3,056	3,516
AI613259	0,071	0,291	SLA	4,085	3,607
THC2128887	0,142	0,268	TNNI1	3,911	3,623
AI613259	0,063	0,265	KCNK7	3,157	3,679
AF130059	0,079	0,241	BC002811	3,628	3,774
THC2162618	0,085	0,208	XTP7	4,126	3,777
A_32_P140122		0,269	BC012876	4,418	3,817
FTH1	0,084		AD7C-NTP	3,404	3,823
A_32_P98162	0,203		NPEPL1	4,054	3,837
THC2115077	0,260		AL137472	4,518	3,895
AI097304	0,200		MGC21675	4,815	3,992
A_32_P95502	0,121		THC2134916	4,073	4,022
BM023129	0,332		A_23_P141785	3,565	4,093
THC2200745	0,074		AK021593	4,529	4,103
AA922712	0,294		FLJ11710	4,862	4,376
THC2160881	0,211		SDK2	3,912	4,410
BM041657	0,074		HAAO	3,885	4,733
AA300289	0,121		AF116619	5,113	5,297
A_32_P8857	0,269		BC012876	4,418	3,817
HNRPC	0,310		ABHD9		3,689
THC2044542	0,193		MKRN4		3,056
THC2136179	0,178		HSD17B1		4,663
BM973227	0,265		DUB3		3,069
THC2122880	0,266		AK024382		3,537
RPL23A	0,288		THC2177248		3,327
BG989839	0,273		TSPYL3	3,973	
BM995362	0,333		RASD1	4,053	
THC2044390	0,200		ASB16	4,027	
AL050041	0,278		CCL19	3,800	

Appendix

RPS15A	0,113	ADM	3,745
BQ029628	0,259	GLTSCR1	3,986
LOC400590	0,306	SLC27A1	3,066
W45382	0,218	TRH	3,015
AI278811	0,164	A_23_P206568	3,847
RPL23A	0,188	HDAC4	3,066
THC2083654	0,286	DLGAP4	4,003
T07777	0,318	PNPO	3,978
THC2166774	0,217	TCF15	4,081
BX350430	0,313	A_23_P348587	3,442
A_32_P51781	0,228	JUND	3,342
AK092531	0,162	FLJ10521	4,374
THC2200669	0,136	ARHGEF15	3,727
N75321	0,192	RHO	4,224
A_32_P46641	0,310	ENST00000304460	3,918
AI752947	0,288	CDKAL1	3,116
AK093548	0,103	TAGLN2	3,349
CB993898	0,309	MGC4606	4,449
A_32_P36412	0,136	DKFZp564K142	3,093
THC2022176	0,185	DPYSL3	3,949
HNRPH1	0,299	AF144054	3,300
BE505021	0,327	dJ222E13.2	3,158
BX398964	0,220	HSPC065	3,102
BE963453	0,065	FLJ90024	4,265
AA399656	0,148	KIAA0406	3,483
D16891	0,198	LENG8	3,086
FTHL7	0,075	TIP120A	3,298
BF109153	0,261	THC2134410	4,095
A_32_P231114	0,191	ZNF403	3,413
BU734416	0,175	AK123446	3,227
15E1.2	0,240	A_32_P12282	3,349
CD370449	0,252	BF960555	4,845
RPS6	0,225	THC2055297	3,977
BQ028747	0,239	AK092875	3,672
BF592096	0,332	THC2138984	3,403
BE963453	0,074	AI500335	3,181
THC2203017	0,295	THC2051912	3,316
THC2205955	0,219	FAM19A4	3,351
BG013371	0,281	THC2182978	4,322
AF155662	0,139		
AI520890	0,299		
AA230176	0,114		

---

Appendix

---

F02250	0,310
BU620016	0,242
LY6K	0,291
AA897210	0,142
BM968705	0,211
BQ614035	0,219
AY117690	0,312
AK094885	0,199
RPS15A	0,137
THC2085413	0,182
AA669846	0,182
AA516102	0,321
THC2084699	0,204
A_32_P182246	0,292
AI918632	0,118
AI354226	0,222
AI937689	0,275
AK128048	0,263
THC2162031	0,261
AI961400	0,070
AF113008	0,311
CK818527	0,328
BQ028747	0,253
THC2044448	0,200
BI003432	0,098
AA081107	0,274
THC2070072	0,228
AU137951	0,132
AA604851	0,249
A_32_P158543	0,118
THC2174183	0,261
THC2166800	0,107
BQ000122	0,162
AI686776	0,252
THC2194550	0,067
BE328348	0,117
THC2130025	0,103
BE695822	0,152
BC071732	0,177
AW673984	0,276
BQ573872	0,107
AI267511	0,294

---

Appendix

---

CB853422	0,254
THC2164322	0,259
THC2200192	0,155
BC065734	0,281
A_32_P127036	0,216
RAN	0,106
AA902595	0,333
AI718865	0,320
AI608782	0,244
BG942819	0,222
AI457687	0,276
A_32_P118959	0,130
RPL23A	0,238
BI031372	0,101
CA775175	0,086
THC2123039	0,239
BE719776	0,262
AB019568	0,062
AY170823	0,303
THC2126165	0,245
THC2166330	0,299
AI985214	0,264
AL138396	0,283
THC2045396	0,131
A_24_P831005	0,187
THC2202467	0,235
AF283771	0,278
A_24_P636834	0,110
THC2159243	0,311
BC000206	0,270
THC2045155	0,269
AW075437	0,314
AW449150	0,274
AI955728	0,158
A_24_P32766	0,328
THC2082102	0,324
AK090440	0,333
AF187554	0,182
AF271776	0,227
THC2177764	0,255
A_23_P65845	0,285
A_23_P158380	0,245

Appendix

---

TRAF4	0,323
ACTB	0,160

---